DC Breakdown Characteristics of C_3F_7CN Gas Mixtures for High Voltage Insulation Applications

A thesis submitted to The University of Manchester for the degree of Doctor of Philosophy in the Faculty of Science and Engineering

2024

FAISAL OMAR BAHDAD

School of Engineering and Department of Electrical and Electronic Engineering

TABLE OF CONTENTS

TABLE OF CONTENTS **2**

LIST OF FIGURES **7**

LIST OF TABLES **15**

LIST OF ABBREVIATIONS **17**

ABSTRACT **18**

DECLARATION **19**

COPYRIGHT STATEMENT **20**

ACKNOWLEDGEMENTS **21**

PUBLICATIONS **23**

1 INTRODUCTION **24**

1.1 Background 24

1.2 Research Aims and Objectives 26

1.3 Thesis Contribution 27

1.4 Thesis Outline 28

2 REVIEW OF GAS INSULATED EQUIPMENT AND INSULATION GASES FOR HIGH VOLTAGE DC APPLICATIONS **30**

2.1 Introduction 30

2.2 Gas Insulated Switchgear (GIS) 31

2.2.1 Disconnector, Isolators and Earthing Switches 31

2.2.2 Surge Arresters 32

2.2.3 Voltage and Current Measurement 32

2.2.4 Interface and Passive Modules 32

2.3 Electron Beam Accelerator 32

2.4 Gas Insulated Lines (GIL) 33

2.4.1 GIL Development History 33

2.4.2 Construction and Installation 35

2.4.3 Advantages of Using GIL 36

2.4.4 Comparison of Current Transmission Technologies 36

2.4.5 DC Gas Insulated Lines (DC-GIL) Design Challenges 38

2.5 Discharge Mechanism in Gas Dielectrics 43

2.5.1 Generation of Charge Particles 43

2.5.2 Degeneration of Charge Particles (Deionisation Processes) 46

2.5.3 Electric Field Distribution 46

2.5.4 Townsend Theory of Breakdown 47

2.5.5 Paschen's Law 51

2.5.6 Streamer Theory of Breakdown 52

2.5.7 Streamer Propagation 54

2.5.8 Leader Transition and Propagation 55

2.6 SF_6 and its Alternative Gases 56

2.6.1 SF_6 Gas 56

2.6.2 Alternative SF_6 Gases and its Mixtures 57

2.6.3 Chemical and Physical Properties Comparison of SF_6 and C_3F_7CN Gas and Mixture Ratio Selection 61

2.6.4 C_3F_7CN Mixture Ratio Selection 62

2.7 DC Breakdown Characteristics of SF_6 and C_3F_7CN Gas and its Mixtures 64

2.7.1 DC Breakdown Characteristics of SF_6 64

2.7.2 Comparative DC Breakdown Characteristics of SF_6 and C_3F_7CN gas and its Mixtures 65

2.8 Effects of Experimental Procedures on the DC Breakdown Voltage of Gases 71

2.8.1 Breakdown Test Method 71

2.8.2 Successive Discharge Test Procedure 74

2.8.3 Mixing Time of Gas Mixtures 75

2.8.4 Effect of Electrode Materials 77

2.8.5 Effect of Electrode Surface Roughness 79

2.8.6 Effect of Electrical Ageing on the Breakdown Voltage 80

2.9 Summary 86

3 EXPERIMENTAL DETAILS 87

3.1 Introduction 87

3.2 Pressure Vessel 87

3.2.1 Small-Scale Vessel for Preliminary Trials 87

3.2.2 Large-Scale Vessel for Prototype Investigations 88

3.3 Electrode Configurations 90

3.3.1 Rod-Plane Configurations 90

3.3.2 Reduced Scale Coaxial Configurations 95

3.4 Gas Handling Setup and Procedure 100

3.4.1 Gas Handling Procedure 101

3.4.2 Gas Analysis 103

3.4.3 Leakage Detection Instruments 104

3.5 High Voltage DC Test Setup 104

3.6 Experimental Technique and Data Analysis 107

3.6.1 Experimental Technique 107

3.6.2 Data Analysis 109

3.7 Summary 114

4 DC BREAKDOWN CHARACTERISTICS OF SF_6 AND ITS ALTERNATIVES IN ROD-PLANE CONFIGURATIONS 115

4.1 Introduction 115

4.2 The Effect of Repeating Breakdown on Negative DC Breakdown Characteristics of a 20% C_3F_7CN / 80% CO_2 Gas Mixture 115

4.2.1 Negative DC Breakdown Characteristics 116

4.2.2 Gas Analysis Measurement 119

4.2.3 Electrode Surface Roughness Measurement 119

4.3 The Effect of DC Polarity and Field Uniformity on the Breakdown of SF_6, CO_2 and the C_3F_7CN/CO_2 Mixture 120

4.3.1 The Effect of Field Uniformity and DC Polarity 120

4.3.2 The Effect of Gas Pressure 122

4.3.3 The Effect of Electrode Size 129

4.4 Summary 133

5 DC BREAKDOWN CHARACTERISTICS OF SF_6 AND ITS ALTERNATIVES IN COAXIAL CONFIGURATIONS 135

5.1 Introduction 135

5.2 The Effect of the Coaxial Ratio 135

5.3 The Effect of Electrode Material 138

5.4 Comparative Investigation Between SF_6 And Its Alternatives in Coaxial Electrodes 139

5.5 Effect of Conductor Surface Roughness in Coaxial Geometry 142

5.6 Summary 149

6 MODELLING OF THE DC BREAKDOWN CHARACTERISTICS OF SF_6 AND ITS ALTERNATIVES 151

6.1 Introduction 151

6.2 Streamer Inception Criterion 151

6.2.1 Rod-Plane Field Line Data Set of E(X) 153

6.2.2 Single Protrusion Field Line Data Set of E(x) for Coaxial Geometries 154

6.2.3 Streamer Criterion Inception Voltage Calculation 155

6.3 Inception Voltage Estimation in Rod-Plane Electrodes 157

6.4 Inception Voltage Estimation in Coaxial Electrodes 161

6.5 Summary 167

7 CONCLUSION AND FUTURE RESEARCH 168

7.1 General Conclusions....168

7.2 Future Research....172

7.2.1 Large-Scale GIL Demonstrator Withstand and Long-Term Energisation Investigations....172

7.2.2 DC Partial Discharge Characterisation....172

7.2.3 Characterisation of Natural Origin Gases as an Alternative to SF_6....173

REFERENCES....174

APPENDIX A: EXTRACTED FIELD LINE DATA SET OF E(X) FROM COMSOL SIMULATION....189

A.1 Rod-Plane Configurations....189

A.2 Coaxial Geometries....209

APPENDIX B: STREAMER CRITERION MATLAB CODE....214

LIST OF FIGURES

Figure 2.1 Modules of DC gas insulated switchgear assemblies [5]. 31

Figure 2.2 Cross-sectional viewing of an AC-GIL [31]. 35

Figure 2.3 GIL installation layouts [31]. 35

Figure 2.4 400 kV transmission losses for OHL, XLPE and GIL (re-drawn from source) [3]. 37

Figure 2.5 Motion of metallic particles under positive and negative DC voltage [34]. 39

Figure 2.6 Particle motion distribution of a 0.5 mm radius aluminium ball shown in the blue line at 6.1 bar SF_6 under positive DC voltage [35]. 40

Figure 2.7 Principle of a particle driver and field-well ring to effectively capture particles under both DC polarities in 5 bar SF_6 gas; blue and red arrows represent the particle motion under positive and negative DC applied voltage, respectively [36], [40]. 41

Figure 2.8 DC electric field distributions on epoxy (a) disk spacer, (b) conical spacer and (c) a semi-conical spacer [40]. 42

Figure 2.9 Main processes for production of the charged particles in a gas discharge [48]. 44

Figure 2.10 An illustration of Paschen's curve. 52

Figure 2.11 An illustration of the breakdown voltage of sphere-plane electrodes for air in red colour based on the discharge mechanism, P value typically around 50 mm while Q is for gap length that is above 1-2 m. Line slop values in each region are for air as an example [60]. 53

Figure 2.12 DC polarity effect in rod-plane electrodes under DC voltage [24].....55

Figure 2.13 Molecular structure of SF_6 gas.....56

Figure 2.14 Dielectric strength trend comparison between air and SF_6 with, $(E/p)_{crit}$ = 2.5 and 8.8 kV/mm/bar respectively in uniform field (redrawn from source) [6]. 57

Figure 2.15 C_3F_7CN gas molecular structure. 61

Figure 2.16 AC breakdown voltage for SF_6 gas and 20% C_3F_7CN and 80% CO_2, air and N_2 gas mixtures in a uniform field with parallel disk electrodes and a 0.25 cm gap distance (redrawn from sources) [14], [74]. 62

Figure 2.17 Saturated vapour pressure as a function of temperature for C_3F_7CN, CO_2 gas and mixtures (filled markers are results from [74] and others are from [17]), (re-drawn from sources). 63

Figure 2.18 DC breakdown characteristics in plane-plane electrodes representing uniform field electrodes for C_3F_7CN/CO_2 mixtures and SF_6 (filled red squares are results from [18] and unfilled squares are from [91], fitted to a linear line) (re-drawn from sources) [18], [90]–[92]. 67

Figure 2.19 DC breakdown characteristics for C_3F_7CN/CO_2 and SF_6 under a quasi-uniform field (re-drawn from sources) [91]–[93]. 68

Figure 2.20 DC breakdown characteristics for 4%, 8% C_3F_7CN mixtures with CO_2 and SF_6 under a non-uniform field; filled blue markers are results from [83] and unfilled blue markers are from [94], fitted to a polynomial of the 3rd order, (re-drawn from sources) [83], [91], [94]. 69

Figure 2.21 AC breakdown characteristics for C_3F_7CN/CO_2 and SF_6 under a non-uniform field (re-drawn from source) [17]. 70

Figure 2.22 An example of multiple level test series [98]. 72

Figure 2.23 An example of successive discharge test series [98]. 73

Figure 2.24 Comparison between successive discharge and multiple level methods for sphere-sphere electrodes with a radius of (a) 2.5 cm and (b) 6.25 cm under atmospheric air [99]. 74

Figure 2.25 Time variation for SF_6 concentrations injected at the bottom of a 1 m high N_2 column with a final ratio of 60% SF_6 / 40% N_2. The calculation was done for a column height of z = 0.1 m and 0.9 m [50]. 76

Figure 2.26 Effect of electrode materials on AC breakdown voltage for SF_6 gas in plane-plane electrodes represented as filled markers [108], with unfilled markers being 10% SF_6 and a 90% N_2 mixture in sphere-sphere electrodes [107] (redrawn from sources). 77

Figure 2.27 Effect of electrode materials on AC breakdown voltage for air at atmospheric pressure in sphere-sphere electrodes, (redrawn from source) [109]. 78

Figure 2.28 Roughness factor ζ calculated as a function of SF_6/N_2 gas mixtures where, (a) 100% SF_6, (b) 50% SF_6, (c) 25% SF_6 and (d) 10% SF_6 [114]. 80

Figure 2.29 200 AC breakdowns for a 13.3% C_3F_7CN and 86.7% CO_2 gas mixture under 3 bar using a needle-plane with a gap distance equal to 10 mm [119]. 81

Figure 2.30 2000 AC breakdowns for a 13.3% C_3F_7CN and 86.7% CO_2 gas mixture under 3 bar using a needle-plane with a gap distance equal to 10 mm [120]. 81

Figure 2.31 GC/MS results for 13.3% C_3F_7CN and 86.7% CO_2 gas mixture under 3 bar (a) before testing, (b) after 200 and (c) after 2000 AC breakdown events [119], [120]. 83

Figure 2.32 CO, CF_4, C_2F_6 and C_3F_8 concentrations after 200 and 2000 breakdown events [119], [120]. 84

Figure 3.1 Small-scale vessel used in the rod-plane configuration and with breakdowns below 100 kV_{DC}. 88

Figure 3.2 Mechanical linear actuator at the bottom of the small-scale vessel to adjust the gap distance between electrodes with a 0.5 mm gap adjustment per revolution. 88

Figure 3.3 Large-scale vessel used for rod-plane and coaxial configurations for breakdowns up to 300 kV_{DC}. 89

Figure 3.4 Mechanical linear actuator at the side of the large-scale vessel to adjust the gap distance between electrodes with a 1.5 mm gap adjustment per complete revolution. 89

Figure 3.5 Analogue and digital pressure gauges used for monitoring the pressure in the vessel. 90

Figure 3.6 Rod-plane test configurations with a rod diameter of 3.5, 6.25 and 12.5 mm. .91

Figure 3.7 A mesh convergence study in COMSOL simulation to find E_{max} using different meshing sizes with electrodes spacing of 3 mm for a 6.25 mm diameter-rod-pane and an applied voltage of 1 kV. 92

Figure 3.8 Electrode simulation results for maximum and minimum element sizes equal to 0.1 mm and to 0.001 mm for the meshing criteria respectively, with the electrode gap equal to 3 mm for a 6.25 mm diameter-rod-pane and an applied voltage of 1 kV. 92

Figure 3.9 Plot of f values for rod-plane configurations with a rod diameter of 3.5, 6.25 and 12.5 mm over the gap spacing range. 93

Figure 3.10 An illustration of R_a and R_z specified in ISO 4287 [134]. 94

Figure 3.11 Surface roughness measurements of a polished electrode surface by (a) the JENOPTIK W5 surface roughness measurement device and (b) a calibration set. 95

Figure 3.12 Cross sectional view of coaxial geometry. 96

Figure 3.13 Electric field simulation for a 10/30 coaxial electrode design with an applied voltage of 1 kV (mesh size: 0.0005 mm minimum element size and 0.5 mm maximum element size).....97

Figure 3.14 Maximum electric field and field utilisation factor against a different outer conductor radius for a fixed enclosure radius of 15 mm with an applied voltage of 1 kV. .97

Figure 3.15 $R_{enclosure}/R_{conductor}$ ratio for the designed GIL as a function of the maximum system operating voltage; data obtained from [136].....98

Figure 3.16 An example of a roughness profile for a 750 CLA conductor using a Keyence VK-X200 laser microscope: (a) conductor used, (b) zoomed image measurement for the width of a protrusion of 500 µm, (c) mean surface roughness line and ridges, (d) height image showing peaks in red and valleys in blue and (e) roughness profile over a sampling length of 5,000 µm with R_a and R_z labelled.....100

Figure 3.17 DILO mini-series compact SF_6 gas service cart for (a) filling/recovery device, (b) vacuum compressor, (c) filter and (d) vacuum pump for air evacuation. 101

Figure 3.18 20% C_3F_7CN / 80% CO_2 gas mixture handling equipment (a) DILO piccolo series gas handling unit and (b) a storage tank for the pre-mixed gas. 102

Figure 3.19 Measurement examples of the used gas analysers: (a) a WIKA GA11 gas analyser, (b) a DILO C_4 multi-gas analyser and (c) a DILO SF_6 volume percentage gas analyser. 104

Figure 3.20 Leak detection devices (a) DILO SF_6 and (B) WIKA C_3F_7CN leakage detector devices.....104

Figure 3.21 Laboratory setup of the HIGHVOLT DC generator: (a) actual equipment, (b) schematic diagram and (c) equivalent DC circuit. 106

Figure 3.22 HiCOs computer-based software for controlling the DC generator. 107

Figure 3.23 Negative DC breakdown voltage of a 20% C_3F_7CN / 80% CO_2 gas mixture using sphere-plane electrodes (25 mm sphere diameter) under 3 bar, a fixed gap of 3 mm and a 2-minute time interval. 108

Figure 3.24 Negative DC breakdown voltage of a 20% C_3F_7CN / 80% CO_2 gas mixture using sphere-plane electrodes (25 mm sphere diameter) under 3 bar, a fixed gap of 3 mm and 5 kV/s ramp rate. 108

Figure 3.25 Positive DC breakdown voltage of a 20% C_3F_7CN / 80% CO_2 gas mixture using coaxial electrodes (conductor/enclosure diameter of 20/60) under 3 bar pressure. 109

Figure 3.26 Positive DC breakdown voltage of a 20% C_3F_7CN / 80% CO_2 gas mixture using coaxial electrodes (conductor/enclosure diameter of 20/60) under 3 bar pressure, with results fitted to (a) Gaussian distribution and (b) Weibull distribution probability plots. R^2 is the coefficient of determination. 111

Figure 3.27 Positive DC breakdown voltage of a 20% C_3F_7CN / 80% CO_2 gas mixture using coaxial electrodes (conductor/enclosure diameter of 20/60) under 3 bar pressure, with results in an ascending order and evaluated based on the median labelled as U_{P50}, 84.13% and 15.78% percentiles with 75% confidence. 112

Figure 4.1 Negative DC breakdown characteristics of a 20% C_3F_7CN / 80% CO_2 mixture tested using a rod-plane configuration (6.25 mm rod diameter), for stainless steel, aluminium and brass, a fixed gap of 3 mm and a pressure of 4.8 bar. The straight lines represent the best fit in each case. 116

Figure 4.2 First and last 20 breakdowns averaged from the 300 breakdowns for 20% C_3F7CN / 80% CO_2 using stainless steel, aluminium and brass electrodes. 117

Figure 4.3 Average values from every 20 breakdowns for ageing experiments of 20% C_3F_7CN / 80% CO_2 tested using stainless steel, aluminium and brass electrodes. 117

Figure 4.4 Negative DC breakdown for 20% C_3F_7CN / 80% CO_2 tested using a rod-plane configuration (6.25 mm rod diameter), for stainless steel, aluminium and brass, a gap of 3 mm and a pressure of 4.8, 3 and 2 bar. 118

Figure 4.5 Comparison of the breakdown voltage in 20% C_3F_7CN / 80% CO_2 and SF_6 at 4 bar with a 6.25 mm rod. The gap distance to f conversion is presented in Figure 3.9.....121

Figure 4.6 Effect of pressure and gap on the breakdown voltage of (a) 20% C_3F_7CN / 80% CO_2 and (b) SF_6 (up to 35 mm due to the bushing limitation) for a 6.25 mm rod.....123

Figure 4.7 Illustration of the corona stabilisation region in the V-p characteristic [83], [142]. 124

Figure 4.8 Effect of pressure and polarity on breakdown voltage for a 20% C_3F_7CN / 80% CO_2 gas mixture using a 6.25 mm rod at a fixed rod-plane gap of 25 mm.....125

Figure 4.9 Effect of pressure and gap spacing using a 6.25 mm rod diameter in CO_2. 125

Figure 4.10 Effect of pressure and gap spacing on E_{max}/p using a 6.25 mm rod-plane configuration for (a) 20% C_3F_7CN / 80% CO_2 and (b) SF_6. 127

Figure 4.11 Breakdown characteristics as a function of p·d for both 20% C_3F_7CN and 80% CO_2 and SF_6 for a 6.25 mm rod configuration under a pressure range of 1 to 5 bar and a gap range of 5 to 55 mm, and for (a) positive and (b) negative polarities. 128

Figure 4.12 Crossover point trend for rod diameters of 3.5 mm, 6.25 mm and 12.5 mm tested in 20% C_3F_7CN / 80% CO_2 under (a) 2 and (b) 3 bar. 130

Figure 4.13 Crossover point trend for rod diameters of 3.5 mm, 6.25 mm and 12.5 mm tested in SF_6 under 3 bar. 131

Figure 4.14 Crossover point trend for rod diameters of 6.25 mm and 12.5 mm tested in CO_2 under 7 and 9 bar. Green circle markers are U_{50} results only calculated for 5 breakdowns. 131

Figure 4.15 Qualitative illustration of the crossover point between both DC polarities due to the influencing factors used in this study. 132

Figure 5.1 Effect of coaxial conductor/enclosure ratio with a fixed inner enclosure of 30 mm diameter on the DC breakdown characteristics of 20% C_3F_7CN / 80% CO_2 for (a) positive and (b) negative DC. 136

Figure 5.2 Effect of the coaxial conductor/enclosure ratio with a fixed inner enclosure of 30 mm in diameter on the DC breakdown characteristics of SF_6 for (a) positive and (b) negative DC. 137

Figure 5.3 Effect of electrode material in a 10/30 mm coaxial configuration for 20% C_3F_7CN / 80% CO_2 for (a) positive and (b) negative DC. 139

Figure 5.4 Comparison of the DC breakdown characteristics between 20% C_3F_7CN / 80% CO_2, 7% C_3F_7CN / 93% CO_2, SF_6 and CO_2 in 10/30 mm coaxial configuration for (a) positive and (b) negative DC. 140

Figure 5.5 Comparison of the DC breakdown characteristics between 20% C_3F_7CN / 80% CO_2, 4% $C_5F_{10}O$ / 96% CO_2 and SF_6 in 15/45 mm coaxial configuration under both DC polarities. 141

Figure 5.6 Comparison of the DC breakdown characteristics between 20% C_3F_7CN / 80% CO_2, SF_6 and CO_2 in 20/60 mm coaxial configuration under both DC polarities. 141

Figure 5.7 DC breakdown characteristics comparison under different conductor surface roughness in a 10/30 coaxial configuration for 20% C_3F_7CN / 80% CO_2 for (a) positive and (b) negative DC polarity.....143

Figure 5.8 DC breakdown characteristics comparison under different conductor surface roughness in a 10/30 coaxial configuration for SF_6 for (a) positive and (b) negative DC polarity. 144

Figure 5.9 DC breakdown characteristics as a function of gas pressure and protrusion height tested in a 10/30 coaxial configuration for (a) 20% C_3F_7CN / 80% CO_2 gas mixture and (b) SF_6 gas.....146

Figure 5.10 Effect of pressure and protrusion height on E_{max}/p in a 10/30 coaxial configuration for (a) 20% C_3F_7CN / 80% CO_2 and (b) SF_6. Filled markers are positive and unfilled markers are negative E_{max}/p values calculated from breakdown results. 147

Figure 5.11 Calculated p·h threshold values of E_{max}/p at a T_p of -0.05 as a threshold criterion in a 10/30 coaxial configuration for (a) 20% C_3F_7CN / 80% CO_2 and (b) SF_6. Filled markers are positive and unfilled markers are negative E_{max}/p values calculated from breakdowns. 149

Figure 6.1 Shortest path field line extracted data set drawn in red for the tested rod-plane electrodes.....153

Figure 6.2 COMSOL simulation of a 10/30 mm coaxial configuration with a single hemispherical protrusion on the high-voltage conductor with a R_z of 121.8 µm for the computation of E(x) at 1 kV applied voltage. 154

Figure 6.3 Streamer criterion evaluation method by comparing the green area (integration of α_{eff} in the positive region) with the constant K. Breakdown is possible when both are equal [50], [52]. 156

Figure 6.4 SF_6 positive DC breakdown voltage for a rod plane with a 6.25 mm-diameter rod compared to U_i (dashed lines). Filled markers are results from [83] for a 6.3 mm diameter rod-plane under 1 and 3 bar. 158

Figure 6.5 SF_6 positive DC breakdown voltage for a rod plane with rod diameters of 12.5 mm and 3.5 mm compared to U_i (dashed lines). Filled markers are results from [150] and [81] for plane-sphere and sphere-sphere configurations. 158

Figure 6.6 CO_2 positive DC breakdown voltage for 12.5 mm and 6.25 mm rod-plane electrodes compared to U_i (dashed lines). 159

Figure 6.7 CO_2 positive DC breakdown voltage for 6.25 mm rod-plane electrodes compared to $U_{i\_corrected}$ (dashed lines).....160

Figure 6.8 20% C_3F_7CN / 80% CO_2 positive DC breakdown voltage for 6.25 mm rod-plane electrodes compared to $U_{i\_corrected}$ (dashed lines).....160

Figure 6.9 20% C_3F_7CN / 80% CO_2 positive DC breakdown voltage for 12.5 mm and 3.5 mm rod-plane electrodes compared to $U_{i\_corrected}$ (dashed lines). 161

Figure 6.10 Comparison of DC breakdown voltages and modelled results shown in dotted lines for: a 20% C_3F_7CN / 80% CO_2 gas mixture in (a) DC (+) and (b) DC (-); SF_6 in (c) DC (+) and (d) DC (-); and (e) DC (+) and (f) DC (-) show 7% C_3F_7CN / 93% CO_2 and 4% $C_5F_{10}O$ / 96% CO_2 gas mixtures and CO_2 gas tested in different coaxial conductor/enclosure designs.....165

Figure 6.11 Comparison of the experimental and calculated (dotted lines) results in the effect of conductor surface roughness of 10/30 mm coaxial configuration for (a) 20% C_3F_7CN / 80% CO_2 gas mixture and (b) SF_6 over different pressures and DC polarities. 166

LIST OF TABLES

Table 2.1 Technical data for the GIL in the Schluchsee Project [3]. 33

Table 2.2 Technical data for the Palexpo GIL Project [3]. 34

Table 2.3 Power losses cost of GIL and OHL with an electricity cost of 0.1 £/kWh and 100 km in length [3]. 38

Table 2.4 500 kV DC GIS prototype test procedure and results [40]. 42

Table 2.5 Natural origin gases and SF_6 GIS design specifications. 58

Table 2.6 Key properties of SF_6 and alternative gases [7], [10], [17], [29], [60], [68]–[71], [73]. 60

Table 2.7 Key properties comparison between C_3F_7CN and SF_6 [7], [14], [17], [74]. 61

Table 2.8 Antoine equation constants for C_3F_7CN and CO_2 [17]. 63

Table 2.9 SST critical field strength comparison for different gases [17], [49], [57], [85]–[89]. 65

Table 2.10 All configurations of the reported DC breakdown tests in the literature of C_3F_7CN in comparison with SF_6 in the subsequent figures. AC results were used for illustration in the non-uniform field. 66

Table 2.11 Ramp rate and time to breakdown calculation adopted by different studies on DC breakdown voltage in gases. 75

Table 2.12 Acute toxicity hazard categories according to the LC_{50} value [124]. 84

Table 2.13 GWP and LC_{50} calculations for 13.3% C_3F_7CN and 86.7% CO_2 gas mixtures before and after 2000 AC breakdown events based on CO, CF_4, C_2F_6 and C_3F_8 concentrations obtained from [120]. 85

Table 3.1 Material specifications for the used stainless steel, aluminium, and brass electrodes. Aluminium alloy could have a higher work function value than the pure one [111], [131]–[133]. 94

Table 3.2 A range of parameters including coaxial geometry, E_{max}, field uniformity and the material tested in this study. 99

Table 3.3 Tested conductor's surface roughness parameters in a10/30 mm coaxial configuration as per ISO 4287 [134]. 99

Table 3.4 Measured gases and tolerances of the used gas analysers. 103

Table 3.5 Comparison of the U_{50G}, U_{50W} and U_{P50} values for 8 randomly selected tests in 20% C_3F_7CN / 80% CO_2. 113

Table 4.1 Gas analysis using a DILO C_4 multi-gas analyser unit for a C_3F_7CN/CO_2 gas mixture before and after 300 breakdowns under 4.8 bar. 119

Table 4.2 Surface roughness measurement using a Jenoptik wave line W5 device before and after 300 breakdowns for stainless steel, aluminium and brass at the centre of the plane electrode. 120

Table 6.1 A, B and K parameters used for streamer calculation [57], [85]–[89], [147]–[149]. 153

Table 6.2 Effect of surface roughness on the E_{max} values obtained from a COMSOL simulation with an applied voltage of 1 kV. 155

Table A.1 Field line data set of E(x) with x is the distance away from the high voltage electrode, for 3.5 mm diameter rod-plane electrodes at 1 kV applied voltage (mesh size: 0.0005 mm minimum element size and 0.5 mm maximum element size). 189

Table A.2 Field line data set of E(x) with x is the distance away from the high voltage electrode, for 6.25 mm diameter rod-plane electrodes at 1 kV applied voltage (mesh size: 0.0005 mm minimum element size and 0.5 mm maximum element size). 193

Table A.3 Field line data set of E(x) with x is the distance away from the high voltage electrode, for 12.5 mm diameter rod-plane electrodes at 1 kV applied voltage (mesh size: 0.0005 mm minimum element size and 0.5 mm maximum element size). 201

Table A.4 Field line data set of E(x) with x is the distance away from the high voltage electrode, for 10/30, 15/45 and 20/60 mm coaxial geometries with a R_z of 8 µm at 1 kV applied voltage (mesh size: 0.0005 mm minimum element size and 0.5 mm maximum element size). 209

Table A.5 Field line data set of E(x) with x is the distance away from the high voltage electrode, for 10/30 mm configuration, with R_z varied between 8.95-121.8 µm at 1 kV applied voltage (mesh size: 0.0005 mm minimum element size and 0.5 mm maximum element size). 211

LIST OF ABBREVIATIONS

SF_6	Sulphur Hexafluoride
C_3F_7CN	Heptafluoro-Iso-Butyronitrile
CO_2	Carbon Dioxide
GWP	Global Warming Potential
ODP	Ozone Depletion Potential
GIL	Gas Insulated Line
GIB	Gas Insulated Busbar
GIS	Gas Insulated Switchgear
AC	Alternative Current
DC	Direct Current
LI	Lightning Impulse
HV	High Voltage
U_{50}	50% Breakdown Voltage
U_i	Streamer Inception Voltage
f	Field Utilisation Factor
E_{mean}	Mean Electric Field
E_{max}	Maximum Electric Field
$(E/p)_{crit}$	Critical Electric Field
E_{max}/p	Pressure-Reduced Breakdown Field Strength
α	Ionisation Coefficient
η	Attachment Coefficient
α_{eff}	Effective Ionisation Coefficient (α - η)
x_c	Critical Avalanche Length

All pressures used in this work are in <u>absolute pressure</u>.

ABSTRACT

The drive towards decarbonising the electricity grid and the high global warming potential (GWP) of sulphur hexafluoride (SF_6), 24,300 times greater than CO_2 and with an atmospheric lifetime of 3,200 years, has led to an increasing level of research activity to find a suitable alternative candidate with a significantly lower GWP. This thesis investigates the technical viability of adopting C_3F_7CN/CO_2 gas mixtures as an alternative insulation medium to SF_6 gas for DC gas insulated lines (GIL) and gas insulated busbars (GIB). A single protrusion streamer criterion model has been developed to accurately predict the DC breakdown voltage for screening new SF_6 alternatives without recourse to experiment. Two types of electrode configurations are used to examine the DC breakdown characteristics of SF_6 and CO_2 gases and mixtures of 4% $C_5F_{10}O$, 7% C_3F_7CN and 20% C_3F_7CN mixed with CO_2 at 1-9 bars of pressure and rod-plane and reduced-coaxial electrodes with a range of field uniformities between 0.07-0.65 and 0.48-0.69 respectively, including the effects of electrode material and conductor surface roughness. This provides a range of field uniformities and conductor practical surface finishes as found in the designs of GILs, GIBs and switches inside ring main units. Results demonstrate that 20% C_3F_7CN / 80% CO_2 and SF_6 have comparable DC breakdown characteristics in the investigated geometries and surface roughness. Thus, 20% C_3F_7CN / 80% CO_2 could provide a valuable alternative to SF_6 in a high-voltage plant. It is also noted that CO_2, 4% $C_5F_{10}O$ / 96% CO_2 and 7% C_3F_7CN / 93% CO_2 show a weaker dielectric performance than SF_6. The calculated results are in strong agreement with experimental results for positive DC breakdown in a rod-plane configuration with a pressure range of 2-9 bars. In coaxial geometry close to the optimal ratio, the majority of the experimental and calculated results are within ±5% for different coaxial sizes, pressures (>1 bar), gas mediums, DC polarities and conductor surface roughness relevant to practical applications. Therefore, this modelling approach has the ability to provide an accurate estimation of DC breakdown voltage over a range of representative test conditions, optimising the selection process of new SF_6 alternatives.

DECLARATION

No portion of the work referred to in this thesis has been submitted in support of an application for another degree or qualification of this at any other university or institute of learning.

COPYRIGHT STATEMENT

I. The author of this thesis (including any appendices and/or schedules to this thesis) owns certain copyright or related rights in it (the "Copyright") and has given The University of Manchester certain rights to use such Copyright, including for administrative purposes.

II. Copies of this thesis, either in full or in extracts, and whether in hard or electronic copy, may be made only in accordance with the Copyright, Designs and Patents Act 1988 (as amended) and regulations issued under it or, where appropriate, in accordance with licensing agreements which the University has from time to time. This page must form part of any such copies made.

III. The ownership of certain Copyright, patents, designs, trademarks and other intellectual property (the "Intellectual Property") and any reproductions of copyright work in the thesis, for example graphs and tables ("Reproductions"), which may be described in this thesis, may not be owned by the author or third parties. Such Intellectual Property and Reproductions cannot and must not be made available for use without the prior written permission of the owner(s) of the relevant Intellectual Property and/or Reproductions.

IV. Further information on the conditions under which disclosure, publication and commercialisation of this thesis, the Copyright and any Intellectual Property and/or Reproductions described in it that may take place is available in the University IP Policy, in any relevant Thesis restriction declarations deposited in the University Library, The University Library's regulations and in The University's policy on Presentation of Theses.

ACKNOWLEDGEMENTS

All praises to Allah and his blessing for the completion of this work

I would like to start by expressing my sincere gratitude to my supervisors Dr. Tony Chen and Prof. Simon Rowland for their absolute support, guidance and encouragement throughout my academic journey. I am grateful to be under their supervision.

I would also like to thank the Faculty of Science and Engineering at The University of Manchester for awarding me one of the highly prestigious Dean's Doctoral Scholar awards and The Department of Electrical and Computer Engineering in King Abdulaziz University for their financial support. I am also grateful to Dr. Richard Gardner, Dr. Vidyadhar Peesapati, Dr. Prem Ranjan, Dr. Paul Coffey, Dr. Ibrahim Iddrissu, Dr. Loizos Loizou, Prof. Qiang Liu and Prof. Ian Cotton for their unconditional support and helpful guidance during my experimental research. Also, I would like to take the opportunity to thank those from the mechanical workshop at The University of Manchester, specifically, Morris Patterson, Daniel Vale and David Joslin, for being particularly helpful in fabricating and polishing experimental conductors. I am also grateful for those colleagues and friends who were around me during my time at The University of Manchester, where I had the pleasure of working with Dr. Qinghua Han, Abir Alabani, Frances Hu, Faisal Aldawsari, Costa Onoufriou, Dr. Niharika Baruah, Maria-Irina Oancea and Raul Negrin.

I have started this sentence in bold in tribute to the most important people in my life. These people not only supported me throughout my PhD but have always been there for me through their provision of infinite love and care.

Words are not always enough to express one's deepest gratitude to their beloved parents, as is the case towards mine, Omar Bahdad and Amal Alsawadi, who have always been by my side offering endless care and support for my education and choices in life. I have been lucky to have them in my life throughout. I would also like to thank my brothers, Abdullah and Ibrahim Bahdad, and my sisters, Sereen and Maria Bahdad, who have always supported me. Thanks also go to my wider family.

I would also like to thank my father- and mother-in-law, Kahiry Abideen and Samia Kalkatawi, and their daughter, Raseel Abideen, for their care and support during my academic journey.

I would be remiss in not mentioning my dearest best friends, Amar Abideen and Khalid Altunisi, for their continued help, support and companionship throughout the years.

Finally, I cannot begin to express my gratitude and thanks to my wife and life, (soon to be Dr.) Dania Abideen, for her selfless, endless, limitless and unconditional love, care and support in all of the years. I have been lucky to have had her by my side. She has brought me the most incredible gift in the world, my son, Amr Bahdad.

PUBLICATIONS

Journal Articles:

F. O. Bahdad, L. Chen and Q. Han, " Modeling of DC Breakdown Characteristic in Coaxial Geometries for SF_6 and its Alternatives," *IEEE Transactions on Dielectrics and Electrical Insulation*, vol. 31, no. 3, pp. 1438-1446, Jun. 2024.

F. O. Bahdad, L. Chen, P. Ranjan and S. Rowland, "Effects of DC Polarity and Field Uniformity on Breakdown of SF_6 and C_3F_7CN/CO_2 Mixture," *IEEE Transactions on Dielectrics and Electrical Insulation*, vol. 29, no. 6, pp. 2227-2235, Dec. 2022.

P. Ranjan, L. Chen, A. Alabani, F. O. Bahdad, I. Cotton and L. van der Zel, "Anomalous First Breakdown Behavior for HFO1234ze(E)," *IEEE Transactions on Dielectrics and Electrical Insulation*, vol. 28, no. 5, pp. 1620-1627, Oct. 2021.

I. Iddrissu, L. Chen, F. O. Bahdad, J. Dabin, D. Joassin, L. Maksoud and Y. Kieffel, "Negative DC Breakdown Characteristics of C_3F_7CN / CO_2 Gas Mixture for Application in High Voltage Accelerators," *IEEE Transactions on Dielectrics and Electrical Insulation*, vol. 28, no. 3, pp. 946-954, Jun. 2021.

Conference Proceedings:

P. Ranjan, Q. Han, F. O. Bahdad, A. Alabani, L. Chen, I. Iddrissu and L. van der Zel, "Lightning Impulse and AC Breakdown Characteristics of SF_6 and its Alternatives," *2022 IEEE 4th International Conference on Dielectrics (ICD)*, Palermo, Italy, 2022, pp. 672-675.

F. O. Bahdad, L. Chen and S. M. Rowland, "Negative DC Breakdown Characteristics of C_3F_7CN and CO_2 Mixture with Different Electrode Materials," *2021 IEEE Conference on Electrical Insulation and Dielectric Phenomena (CEIDP)*, Vancouver, BC, Canada, 2021, pp. 510-513.

1 INTRODUCTION

1.1 Background

In response to increasing electricity demand, more compressed gas insulated equipment will need to be installed, including gas insulated switchgear (GIS), gas insulated busbars (GIB) and gas insulated lines (GIL), due to these types of equipment having proven their efficiency, reliability and capability in power networks over the years. In addition, security of supply and network reliability are compulsory factors due to the cost of loss of supply and blackouts costing more than securing it [1]. In the USA in 1960, gas insulated technology using sulphur hexafluoride (SF_6) gas as an insulator medium was first proposed. The first connected GIL was used in Germany at Schluchseewerk hydro power plant in 1974 for alternating current (AC) transmission [2], [3].

Today, renewable energy generation and interconnectors used to connect countries are operated under high voltage direct current (HVDC) systems [4]. Additionally, with the increasing number of installations of offshore wind platforms where space is at a premium, DC-GIS offers a more compact solution [5]. In addition, compared to the current used in an HVDC transmission system where which uses a cross-linked polyethylene cable (XLPE), DC-GIL could not only provide lower losses but also higher efficiency and power transmission capability. Furthermore, DC transmission is desired to transmit energy over a long distance as it will provide lower losses when compared to an AC transmission system. However, many technical challenges remain with the DC-GIL design, such as floating metallic particles under the DC field having different behaviours than the AC-GIL due to voltage polarity dependences. Thus, a new design of metallic particle trap for a DC-GIL is required. Moreover, charge accumulation in the solid insulator inside the enclosure presents another dilemma [2].

The most commonly used insulating medium in compressed gas-insulated equipment is SF_6 due to its chemically stability with a high arc quenching capability and dielectric strength approximately three times higher than air at atmospheric pressure under a uniform field [6]. Pressurised SF_6 has even higher dielectric strength, which could help reduce the equipment footprint in order to save space. However, the main downside of this gas is its high global warming potential (GWP) 24,300 greater than CO_2 and its 3,200 year atmospheric lifetime [7], [8]. The installation of more SF_6 equipment would have a significant cumulative

environmental impact [9]. The high GWP of SF_6 gas has led to increasing research activity to find a suitable alternative candidate with a significantly lower GWP. Recently, many alternatives to SF_6 have been examined, including natural origin gases (dry air, N_2 and CO_2) and fluorinated gases (such as C_3F_7CN, $C_5F_{10}O$, $C_3H_2F_4$, CF_3I and others) but they all have drawbacks in terms of liquefaction temperature, dielectric strength and toxicity, as detailed in [10], [11].

Current investigations focus on replacing SF_6 by either a complete replacement with new equipment using natural origin gases such as dry air, N_2 and CO_2 and low C_3F_7CN mixture concentrations at an elevated operating pressure [10], [12], or a retrofill solution of existing SF_6 equipment at a comparable operating pressure [13]. C_3F_7CN is a gas developed by 3M™ and known commercially as Novec™ 4710. This gas has many similarities to SF_6 in terms of chemical and physical properties, and has a GWP 2,100 greater than CO_2 [14]. It is usually used in mixtures to avoid liquefaction under higher pressure. A mixture of 20% C_3F_7CN content has a GWP of 1,100 [15], matching the breakdown strength of SF_6 in uniform and quasi-uniform field configurations only, with some differences in the breakdown strength also observed in non-uniform fields, under lightning impulse (LI) [16], AC [17] and DC [18] voltage stresses.

With the current regulation of Fluorinated gases (F-gases) in progress, as well as the determination of the minimum allowable GWP limit for the insulation gases to decarbonise the electricity sector [19]–[21], this creates uncertainty in finding an optimal alternative gas to SF_6. For every alternative gas candidate and mixture ratio used, a complete set of experimental research that includes different electrode configurations, surface roughness and gas pressures is required to study the breakdown characteristics of the candidate. Thus, if a generalised modelling approach is developed that could estimate the DC breakdown characteristics of different gases prior to any experimental research that takes into account representative practical conditions, it would help optimise the selection process of any new SF_6 alternatives for high voltage DC insulation applications without recourse to experiment.

1.2 Research Aims and Objectives

This research aims to investigate the feasibility of adopting C_3F_7CN gas mixtures as an environmentally friendlier alternative to SF_6 gas for DC-GILs for long distance power transmission. This will lead to an eco-friendly and high-efficiency transmission system. Prior to deployment, extensive testing and optimisation is necessary. The breakdown characteristics of C_3F_7CN gas mixtures when compared to SF_6 gas will be investigated using DC voltage for both polarities at different gas pressures, field uniformities and electrode designs. This is to develop a systematic modelling approach capable of screening SF_6 alternatives and to estimate the DC breakdown voltage under representative conditions for different insulating gases.

The key research objectives are as follows:

I. Review of relevant literature to identify current knowledge and directions that will help identify key research gaps. This includes, HVDC equipment, DC-GIL benefits and design challenges, evaluation of SF_6 alternative gases in terms of dielectric strength, boiling point and toxicity, and factors that affect HVDC breakdown voltage in gases from a test procedure perspective.

II. Design and develop a reliable HVDC test rig, pressurised test vessel and varying field uniformity small-scale electrode configurations that include different sized rod-plane and reduced-scale coaxial geometries of different electrode materials and surface roughness for the purpose of characterising the electric field distribution in a large-scale GIL.

III. Conduct HVDC breakdown tests on different proposed SF_6 alternative gases and mixtures, including SF_6 gas, for comparison of the dielectric performance at elevated pressure in the designed test electrodes. A 50% probability of breakdown (U_{50}) will determine the breakdown voltage characteristics.

IV. Develop a mathematical model able to predict the DC breakdown voltage of different insulation gases and mixtures by considering representative practical conditions. This model will initially be applied to the experimental results of this current study and expanded to other gases reported in the researched literature.

1.3 Thesis Contribution

The major contributions of this thesis are listed as follows:

I. A comparative experimental study was carried out using three different sized rod-plane electrodes with a varying gap distance, field uniformities and gas pressure between 20% C_3F_7CN / 80% CO_2 and SF_6 under positive and negative DC polarities.

II. An experimental investigation was conducted on SF_6 and CO_2 gases, a mixture of $C_5F_{10}O/CO_2$ and two different mixtures of C_3F_7CN/CO_2 in five different sized reduced-scale coaxial electrodes systems including the effect of conductor surface roughness under both DC polarities. This is the most representative electrode design for an actual GIL.

III. A systematic modelling approach was developed based on streamer criterion theory capable of estimating the DC breakdown voltage of different insulation gases in rod-plane electrodes and reduced-scale coaxial geometries.

IV. A reliable test procedure was established to setup and perform a HVDC breakdown test for SF_6 and its alternative gases starting from addressing the factors affecting DC breakdown voltage values, such as the effect of the time intervals between breakdown and next voltage ramp, ramp rate, effect of electrode materials and ageing of electrodes that are subjected to many breakdown events, based on prior literature and preliminary testing.

1.4 Thesis Outline

The structure of the chapters in this thesis are as follows:

Chapter 2: *Review of Gas Insulated Equipment and Insulation Gases for High Voltage DC Applications*

This chapter reviews the gas insulated equipment used for high voltage insulation and control, the development of the GIL transmission system, the benefits of this transmission system in comparison with other systems and the challenges associated with moving from AC-GIL to DC-GIL. It also reviews possible alternative gases to replace SF_6. C_3F_7CN gas is a promising alternative and has been extensively compared with SF_6 gas in terms of chemical and physical properties, and previous DC breakdown investigations based on factors affecting gases breakdown voltage values during previous testing procedures.

Chapter 3: *Experimental Details*

This chapter describes the laboratory test equipment and testing method adopted for the DC breakdown voltage investigation. It includes the used test vessel and electrodes design, high voltage laboratory test circuit and gas handling procedure for gas mixtures.

Chapter 4: *DC Breakdown Characteristics of SF_6 and Its Alternatives in Rod-Plane Configurations*

This chapter provide a preliminary investigation of the effect of electrode materials and ageing electrodes on the breakdown voltage value in a rod-plane configuration, resulting from the DC polarity effect on a 20% C_3F_7CN / 80% CO_2 gas mixture when compared to SF_6 gas under both DC polarities using three different sized rod-plane configurations and a varying gap distance that can change the field uniformity from a quasi-uniform to non-uniform field.

Chapter 5: *DC Breakdown Characteristics of SF_6 and Its Alternatives in Coaxial Configurations*

This chapter presents an experimental investigation of SF_6 and CO_2 gases and mixtures of 4% $C_5F_{10}O$, 7% C_3F_7CN and 20% C_3F_7CN with CO_2 in reduced-scale coaxial configurations of different sizes under both DC polarities. The effect of conductor surface roughness on the

breakdown voltage and the threshold values are examined for both SF_6 gas and the 20% C_3F_7CN / 80% CO_2 gas mixture.

Chapter 6: *Modelling of the DC Breakdown Characteristics of SF_6 and Its Alternatives*

This chapter presents a systematic modelling approach based on streamer criterion theory to predict the DC breakdown voltage in both rod-plane and coaxial geometries. Experimental results from previous chapters will be compared with the calculated values.

Chapter 7: *Conclusion and Future Research*

This chapter presents the overall conclusion of the research carried out in this report and potential future research directions.

2 REVIEW OF GAS INSULATED EQUIPMENT AND INSULATION GASES FOR HIGH VOLTAGE DC APPLICATIONS

2.1 Introduction

Gas insulated equipment is used widely due to its capability of withstanding and delivering large amount of power to satisfy increasing demand with minimum losses when compared to other transmission systems. The main insulation medium for gas insulated equipment is SF_6 gas, which has valid negative environmental impacts. SF_6 is one of the most potent greenhouse gases, due to its high GWP 24,300 times greater than CO_2 and an atmospheric lifetime of thousands of years [7], [8]. Thus, there is urgency in finding a suitable gas to replace SF_6 in global power system networks and to satisfy environmental agreements currently in place, such as F-gas regulations [19]–[21]. Several alternative gases, such as perfluorocarbons, fluoroketones, natural origin gases and others, have all been studied but they all present limitations in terms of liquefaction temperature, dielectric strength and toxicity [10]. One proposed candidate is C_3F_7CN, which matches the dielectric performance of SF_6 when used with other buffer gases [13].

In this chapter, an extensive review will be provided by focusing on HVDC equipment, starting with its GIS components, accelerators, GIL and other transmission technologies, which will all be compared, with the challenges from moving from AC-GIL to DC-GIL presented as a potential future solution. Then, the discharge mechanism in gas dielectrics will be outlined to establish an analytical foundation for the ensuing experimental findings. The properties of SF_6, followed by research into potential alternative gases focusing on the possibility of a comparable candidate and previous experimental investigations into the breakdown characteristics of SF_6 and C_3F_7CN as the proposed candidate with DC applied voltage, will be focused on to address the effect of DC polarity on the breakdown voltage, as will the DC characteristics of alternative gases that have been rarely reported on to date. Ultimately, key factors affecting the DC breakdown voltage in terms of test procedure, technique and setup will also be presented.

2.2 Gas Insulated Switchgear (GIS)

Switchgear is a broad term that includes a disconnector, circuit breakers and other equipment used for measuring, controlling, protecting, regulating and interrupting in the electrical power system. Thus, this equipment is directly linked to the reliability of the entire electricity network. GIS components are mainly insulated with SF_6 and used where space is limited to provide a compact equipment design due to its high dielectric strength [22], [23]. A DC-GIL provides a compact technical solution optimised for converter stations offshore or onshore, and transition stations. The development of DC-GIS relies on the technology used for AC-GIS but with a newly designed DC insulator to meet the requirements of DC electric field distribution. Figure 2.1 presents the modules of DC-GIS without a circuit breaker [5].

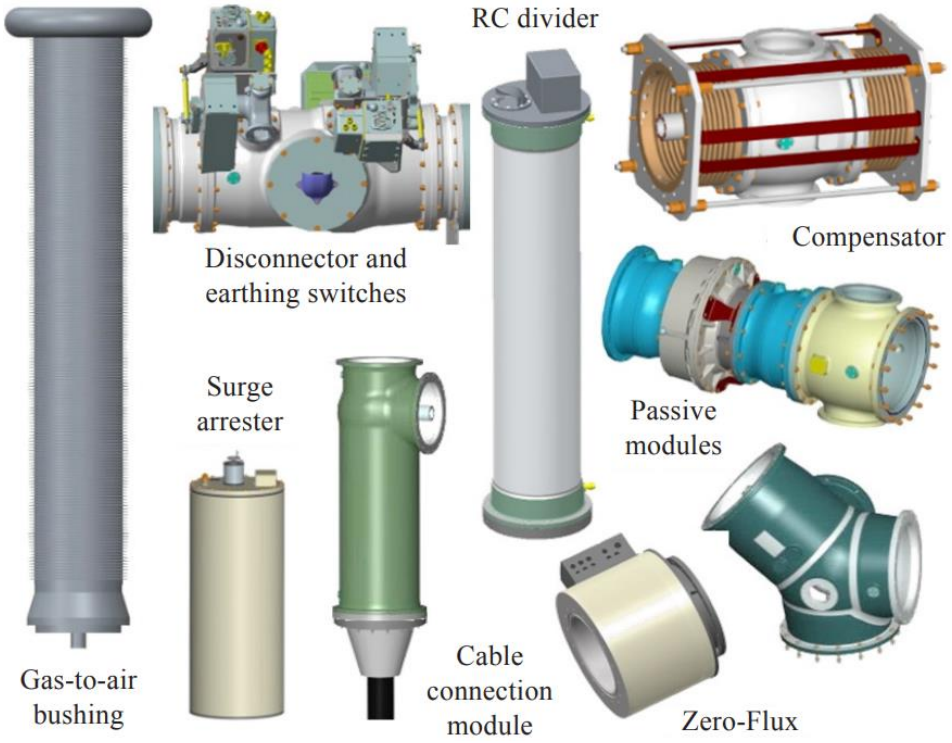

Figure 2.1 Modules of DC gas insulated switchgear assemblies [5].

2.2.1 Disconnector, Isolators and Earthing Switches

In order to perform maintenance on apparatus, it is necessary to disconnect the device from the network and apply a visual earthing which can be achieved by using disconnectors, isolators and earthing switches. Disconnectors and isolators only operate under a no-load condition when the circuit breaker is open due to the lack of any arc rupturing capacity. Earthing switches also allow the safe discharge of potential resulting from residual DC charges [5], [24].

2.2.2 Surge Arresters

Surge arresters ensure protection against overvoltage surges directly in the equipment. It consists of metal oxide resistors with a nonlinear current and voltage characteristic and is grounded to safely dissipate excessive voltage and current surges into the earth. This to ensure that the overvoltage and current surges do not damage the connected equipment. DC systems usually require higher overvoltage surge protection than AC systems. Accordingly, more than one surge arrester may be required in the system [5], [24].

2.2.3 Voltage and Current Measurement

To obtain the system voltages and currents in AC-GIS, instrumental traditional voltage transformers (VT's) and current transformers (CT's) are used. VT's are high impedance shunt devices similar to power transformers, whilst CT's are low impedance series devices [24]. In DC-GIS, voltage measurement can be conducted using gas-insulated resistive-capacitive voltage dividers that provide a low power output sufficient for modern protection and metering systems. In the case of current measurements, a special DC measurement transformer design that relies on the zero-flux current principle for a rated current up to 5000 A is used [5], [25].

2.2.4 Interface and Passive Modules

Interface modules allow transition from GIS to other equipment, such as gas to air bushing, for transition to an overhead line. Passive modules can be used for flexible configuration and special compensation requirements to deal with heat dilatation [5].

2.3 Electron Beam Accelerator

The Dynamitron® is an electron beam accelerator (DC-accelerator) [18], [26], [27], that accelerates electrons in a linear path from the high DC voltage side of the accelerator to the lower DC voltage side, with this voltage gradient acting as the driving force of the accelerator. The resulting beam current is related to the strength of the high voltage field and operates under negative DC polarity. The energy level of a Dynamitron® lies typically between 0.5-5 MeV. The Dynamitron® is widely used for industrial applications in the polymer crosslinking of wires, cables and tires, as well as to provide non-intrusive sterilisation of medical devices. The accelerator is constructed within a cylindrically shaped

pressure vessel that houses the accelerator and its subsystems. Fundamentally, the structure of a Dynamitron® can be represented as a coaxial geometry similar to GIL and GIB. The Dynamitron® uses SF_6 as an insulation medium, at an operating pressure of 9.6 bar and 7.2 bar for typical 4.5–5 MeV and below 4 MeV rated machines, respectively.

2.4 Gas Insulated Lines (GIL)

2.4.1 GIL Development History

First GIL Generation

The first generation of GIL were filled with 100% SF_6 gas. In the 1960s, the first investigation using SF_6 gas in a closed compartment was conducted under high voltage AC and DC. The experiment used a pipe-type conductor and enclosure made of aluminium, held together with solid insulators, and filled with 100 % SF_6. It was found that DC voltage has lower losses than AC. Accordingly, DC voltage was considered in the initial GIL design [3], [28]. At that time, DC had many issues related to the stability of the dielectric of the solid insulator due to some not fully understood phenomena at that time, including the space charging of insulators. As a result, AC-GIL development was undertaken [3]. In 1974, the first GIL installed application was in the Black Forest in Germany at the cavern hydropower plant of Schluchseewerke at a voltage level of 420 kV. This was due to the failure of the oil cable in the pumping storage power plant that caused significant damage to both the cable and the tunnel. Therefore, due to the non-flammability that GIL can assure, and differing from the use of oil cables, the company decided to use GIL as a solution. Table 2.1 presents the technical data for the GIL in the Schluchsee project [2], [3], [28], [29].

Table 2.1 Technical data for the GIL in the Schluchsee Project [3].

Type	Value
Nominal voltage	380 kV
Nominal current	2000 A
Lighting impulse voltage	1640 kV
Switching impulse voltage	1200 kV
Power frequency voltage	750 kV
Rated short-time current	135 kA
Rated gas pressure	7 bar
Insulating gas mixture	100% SF_6

In 1998, due to there being different names for GIL, such as gas insulated bus duct, gas insulated transmission line (GITL) or gas insulated line (GIL), IEC 61640 [30] introduced the name 'Gas-Insulated Transmission Line' using 'GIL' as its designated abbreviation worldwide.

Second GIL Generation

The second generation of GIL was filled with 20% SF_6 and 80% N_2 due to the environmental concerns of the SF_6 gas, the cost of the first GIL design and the boiling point of pure SF_6 gas when used in cold countries. These reasons were the basis for establishing programmes in 1994 to find solutions for future GIL, with the key technical data for this future design set by Electricity de France (EDF). They requested that the new GIL design had to be capable of transmitting high power in a range of 3000-4000 MW and be underground transmission solution for up to 100 km. As a result, ABB, Alstom and Siemens GIL design teams developed two basic solutions, one three-phase and two single-phase GIL designs [3].

The first application for the second GIL generation was built in Palexpo, Geneva due to Geneva hosting the Telecom 2003 international exhibition. It was laid in an underground tunnel below the Palexpo exhibition venue. This GIL was chosen due to its high-power transmission capability and low magnetic field, with the exhibition area having a magnetic field limitation of 1 μT. Only this GIL could achieve this requirement without requiring additional expensive shielding of the tunnel with a 0.3 μT at its rated current. The technical data for the GIL in the Palexpo project is presented in Table 2.2 below [3], [28], [29].

Table 2.2 Technical data for the Palexpo GIL Project [3].

Type	Value
Nominal voltage	300 kV
Nominal current	2000 A
Lighting impulse voltage	1050 kV
Switching impulse voltage	850 kV
Power frequency voltage	460 kV
Rated short-time current	50 kA / 1s
Rated gas pressure	7 bar
Insulating gas mixture	20% SF_6 and 80% N_2

2.4.2 Construction and Installation

GIL are basically made of two aluminium pipes in a concentric position that forms a coaxial cylindrical electrode arrangement, with the outer pipe named as an enclosure and the inner one named the conductor, which is centred using solid insulators/supporters. The whole enclosure is filled with a 20% SF_6 and 80% N_2 gas mixture as the main insulating medium. Figure 2.2 below shows a cross-sectional area view of a GIL [31].

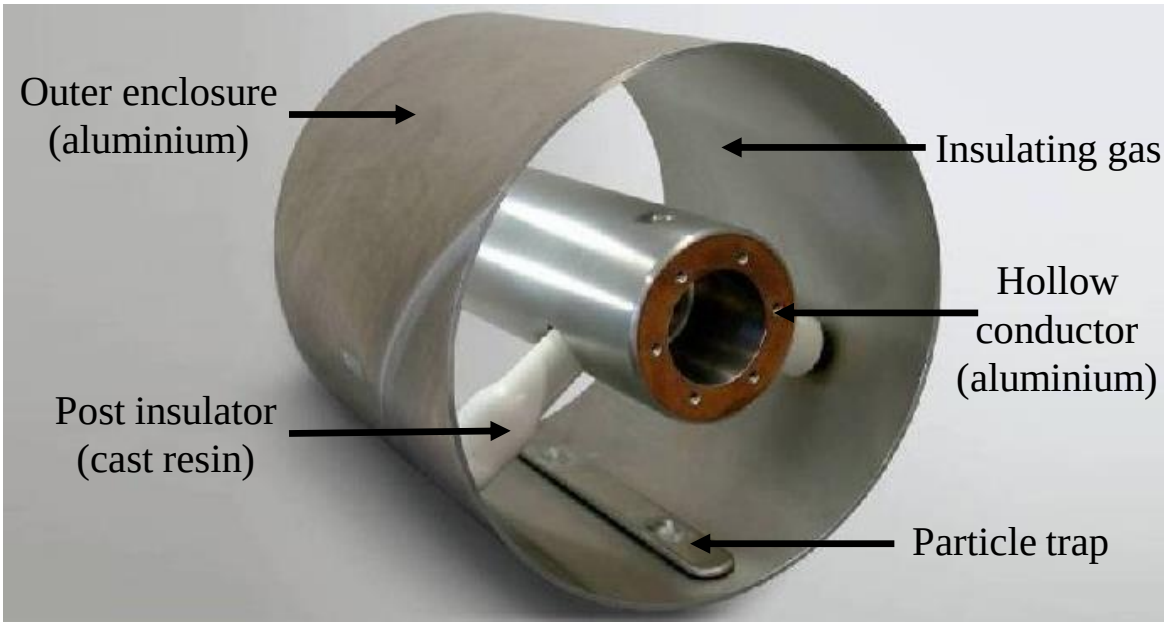

Figure 2.2 Cross-sectional viewing of an AC-GIL [31].

There are many different layouts that a GIL can be installed to overcome steeply inclined slopes, passing around different buildings above and below ground, and that can follow serpentine routings without the need of angle units. Figure 2.3 presents different GIL installation layouts [31].

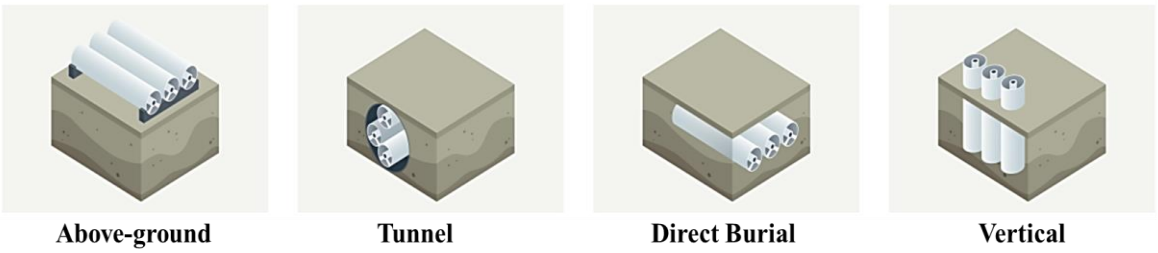

Figure 2.3 GIL installation layouts [31].

Recently, a new technology has been proposed as a transmission solution, named as Pressurised Air Cables (Hivoduct), where it is essentially a GIL using a pressurised air as an insulating medium up to 10 bar pressure. It has a large conductor cross section area with a new compact flange design without bolts or welding required, allowing more flexibility and capability in the installation. It has been successfully tested up to a voltage level of 145 kV [32], [33].

2.4.3 Advantages of Using GIL

There are many benefits for using GIL technology for transmission. This includes providing minimum losses with the maximum power delivery when compared with other transmission systems, due to its large cross-sectional areas that allow for better heat dissipation. In addition, it has minimum electromagnetic field exposure when compared with others, making it suitable for high, strict regulation areas such as hospitals and airport control centres due to the enclosure of the GIL being made from aluminium that is induced with a reverse current of the same magnitude of the conductor current. As a result, the resultant electromagnetic field is close to zero. Moreover, the GIL design provides a non-flammable, high level safety solution suitable for public infrastructures due to its metallic design. A summary of the merits of using GIL technology are listed below [3], [29], [31].

a. High efficiency and power capacity transmission.
b. High reliability and long-life operation.
c. Minimum electromagnetic exposure.
d. Non-flammability and high level of safety.

2.4.4 Comparison of Current Transmission Technologies

There are three possible transmission systems that can be used to transmit power: overhead lines (OHL), underground cables (cross-linked polyethylene: XLPE) and GIL. For OHL, this type of transmission system has the highest transmission losses, and uses air as the main insulator medium, which has low dielectric strength when compared with other insulator gases, as well as requiring well-known clearances for each voltage level to avoid flashover. Therefore, OHL do not provide an optimised solution. In addition, public objections have affect the obtaining of construction approval for new OHL projects.

For XLPE, it uses solid insulators as the main insulator medium due to this type of insulator being non-recoverable after breakdown and causing an additional environmental impact from its materials. Concerning GIL technology, it has the potential to deliver the power at both high efficiency and reliability, and with the minimum visual impact, as well as having the lowest transmission losses due to its large cross-sectional area that provides low resistive losses and better heat dissipation.

The following comparison in Figure 2.4 has been undertaken based on the AC transmission losses for 400 kV due to the lack of resources for the DC-GIL in which the DC transmission systems always have lower transmission losses than AC systems. It compares the transmission losses of OHL with a bundle of four 240 mm^2 aluminium wires and 40 mm^2 of steel, a cross bounded XLPE with a copper cross section area equal to 1600 mm^2 and two GIL designs with power rating equal to 2000 and 3000 MVA [3], [29].

From Figure 2.4, both GILs have lower losses when compared to others. This will reduce the power losses cost and contributes to reducing the GWP due to lower power needs to be generated for demand fulfilment. The following Table 2.3 shows the operating cost comparison between GIL 3000 MVA and OHL transmission systems at 400 kV, obtained from Figure 2.4 below, when assuming the electricity cost is 0.1 £/kWh and the line length is 100 km.

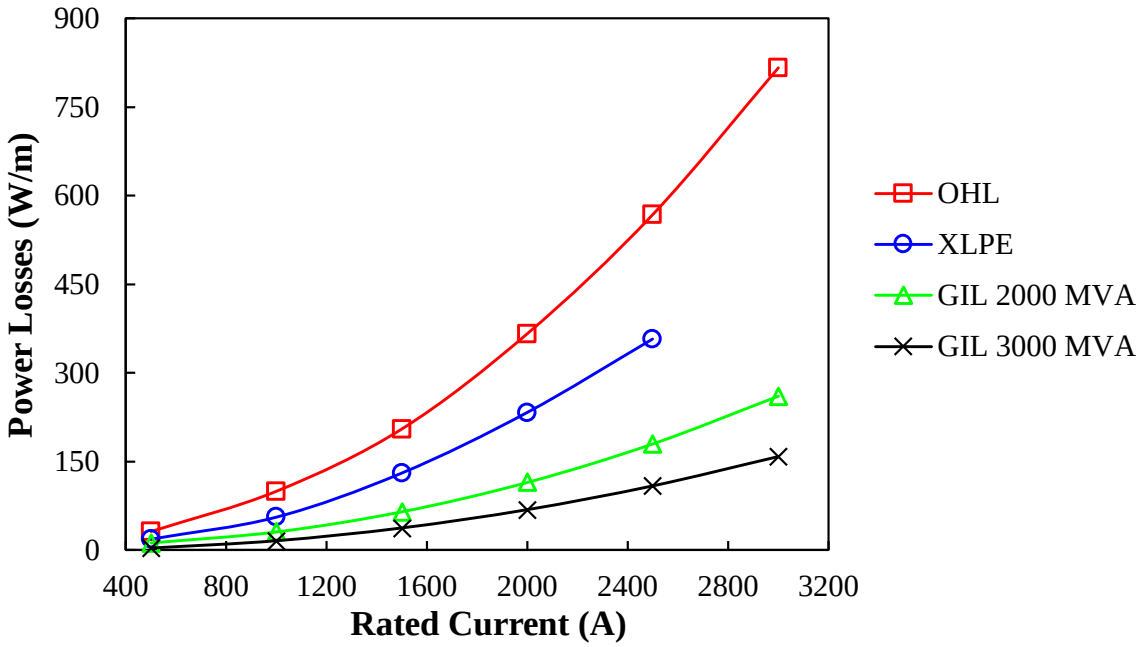

Figure 2.4 400 kV transmission losses for OHL, XLPE and GIL (re-drawn from source) [3].

Table 2.3 Power losses cost of GIL and OHL with an electricity cost of 0.1 £/kWh and 100 km in length [3].

Type	GIL	OHL
Voltage Level (kV)	400	400
Rated Current (A)	3000	3000
Losses per 1 km length (kW/km)	160	820
Losses of a 10 km system (MW)	1.6	8.2
Difference between GIL and OHL (MW)	6.6	
Cost of additional losses caused by OHL for one year (£/year)	**5,781,600**	

In terms of investment cost, underground GIL and cables are more expensive than OHL for voltage levels up to 420 kV and 550 kV. When using a higher level, such as 800 kV and 1000 kV, the cost of GIL will be closer to the OHL because at a voltage level of 420-550 kV, the OHL tower has a height of 30-35 m with up to 4 wire bundles. When the voltage level reaches 800-1000 kV, the OHL tower has a height of 60-80 m with a bundle of 8-10 wires to meet the clearance requirements[3]. On the other hand, the GIL will increase from a 500 mm pipe radius to a 630 mm pipe radius for voltage increments from 420-550 kV to 800-1000 kV.

The cost relationship between different transmission systems can be summarised as follows, where it varies from project to project, but generally, a 420-550 kV GIL has a cost factor approximately 6-8 times higher than OHL. For a 800 kV GIL, the factor reduces to 3-4 times, and for a 1000 kV GIL, a cost factor of 2-3 times can be expected [3]. The cost relationship comparison between cables and GIL at a voltage level of 420 kV is mainly defined by the power rating where, at around 1800 MVA systems, a GIL has a cost advantage due to it using a single circuit system compared with the two circuit system needed in cables, which is mainly due to the large cross sectional area offered by the GIL [3].

2.4.5 DC Gas Insulated Lines (DC-GIL) Design Challenges

AC-GIL have proven their reliability over several decades, with their high level of safety and capability in delivering high power with minimum losses. Due to the difference in the field between the AC and the DC voltage in GIL, the AC-GIL design is unsuitable for the DC-GIL. Therefore, a new design is required to consider these field differences. The two main challenges associated with the DC-GIL are the behaviour of particles that will affect

the particle trap design and charge accumulation in the solid insulator, both of which are significant challenges that will be discussed in the following [34]–[37].

DC-GIL Particle Trap

The existence of particles in GIL could be the result of mechanical vibrations and thermal expansion friction caused throughout assembly, transportation and operational processes [38]. These particles adversely affect the dielectric strength of the gas, particularly at high-pressure ranges where the presence of particles can largely eliminate the advantages of pressurised gas [39]. Therefore, they need to be captured by particle traps in a way that prevents any reactivations of these particles during operation or polarity reversal.

The main differences between particle motion in SF_6 gas under DC voltage when compared to AC voltage are particle mobility in DC being much higher than in AC and observed voltage polarity dependency; when in positive polarity, the particles move between the conductor and enclosure with much stronger mobility than in AC voltage. In negative polarity, particles hold up at the surface of the conductor and bounce around in a motion named as a "firefly" phenomenon (see Figure 2.5) [2], [34].

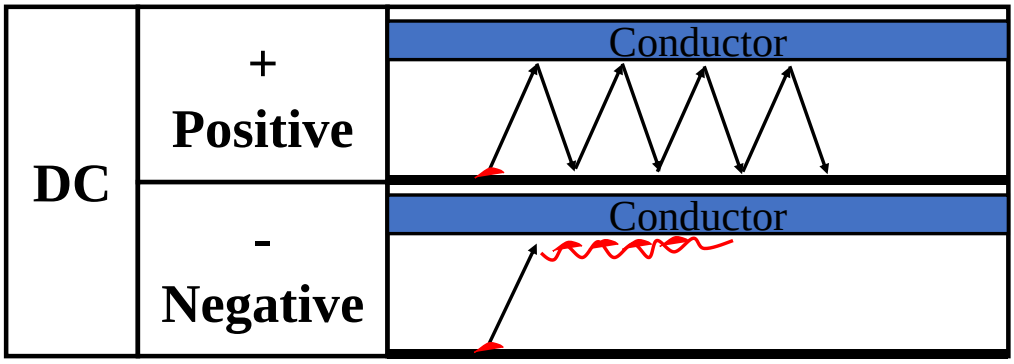

Figure 2.5 Motion of metallic particles under positive and negative DC voltage [34].

An experiment has been conducted to determine the distribution of particle trajectory by applying 140, 180, 220 and 260 kV DC for 10 minutes to an aluminium coaxial cylindrical electrode with a 20 mm conductor radius and a 60 mm shell of an enclosure radius, and a 0.5 mm radius of an aluminium ball under 6.1 bar SF_6. The motion of the ball was observed using a high-speed camera (see Figure 2.6 below) [35].

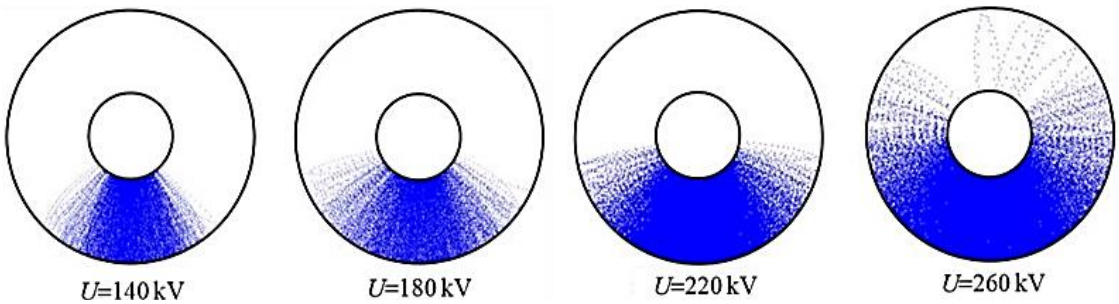

Figure 2.6 Particle motion distribution of a 0.5 mm radius aluminium ball shown in the blue line at 6.1 bar SF_6 under positive DC voltage [35].

In Figure 2.6, as the voltage is increasing, the particle distribution trajectory range is increasing, with the particle reaching the upper half side of the GIL when the applied voltage is 260 kV. This experiment only shows a certain distribution attribute in a GIL because particles tend to have a random reflection angle after collision, resulting in an undetermined trajectory [35].

Existence of these particles inside a GIL is unavoidable. Therefore, an optimised DC particle trap design is required. One potentially proven design is the use of a particle driver with a field-well ring on the conductor side and a particle trap on the enclosure side [36]. This will guide particles to the trap, especially under negative polarity when particles bounce near the HV side. This mechanism is based on unbalancing the forces acting on a particle by weakening the electric field locally, which can be achieved by using a ring shield, called a field-well ring, installed on the conductor side that will create a low field region. When a particle comes to this region, the lifting force will be lower than the gravitational force and will make the particle drop into the trap (as shown in Figure 2.7).

Selection of the height and width of the field-well ring needs to be optimised to satisfy the required field strength where it is desirable to have a large width. However, too large a width will significantly increase the ring's field strength [36]. An experimental investigation was conducted to assess this design using optimised values for the width and height of the field-well ring inside a sheath 500 mm in diameter and filled with 5 bar SF_6 gas, with many 3 mm long aluminium particles placed on the sheath below the particle driver and by applying 250 kV DC voltage [40]. The result shows that without using the field-well ring and particle driver, nearly 50% of the particles were not trapped. When both were installed, all the particles were successfully trapped. This creative design led to an effective particle trap that can deal with particles under DC voltage inside the DC-GIL [36], [40]. To be able to fully

replace the SF_6 gas used in the DC-GIL, similar investigations need to be assessed concerning the alternative gases that could be used.

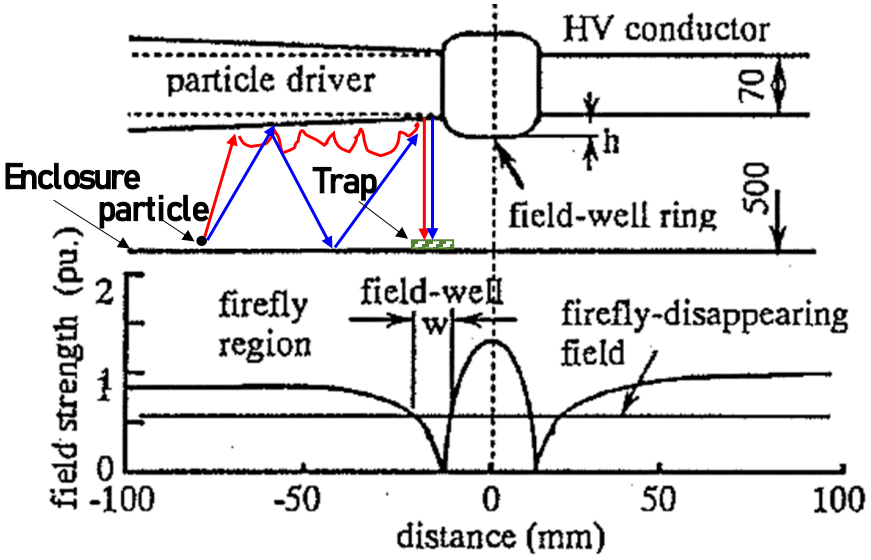

Figure 2.7 Principle of a particle driver and field-well ring to effectively capture particles under both DC polarities in 5 bar SF_6 gas; blue and red arrows represent the particle motion under positive and negative DC applied voltage, respectively [36], [40].

DC-GIL Solid Insulator

Due to the field distribution difference between AC and DC voltage along the solid insulator used inside GIL, under AC voltage, the field distribution will be dependent on the dielectric constant of the insulation material. In contrast, under DC voltage, the distribution will have two stages: (i) the distribution will be determined by the capacitive grading, and (ii) over extended DC energisation time, the distribution will be determined by the resistivity and geometry of the insulation material as the field transits into stationary resistive field distribution. This capacitive-resistive field transition is accompanied by charge accumulation on the insulator surface [36], [37], [40], [41]. There are some parameters that influence the charge accumulation on the insulator surface, including insulator shape, properties, surface roughness. Optimisation of these parameters will lead to a suitable spacer design for DC-GIL [37].

Different authors have investigated the influence of insulator shape on the breakdown field strength of an insulator [40], [42]–[45]. An investigation led by Hasegawa [40] concluded that the ideal insulator geometry is the one with the minimum electric field from the insulation strength point of view, with a lower tangential electric field (E_t), which is the electric field that lies on the insulator surface at which it will contribute to reducing particle-

initiated breakdown, and with the minimum normal electric field (E_n) which is the electric field perpendicular to the insulator surface contributing to charge accumulation. Figure 2.8 shows the electric field distribution of three differently shaped insulators. The highest E_t is obtained from the disk spacer (a), while the lowest E_t and highest E_n is obtained from the conical spacer (b). Spacer (c), which is the semi-conical spacer, provides the optimal solution due to having a lower E_n and E_t.

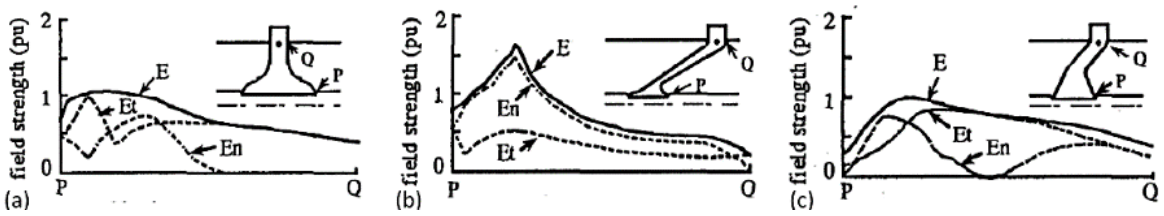

Figure 2.8 DC electric field distributions on epoxy (a) disk spacer, (b) conical spacer and (c) a semi-conical spacer [40].

The shape of the semi-conical spacer in Figure 2.8 (c) was optimised to meet the specification of testing different waveforms and used in a full-scale prototype of 500 kV DC GIS of a total length of 13 m and busbar diameter of 1 m. The rated pressure of the equipment is 5 bar filled with SF_6 gas. Table 2.4 shows the insulation test procedure and results. Table 2.4 presents how the 500 kV DC GIS prototype has high insulation reliability and passed the proposed tests with a margin of 20% [40].

Table 2.4 500 kV DC GIS prototype test procedure and results [40].

Voltages	Specifications	Results
Lighting impulse	± 1300 kV (3 times)	± 1560 kV withstood (3 times)
Switching impulse	± 1175 kV (3 times)	± 1414 kV withstood (3 times)
AC	645 kV (5 min) 559 kV (30 min) 559 kV (30 min)	Withstood, no partial discharge up to 645 kV
DC	± 900 kV (1 min) ± 750 kV (2 h) ± 750 kV (2 h)	Withstood, no partial discharge up to ± 750 kV
Polarity reversal	± 625 kV (2 h) DC or SI ∓625 kV (30 min)	**DC** **SI** + 750 kV → - 750 kV - 750 kV → + 750 kV Withstood

Currently, there are many large-scale prototypes of the DC-GIL that have successfully passed the extensive preliminary tests and are now on-site and been tested for a long time. Their typical ratings are up to ± 550 kV DC and a rated current of 5000 A [2], [46], [47]. The length of the GIL in [46] is 100 m while in [47] it is 22 m. In both studies, the proven long-term performance of the DC-GIL was reported, with commissioning experiences, long-term testing and recommendations further proposed. By the completion of these tests, DC GIL, which will be state of the art, will be widely commissioned due to it providing maximum reliability with minimum transmission losses.

2.5 Discharge Mechanism in Gas Dielectrics

2.5.1 Generation of Charge Particles

At normal temperature and pressure gases are excellent insulators. When an electric field is applied on electrodes with an insulated gas in between, conduction current will flow if there are charge carriers presented in the gas. These charge carries can take a form of: (i) electrons (e^- negatively charged), (ii) positive ions (a^+ neutral atom missing an electron) and (iii) negative ions (a^- neutral atom with an excess electron). The generation of these charged particles are associated with ionisation procedures under applied field stresses as shown in Figure 2.9 [48].

The development of electrical breakdown in gas are mainly caused by the charge carries (free electrons in this case) as they are light and fast-moving particles causing a significant ionisation. On the other hand, heavy and slow-moving ions are considered comparatively stationary and unable to accumulate sufficient energy to cause ionisation resulting a reduced effect on the breakdown development process [49].

The main source of free electrons generation in gas comes through primary ionisation processes such as ionisation of neutral molecules by collision or from detachment of negative ions. Secondary ionisation processes can also enhance the number of free electrons, and this includes the release of electrons from cathode surface. In contrast, deionisation processes such as electrons attachment process, can inhabit the electrical breakdown development in the gas by reducing the number of free electrons. The following sections are a brief description of the ionisation and deionisation processes in a gas [24], [48], [49].

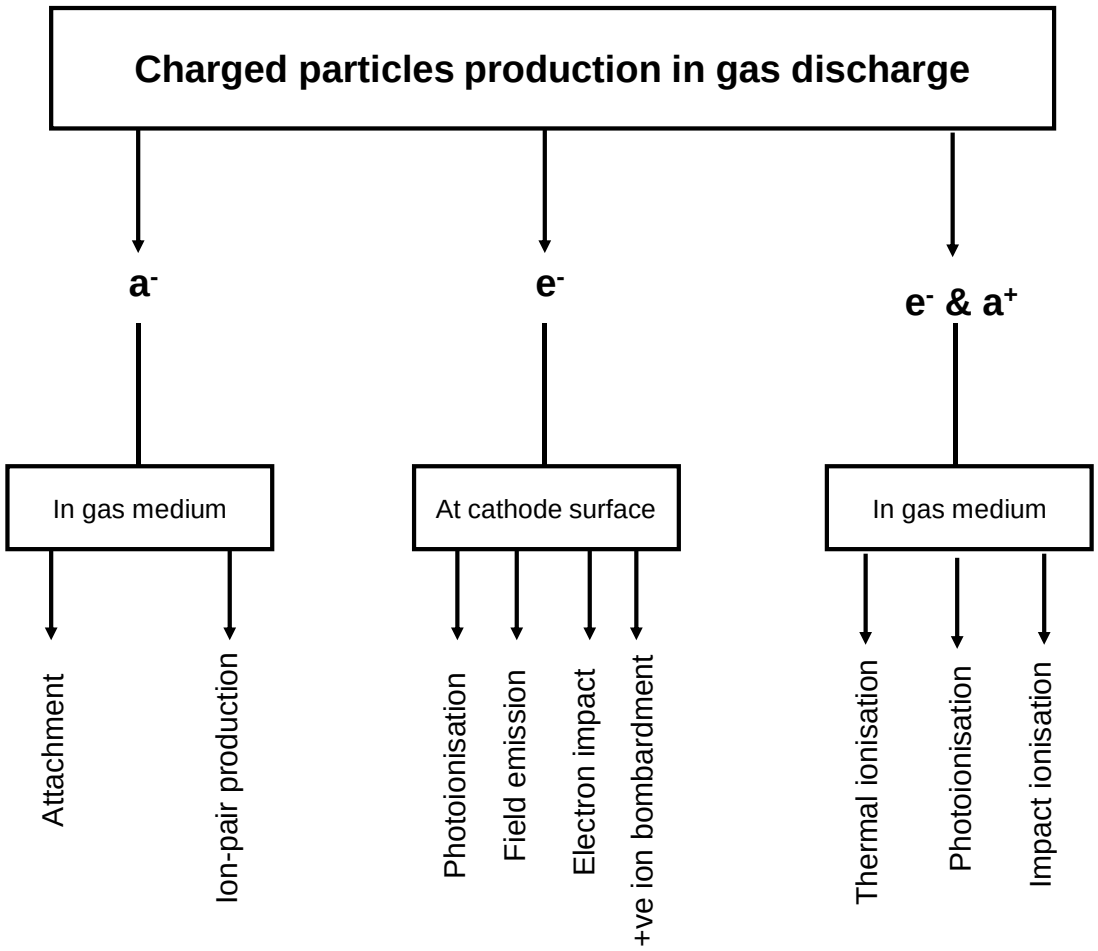

Figure 2.9 Main processes for production of the charged particles in a gas discharge [48].

Ionisation by Collision (Impact Ionisation)

This process is initiated by the existence of free electrons in the atmosphere as a result of ionisation by cosmic radiation. Initial electron gains energy from the applied field and is accelerated in the field towards the anode. On their way, electron go through collisions with neutral gas molecules. If the energy acquired by the initial electron is sufficient but less than the ionisation energy of the gas molecule, it may, during an inelastic collision, transfer some of its kinetic energy to the gas molecule and excite them. If the gained energy exceeds the ionisation energy of the gas molecule, one or more electrons may leave their orbits and the atom will become a positive ion as illustrated in Equation 2.1 [48], [49]. The positive ion will be attracted to the cathode while the free electrons will attain energy accelerating toward the anode ionising more molecules.

$$a + e^- = a^+ + e^- + e^- \tag{2.1}$$

Photoionisation (Ionisation by Radiation)

when the excited gas molecule returns to its stable ground state, it emits the excess energy as photon which may lead to ionisation as the following Equation 2.2:

$$a^* \rightarrow a + hf_p$$

$$a + hf_p \rightarrow b^+ + e^- \tag{2.2}$$

Where a* denotes the excited state of molecule a and hf_p is the photon energy assumed to be more than that the ionisation energy of molecule b. External sources such as x-rays, nuclear radiation or cosmic rays may also cause photoionisation via radiation energy and excite or ionise gas molecules [48], [49].

Thermal Ionisation

A sufficient increase in gas temperature will increase the kinetic energy of its particle causes them to move faster. Thus, it may cause ionisation on collision between gas atoms or molecules. Thermal energy (W_t) can cause ionisation by itself at high temperature as in Equation 2.3 [24], [48], [49]:

$$a + W_t \rightarrow a^+ + e^- \tag{2.3}$$

Electron Detachment

Although electron detachment from negative ions does not increase the number of charged particles, electron detachment is considered to be an ionisation process as it will provide free electrons that can cause ionisation more effectively than the negative ions. This is due to converting slow-moving and heavy negative ions into a fast-moving light mass electrons that can acquire higher kinetic energy leading to enhance the ionisation process as shown in Equation 2.4 [48], [49]:

$$a^- \rightarrow a + e^- \quad (2.4)$$

Cathod Ionisation Process

The charged particles can be supplied from the cathode electrode as in the absence of the electric field, these particles are bounded with the cathode electrode through electrostatic forces between electrons and ions in the lattice. electrons can escape the cathode surface when a minimum specified energy is exceeded, known as work function, which is highly dependent on the electrode material. The source of energy required for electrons to break free can come from the positive ion and excited atom bombardment, photoemission, thermionic emission and field emission [48], [49].

2.5.2 Degeneration of Charge Particles (Deionisation Processes)

Deionisation is the process that opposing the ionisation process at which the number of charged particles especially the electrons decrease. This will inhibit the avalanche growth where it is a desirable feature in insulation gases.

There are two main deionisation process, (i) Recombination: when positive and negative ions recombine to form a neutral atom and (ii) some gases such as SF_6 have the property of attaching free electrons to their molecules and atoms and form a stable negative ion (exhibits electron attachment property that inhibits breakdown development) where, the energy difference between initial state and final state during the attachment process is denominated as electron affinity. Contrariwise, this energy is equivalent to that required for detachment of electrons [50]. As described before, these heavy ions are unable to accumulate enough energy to cause ionisation leading to inhibit the electron avalanche development. Therefore, gas molecules with a high electron affinity are desirable for a high dielectric strength [24], [48], [49].

2.5.3 Electric Field Distribution

The electrical breakdown is significantly influenced by the field distribution where, the characteristics of the electric field located between the ground and high voltage electrodes could be categorised into three different categories based on the field uniformity or field utilisation factor (f) of the test electrodes: uniform field, quasi-uniform field and non-uniform field. In an

ideal electric field distribution, f = 1. Practically, the range of f values vary from highly non-uniform fields close to 0 when using needle/point-plane to highly uniform fields close to 1, such as Rogowski profile planes. However, f values do not represent distinctive geometry due to the field uniformity being changed by increasing or decreasing the spacing between the electrodes or modifying the electrode design [16]. The f factor can be calculated using the following Equation 2.5 [51]:

$$f = \frac{E_{mean}}{E_{max}} \tag{2.5}$$

where, E_{mean} is the mean electric field and can be calculated using Equation 2.6 as follows:

$$E_{mean} = \frac{V}{d} \tag{2.6}$$

where, V is the applied voltage and d is the gap distance.

2.5.4 Townsend Theory of Breakdown

Townsend theory explains breakdown phenomena using small electrodes spacing under uniform field and low-pressure ranges, typically, for air Pressure·Gap < 13 bar·mm and SF_6 Pressure·Gap < 10 bar·mm [50]. While for gaps with larger Pressure·Gap values usually the streamer theory of breakdown is dominant where it will be described in the next section [48].

Townsend theory assumes that [24], [48]–[50], n_0 electrons are being emitted by the ultraviolet light from the cathode electrode per second. α is the Townsend's first ionisation coefficient and defined as the number of ionising collisions in per unit distance made by an electron as it travels towards the anode. This is dependent on gas pressure and electric field. The number of electrons that are being generated at a distance x away from the cathode will be n and is given by:

$$\frac{dn}{dx} = \alpha \cdot n \tag{2.7}$$

Then, integration of Equation 2.7 is:

$$n = n_0 \cdot e^{\alpha \cdot d} \tag{2.8}$$

The average current in the gap, I, that is numerically proportional with the number of travelling electrons per second can be described as:

$$I = I_0 \cdot e^{\alpha \cdot d} \tag{2.9}$$

Where I_0 is the initial current generated at the cathode. The term $e^{\alpha \cdot d}$ is the number of produced electrons by a single electron travelling from cathode to anode and it increases exponentially with the distance x, such a process is called an electron avalanche.

Since the energy gained by one electron moving towards the anode is proportional to the electric field E, and the mean free path is proportional to the temperature/pressure, then, the ionisation will depend on the gas density or pressure at a constant temperature. Thus, a general relation for the ionisation coefficient and E can be written as following:

$$\alpha \propto p(\frac{E}{p}) \tag{2.10}$$

or normally is given as an empirical function as shown in the following:

$$\frac{\alpha}{p} = f(\frac{E}{p}) \tag{2.11}$$

where f(E/p) is a function of the pressure reduced electric field.

Considering the attachment of free electrons in the process such as in high electron affinity gases as discussed earlier, η is the attachment coefficient that defined as the number of attachments produced by an electron travelling towards the anode which will cause current loss by forming negative ions. Thus, the effective ionisation coefficient α_{eff} can be calculated as the following:

$$\alpha_{eff} = \alpha - \eta \tag{2.12}$$

Ionisation and attachment are two competitive processes determine the current together. Also, the effective ionisation coefficient follows a relationship with the electric field:

$$\frac{\alpha_{eff}}{p} = f(\frac{E}{p}) \tag{2.13}$$

In Equation 2.13, pressure reduced electric field E/p is equivalent with the density reduced electric field E/N. Pressure or density reduced critical electric field, $(E/p)_{crit}$ or $(E/N)_{crit}$ is a parameter used to characterise the dielectric performance of an insulation gas, where $(E/p)_{crit}$ is the value of E/p when α_{eff} is equal to zero, that is when ionisation and attachment process balancing each other. The $(E/p)_{crit}$ value is the lowest E/p value at which the discharge process can remain self-sustained. The higher the $(E/p)_{crit}$ value, the better is the insulation performance. At a fixed ambient temperature, the approximated relation of E/N to E/p is given by the following Equation 2.14 [49], [52]:

$$40.4 \cdot \frac{E}{p}\ in\ (\frac{kV}{mm \cdot bar}) = \frac{E}{N}\ in\ (Td) \tag{2.14}$$

During the electrons amplification in the field by the α_{eff} process, further electrons are being liberated within the gap by secondary processes as well leading to progress their own avalanche. These secondary processes include positive ion bombardment on cathode photoionisation and detachment process. γ is Townsend second ionisation coefficient defined as the net number of secondary electrons being produced per primary electron leaving the cathode. γ coefficient is also a function of E/p and electrode material. To consider the influence of the secondary process on the current growth, let n_s is the number of secondary electrons generated at the cathode, n_t is total number of electrons leaving the cathode which is equal to n_0+n_s. Then, n_d is the total number of electrons arriving the anode can be calculated as:

$$n_d = n_t \cdot e^{\alpha \cdot d} = (n_0 + n_s) \cdot e^{\alpha \cdot d} \tag{2.15}$$

Therefore,

$$n_s = \gamma \cdot (n_d - (n_0 + n_s)) \tag{2.16}$$

Then,

$$n_d = \frac{n_0 \cdot e^{\alpha \cdot d}}{1 - \gamma \cdot (e^{\alpha \cdot d} - 1)} \tag{2.17}$$

Thus, the increased current growth with the presence of both α and γ processes is given as:

$$I = \frac{I_0 \cdot e^{\alpha \cdot d}}{1 - \gamma \cdot (e^{\alpha \cdot d} - 1)} \tag{2.18}$$

For a self-sustained discharge, at breakdown, I/I_0 is infinite:

$$\gamma \cdot (e^{\alpha \cdot d} - 1) = 1 \tag{2.19}$$

Considering the attachment in the process, Equation 2.19 can be approximated to the following:

$$\gamma \cdot \left(e^{\alpha_{eff} \cdot d} - 1\right) = 1 \tag{2.20}$$

This Equation 2.20 called Townsend criterion. As both α and γ processes are E and p dependant, for a specific value of d there is an E value and hence V_b which will satisfy the

Townsend breakdown criterion representing the sparkover or breakdown voltage. Equation 2.20 can also be re-written as follows:

$$\alpha_{eff} \cdot d = \ln\left(\frac{1}{\gamma} + 1\right) = k \tag{2.21}$$

Where k is a constant depending on the cathode material and properties of the gas representing how many electrons and positive elementary charges have to be generated for releasing a secondary electron from the cathode which is also approximately equivalent to γ factor. It is usually treated as a constant for a Townsend discharge in the order of 7-10 [50], [53].

2.5.5 Paschen's Law

From Townsend breakdown criterion, a relation can be established between breakdown voltage and the Pressure·Gap, where in uniform field, $E=V_b/d$, by substituting this into Equations 2.13 and 2.21 [24], [48], [49]:

$$\frac{k}{\text{Pressure} \cdot \text{Gap}} = f\left(\frac{V_b}{\text{Pressure} \cdot \text{Gap}}\right) \tag{2.22}$$

Equation 2.22 knows as Paschen's law, where V_b is a function of Pressure·Gap. Figure 2.10 shows an illustration of the relation between V_b and Pressure·Gap (Paschen's curve) for a gas. Paschen minimum V_b value is dependent on the gas characteristics where for SF_6 it occurs at 0.0035 bar·mm with a breakdown voltage equal to 507 V [54], while air occurs at 0.0073 bar·mm with a breakdown voltage minimum of 352 V [55].

Generally, in breakdown experiments, the focus is usually within the right side of the Paschen's curve where test results follow Paschen's law, until a deviation that can occur under higher pressures as the effect of space charge becomes dominant and no longer negligible, resulting a transition to space-charge-dominated streamer discharge [24], [48], [50].

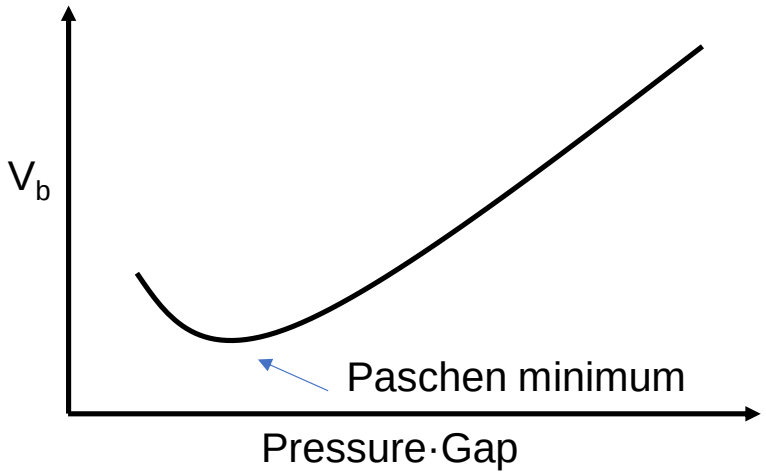

Figure 2.10 An illustration of Paschen's curve.

2.5.6 Streamer Theory of Breakdown

The growth of the avalanche was studied by Raether, Loeb and Meek during the breakdown of different gap lengths and pressures. They observed specifically for longer gaps, deviations from Townsend theory (and Paschen's Law). Also, if the avalanche length becomes large, a field distortion was observed as a result of the negative and positive charges being generated to an extent that will start new avalanches ahead of the original one, leading to a breakdown event [24]. For an avalanche to streamer transition, this is triggered by the number of electrons being generated during the initial avalanche, if it reaches a critical number between 10^4 to 10^8 electrons, the electric field at the head of the avalanche is distorted and increased where it is significantly influenced by space charges, leading to further ionising collisions and photon-emitting recombination causing photoionisation at which consecutive avalanches can be triggered that will generate a conductive streamer channel known as streamer mechanism [24], [48]–[50]. Considering α_{eff} is no longer constant as the field is not fixed, Equation 2.23 representing an empirical streamer breakdown criterion:

$$e^{\left(\int_0^{x_c} \alpha_{eff}(x)\cdot dx\right)} = N_c \tag{2.23}$$

Then,

$$\int_0^{x_c} \alpha_{eff}(x) \cdot dx = \ln\left(N_c\right) = K \tag{2.24}$$

where α_{eff} is the effective ionisation coefficient at the head of the avalanche, x_c is the length of a critical avalanche at the instant of streamer initiation and K is a constant calculated from the logarithm of critical avalanche size at which streamer criterion is satisfied (N_c). In the literature, the range of N_c chosen as a critical size, enabling an avalanche to transform into a streamer, falls between 10^4 and 10^8 electrons, which associates with K values of 9.5-20. Note that, streamer criterion K factor is different from that used in Townsend criterion, k=ln(1/ γ+1), where the latter being related to the γ coefficient (secondary electrons being released from the cathode) [24], [48]–[50], [56]–[58].

The formation of the streamer will usually lead to breakdown event in uniform and quasi-uniform or weakly non-uniform fields [48], [59]. This is called streamer inception region where it is a precursor for the breakdown. Figure 2.11 illustrates the relationship between the breakdown voltage and the gap distance d in a sphere-plane electrodes [60]. It identifies three regions, namely, streamer inception, streamer propagation and leader propagation. The curve 1 in Figure 2.11 represents the characteristics of inception voltage U_i with the gap distance. P correspond to the transition limit between quasi-uniform and non-uniform fields. It is typically around 50 mm for air at atmospheric pressure. For smaller gap than P, U_i will lead directly to breakdown at which Equation 2.24 is sufficient to calculate the breakdown voltage [60]. The other mechanisms will be briefly discussed in the next sections.

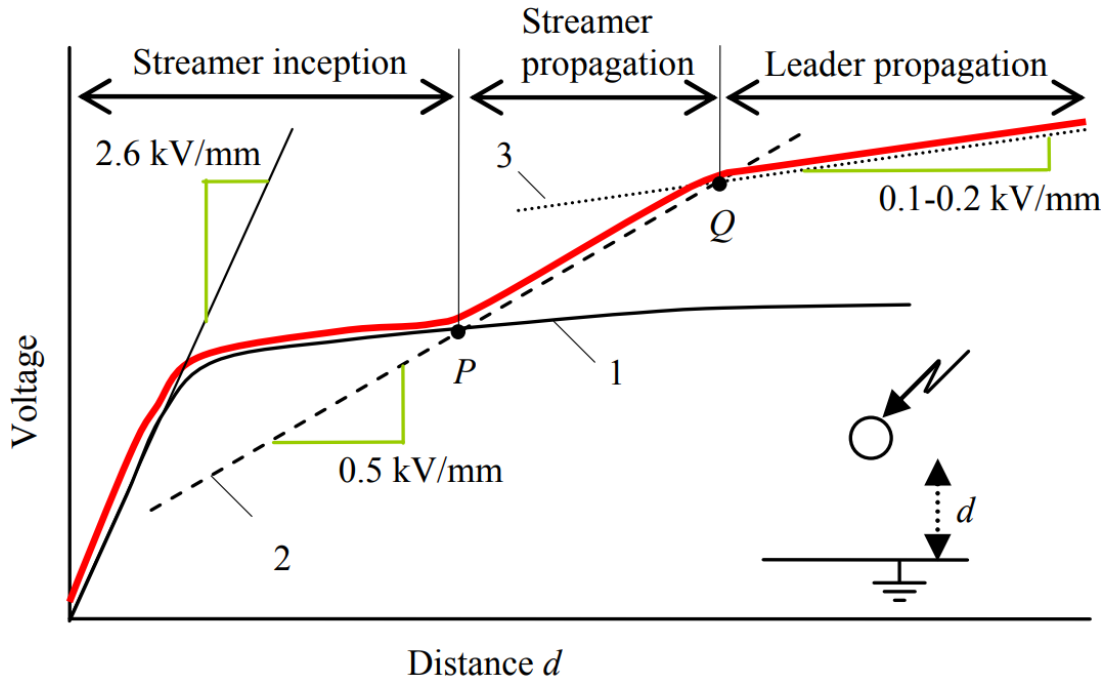

Figure 2.11 An illustration of the breakdown voltage of sphere-plane electrodes for air in red colour based on the discharge mechanism, P value typically around 50 mm while Q is for gap length that is above 1-2 m. Line slop values in each region are for air as an example [60].

2.5.7 Streamer Propagation

Streamer propagation is used in non-uniform fields, typically for gap distances shorter than 1-2 m but longer than 50 mm in the case of air at atmospheric pressure. Streamer head will propagate in the direction of the opposite electrode. To reach that electrode, a higher applied voltage that is larger than the U_i is required for maintaining a stable propagation process, meaning that, the field in front of the streamer head has to fulfil a criterion that is similar to U_i requiring a sufficiently high voltage drop between streamer head and the opposite electrode to progress [49], [60].

The minimum applied voltage enabling streamer propagation in a non-uniform field can be approximated as in the following Equation 2.25 [49], [60]:

$$U_p = U_0 + d \cdot E_{st} \tag{2.25}$$

Where U_p is the streamer propagation breakdown voltage, d is the inter electrodes gap distance (50 mm > d > 1-2 m), E_{st} is the is external field required for a stable streamer propagation and U_0 denotes the required voltage potential for the streamer head to generate a breakdown. In the case of air, E_{st} and U_0 is approximated to 0.5 kV/mm (positive streamer) and between 20-30 kV respectively [49], [60]. A typical streamer propagation characteristics can be seen above in Figure 2.11 by the dashed line 2 beyond the P value at which the field is considered to be a non-uniform field [60].

The value of E_{st} can vary up to ±20% depending on humidity, applied voltage waveform and voltage polarity. In the case of negative streamer propagation, it requires a much higher field strength to maintain a stable propagation (air E_{st} = 1.2 kV/mm) as the negative streamer propagates with direction of low field region [50]. Thus, the negative breakdown voltage is much higher than the positive one in this case (non-uniform field) [24]. This is also related to the corona discharges differences where it is highly dependent on the voltage polarity [50].

Generally, positive and negative breakdown voltages in a uniform field are comparable, with this being the ideal case. In a quasi-uniform field, positive breakdown is higher than the negative one, as in both cases, the electrons being produced through the detachment process from a

negative ion or the ionisation of neutral molecules, but a negatively charged electrode can also provide an additional source of electrons (field emission) that will maintain and enhance the ionisation process, potentially leading to breakdown at a lower applied voltage when comparison to a positively charged electrode [16]. In the case of a non-uniform field, the negative breakdown voltage is higher than positive counterparts. In the case of a positive applied voltage, the heavy positive space charges will create an extension of the sharp electrode. Thus, the gap distance will be reduced, which will increase the field stress in the rest of the gap. In the case of a negative applied voltage, positive space charges have a different polarity to the high voltage electrode. As a result, the field will be reduced in the rest of the gap, which will then require a higher applied voltage to maintain a stable propagation of the negative streamer to cause a breakdown as mentioned earlier [24], [50]. Figure 2.12 presents an illustration of the charge distribution in both cases.

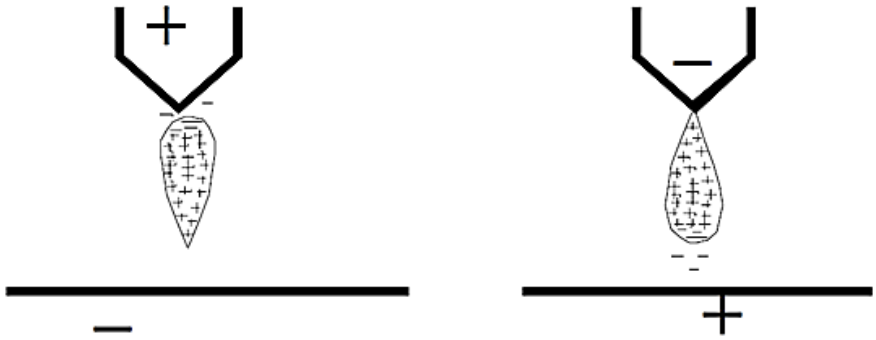

Figure 2.12 DC polarity effect in rod-plane electrodes under DC voltage [24].

2.5.8 Leader Transition and Propagation

Leader mechanism is applicable for gaps longer than 1-2 m as in Figure 2.11 beyond Q. The initiation of the leader usually occurs with the presence of corona discharges, where some streamer branches will grow into leader. While streamer branches propagate towards the opposite electrode, some of the branches have an ionisation intensity that is higher than the others, this results in a higher energy exchange between the energetic electrons and neutral molecules, leading to a significant heating in these specific branches because of the increasing ohmic loss of energy. At that region, the gas temperature increases leading to a reduction of the molecule's density. Thus, the ionisation becomes more efficient developing a highly conductive, high temperature, arc like channels having a different characteristic than those related to streamer branches. These channels are called leader, also known as arc or plasma, and it is normally precursor of breakdown events in long gaps (d < 1-2 m) [49], [60].

The internal field strength along a leader is around 0.1-0.2 kV/mm in the case of air as shown in Figure 2.11 from the dotted line 3 passed the Q value. Consequently, the leader can propagate over a distance that is longer than the streamer one. The transition into leader depends on its capacitive coupling with the surrounding electrodes. This can be estimated in simple geometries using empirical formulations. However, this is not always the case in real geometries [60].

2.6 SF_6 and its Alternative Gases

SF_6 gas is used extensively in gas insulated equipment as an insulating medium but has a high environmental impact. Currently, several alternatives have been proposed to replace this gas, all of which has their own specific advantages and disadvantages. This section reviews possible alternative gases to replace SF_6. One possible candidate is a C_3F_7CN gas mixture, for which a detailed comparison will be provided.

2.6.1 SF_6 Gas

SF_6 gas consists of one sulphur atom in the centre that is surrounded by six fluorine atoms attached to it with a single bond, creating an octahedral shape (see Figure 2.13) [61].

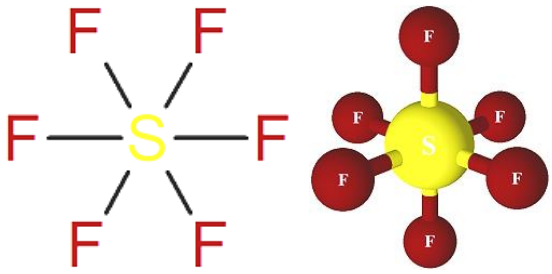

Figure 2.13 Molecular structure of SF_6 gas.

Physically, SF_6 gas is colourless, odourless, non-flammable, non-corrosive, non-toxic and chemically stable. In addition, SF_6 gas has a high electron affinity property, which is the ability to attract free electrons that can be produced by arcing and a self-healing property that allows it to recover after discharges [61], [62]. Moreover, it has a dielectric strength around three times higher than air and CO_2 in uniform field under atmospheric pressure [6], [49]. Figure 2.14 shows the breakdown performance comparison between SF_6 and air in a uniform-field that highlights the benefit of using high pressure on dielectric performance [6].

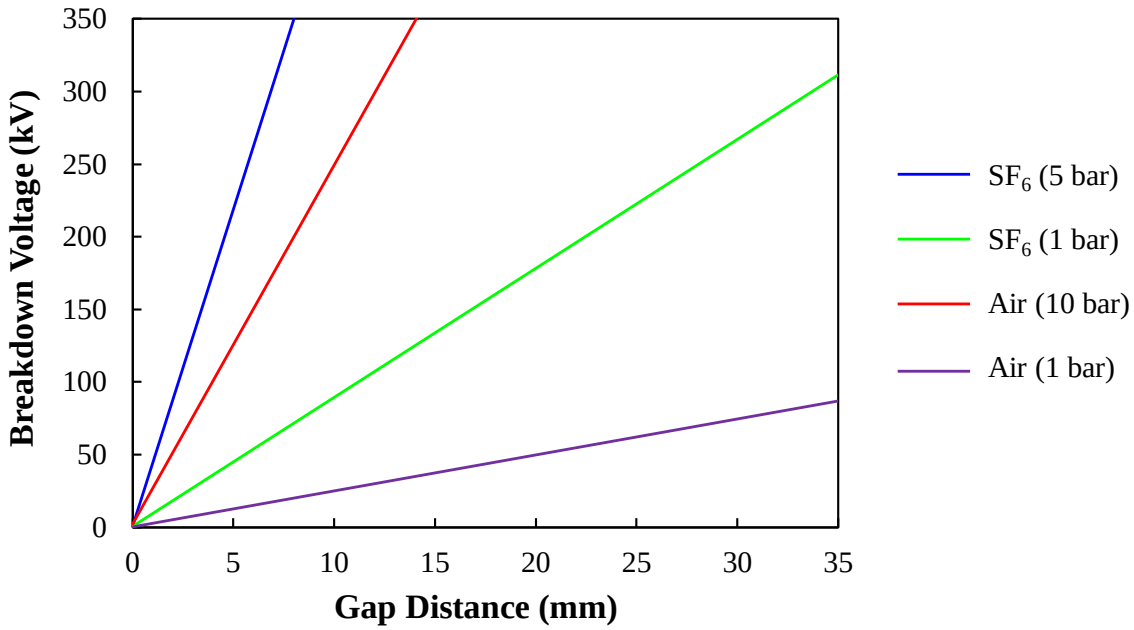

Figure 2.14 Dielectric strength trend comparison between air and SF_6 with, $(E/p)_{crit}$ = 2.5 and 8.8 kV/mm/bar respectively in uniform field (redrawn from source) [6].

SF_6 provides high dielectric strength when used under pressure, reducing the equipment footprint in situations when it is essential due to space being at a premium. However, the environmental concern is a key downside for SF_6 gas due to its high GWP when combined with its long atmospheric lifetime. Typically, it has an atmospheric lifetime of 3,200 years, 23,500-24,300 times longer than CO_2 GWP, making it a potent greenhouse gas [7], [8]. With this very long atmospheric lifetime, the SF_6 emissions accumulate in the atmosphere leading to an increase in its environmental damage over time. Thus, its use in industry is becoming increasingly regulated and restricted [19]–[21].

2.6.2 Alternative SF_6 Gases and its Mixtures

A summary of the SF_6 alternatives comparison in terms of dielectric strength, GWP and boiling temperature is presented in Table 2.6 and will be discussed in detail in the following.

Natural Origin Gases (CO_2, N_2, O_2)

These gases freely exist in the atmosphere with 78.09% N_2 and 20.95% O_2 from the chemical composition of dry air. They are commonly used as insulating materials and an arc extinguish medium in high voltage equipment. Environmentally, natural origin gases have no ozone depleting potential (ODP), with a GWP $\leq$ 1 making them the most suitable candidates. However, the main drawback is their weak dielectric strength when compared to

SF_6 gas. To have comparable dielectric strength to SF_6 gas, natural origin gases need to have at least 2-3 times higher pressure than SF_6 gas. It could also require a larger equipment footprint than SF_6 due to increasing the pressure only leading to an impractical level of pressure, mainly due to the breakdown voltage tending to saturate when the pressure increases at a high range [13]. Thus, a new mechanical structure would be needed to withstand such high pressure, leading to an additional and significant economic impact when such a solution is considered [10], [63], [64].

Currently, synthetic air (20% O_2, 80% N_2), CO_2 and CO_2/O_2 mixtures have been adopted by some manufacturers as an alternative to SF_6 in newly designed GIS, with its applications at different voltage levels ranging between 52-420 kV [19], [64]–[69]. Table 2.5 summarises a comparison between current SF_6 applications and the new equipment designed for natural origin gases concerning operating voltage, gas pressure and equipment footprint. From the comparison, an equivalent equipment footprint was achieved for a medium voltage level (MV < 52 kV) and up to a HV level of 84 kV at 3 times higher than SF_6 rated pressure. Higher than that level, the equipment footprint needs to be increased by approximately 60% more at a voltage level of 420 kV at around double that required for SF_6 and its current operating pressure. Consequently, natural origin gases are not the most optimal option when there is space constraint.

Table 2.5 Natural origin gases and SF_6 GIS design specifications.

Medium voltage GIS at 52 kV [64]				
Gas	SF_6		Synthetic Air (20% O_2, 80% N_2)	
Pressure (bar)	< 1.2		≈ 3	
Footprint ratio	1		1	
High voltage GIS at 84 kV [65], [68], [69]				
Gas	SF_6		Synthetic Air (20% O_2, 80% N_2)	
Pressure (bar)	≈ 1.7		≈ 5 - 5.6	
Footprint ratio	1		1	
High voltage GIS (circuit breaker) at 168 kV [66]				
Gas	SF_6	CO_2	70% CO_2 / 30% O_2	70% CO_2 / 30% O_2
Pressure (bar)	4	8	8	14
Footprint ratio	1	1.59	1.22	0.91
Extra high voltage GIS at 420 kV [19], [67]				
Gas	SF_6		Synthetic Air (20% O_2, 80% N_2)	
Pressure (bar)	≈ 5-6		11	
Footprint ratio	1		1.5 - 1.6	

Trifluoroiodomethane (CF_3I)

This gas has a dielectric strength 1.2 times higher than SF_6 in its pure form. It is an inert, non-flammable, colourless, electronegative gas with a very low GWP of less than 1, a very short atmospheric lifetime equal to 0.005 year and a very low ODP equal to 0.07 [10]. A key disadvantage of this gas is its high boiling temperature when compared to SF_6. Therefore, it is best used as part of a mixture with buffer gases to reduce the overall liquefaction temperature. This reduces its breakdown voltage to lower than that of SF_6. Also, the weak C-I bond result in iodine deposits can affect the insulation performance and cause surface flashover. Moreover, it is categorised as both a carcinogen and mutagen [10], [29].

Hydrofluoroolefin (HFOs)

The generalised formula of this category is $C_n(H,F)_{2n,}$ such as $CF_3CH=CHF$, $CF_3CF=CH_2$ and $C_4H_2F_6$, commercially known as HFO-1234ze(E), HFO-1234yf and HFO-1336mzz-Z. They have a very low GWP and a comparable dielectric strength to SF_6. Having HFO-1234ze as a replacement candidate has two limitations: (i) 0.83 of SF_6's dielectric strength and (ii) a higher boiling point than SF_6. Concerning HFO-1234yf, this gas has a concern of flammability that makes it a non-suitable substitution for SF_6. Also, for HFO-1336mzz-Z, this gas becomes liquid at room temperature due to its high boiling temperature [10]. Moreover, the main drawback for this category, the HFO group, can lead to a carbon deposit appearing in the solid insulator after a sufficient number of arcing events [70]. Thus, this layer is conductive and can short circuit the solid insulators inside the GIS [71].

Fluoroketone (i.e., $C_5F_{10}O$)

This group has a chemical form of $C_nF_{2n}O$, such as, $C_5F_{10}O$ (Novec 5110) and $C_6F_{12}O$. They have a very low GWP and a dielectric strength at least two times that of SF_6. Despite the fact that they have more than two times the dielectric strength than SF_6, they have a very high boiling temperature. As a result, they tend to liquefy at atmospheric pressure under 27°C for $C_5F_{10}O$ and 49°C for $C_6F_{12}O$, making the maximum operation pressure of 0.8 bar and 0.3 bar, respectively. Thus, it is impossible to utilise this group for high voltage equipment where higher pressures are required [72], [73].

Fluoronitrile (i.e., C_3F_7CN)

The general formula for this family is $C_nF_{2n+1}CN$, such as C_3F_7CN gas. This gas commercially, known as Novec 4710, has been developed by 3M. It has more than double the dielectric strength of SF_6 when tested using uniform gaps at atmospheric pressure [74]. It is considered practically non-toxic, with the GWP of pure C_3F_7CN being 2,100 with a 30-year atmospheric lifetime. C_3F_7CN is usually used in a mixture with non-condensable gases to reduce the boiling temperature and meet operational requirements.

Currently, ongoing investigations have been conducted focusing on two different scenarios: (i) complete equipment replacement with new-build equipment under a higher operating pressure using a low concentration of C_3F_7CN of less than 7% [10], [75] or (ii) as a retrofill solution for existing SF_6 equipment through use of a 20% C_3F_7CN concentration in the mixture but at a comparable operating pressure to SF_6, resulting in a cost effective solution [13]. A mixture of 18-20% C_3F_7CN and 82-80% non-condensable gases, as reported in [13], [74] matches the SF_6 dielectric strength, making it suitable for a retrofill in current SF_6 equipment. A 20% C_3F_7CN mixture has a GWP of approximately 1,000-1,100 at which it will provide a 96% GWP reduction compared to the SF_6 one [13], [74]. A further comparison of SF_6 gas properties will be discussed in the following sections. Table 2.6 presents a summary of the comparison between SF_6 and its alternatives.

Table 2.6 Key properties of SF_6 and alternative gases [7], [10], [17], [29], [60], [68]–[71], [73].

Gas	Relative Dielectric Strength to SF_6 (p.u)	GWP	Boiling Temperature (°C)
SF_6	1	24,300	-63.9
Air	≈ 0.3	-	-194.4
N_2		0	-195.8
CO_2		1	-78.5
CF_3I	1.3	1	-22.5
$CF_3CH=CHF$	0.83	6	-19.4
$CF_3CF=CH_2$	-	4	-29.4
$C_4H_2F_6$	2.2	8.9	33.4
$C_5F_{10}O$	> 2	1	26.9
$C_6F_{12}O$	2.8	1	49.2
C_3F_7CN	≈ 2.7	2,100	-4.7

2.6.3 Chemical and Physical Properties Comparison of SF_6 and C_3F_7CN Gas and Mixture Ratio Selection

C_3F_7CN gas is chemically known as 2, 3, 3, 3-tetrafluoro-2-(trifluoromethyl)-propanenitrile $(CF_3)_2CFCN$ [14]. Figure 2.15 presents its molecular structure [74].

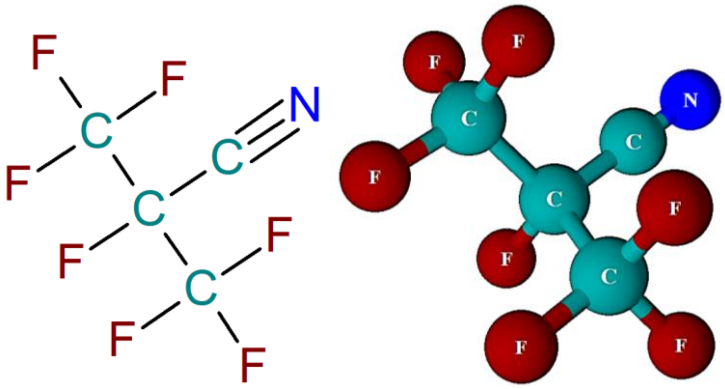

Figure 2.15 C_3F_7CN gas molecular structure.

Based on the comparison of C_3F_7CN and SF_6 gas in terms of the chemical and physical properties shown in Table 2.7, both gases share a number of similar properties. They are both non-flammables, colourless and odourless. C_3F_7CN has more than double the dielectric strength of SF_6. SF_6 has a much lower boiling point in comparison to C_3F_7CN. Therefore, SF_6 remains in its gaseous form at a much higher pressure. The boiling temperature of C_3F_7CN can be reduced to meet operational requirements by mixing it with non-condensable gases such as dry air, N_2 and CO_2.

Table 2.7 Key properties comparison between C_3F_7CN and SF_6 [7], [14], [17], [74].

Property	C_3F_7CN	SF_6
Colour	Colourless	Colourless
Odour threshold	Odourless	Odourless
Flammability	Non-flammable	Non-flammable
Molecular Weight (g/mol)	195	146
Boiling Point at 1 atm (°C)	-4.72	-68.3
Critical Field Strength $(E/P)_{crit}$ (kV/mm/bar)	≈ 24	8.8-8.9
Global Warming Potential	2100	24300
Atmospheric Lifetime (years)	30	3200
Ozone Depletion Potential (ODP)	0	0

2.6.4 C_3F_7CN Mixture Ratio Selection

The initial gas mixture selection is made through consideration of a simple trade-off between dielectric performance and liquefaction temperature that depends on the mixture ratio. The requirement for the initial selection of an ideal mixture ratio needs to match the dielectric strength of SF_6 to enable a retrofill under similar working pressure. C_3F_7CN can be comparable to the dielectric strength of SF_6 when it is mixed in a ratio of 20-18% C_3F_7CN and 80-82% buffer gases under a uniform field (as shown in Figure 2.16) [13], [74].

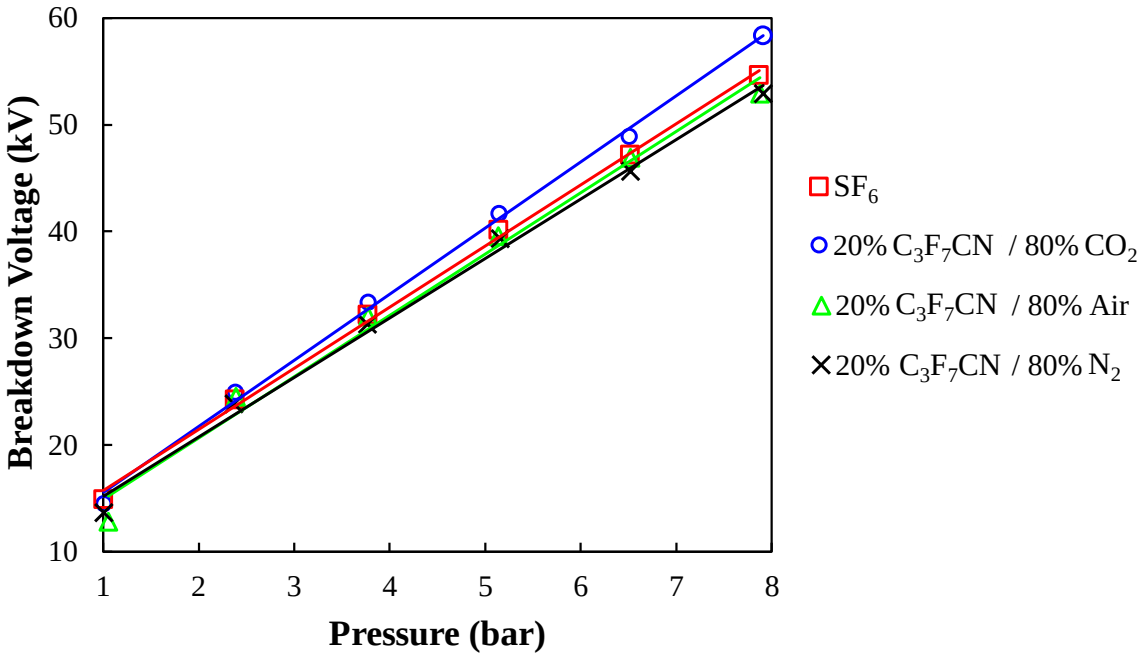

Figure 2.16 AC breakdown voltage for SF_6 gas and 20% C_3F_7CN and 80% CO_2, air and N_2 gas mixtures in a uniform field with parallel disk electrodes and a 0.25 cm gap distance (redrawn from sources) [14], [74].

As shown in Figure 2.16, a 20% C_3F_7CN and 80% CO_2 mixture has scored the highest breakdown voltage in comparison with other buffer gases. Thus, CO_2 exhibits the most favourable dielectric properties in comparison with the others, making it an ideal candidate for use as a carrier gas in this mixture.

Concerning the boiling point and the maximum operating pressure for the selected ratio of 20% C_3F_7CN / 80% CO_2, fulfilment of the minimum operating temperature for the gas insulated equipment is essential. Although the use of a lower C_3F_7CN concentration lower than 20% in the mixture with a buffer gas will improve the liquefaction temperature limit, it will reduce the dielectric performance of the mixture [10], [17], [74]. An Antoine semi-empirical equation (Equation 2.26) was used to calculate the vapour pressure and its related temperature for pure C_3F_7CN and CO_2 gas as follows [77].

$$\log_{10} p = T_A - \frac{T_B}{T_C + T} \tag{2.26}$$

where, p is the vapour pressure, T is the temperature and T_A, T_B and T_C are component specific constants. Table 2.8 shows the parameters for both gases.

Table 2.8 Antoine equation constants for C_3F_7CN and CO_2 [17].

Gas	T_A	T_B	T_C
CO_2	7.81	987.4	290.9
C_3F_7CN	6.24	599. 1	182

By using the Antoine equation with previous parameters, the liquefaction temperature for CO_2 and C_3F_7CN can be calculated, and from them the C_3F_7CN/CO_2 mixtures estimated based on the partial pressure, as in [17] and compared with the one in [74] (see Figure 2.17).

According to Figure 2.17, a 20% C_3F_7CN / 80% CO_2 mixture has a liquefaction temperature of -8°C at 5 bar pressure. This meets the minimum temperature requirement for outdoor applications in hot-climate countries and indoor applications for cold-climate countries in accordance with IEC 62271-203: 2011 [78]. Therefore, the maximum tested pressure for the 20% C_3F_7CN / 80% CO_2 mixture in this current experimental research will not exceed 5 bar to avoid liquefaction.

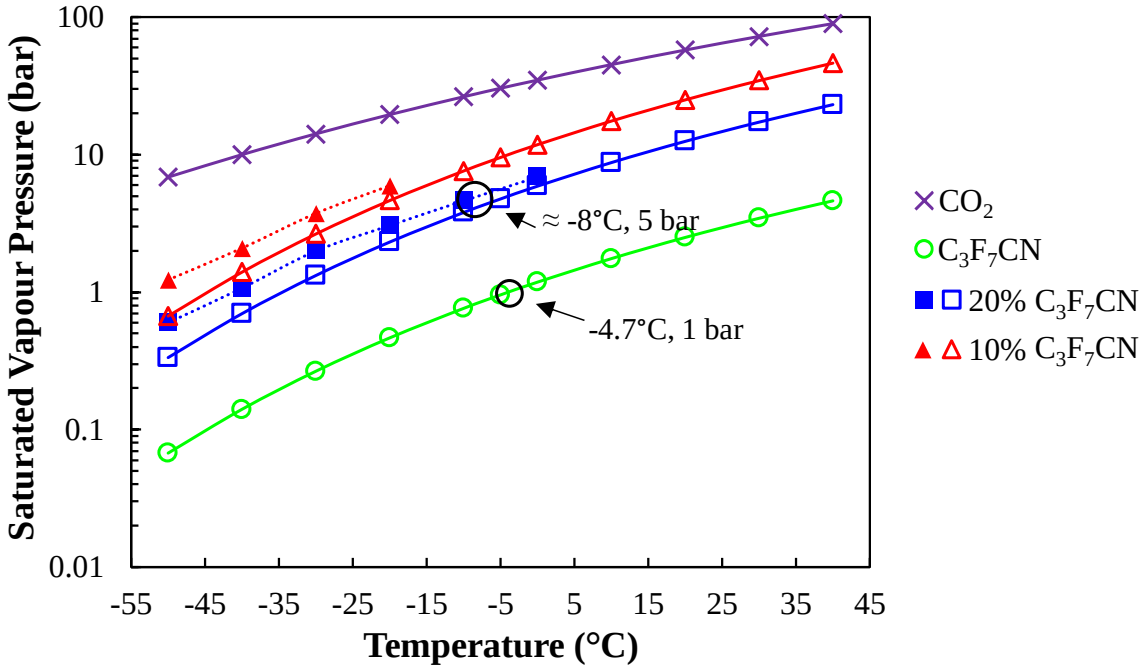

Figure 2.17 Saturated vapour pressure as a function of temperature for C_3F_7CN, CO_2 gas and mixtures (filled markers are results from [74] and others are from [17]), (re-drawn from sources).

2.7 DC Breakdown Characteristics of SF_6 and C_3F_7CN Gas and its Mixtures

This section compares the breakdown characteristics between SF_6 and C_3F_7CN gas, and its mixtures under positive and negative DC voltage polarities, as up to this date, DC breakdown characteristics of C_3F_7CN gas and its mixtures have rarely being reported in previous investigations, where AC and lighting impulse (LI) characteristics have been extensively studied in [13], [16], [17], [79], [80]. The investigation will be categorised based on the field f factor of the test electrodes and gap distance (refer to Section 2.5.3 for f factor categorisation).

2.7.1 DC Breakdown Characteristics of SF_6

Uniform Field (f ≈ 1)

DC breakdown performance under a uniform field was reported in 1978 [81], where the breakdown voltage of SF_6 was studied in a 150 mm diameter plane-plane configuration for a gap distance between 5-30 mm and a fixed pressure of 3.4 bar. From the results, the breakdown voltage under both polarities were comparable. Generally, in uniform field breakdown voltage can be represented with the theoretical calculated $(E/p)_{crit}$ value, which is equal to 8.8-8.9 kV/mm/bar in the case of SF_6 gas [57].

Quasi-Uniform Field (0.75 < f < 0.25)

An investigation in 1978 [81] studied the characteristics under a quasi-uniform field using coaxial geometry with a 80/200 mm diameter coaxial configuration. Results show that there was not any remarkable difference in the breakdown voltage between positive and negative polarities up to 1 bar pressure. At pressure above 1 bar, positive polarity becomes higher than the negative one. At 2 bar, the negative breakdown voltage is 31% less than the positive one. Another study in 2016 [82] reported on the characteristics under a quasi-uniform field using a sphere-sphere electrode with a 10 mm diameter sphere and a gap distance equal to 10 mm. Results conclude that SF_6's DC breakdown voltage is more than two times higher than that of CO_2 and N_2, as expected. Overall, positive DC breakdown voltage under a quasi-uniform field tends to be higher than the negative one [83].

Non-Uniform Field (0.25 > f > 0)

In 1953 [84], an investigation of the DC breakdown characteristics of SF_6 under a non-uniform field was conducted using a 0.8 mm radius for a hemispherical rod and a 142 mm width plane placed in a steel tank filled with SF_6 gas of a 152 mm radius. The effect of gap length and pressure were extensively tested. It was found that for point to plane, generally the positive breakdown voltage is lower than the negative one. A similar observation was found in [83]. However, for some very short gaps, the opposite was observed [83]. Moreover, a positive breakdown voltage increases rapidly with the gap increasing over a wide range of pressures until situation in which a considerable increase in the gap distance does not yield any appreciable increase in the breakdown voltage [83].

2.7.2 Comparative DC Breakdown Characteristics of SF_6 and C_3F_7CN gas and its Mixtures

A comparison of the $(E/p)_{crit}$ values of SF_6, CO_2 gases and mixtures of 4-20% C_3F_7CN, with the CO_2 obtained experimentally under a steady-state Townsend (SST) test condition shown in Table 2.9. These values represent an overall evaluation of the dielectric strength capability of the gas. This SST test condition was formulated based on a small gap distance in which the relation between gap length and breakdown voltage is linear under a uniform field [17].

Table 2.9 SST critical field strength comparison for different gases [17], [49], [57], [85]–[89].

Gas	$(E/p)_{crit}$ (kV/cm·bar)	Ratio to SF_6
4.5% C_3F_7CN / 95.5% CO_2	5.2	0.58
7% C_3F_7CN / 93% CO_2	5.9 - 6.8	0.67 - 0.76
10% C_3F_7CN / 90% CO_2	7.7 - 7.9	0.87 - 0.88
18.5% C_3F_7CN / 81.5% CO_2	8.8	0.99
20% C_3F_7CN / 80% CO_2	8.9 - 9.1	1.01 - 1.02
SF_6	8.8 - 8.9	1
CO_2	2.6 - 2.9	0.29 - 0.33

According to Table 2.9, the $(E/p)_{crit}$ value of SF_6 gas is around three times higher than CO_2, while it is comparable with the 18-20% C_3F_7CN and 80-82% CO_2 gas mixture. In the case of 4.5-10% C_3F_7CN/CO_2, the dielectric performance achieved an approximate 58-88% for both SF_6 and 20% C_3F_7CN / 80% CO_2.

Based on the electrodes' dimensions, configurations and gap distances used in the literature studies for SF_6 and C_3F_7CN under DC voltage in this section, with COMSOL Multiphysics

version 5.5 software used to simulate the maximum electric field (E_{max}) and computed based on a finite element analysis (FEA). Then, f factor will be calculated as in Equations 2.5 and 2.6. The f factor indicates the uniformity of the applied field on the gap through which it can be controlled by the gap distance and electrode geometry. The range for this value is from one for a uniform field and close to zero for a non-uniform field as discussed earlier in Section 2.5.3. Table 2.10 summarises the f factor values and test conditions for the used electrode configurations from the literature in this section.

Table 2.10 All configurations of the reported DC breakdown tests in the literature of C_3F_7CN in comparison with SF_6 in the subsequent figures. AC results were used for illustration in the non-uniform field.

Electrode (mm)	Gap (mm)	Pressure (bar)	f factor	Reference
Plane width 45 - plane width 45	3	3 - 7.2	0.95	[18]
Plane width 50 - plane width 50	3	3 - 7	0.96	[90]–[92]
Sphere radius 25 - sphere radius 37.5	1 - 9	6	0.97 - 0.85	[93]
Sphere radius 25 - plane width 50	5	3 - 7	0.88	[91], [92]
Needle with 0.41 tip - plane width 135	20	1 - 5	0.045	[83]
Needle with 0.025 tip - plane width 50	5	3 - 7	0.05	[91]
Needle with 0.015 tip - plane width 49.5	10	0.5 - 4	0.02	[94]
Needle with 0.02 tip - plane width 50 (AC)	20	0.1 - 2	0.013	[17]

Uniform Field (f ≈ 1)

Figure 2.18 presents the outcome of the investigations in [18], [90]–[92] using plane-plane electrodes of 45 and 50 mm in width at a 3 mm gap distance. Pressure was varied between 3-7.2 bar when testing SF_6, and 4, 6, 8 and 20% C_3F_7CN with CO_2. From the results, breakdown voltage values for all the tested gases increase linearly with the Pressure·Gap. 20% C_3F_7CN and 80% CO_2 has a slightly higher breakdown voltage than SF_6, behaviour matching the reported result under an AC uniform field (previously shown in Figure 2.16) [14], [74]. For the other low mixture ratios' breakdown voltage is significantly lower than both SF_6 and the 20% ratio, the higher the concentration of C_3F_7CN, the higher the breakdown voltage. In addition, the differences between positive and negative breakdown voltage values in a uniform field are negligible, as seen in the 8%, 6% and 4% C_3F_7CN

mixture ratios. This is similar to what has been previously reported for SF_6 polarity behaviour under a uniform field [81].

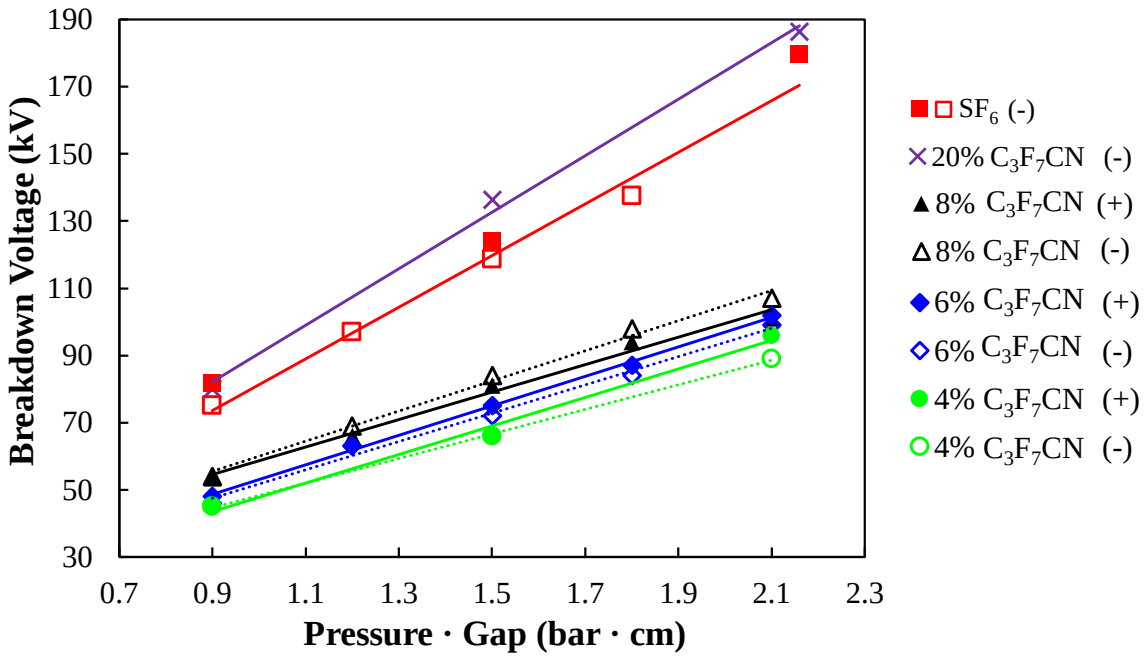

Figure 2.18 DC breakdown characteristics in plane-plane electrodes representing uniform field electrodes for C_3F_7CN/CO_2 mixtures and SF_6 (filled red squares are results from [18] and unfilled squares are from [91], fitted to a linear line) (re-drawn from sources) [18], [90]–[92].

Quasi-Uniform Field (0.75 < f < 0.25)

Figure 2.19 shows the results obtained from [91]–[93]. The experimental investigations were conducted on SF_6 and C_3F_7CN/CO_2 mixtures using sphere-sphere configuration of a 25 mm and 37.5 mm radius at 6 bar of pressure and a gap distance varied between 1-9 mm [93], and sphere-plane configuration of 25 mm radius at a fixed gap distance of 5 mm and varying pressure between 3-7 bar [91], [92]. Both configurations are considered as a quasi-uniform field of a high f factor range.

From Figure 2.19, SF_6 and the 20% C_3F_7CN mixture have a comparable breakdown voltage, with SF_6 being comparatively higher. This is opposite to the case for the uniform field (as in Figure 2.18) in which 20% C_3F_7CN was comparatively higher than SF_6. This suggests that a 20% C_3F_7CN mixture could be more sensitive towards field uniformity than SF_6. A further comparison will be conducted in a non-uniform field in the next section in which this effect will be at its maximum. The 1% concentration difference between the C_3F_7CN ratio concentrations will not have a measurable effect.

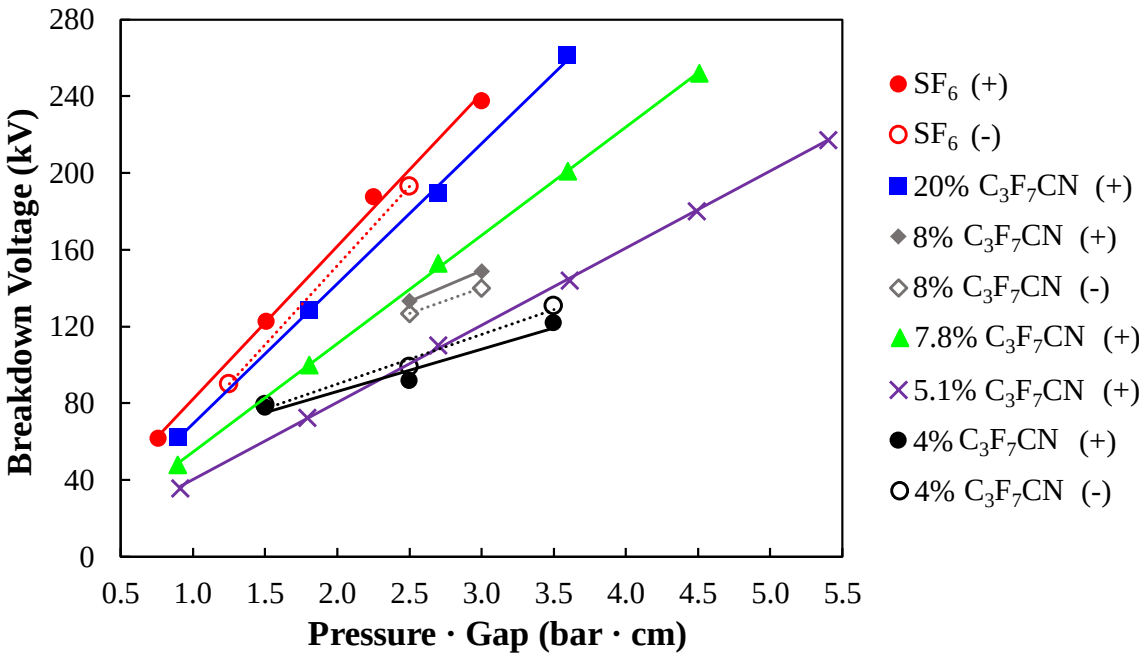

Figure 2.19 DC breakdown characteristics for C_3F_7CN/CO_2 and SF_6 under a quasi-uniform field (re-drawn from sources) [91]–[93].

Concerning the effect of DC polarities on the breakdown voltage, SF_6's positive breakdown voltage attains a higher breakdown when compared with the negative one. Since the applied field is quasi-uniform with a high f factor, the margin between polarities is small, with both polarities increasing linearly with the Pressure·Gap, with the positive one being higher. In [83], the DC polarity effect of SF_6 was extensively investigated under varying field uniformity and gas pressure in a hemispherical rod-plane configuration. Results conclude that the margin between positive and negative polarity breakdowns is larger at a quasi-uniform field with a low f factor (f between ≈ 0.7 - 0.2) and that it is pressure dependant. Further decreasing of field uniformity ($f < \approx 0.2$), via increasing the gap distance or reducing rod diameter, would expect to see a transition to a non-uniform field in which negative polarity exceeds positive polarity. This is known as transition from streamer inception into propagation region as discussed earlier (see Section 2.5.7).

The 8% C_3F_7CN ratio shows similar behaviour to SF_6 with the positive breakdown voltage being comparatively higher than the negative one. 4% C_3F_7CN shows the opposite effect. In both results, a large uncertainty margin is associated with the results, with both polarities error bars overlapping, making judgments of the behaviour uncertain [91], [92]. However, it is anticipated to follow a similar trend to SF_6 in the results in [83] for DC voltage, with both SF_6 and 20% C_3F_7CN in [16] for LI voltage under a quasi-uniform field using a hemispherical rod-plane with a 15 mm radius and coaxial geometry with a 4/30

conductor/enclosure radius at which positive breakdowns are higher than the negative results.

Non-Uniform Field (0.25 > f > 0)

Figure 2.20 presents the results obtained from [83], [91], [94] in a non-uniform field using needle-plane configurations under both DC polarities. All the investigations have a fixed gap at 5, 10 and 20 mm, respectively, with varying pressure, configuration specifications (shown earlier in Table 2.10). Both SF_6 and mixtures of 4% and 8% C_3F_7CN show a similar trend but at different Pressure·Gap ranges. Positive breakdown voltage tends to saturate, while negative breakdown voltage increases almost linearly with the increasing of the Pressure·Gap, leading to a more non-uniform field effect.

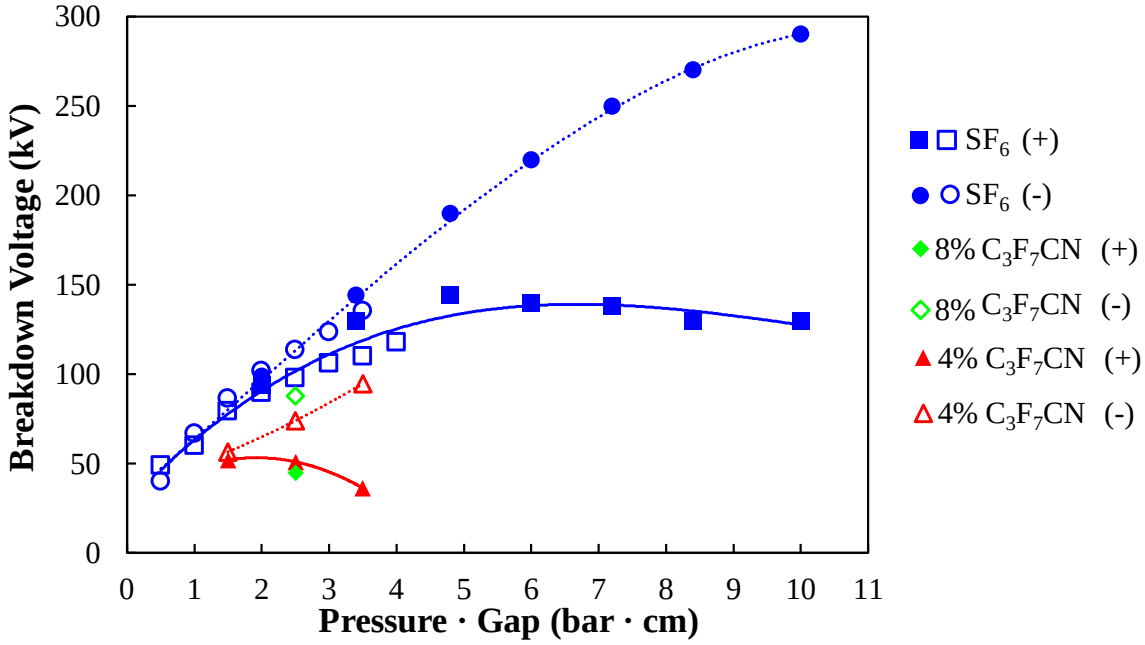

Figure 2.20 DC breakdown characteristics for 4%, 8% C_3F_7CN mixtures with CO_2 and SF_6 under a non-uniform field; filled blue markers are results from [83] and unfilled blue markers are from [94], fitted to a polynomial of the 3rd order, (re-drawn from sources) [83], [91], [94].

Due to the lack of results in the literature for DC breakdown voltages in C_3F_7CN mixtures, the following Figure 2.21 shows a study under AC voltage from [17], conducted for the purpose of comparing the dielectric performance of SF_6 gas and different C_3F_7CN mixtures under a non-uniform field using a needle with a tip head of 0.02 mm radius, a plane with 50 mm in width and a gap distance equal to 20 mm under varying pressure.

From Figure 2.21, under non-uniform field AC voltage, SF_6 has a higher breakdown voltage than the 20% C_3F_7CN and 80% CO_2 mixture with around 30 kV higher at 2 bar pressure,

while in a uniform field, this mixture ratio is comparatively higher than SF_6. One of the reasons for this decreasing trend could be the effective ionisation coefficient of the C_3F_7CN/CO_2 gas mixture increases with the electric field at a greater rate than SF_6, as highlighted in [17], [88]. Thus, it indicates that the 20% C_3F_7CN / 80% CO_2 gas mixture is more sensitive towards varying field uniformity.

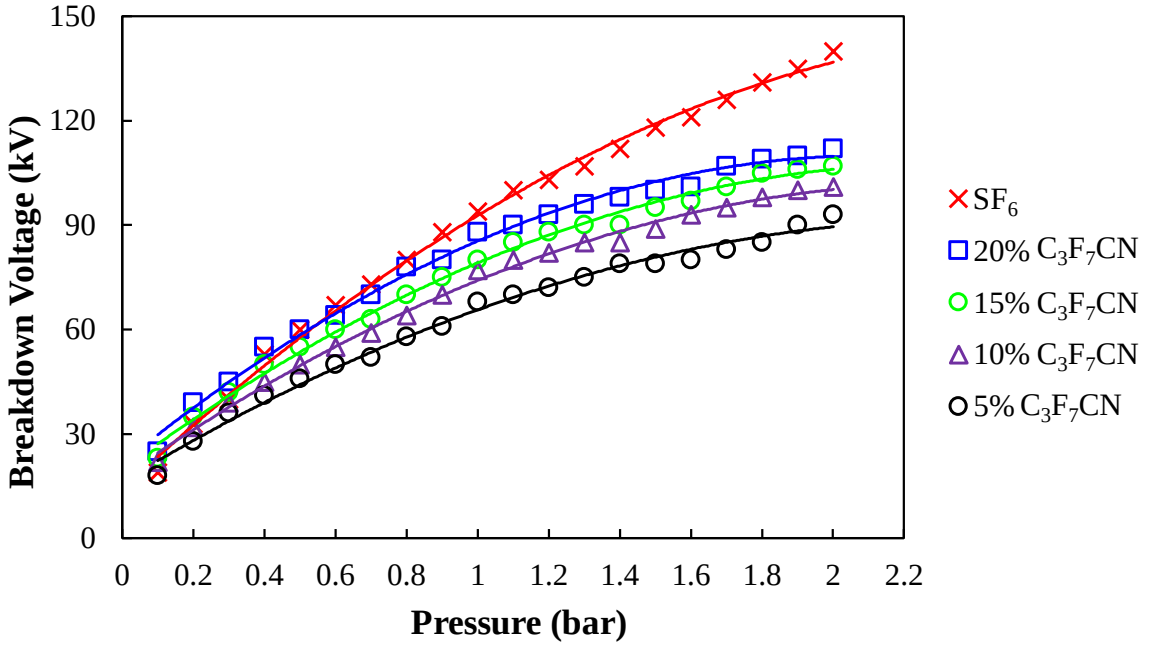

Figure 2.21 AC breakdown characteristics for C_3F_7CN/CO_2 and SF_6 under a non-uniform field (re-drawn from source) [17].

While the field is changing from quasi-uniform to non-uniform via increasing the gap distance typically in rod-plane configurations, increasingly non-uniform fields lead to saturation in the case of the positive breakdown voltage, while in the negative polarity case, the breakdown voltage increases linearly. As a result, the two polarities' breakdown voltage magnitudes crossover with the negative breakdown being higher (see Figure 2.20). This is a result of the breakdown mechanism changes to streamer propagation as discussed in Section 2.5.7 earlier. This was also observed in SF_6, CO_2, N_2 and C_3F_7CN gases and mixtures under LI and DC voltages in [16], [83], [95], [96]. Also, each gas medium has different conditions at which polarity crossover occurs. Thus, a comprehensive investigation concerning the effects of DC polarity and field uniformity on the breakdown voltage of SF_6 in comparison with C_3F_7CN mixtures is essential to address these influencing conditions where it could further elaborate the observed differences between the dielectric performance of 20% C_3F_7CN and SF_6 under a non-uniform field as in Figure 2.21.

2.8 Effects of Experimental Procedures on the DC Breakdown Voltage of Gases

There are several ways to investigate breakdown characteristics under DC voltage, such as the successive discharge and multiple level methods. As a result, this could introduce some differences in the breakdown voltage value. In addition, different electrode materials will lead to different breakdown voltage. Moreover, aged gas and electrodes will have a significant effect on the breakdown voltage value. Thus, this section will assess those factors influencing the breakdown voltage value in terms of the used DC test method, time required for gases to be fully homogenous, the effect of different electrode materials, surface roughness and ageing analysis for the gas mixture after many breakdown events.

2.8.1 Breakdown Test Method

There are currently not any specified type testing standards for a DC-GIL system. CIGRE SC D1 installed a working group to define recommendations for this type of equipment [97]. Concerning DC voltage breakdown testing, there are two methods that are used that accord to the BS EN 60060-1:2010 standard [98]: the multiple level test and successive discharge test. The standard recommends the successive discharge tests best used when performing DC voltage testing.

Multiple Level Technique

This test requires at least 5 levels of voltage (L) and 10 events in each voltage level (N), with an initial estimation of the breakdown voltage U also required to obtain step (ΔU) between the levels, which is 3% of the U.

Considering N is the voltage application in each level that will cause a breakdown event B_d in some of them where $B_d \leq N$. This is applied to each L voltage level. The outcome of this test will be number of the voltage application N and the breakdown B_d in each L voltage level. For the processing of results, the discharge frequency in each level can be calculated from the number of voltage applications and the breakdown number in each voltage level to estimate the discharge probability at each voltage level. Then, the discharge probability at each level is fitted to an assumed probability distribution function, with its parameters U_{50} (voltage at a 50% probability of breakdown) and σ (standard deviation) = $U_{50} - U_{16} = U_{84} - U_{50}$. This has been done traditionally by plotting the discharge frequency versus the voltage

level on special graph paper designed for the required distribution, such as the Gaussian distribution function. Figure 2.22 below shows an example of a multiple level test series [98].

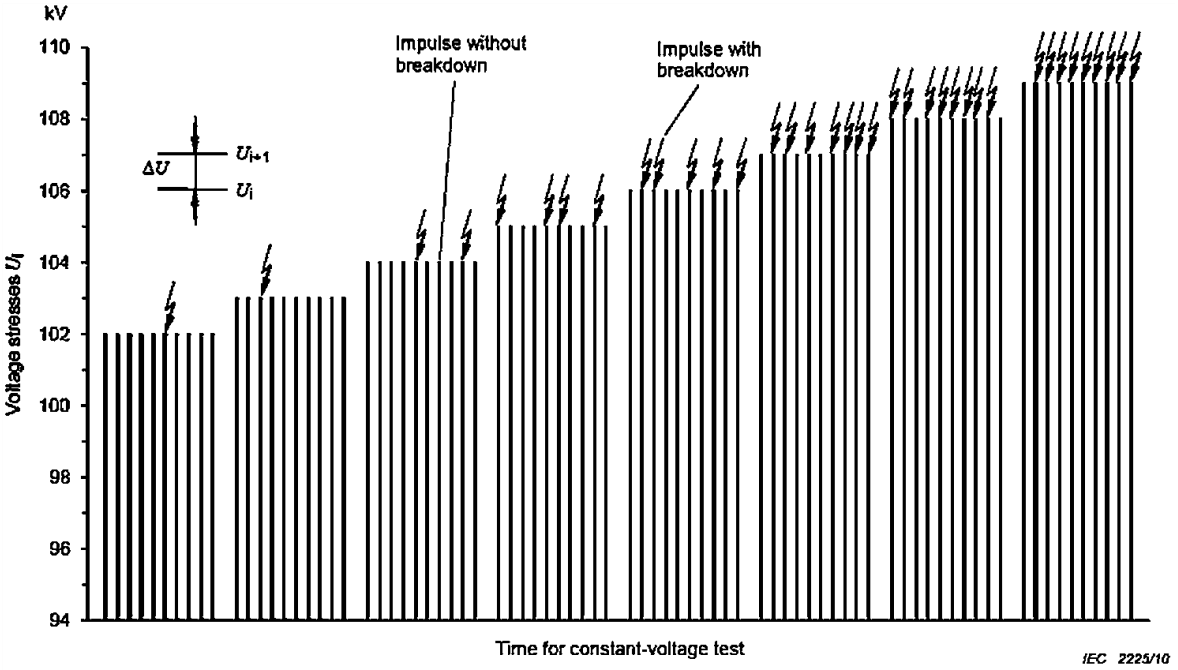

Figure 2.22 An example of multiple level test series [98].

Successive Discharge Technique

This method is commonly used for DC breakdown investigations. In this testing method, all events (n) lead to a disruptive discharge. The test voltage is increased continuously until the test object breakdown. The outcome of this test will be the voltage at the time of breakdown (U_i). This method requires at least 10 breakdown events. To process the data, calculating the U_{50} and the σ can be done based on the Gaussian distribution using Equations 2.27 and 2.28 [98]. An example for this test is shown in Figure 2.23 below.

$$U_{50} = \sum \frac{U_i}{n} \tag{2.27}$$

$$\sigma = \left(\sum \frac{(U_i - U_{50})^2}{n-1} \right)^{\frac{1}{2}} \tag{2.28}$$

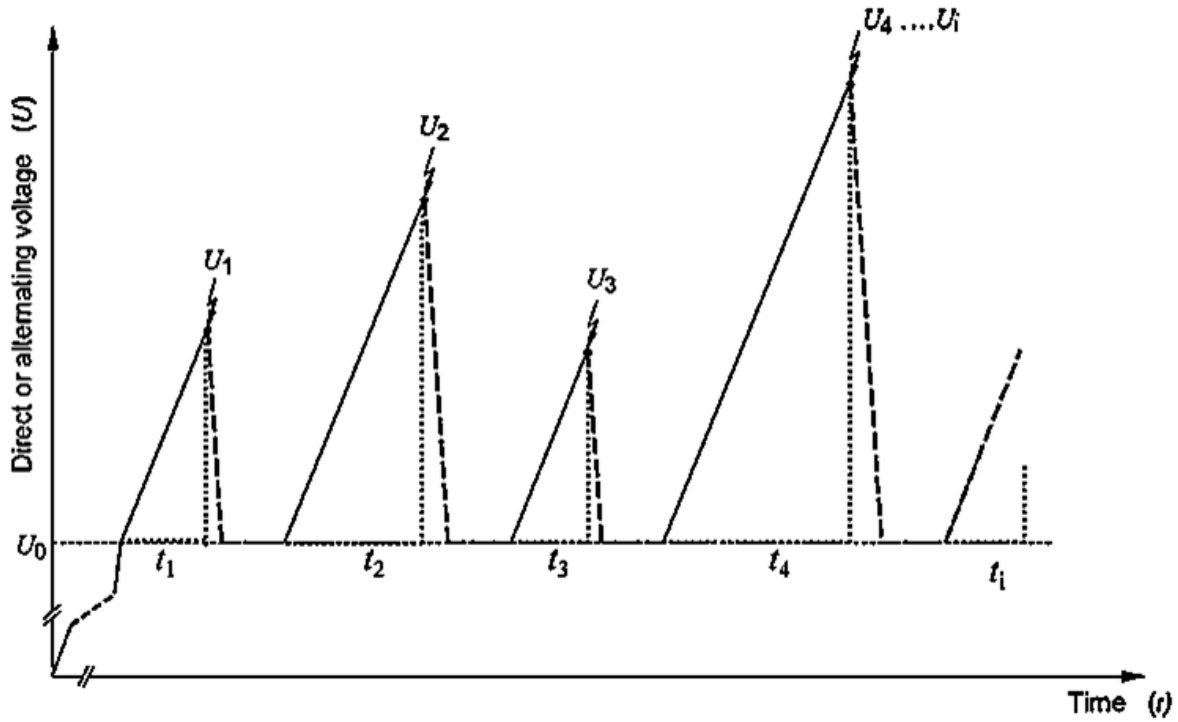

Figure 2.23 An example of successive discharge test series [98].

Research conducted in [99] compares a multiple level test and successive discharge tests under positive DC voltage using a sphere-sphere electrode with a radius of 2.5 cm and a radius of 6.25 cm in air at atmospheric pressure. Test results are shown for both electrode sizes in Figure 2.24.

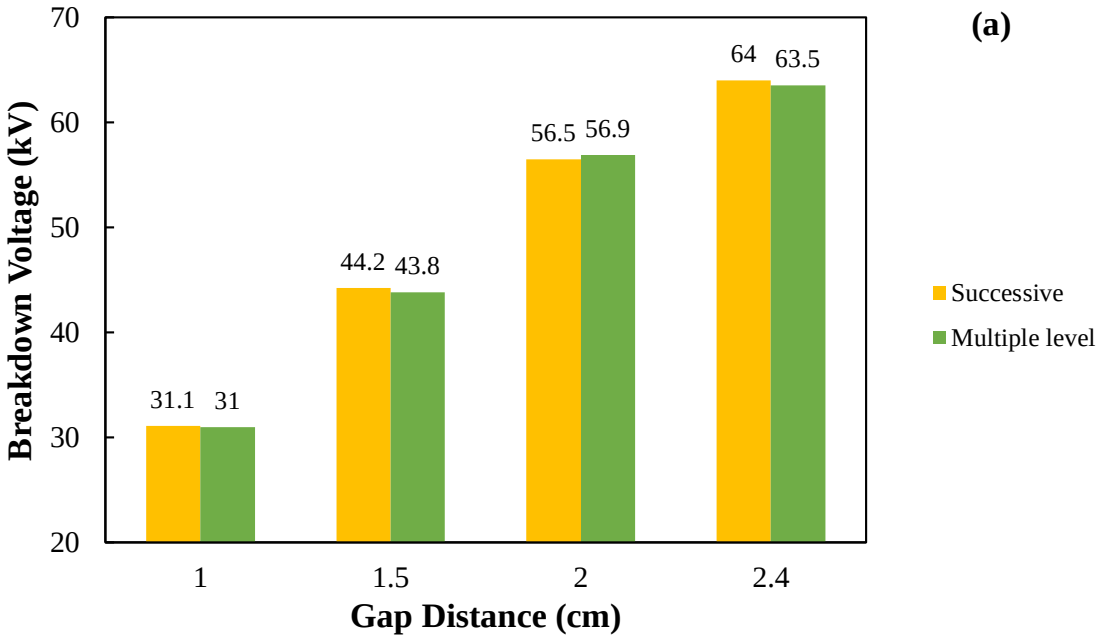

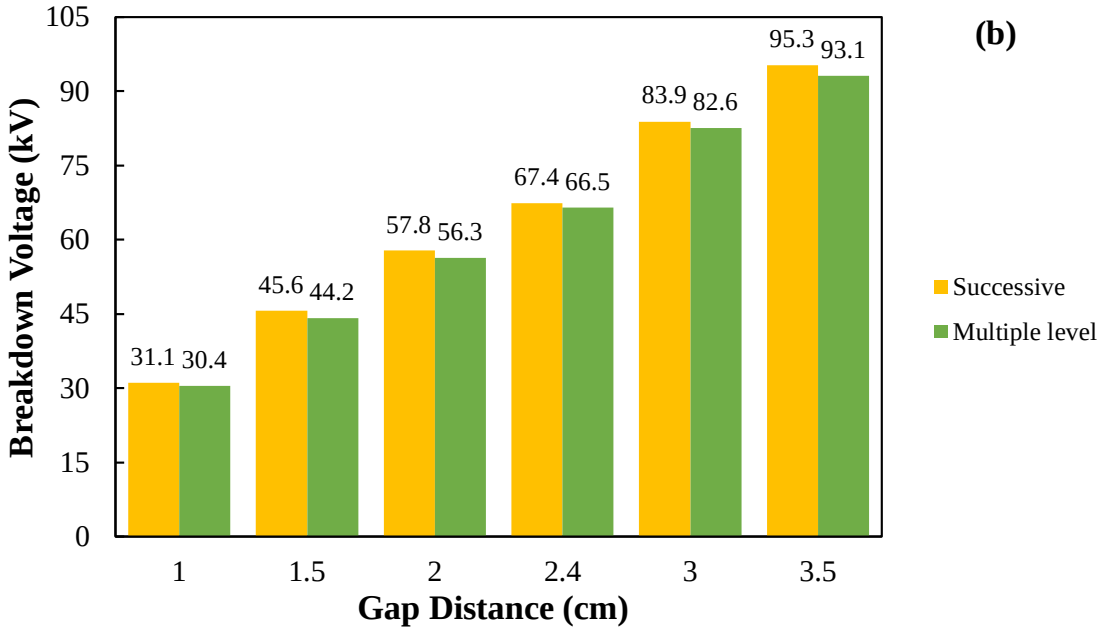

Figure 2.24 Comparison between successive discharge and multiple level methods for sphere-sphere electrodes with a radius of (a) 2.5 cm and (b) 6.25 cm under atmospheric air [99].

In the case of the 2.5 cm sphere radius shown in Figure 2.24(a), the average difference between both methods is 0.7%, with overlapping between two test results. For the case of the 6.25 cm sphere radius in Figure 2.24(b), the average difference between the successive discharge test and multiple level test is 2% [99]. Ultimately, for the two electrodes' radiuses used in this experiment, the obtained results from both test methods are similar. Thus, both methods can be used to evaluate the DC breakdown voltage of gases.

2.8.2 Successive Discharge Test Procedure

In this method, as discussed earlier, the voltage will rise until breakdown. There are different ways to ramp the voltage up to the point of breakdown, such as increasing it with a different ramp rate, for example 0.5 kV/s, 1 kV/s and 5 kV/s. Another way to ramp the voltage is using two ramp rates, one 60% fast and one 40% slow as an example, 5 kV/s up to 60% of the breakdown point and the rest will increase in 0.5 kV/s. In the standard, it is only for the liquid DC breakdown procedure according to IEC 60243-1: 1998 [100] where this rate should be in a range that will cause the object to breakdown between 10 to 20 seconds, with it being satisfactory if the majority of the breakdowns fall inside this time.

In addition, there is not any recommendation about the time interval between each breakdown for DC voltage where it will allow the gas to recover for the next breakdown. These factors could introduce uncertainty to the results and might make them non-repeatable.

Therefore, investigation of the test procedure for this method needs to be standardised to both obtain a reliable result and unify the procedures for all other researchers' outcomes.

According to [91], the rate used for their DC breakdown experiment was 1 kV/s, with a time interval between each breakdown equal to 5 minutes. In addition, they used another rate of 2 kV/s and a time interval equal to 10 minutes for their DC insulator flashover experiment. Another research [101], used 1 kV/s as its ramp rate with 2 minutes time interval for the DC breakdown investigation. Another study [18], used 5 kV/s, stating that there will be no significant difference in breakdown voltage value when using ramp rates of 0.2 kV/s, 1 kV/s and 5 kV/s. Table 2.11 shows the maximum and minimum time to breakdown based on the adopted ramp rates for the breakdown voltage experiments in those studies investigating DC breakdown voltage in gases dielectric. From Table 2.11, using a very slow ramp rate, such as 0.1 kV/s, will require a long time to breakdown. Most studies adopted a ramp rate of 1 kV/s. Time to breakdown is different for each study, which is the time for stressing the gas until discharge occurs, which is dependent on the breakdown voltage value and ramp rate.

Table 2.11 Ramp rate and time to breakdown calculation adopted by different studies on DC breakdown voltage in gases.

Ramp rate (kV/s)	Minimum breakdown (kV)	Maximum breakdown (kV)	Minimum time to breakdown (s)	Maximum time to breakdown (s)	Reference
1	45	135	45	135	[91]
2	75	140	37.5	70	[91]
0.1	28	255	280	2550	[93]
5	80	180	16	36	[18]
1	3	35	3	35	[101]
1	15	90	15	90	[102]

2.8.3 Mixing Time of Gas Mixtures

In order to have a gas mixture, at least two gases are filled in a vessel, with the total pressure equal to the partial pressure of each gas according to Dalton's law of partial pressures [103]. The only issue is to confirm, after filling the mixture, how homogenous the mixture is. According to the CIGRE guide for mixing SF_6 with N_2 [104], after finishing mixing, it is sometimes necessary to allow for their diffusive mixing before any operations are undertaken. The diffusive mixing time is dependent on the dimension and shape of the chamber. A calculation of the time for diffusion of the SF_6 and N_2 gas mixture is conducted in an N_2 gas column of 1 m height, with the SF_6 injected from the bottom of the column until

the final mixing ratio of 60% SF_6 and 40% N_2 is reached. Figure 2.25 shows the time required for the diffusion process before the gas mixture becomes homogenous, with the calculations made for two different column heights, z= 0.9 and 0.1 m [50].

From Figure 2.25, the 60% SF_6 and 40% N_2 gas mixture in a 1 m high column required at least 20 hours to be fully mixed and homogenous. Studies in [105], [106], investigated the characteristics of the SF_6 and N_2 gas mixture where, they recommended that, after filling the gas mixture, it is important to leave the mixture for up to 24 hours before conducting any testing.

For a typical concentration of 20% of C_3F_7CN in CO_2, the gas mixture should remain homogenous, unless condensation occurs [16]. The time required for mixing the gas to be fully homogenous at room temperature and under atmospheric pressure could be in order of days, with the time required increasing when using lower temperature and higher pressure. Therefore, it is recommended to pre-mix the gas in a storage tank and leave it for a period of time before filling any equipment [13], [16].

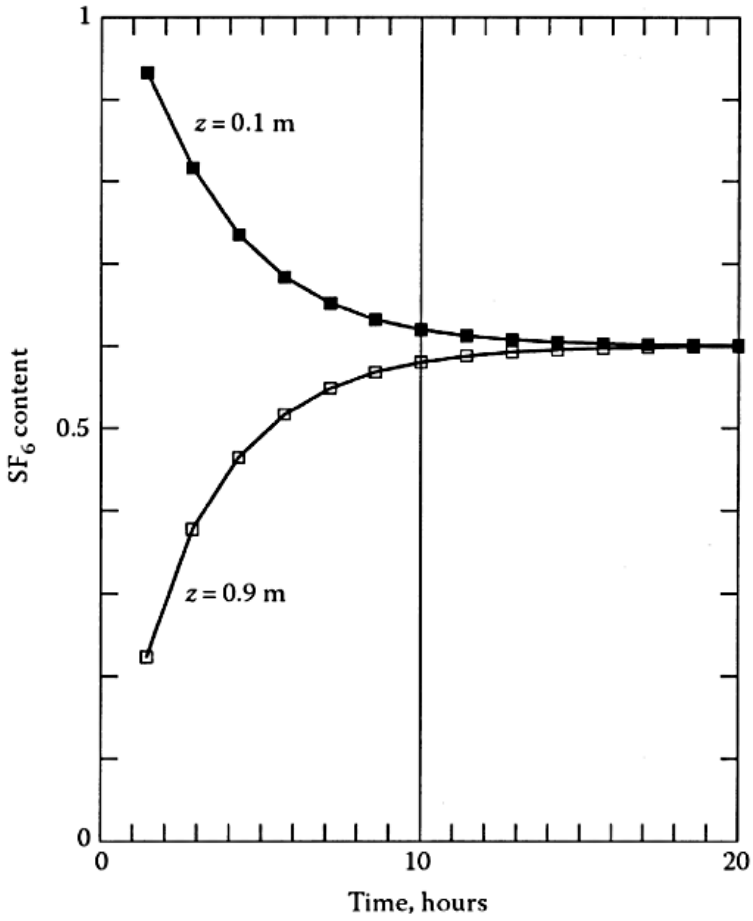

Figure 2.25 Time variation for SF_6 concentrations injected at the bottom of a 1 m high N_2 column with a final ratio of 60% SF_6 / 40% N_2. The calculation was done for a column height of z = 0.1 m and 0.9 m [50].

2.8.4 Effect of Electrode Materials

Several researchers have reported an influence of electrode materials on the breakdown voltage in SF_6 gas and its mixtures, air and vacuum [107]–[110]. The commonly used material in gas insulated equipment is aluminium but for testing purposes, other materials such as stainless steel, brass and copper, have also been investigated.

In [107], the effect of using copper, brass and aluminium electrodes on the AC breakdown voltage was reported for 5%, 10% and 15% SF_6 and (N_2 or CO_2) gas mixtures using a sphere-sphere configuration with a sphere radius of 10 mm and a fixed gap distance of 4 mm under varying pressure. In [109], a similar electrode configuration was used for air at atmospheric pressure and a varied gap distance from 0.5 mm to 5 mm using stainless steel, copper and aluminium electrodes. Also, in [108], the AC breakdown voltage was investigated in SF_6 gas using stainless steel, copper and aluminium plane-plane electrodes with a plane width of 150 mm and at a fixed gap of 5 mm. Figure 2.26 shows the effect of different electrode materials on the AC breakdown voltage of SF_6 and a mixture of 10% SF_6 and 90% N_2, while in Figure 2.27, the results are shown in air.

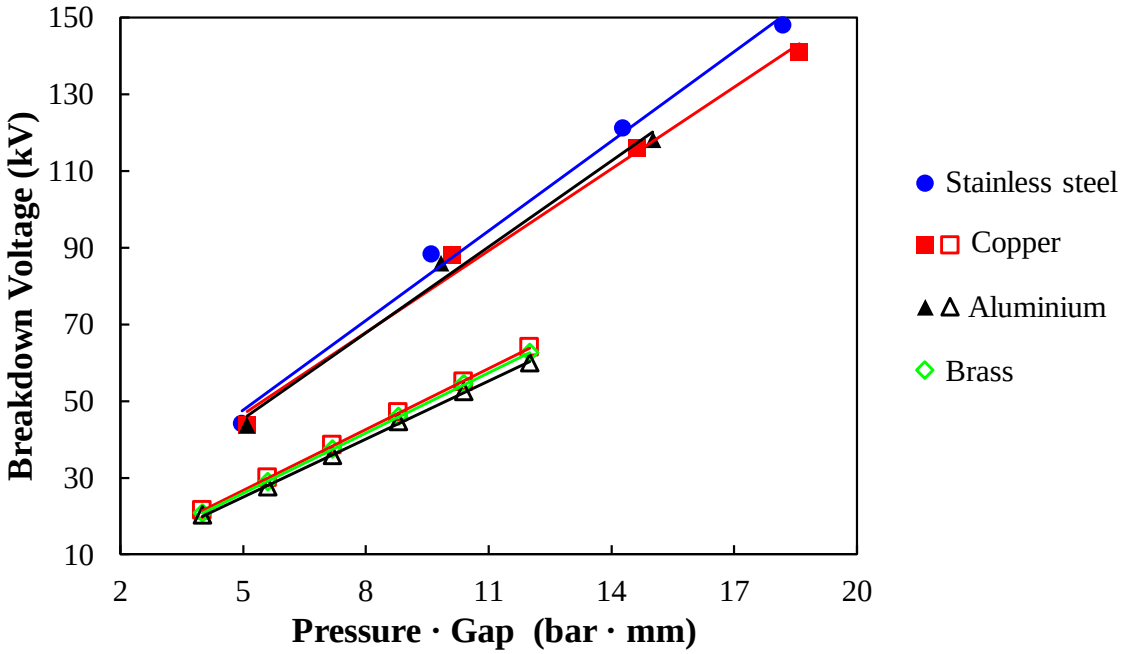

Figure 2.26 Effect of electrode materials on AC breakdown voltage for SF_6 gas in plane-plane electrodes represented as filled markers [108], with unfilled markers being 10% SF_6 and a 90% N_2 mixture in sphere-sphere electrodes [107] (redrawn from sources).

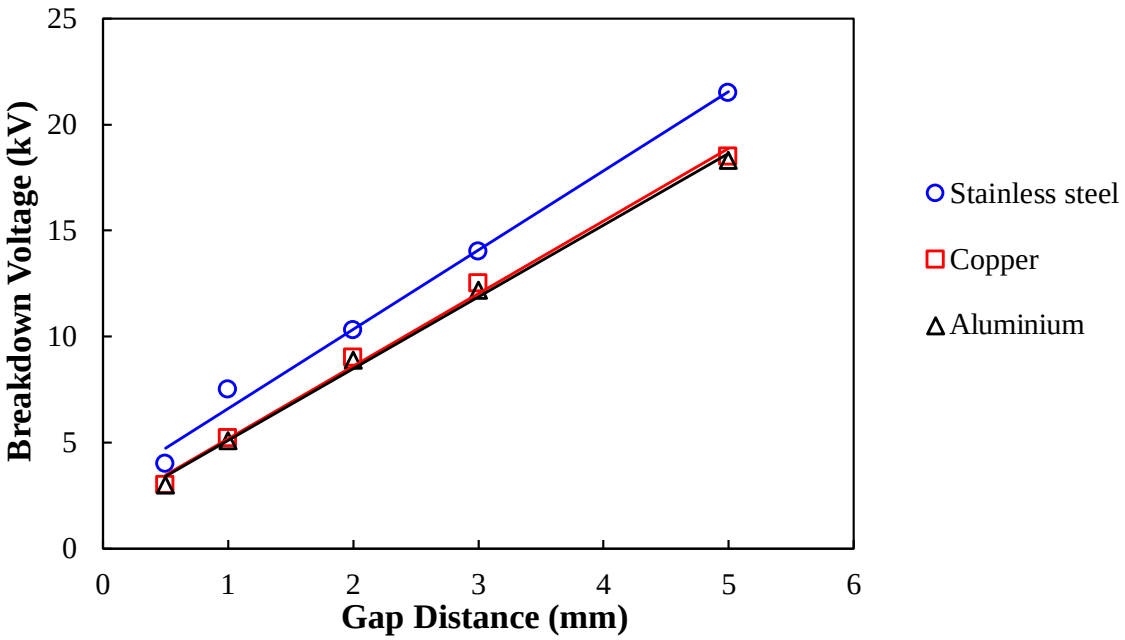

Figure 2.27 Effect of electrode materials on AC breakdown voltage for air at atmospheric pressure in sphere-sphere electrodes, (redrawn from source) [109].

From Figures 2.26 and 2.27, there is a noticeable effect of the electrode material on the breakdown voltage, which becomes more visually distinct as the Pressure·Gap increases. Stainless steel attains the highest breakdown voltage in comparison with other electrode materials tested in SF_6 and air. It is also worth mentioning that, in [107], other SF_6/N_2 and SF_6/CO_2 mixtures were also investigated, with the results showing that the effect of electrode material on the breakdown voltage was mainly influenced by the work function of the electrode material. The main reason for this effect is the difference in the work function and the first ionisation energy between different electrode materials. First ionisation energy is the energy required to remove an electron from the electrode atom in order to enable the departure from the metal surface to a point outside it. As high as the work function, resulting in a higher applied voltage to cause a breakdown. However, it is known that the breakdown voltage value is usually not strictly following the work function order, due to oxide layers effect on some materials [110]. Thus, in some cases, copper performs better when compared to brass and aluminium [107]. While in [108], copper and aluminium breakdown voltages were matching. Additional interpretation of this trend is the used aluminium could be an alloy with a higher work function value [111].

2.8.5 Effect of Electrode Surface Roughness

In ideal cases, when electrodes are fabricated to a mirror finished (polished) condition, the experimental critical field strength of gas dielectrics can be close to theoretical values ($(E/p)_{crit}$ SF_6 = 8.9 kV/mm·bar [49] and $(E/p)_{crit}$ 20% C_3F_7CN and 80% CO_2 = 9.1 kV/mm·bar [85]). However, at a large scale, this value cannot be sustained with the practical surface finishes used for the equipment. As a result, increased ionisation will occur on the protrusion of microscopic surface roughness, resulting in a reduction in the breakdown voltage by a factor of ζ [49]. Several studies have investigated the effect of microscopic protrusion height and gas pressure (p·h) on ζ factor in SF_6 gas and its mixtures under AC voltage [112]–[117]. Results show that after a threshold value for p·h (AC voltage SF_6 threshold p·h value ≈ 40-50 bar·µm), the breakdown voltage will significantly drop when compared to those with a mirror finished surface until this effect is saturated at a large p·h range. Figure 2.28 shows a calculation of the threshold p·h value in different SF_6/N_2 mixture ratios. From the results, increasing SF_6 concentration in the SF_6/N_2 mixture will increase the sensitivity facilitated by surface roughness.

Concerning the C_3F_7CN/CO_2 gas mixture, it has been reported under DC voltage in [90] for a 6% C_3F_7CN / 94% CO_2 gas mixture, that negative DC polarity is significantly more sensitive to surface roughness where it shows a significant drop in the breakdown voltage value compared with the positive one. Also, a 6% C_3F_7CN / 94% CO_2 gas mixture is less sensitive to electrode surface roughness than SF_6 gas. Another investigation conducted in [118] under AC voltage, had a p·h threshold value for a 10% C_3F_7CN / 90% CO_2 gas mixture equal to 52 bar·µm, with their investigated SF_6 value being 43 bar·µm. Thus, a 10% C_3F_7CN / 90% CO_2 gas mixture is less sensitive towards surface roughness than SF_6. However, it is close to the SF_6 range between the 40-50 bar·µm presented in other studies [49], [112]. Through the calculation used in [118], a mixture between 3-20% C_3F_7CN concentrations should have comparable surface roughness characteristics to SF_6. Overall, different gases and mixtures reacted differently towards electrode surface roughness. Therefore, it is essential to study these characteristics when selecting alternative SF_6 gases as a design consideration when using gas insulated equipment.

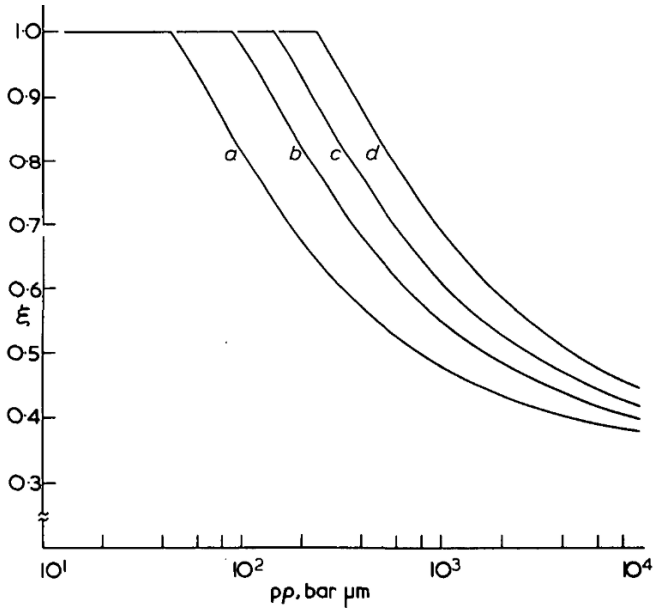

Figure 2.28 Roughness factor ζ calculated as a function of SF_6/N_2 gas mixtures where, (a) 100% SF_6, (b) 50% SF_6, (c) 25% SF_6 and (d) 10% SF_6 [114].

2.8.6 Effect of Electrical Ageing on the Breakdown Voltage

Electrical ageing is when an insulation gas or mixture and the electrode setup are subjected to many breakdown events that lead to drop in the breakdown voltage value. This is mainly due to the damage on the surface of the electrodes where surface roughness increases, as well as due to the generated by-products that will have lower dielectric strength than the original gas.

An investigation carried out in [27] exposing a 20% C_3F_7CN / 80% CO_2 gas mixture to 1000 negative DC breakdowns using 5.8 mm diameter spark gaps at a 1 mm gap distance under a pressure of 7.2 bar, concluded that within the first 200 breakdowns for the tested configuration, breakdown result of 20% C_3F_7CN / 80% CO_2 is not as stable as SF_6 after a significant drop in the performance, which was mainly due to the surface roughness effect rather than gas decomposition. This could be a result of the small gap distance used in the investigation at which the effect of gap distance highly influences the breakdown voltage.

Other investigations carried out by [119], [120] assessed the by-products produced from a 13.3% C_3F_7CN and 86.7% CO_2 gas mixture at 3 bar pressure when exposed to AC breakdowns at 200 events in [119] and extended to 2000 in [120] . This was achieved by using needle-plane electrodes with a gap distance of 10 mm, with the needle tip head radius equal to 0.25 mm. By using a COMSOL simulation, the f factor is determined as 0.042, resulting in a non-uniform field. The AC breakdowns are shown in Figures 2.29 and 2.30.

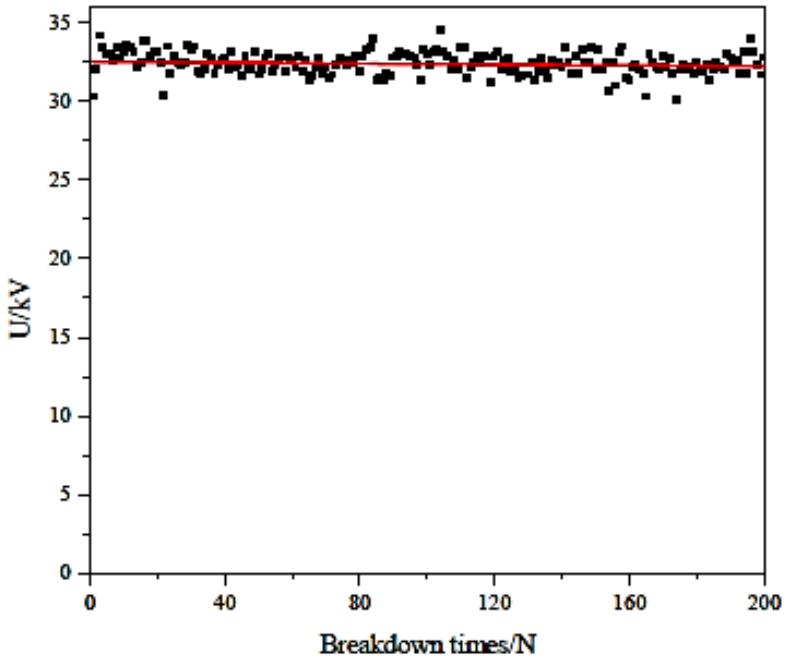

Figure 2.29 200 AC breakdowns for a 13.3% C_3F_7CN and 86.7% CO_2 gas mixture under 3 bar using a needle-plane with a gap distance equal to 10 mm [119].

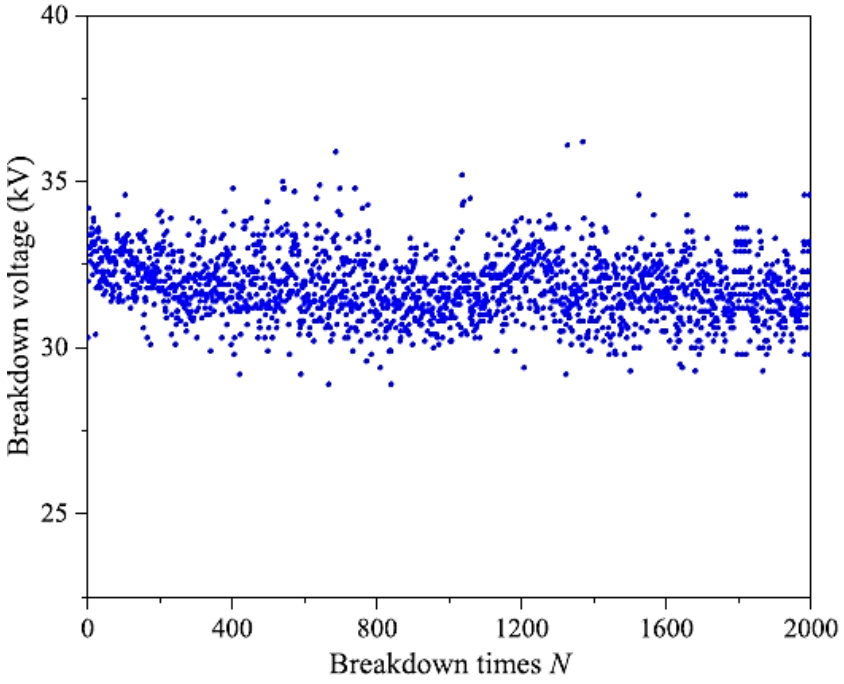

Figure 2.30 2000 AC breakdowns for a 13.3% C_3F_7CN and 86.7% CO_2 gas mixture under 3 bar using a needle-plane with a gap distance equal to 10 mm [120].

From Figures 2.29 and 2.30, the AC breakdown voltage shows a small decreasing trend as the breakdown number increases. The first few breakdowns were stacked around 33-34 kV and the last few gathered around 31 kV. Also, in the first 200 breakdowns, the variation in

the results remained at a minimum but then started to vary rapidly. Theoretically, due to the electrode used in this experiment being a needle, it is difficult to assess the reduction of the breakdown voltage because the f factor will change every time breakdown occurs because of damage at the tip of the needle. Thus, it will make the needle dull and lead to higher breakdown voltages up to some point. Concerning the produced by-products, gas chromatography-mass spectrometry (GS/MS) technology was used to analyse the gas condition before and after 200 and 2000 breakdowns, with results shown in Figure 2.31.

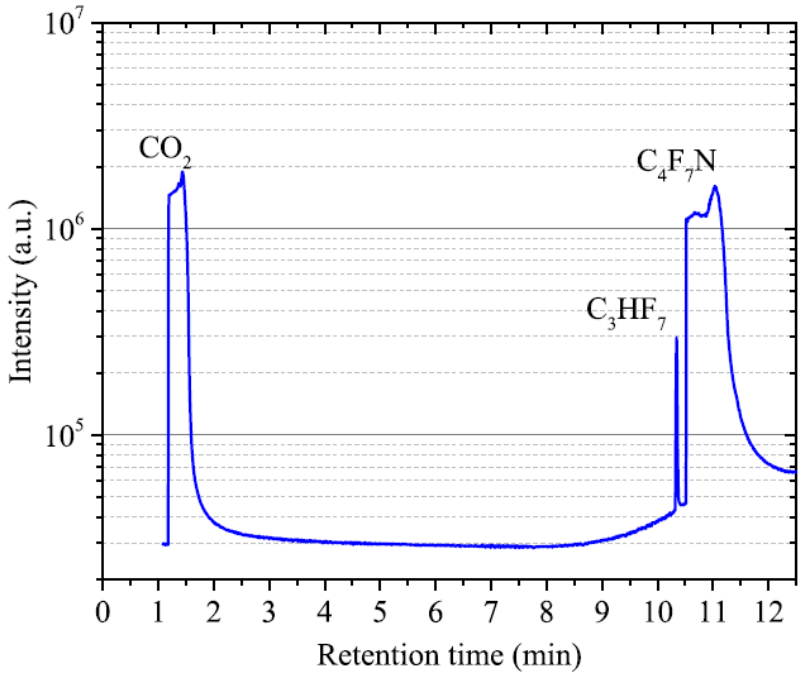

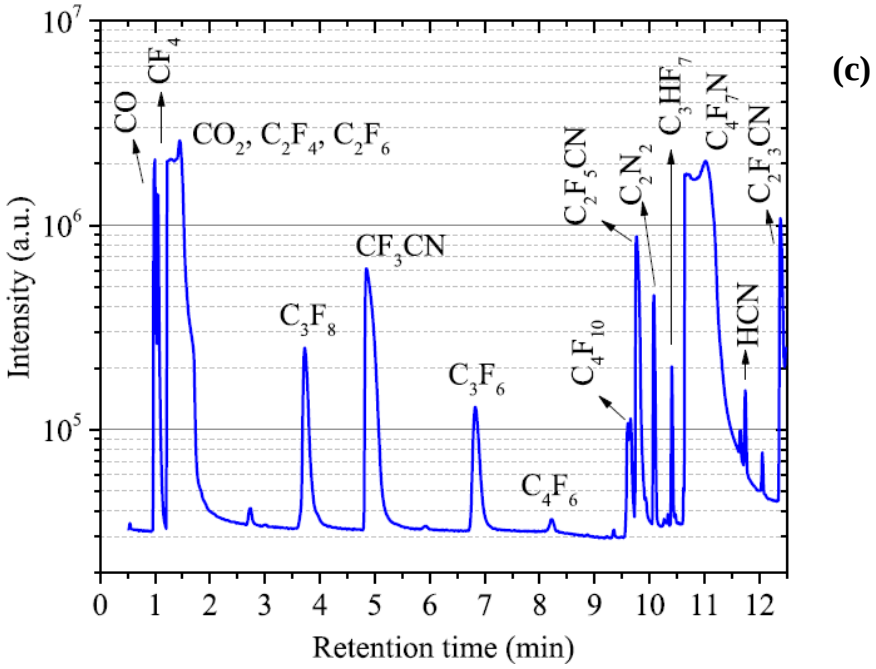

Figure 2.31 GC/MS results for 13.3% C_3F_7CN and 86.7% CO_2 gas mixture under 3 bar (a) before testing, (b) after 200 and (c) after 2000 AC breakdown events [119], [120].

Before the test, there was a small amount of C_3HF_7 gas, which is an impurity that comes with the C_3F_7CN from the supplier.

After the first 200 AC breakdown events, the decomposed products are CO, CF_4, C_2F_6, C_3F_8, C_3F_6, C_2F_4, C_4F_6, $C_4F_{10}O$, C_2F_3CN, C_2F_5CN, CF_3CN, C_2N_2 and HCN. The highest three concentrations of standard gas are CF_4 at 570 ppm_v, CO at 550 ppm_v and C_3F_8 at 20 ppm_v [119]. CF_4 has a low level of toxicity but a lethal concentration in 50% of the test population (LC_{50}) 895000 ppm_v / 15 min, and a high GWP of 6300 [76], [121]. C_3F_8 has a value of LC_{50} equal to 6100 ppm_v / 4 h, with its GWP equal to 8900 [120], [122]. CO has a high toxicity level and, if inhaled, can cause dizziness, headaches, nausea and a loss of physical co-ordination with LC_{50} value equal to 1807 ppmv / 4 h [120]. CO gas plays an important role in governing OH abundancies in the troposphere layer, with its estimated GWP being approximately 8 [123].

After the 2000 AC breakdown events, the by-products are the same as for 200 breakdowns, with the only difference being that the concentrations increase. The most dominant decomposition gas after the 2000 breakdowns is CO, reaching 4200 ppm_v due to most of the gas mixture being CO_2 that will decompose to CO. The second most dominant decomposed gas is CF_4, with its concentration reaching 2500 ppm_v. Figure 2.32 shows a comparison of the concentrations for the dominant decomposed gases after 200 and 2000 breakdowns.

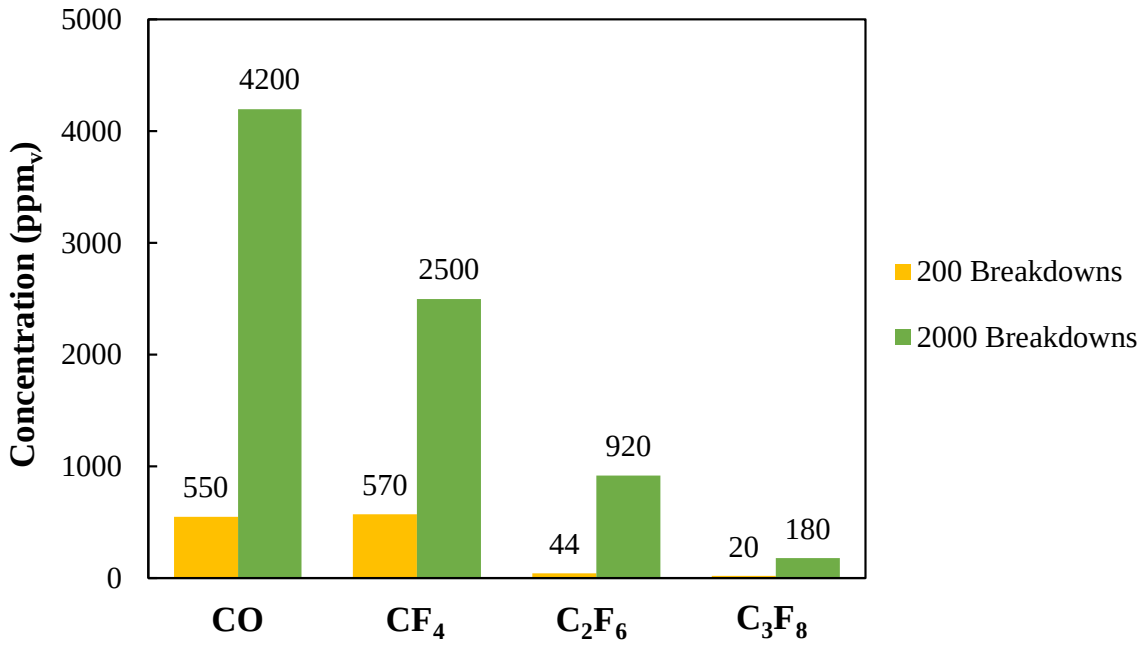

Figure 2.32 CO, CF_4, C_2F_6 and C_3F_8 concentrations after 200 and 2000 breakdown events [119], [120].

LC_{50} provides a standard measurement of the toxicity for the medium, with the lower the LC_{50} value, the more toxic the surrounding medium becomes. There are five acute toxicity categories to classify hazards caused by the substances shown in Table 2.12.

Table 2.12 Acute toxicity hazard categories according to the LC_{50} value [124].

Classification	Category 1	Category 2	Category 3	Category 4	Category 5
Inhalation-Gases (ppm_v)	$LC_{50} \leq 100$	$100 < LC_{50} \leq 500$	$500 < LC_{50} \leq 2{,}500$	$2{,}500 < LC_{50} \leq 20{,}000$	Practically non-toxic [125]

To calculate the overall LC_{50} in ppm_v and the GWP for the 13.3% C_3F_7CN and 86.7% CO_2 gas mixture after 2000 breakdowns, the following Equations 2.29 and 2.30 were used [126], [127]:

$$LC_{50mixture} = \frac{10^6}{\frac{ppm_v\ of\ gas\ 1}{LC_{50}1} + \frac{ppm_v\ of\ gas\ 2}{LC_{50}2} + \cdots} \tag{2.29}$$

$$GWP_{mixture} = \frac{mass_1 * GWP_1 + mass_2 * GWP_2 + \cdots}{mass_1 + mass_2 + \cdots} \tag{2.30}$$

where, $mass_1$ and $mass_2$ are the ratio of the gas molecular mass in the mixture, with the estimated values for the LC_{50} and the GWP for the aged gas mixture based on CO, CF_4, C_2F_6 and C_3F_8 concentrations shown in Table 2.13.

Table 2.13 GWP and LC_{50} calculations for 13.3% C_3F_7CN and 86.7% CO_2 gas mixtures before and after 2000 AC breakdown events based on CO, CF_4, C_2F_6 and C_3F_8 concentrations obtained from [120].

Gas	**Concentration (ppm_v)**	**Mole (%)**	**Molecular Weight (g/mol)**	**GWP** [120], [122]	**LC_{50} / 4 h (ppm_v)** [120], [121], [128]
CO_2	866958	86.6958	44.01	1	>300000
C_3F_7CN	132964	13.2964	195	2100	>10000
CO	4200	0.0042	28.01	≈ 8	1807
CF_4	2500	0.0025	88.0043	6300	> 14320000
C_2F_6	920	0.00092	138.01	11000	> 400000
C_3F_8	180	0.00018	188.02	8900	6100
13.3% C_3F_7CN / 86.7% CO_2 before testing				**850**	**61767**
13.3% C_3F_7CN / 86.7% CO_2 after 2000 breakdowns				**850**	**53930**

From Table 2.13, the concentration's drop of the 13.3% C_3F_7CN / 86.7% CO_2 mixture after 2000 AC breakdowns are around 0.02%, and 0.005% respectively. Thus, the influence of this marginal drop should not affect the dielectric performance of the mixture. This suggests other factors such as the effect of surface roughness and change of the needle f factor may have influenced the observed trend in the breakdown voltage in Figures 2.29 and 2.30.

The GWP of the 13.3% C_3F_7CN / 86.7% CO_2 gas mixture does not change after 2000 AC breakdowns, with the by-product's concentration being very low. In addition, LC_{50} has decreased as expected due to the by-product's toxicity. According to the calculated LC_{50} for the aged gas mixture under AC breakdowns in [120], it still falls under category five and is considered practically non-toxic [125]. This is similar to the estimated LC_{50} category reported in [27] under DC breakdowns. However, extreme caution must be considered when handling C_3F_7CN, with a recent study in [129] reporting that acute exposure to C_3F_7CN is neurotoxic in mice brains. It is strongly recommended to use adequate eye and respiratory protection, and avoid inhaling or contacting C_3F_7CN at all times [128].

2.9 Summary

This chapter has provided an overview of gas insulated equipment and transmission system comparison where GIL has been deemed to have the strongest capability of delivering power transmission with minimum losses. Also, the design challenges from moving to DC-GIL have been addressed and discussed. A summary of SF_6 alternative gases has been shown for each gas category, with the C_3F_7CN/CO_2 gas mixture providing a promising alternative. Finally, a review was conducted on previous investigations using C_3F_7CN/CO_2 gas mixtures under DC voltage, along with one on the experimental factors that can influence the DC breakdown voltage in gases. These helped identify the following important research gaps:

- It is clear that there is a lack of experimental investigations under DC voltage for C_3F_7CN/CO_2 gas mixtures when compared to SF_6 that could establish a fair one to one comparison under varying pressure and field uniformity, especially at conditions that is similar as found in practical DC GIB/GIL equipment.

- There is a lack of detailed studies on the effects of DC polarity and field uniformity on the breakdown characteristics of C_3F_7CN/CO_2 gas mixtures when compared to SF_6 and the influencing factors that led to the observed saturation in the positive breakdown voltage with increasing electrodes gap distance or decreasing the field uniformity at which equipment insulation level must be designed to withstand the DC voltage polarity that gives the lowest breakdown voltage.

- There is a lack of preliminary investigations on the DC breakdown procedure concerning the effect of adopting different ramp rates until successive discharge occurs, as well as a lack of studies investigating the effect of waiting time between a successive discharge and the next voltage ramp on the average breakdown voltage value.

Addressing the abovementioned research gaps would provide key fundamental knowledge needed to characterise varying C_3F_7CN/CO_2 gas mixtures as an insulation medium in DC-GIL applications.

3 EXPERIMENTAL DETAILS

3.1 Introduction

This chapter discusses the designed and used test equipment, namely the high pressure vessels, test electrodes, gas handling equipment and DC test circuit, used to investigate the breakdown characteristics of SF_6 and its alternative gases under DC voltage. In addition, the successive discharge method will be used for the DC breakdown investigations in this current thesis.

3.2 Pressure Vessel

Two different sized vessels were used in the experiment for different experimental purposes. The specifications of each vessel are described in the following sections.

3.2.1 Small-Scale Vessel for Preliminary Trials

A 5-litre stainless steel pressure vessel that can withstand up to 10 bar pressure was fabricated and incorporated with a bushing rated up to 100 kV_{DC} (shown in Figure 3.1). A side window was fitted to allow visual viewing of breakdown events. The vessel has an inner diameter of 160 mm and a height of 300 mm.

A linear mechanical actuator with a maximum movement of 19 mm was fitted to the bottom side of the vessel shown in Figure 3.2 and used to enable control of the gap distance between the electrodes under pressure without any leakage. One complete revolution of the actuator probe (clockwise or anti-clockwise) allows the electrode gap distance to be adjusted up or down by 0.5 mm. The micro spindle main divisions have accuracy in the range of 10 µm per division, allowing for high accuracy movement and precision when setting the gap distance. This small-scale vessel was only used for the rod-plane experiment that has a maximum breakdown voltage of no more than 90 kV_{DC} and for the electrical ageing experiment with decomposition by-products due to the smaller volume.

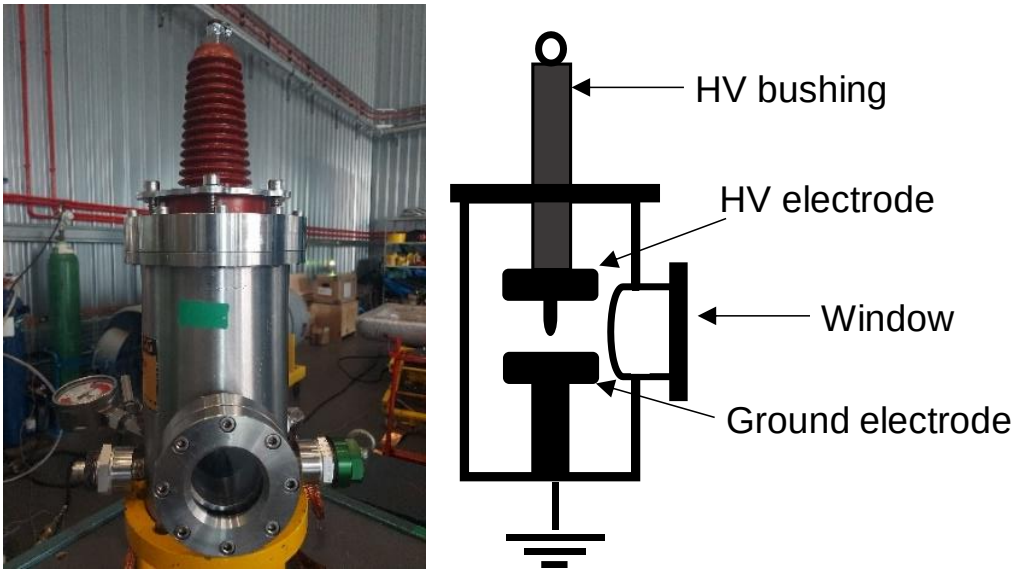

Figure 3.1 Small-scale vessel used in the rod-plane configuration and with breakdowns below 100 kV_{DC}.

Figure 3.2 Mechanical linear actuator at the bottom of the small-scale vessel to adjust the gap distance between electrodes with a 0.5 mm gap adjustment per revolution.

3.2.2 Large-Scale Vessel for Prototype Investigations

This vessel consists of two sections: a bushing zone and test zone. The bushing zone is always filled with SF_6 above 4.5 bar that is capable of withstanding up to 325 kV AC_{rms} (with a maximum operating pressure of 8.7 bar at 20°C). The test zone is used for filling the test gas and rated up to 10 bar of pressure. An animation of the vessel is shown in Figure 3.3.

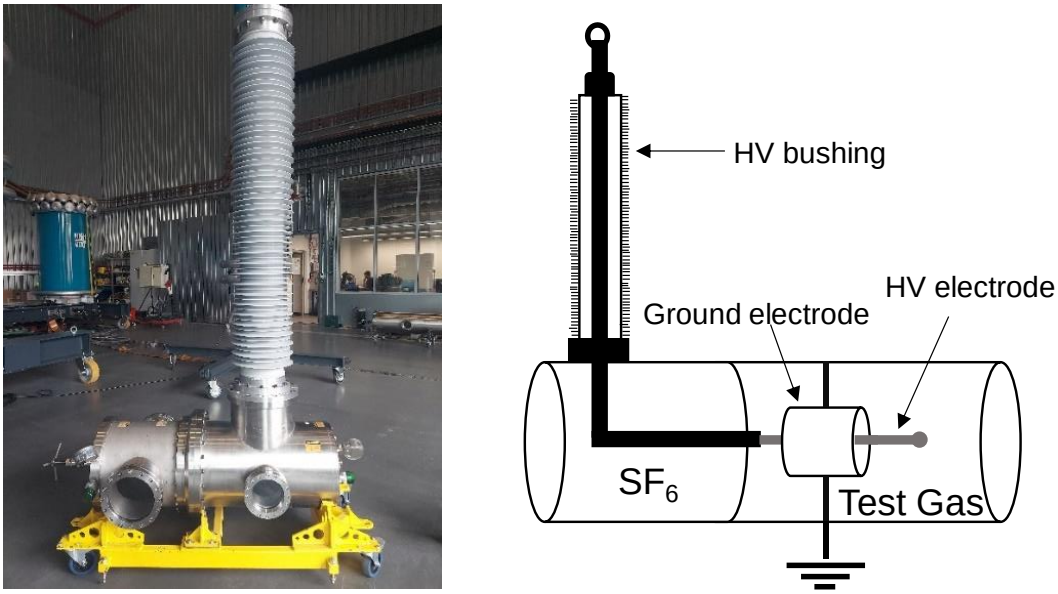

Figure 3.3 Large-scale vessel used for rod-plane and coaxial configurations for breakdowns up to 300 kV_{DC}.

Viewing windows were fitted in the test zone and the bushing zone to visually observe the breakdowns. Since the bushing rating is 325 kV $AC_{rms,}$ which is assumed to be DC equivalent, this vessel was used for both rod-plane and coaxial configurations up to 300 kV DC to avoid bushing failure. A linear mechanical actuator mounted on the side of the vessel with a step of 0.5 mm per section and 1.5 mm per revolution was fitted on the side of the testing zone (see Figure 3.4). The actuator is only used in the rod-plane configuration to adjust the gap distance under pressure, allowing a maximum of 100 mm gap per adjustment. The first tested inter-electrode gap spacing was set using a slip gauge prior to any experiment, with the gap distance then adjusted using the actuator while under pressure. Further verification was undertaken using slip gauges to cross-check the gap distance after opening the vessel.

Figure 3.4 Mechanical linear actuator at the side of the large-scale vessel to adjust the gap distance between electrodes with a 1.5 mm gap adjustment per complete revolution.

Vessels were filled with N_2 gas at 10 bar for 30 minutes. Leak detection was performed during that time and there was no noticeable drop observed in the pressure. Also, each vessel has an analogue pressure gauge mounted on the side of the vessel to monitor the pressure reading inside the vessel, as well as a plug-in digital gauge calibrated with a five-point pressure calibration certificate to cross-check the pressure readings for all gas filling stages (see Figure 3.5). To ensure safety measures, a pressure relief valve was attached to each vessel with the maximum release pressure set at 10 bar. Exceeding that pressure will ensure that the gas is evacuated from the vessel.

Figure 3.5 Analogue and digital pressure gauges used for monitoring the pressure in the vessel.

3.3 Electrode Configurations

3.3.1 Rod-Plane Configurations

Rod-Plane Electrode Design and Dimensions

Three differently sized hemispherical rod-plane configurations with rod diameters of 3.5 mm, 6.25 mm and 12.5 mm made of stainless steel, unless specified otherwise and shown in Figure 3.6, were selected to provide a range of field uniformities as found in the designs of GILs and GIBs (quasi-uniform), and contact switches inside ring main units (non-uniform) using different rod diameters at a varying gap distance of 5-55 mm [16], [130]. The interelectrode gap distance was set prior to an experiment using a slip gauge and then

adjusted for other gaps using the mechanical actuator while under pressure, before cross-checking again after the experiment using a slip gauge.

In order to find the E_{max} point on the electrodes and f factors, COMSOL was used to compute the electric field based on FEA simulation. Figure 3.7 shows a mesh convergence study by evaluating the effect of meshing size on the accuracy of computing the E_{max} value for the 6.25 mm rod-plane at an interelectrode gap distance of 3 mm. In Figure 3.7, considering the accuracy of E_{max} and the time required for computation, a maximum element size equal to 0.1 mm and a minimum element size equal to 0.001 mm were chosen for the E_{max} simulation shown in Figures 3.8 and 3.9. In addition, since the physics-controlled at an extremely fine mesh level is also an acceptable meshing criterion as the difference between the E_{max} obtained from the user defined mesh and the physics-controlled at an extremely fine level is marginal, thus, for other simulations in this work, a maximum element size equal to 0.5 mm and a minimum element size equal to 0.0005 mm were adopted for a faster computation time while maintaining an acceptable accuracy level of the results.

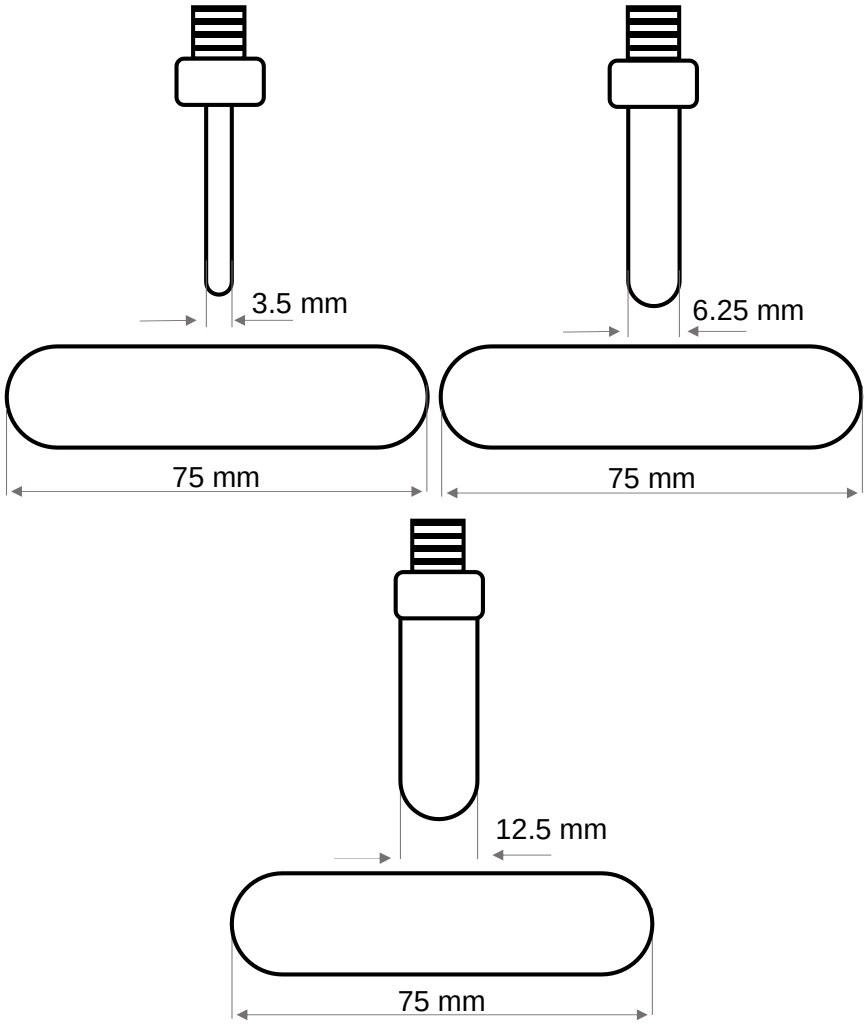

Figure 3.6 Rod-plane test configurations with a rod diameter of 3.5, 6.25 and 12.5 mm.

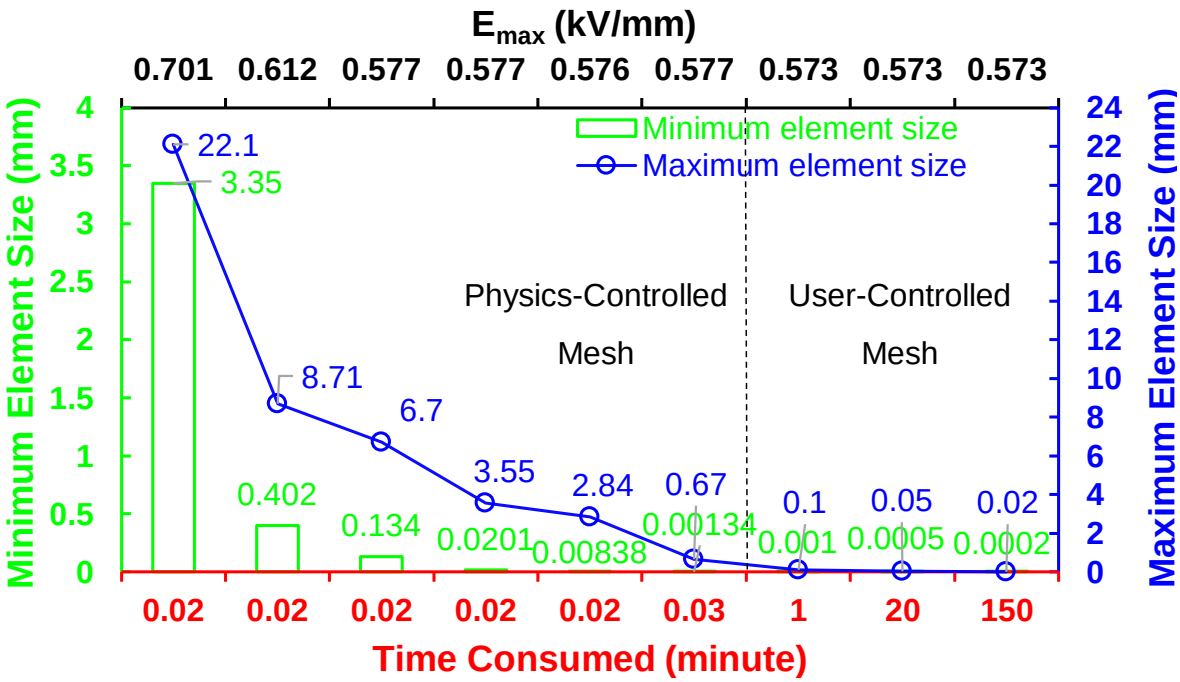

Figure 3.7 A mesh convergence study in COMSOL simulation to find E_{max} using different meshing sizes with electrodes spacing of 3 mm for a 6.25 mm diameter-rod-pane and an applied voltage of 1 kV.

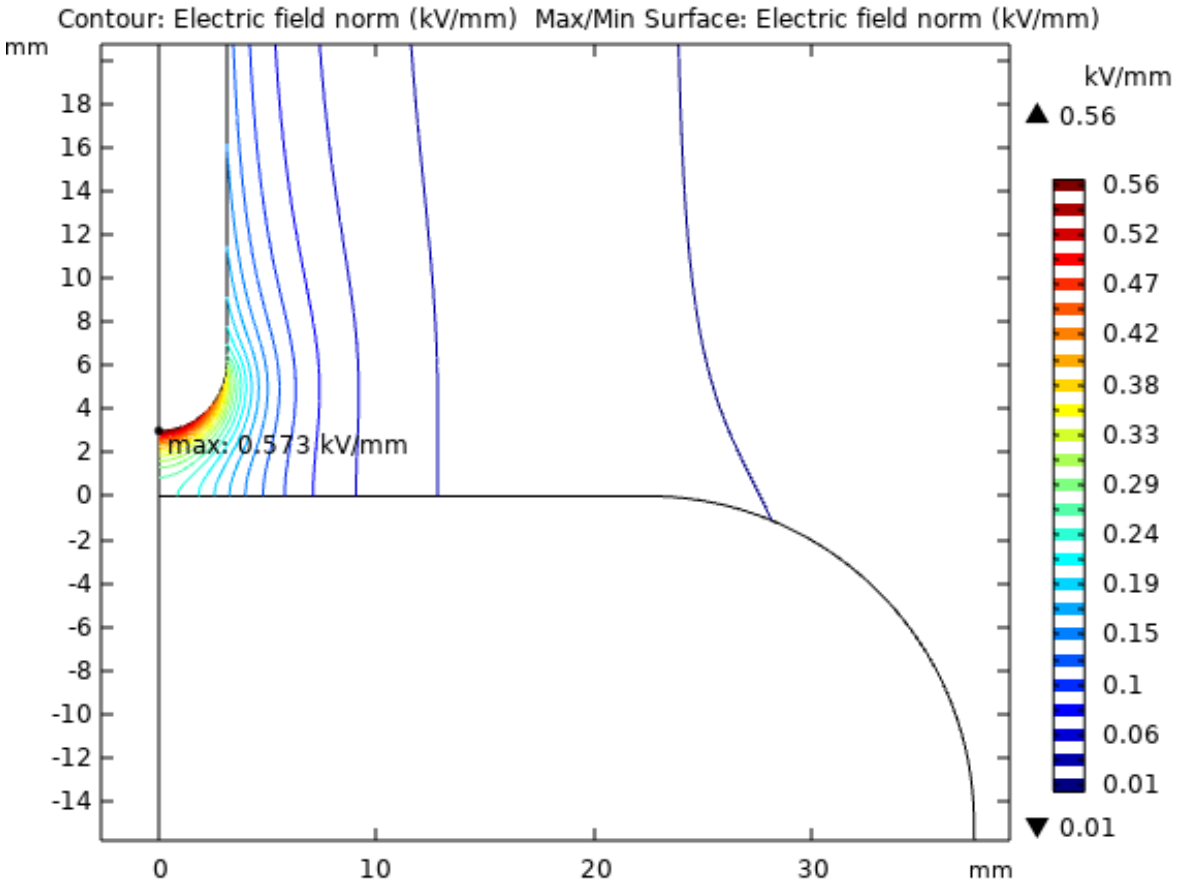

Figure 3.8 Electrode simulation results for maximum and minimum element sizes equal to 0.1 mm and to 0.001 mm for the meshing criteria respectively, with the electrode gap equal to 3 mm for a 6.25 mm diameter-rod-pane and an applied voltage of 1 kV.

As shown in Figure 3.8, the location of E_{max} is at the head of the rod where it should be. The f factor can be calculated using Equations 2.5 and 2.6 shown previously, with the f factor equal to (1/3/0.573) = 0.582, which is comparable to the f found in GIL [16].

Changing the gap distance or rod diameter will modify the f factor. For the rest of the used rod-plane electrode configurations at varying rod diameters and gap distances between 3.5-12.5 mm and 5-55 mm, respectively, a similar criterion to Figure 3.8 was used to simulate the E_{max} for each case, with the f factor then calculated as the ratio of the mean electric field and E_{max}. The calculated f values for the three test configurations over a range of gaps are presented in Figure 3.9.

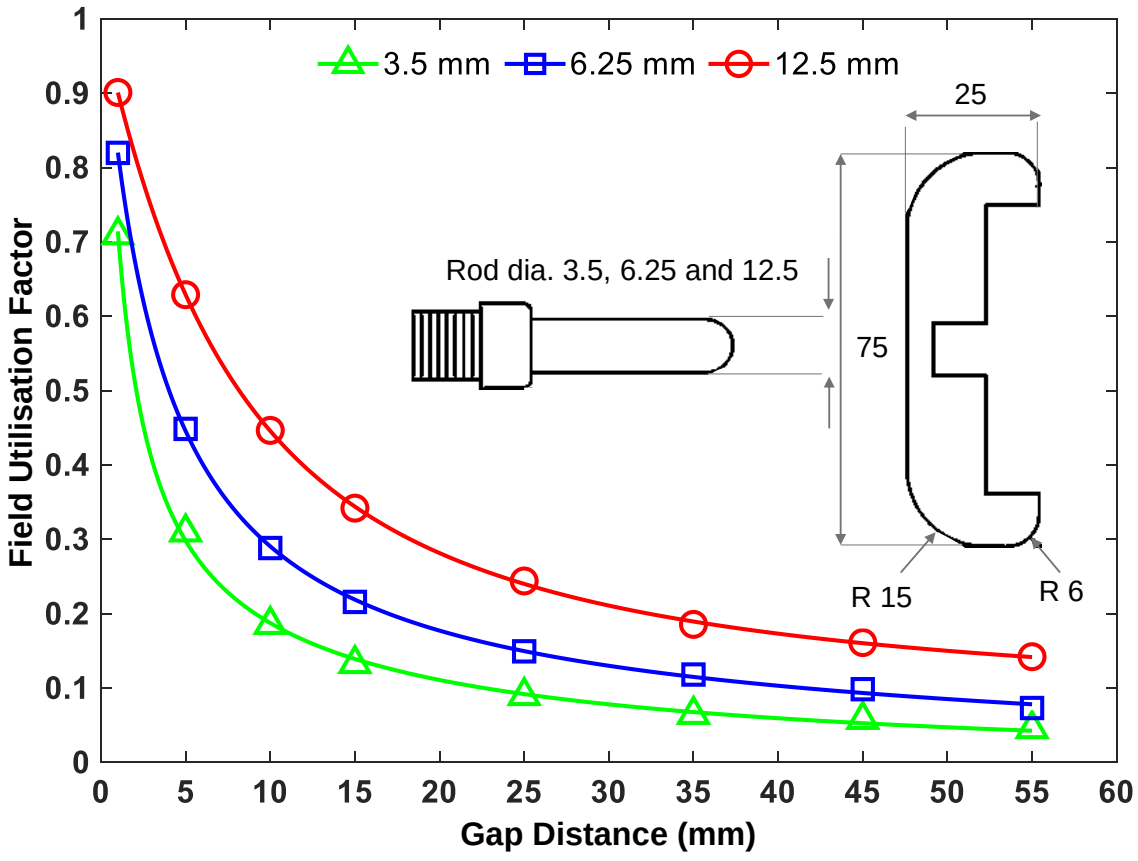

Figure 3.9 Plot of f values for rod-plane configurations with a rod diameter of 3.5, 6.25 and 12.5 mm over the gap spacing range.

Rod-Plane Electrode Material

Three identical sized rod-plane electrodes with a rod diameter of 6.25 mm were fabricated in stainless steel, brass and aluminium as they are the commonly used materials for electrical discharge experiments assessing the effect of electrode materials on the breakdown voltage when investigating the effect of exposing an insulation gas to 300 breakdown events. The key properties of stainless steel, aluminium and brass are summarised in Table 3.1. In terms

of material robustness, stainless steel provides the highest mechanical robustness property, followed by brass and then aluminium. The work function of stainless steel and aluminium is comparable.

Table 3.1 Material specifications for the used stainless steel, aluminium, and brass electrodes. Aluminium alloy could have a higher work function value than the pure one [111], [131]–[133].

Material	Tensile Strength (MPa)	Hardness (HB)	Melting Point (°C)	Work Function (eV)
Stainless steel 316L	485 - 561	95 - 217	≈1375	≈4.9
Aluminium HE30 alloy	295 - 354	95 - 110	≈555	≈4.6 (pure aluminium)
Brass CZ121	360 - 429	90 - 160	≈900	≈3.4

Rod-Plane Electrode Surface Roughness and Measurement

All fabricated rod-plane electrodes were polished to a mirror surface finish with an average surface roughness (R_a) of 0.2 µm and a maximum surface roughness (R_z) of less than 2 µm. The Jenoptik wave line W5 device was used to measure R_a and R_z values as per ISO 4287 [134] before and after testing, with at least three measurements taken to obtain average roughness parameters. The definition of R_a and R_z is shown in Figure 3.10.

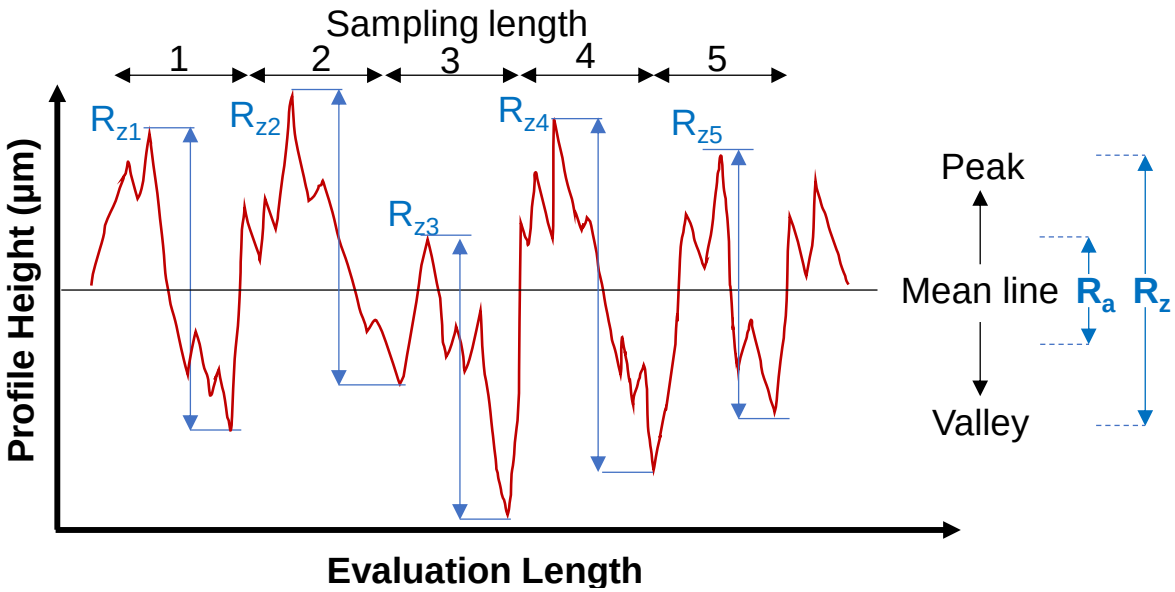

Figure 3.10 An illustration of R_a and R_z specified in ISO 4287 [134].

All measurements were obtained from the middle of the rod-plane electrode where most of the discharges occur. The sampling length was set at 1.5 mm distance at a speed of 0.15 mm/sec along the electrode's surface. Before measuring surface roughness, the accuracy of the measuring probe was checked against a calibration set (a pre-determined surface

roughness block) to ensure the accuracy of the subsequent measurement. Figure 3.11 shows photographic examples of surface roughness measurements and the calibration surface.

(a)

(b)

Figure 3.11 Surface roughness measurements of a polished electrode surface by (a) the JENOPTIK W5 surface roughness measurement device and (b) a calibration set.

3.3.2 Reduced Scale Coaxial Configurations

Optimal Coaxial Electrode Ratio

The most common geometry in gas insulated equipment such as GIB and GIL is a coaxial cylindrical design, which is considered to be a quasi-uniform field. It consists of two concentric pipes (conductor and enclosure) (as illustrated in Figure 3.12) made of aluminium (Al) [2].

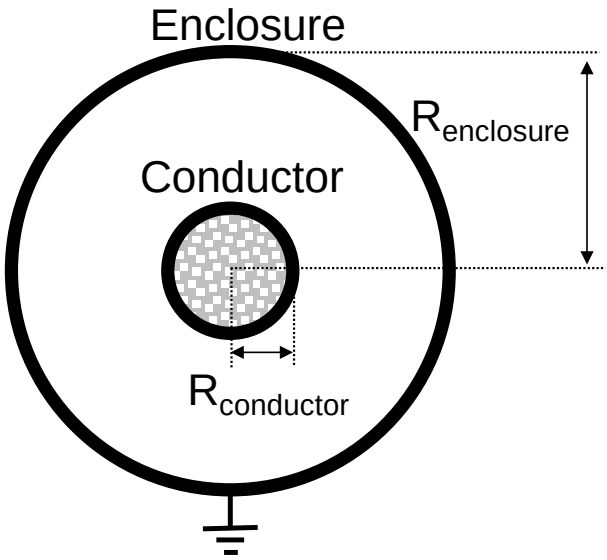

Figure 3.12 Cross sectional view of coaxial geometry.

In the coaxial design, there is a trade-off between gap distance and maximum electric field or field uniformity between the outer conductor radius ($R_{conductor}$) and the inner radius of the enclosure ($R_{enclosure}$). The maximum breakdown voltage is attained at the optimal ratio between $R_{enclosure}$ and $R_{conductor}$, with this ratio found when $\ln(R_{enclosure}/R_{conductor}) = 1$, where $R_{enclosure}/R_{conductor}$ is equal to ≈ 2.72 or within a range of 2.5-3, resulting in the lower E_{max} values [135]. E_{max} in coaxial designs should be located at the surface of the inner conductor where breakdown is likely to occur and influenced by the applied voltage level (U), $R_{conductor}$ and $R_{enclosure}$. Equations 3.1 and 3.2 show the calculated E_{max} and f factor in coaxial geometry, respectively [15].

$$E_{max} = \frac{U}{R_{conductor} \cdot \ln\left(\frac{R_{enclosure}}{R_{conductor}}\right)} \tag{3.1}$$

$$f_{coaxial} = \frac{E_{mean}}{E_{max}} = \frac{R_{conductor} \cdot \ln\left(\frac{R_{enclosure}}{R_{conductor}}\right)}{R_{enclosure} - R_{conductor}} \tag{3.2}$$

Considering a coaxial design example, with an inner enclosure diameter equal to 30 mm and an outer conductor diameter equal to 10 mm (10/30 coaxial electrode design), FEA was conducted using COMSOL to determine the E_{max} for different $R_{conductor}$ varying from 2-10 mm and then validated through the calculated values obtained from Equations 3.1 and 3.2. The results are shown in Figures 3.13. and 3.14.

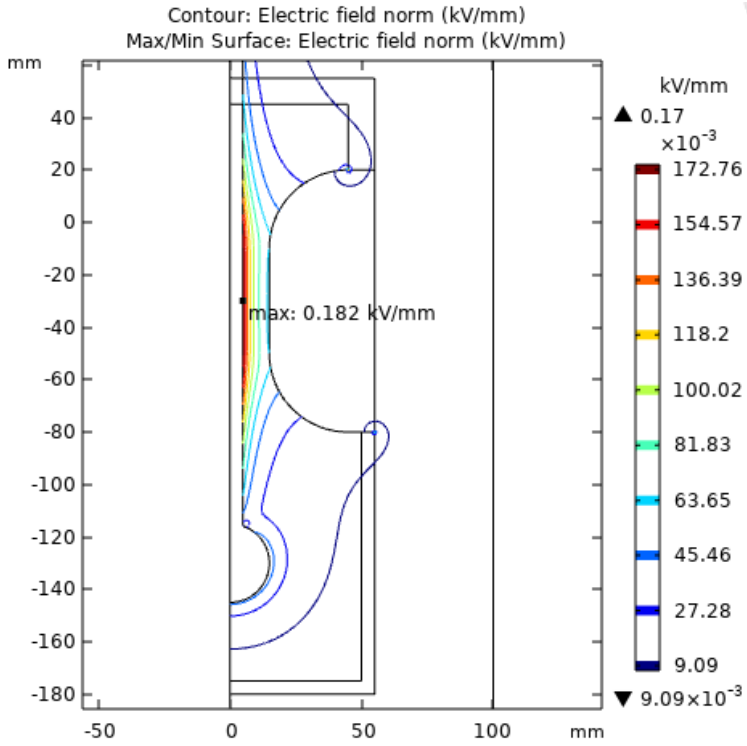

Figure 3.13 Electric field simulation for a 10/30 coaxial electrode design with an applied voltage of 1 kV (mesh size: 0.0005 mm minimum element size and 0.5 mm maximum element size).

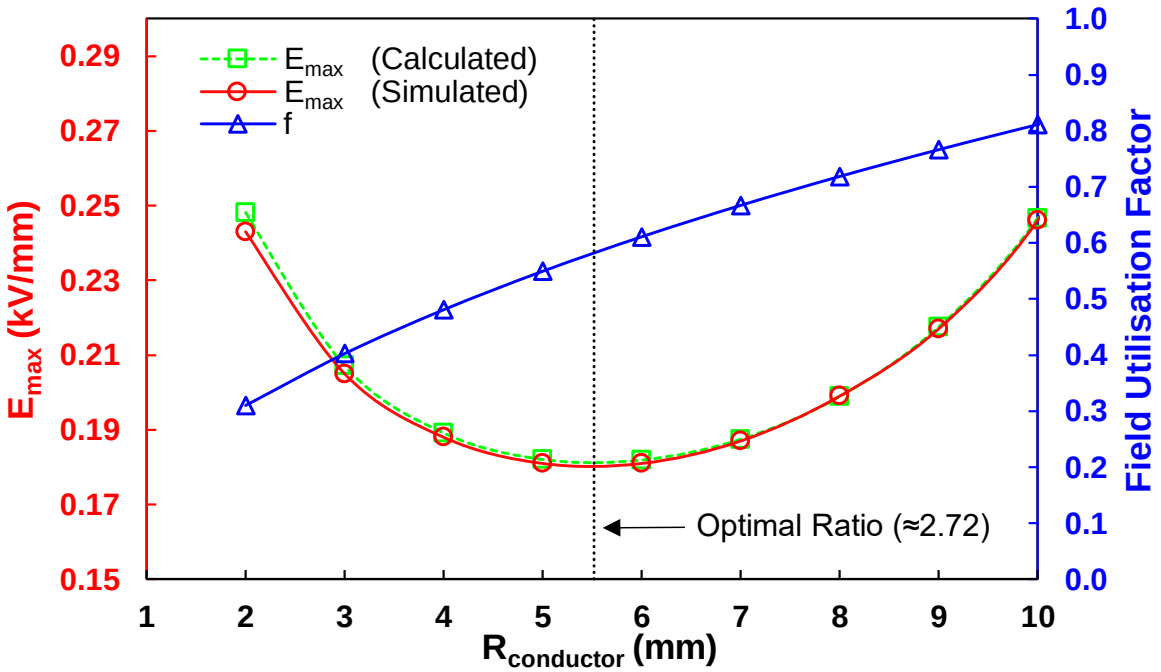

Figure 3.14 Maximum electric field and field utilisation factor against a different outer conductor radius for a fixed enclosure radius of 15 mm with an applied voltage of 1 kV.

As Figure 3.14 shows, for $R_{enclosure}/R_{conductor}$ ratios of 2.5-3, which is close to the optimal ratio (≈2.72), E_{max} will be close to its minimum value. Thus, the minimum electric field intensity will be applied that most likely to have the maximum breakdown voltage in comparison with other $R_{enclosure}/R_{conductor}$ ratios [79].

The coaxial optimal ratio has been adopted worldwide in the design of the geometrical dimensioning of GIL systems, as reported by AZZ CGIT [136]. Detailed dimensions are shown for all their GIL systems for a voltage range between 72.5-1200 kV. The maximum system operating voltage was plotted against the $R_{enclosure}/R_{conductor}$ ratio shown in Figure 3.15, with the $R_{enclosure}/R_{conductor}$ ratio close to the optimal ratio (2.5-3). Moreover, for voltage levels of 800 kV and 1200 kV, the $R_{enclosure}/R_{conductor}$ ratio reaches around 3.7. This indicates for extra high voltage levels, gap spacing is more dominant on field uniformity.

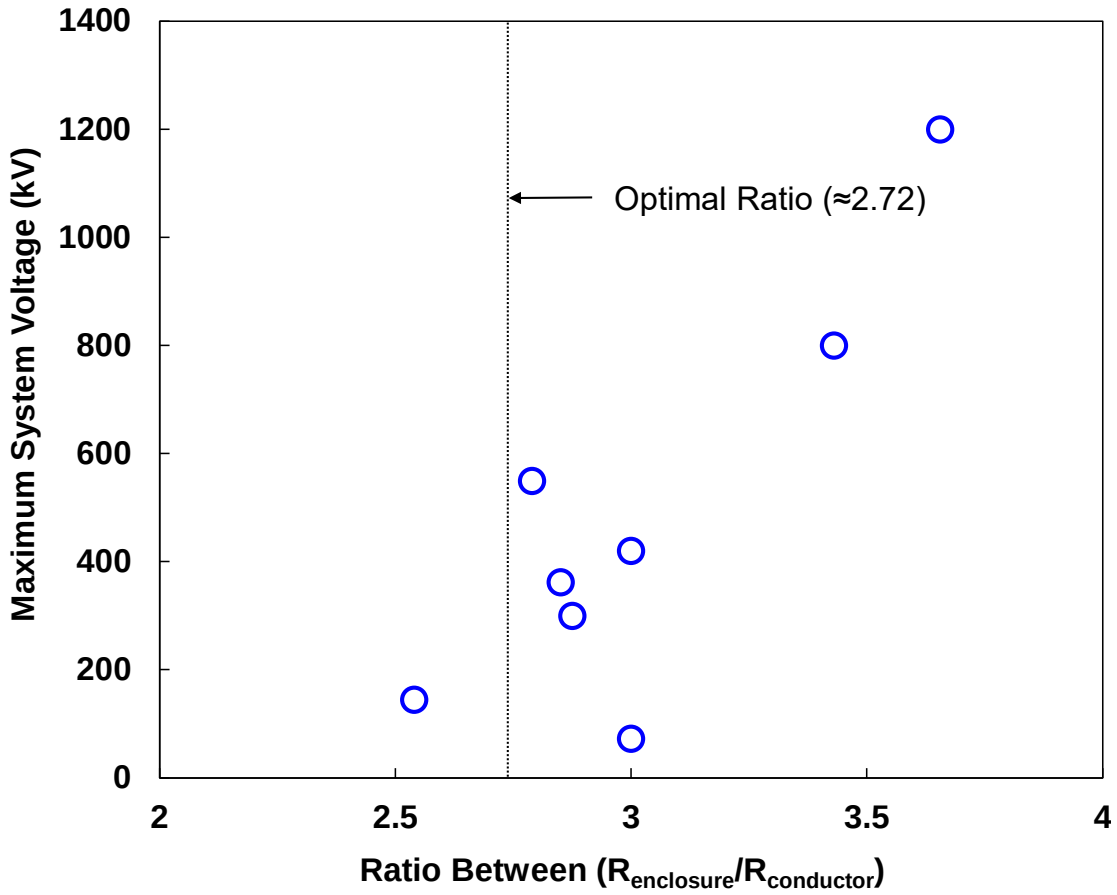

Figure 3.15 $R_{enclosure}/R_{conductor}$ ratio for the designed GIL as a function of the maximum system operating voltage; data obtained from [136].

Coaxial Electrode Design and Dimensions

Table 3.2 shows all tested coaxial configurations and materials in this current study. Three differently sized conductor/enclosure diameters of 8/30, 10/30 and 15/30 mm were tested to address the effect of the $R_{enclosure}/R_{conductor}$ ratio on the breakdown voltage of different insulation gases. The effect of electrode material was investigated by testing both Al and stainless steel (SS) electrodes in a 10/30 coaxial configuration. All electrodes were made from Al unless specified otherwise. Moreover, the 10/30 coaxial ratio was scaled up to 15/45 and 20/60 to examine the DC breakdown characteristics for a comparative analysis.

Table 3.2 A range of parameters including coaxial geometry, E_{max}, field uniformity and the material tested in this study.

	Coaxial Electrode Diameter (Conductor/Enclosure)					
	10/30		**8/30**	**15/30**	**15/45**	**20/60**
$R_{enclosure}/R_{conductor}$	3		3.75	2	3	3
d (mm)	10		11	7.5	15	20
E_{max} (kV/mm)	0.182		0.189	0.192	0.121	0.091
f	0.55		0.48	0.69	0.55	0.55
Material	Al	SS	Al			

The calculated f values shown in Table 3.2 correspond to the ratio between the E_{mean} and E_{max} as in Equation 3.2. While E_{max} can be computed either using Equation 3.1 or based on FEA simulation using COMSOL.

Coaxial Electrode Conductor Surface Roughness and Measurement

All the tested coaxial electrodes were mirror-finished with a R_a of 0.9 μm and R_z of 8 μm, unless specified otherwise. For the investigations examining the effect of conductor surface roughness on the breakdown voltage in a 10/30 coaxial configuration made from Al, five 10 mm diameter conductors with different machine turned lathe surface finishes were tested and compared (see Table 3.3).

Table 3.3 Tested conductor's surface roughness parameters in a10/30 mm coaxial configuration as per ISO 4287 [134].

Designed Center Line Average (CLA)	**Measured R_a (μm)**	**Measured R_z (μm)**
8 (mirror-finish)	0.86	8.00
16	1.21	8.95
32	1.32	14.65
250	10.74	46.58
750	40.40	121.80

The roughness parameters in Table 3.3 were obtained by following the process illustrated in Figure 3.16 for a 750 CLA conductor using a confocal laser (Keyence VK-X200 laser microscope). All surface measurements and parameters were calculated as per ISO 4287 [134] with a sampling length of 5,000 μm. R_a and R_z in Table 3.3 are the average values of two different locations on the surface of the conductors.

As per ISO 4287 [134], R_a represents the average deviation from the mean line shown in the middle of Figure 3.16(e) as a dashed line, where it does not represent the highest peak/valley.

R_z is the average of five sampling lengths of R_{zi} (average of R_{z1}, R_{z2}, ...) representing the best estimation of the profile, which was used for the analyses presented in this work.

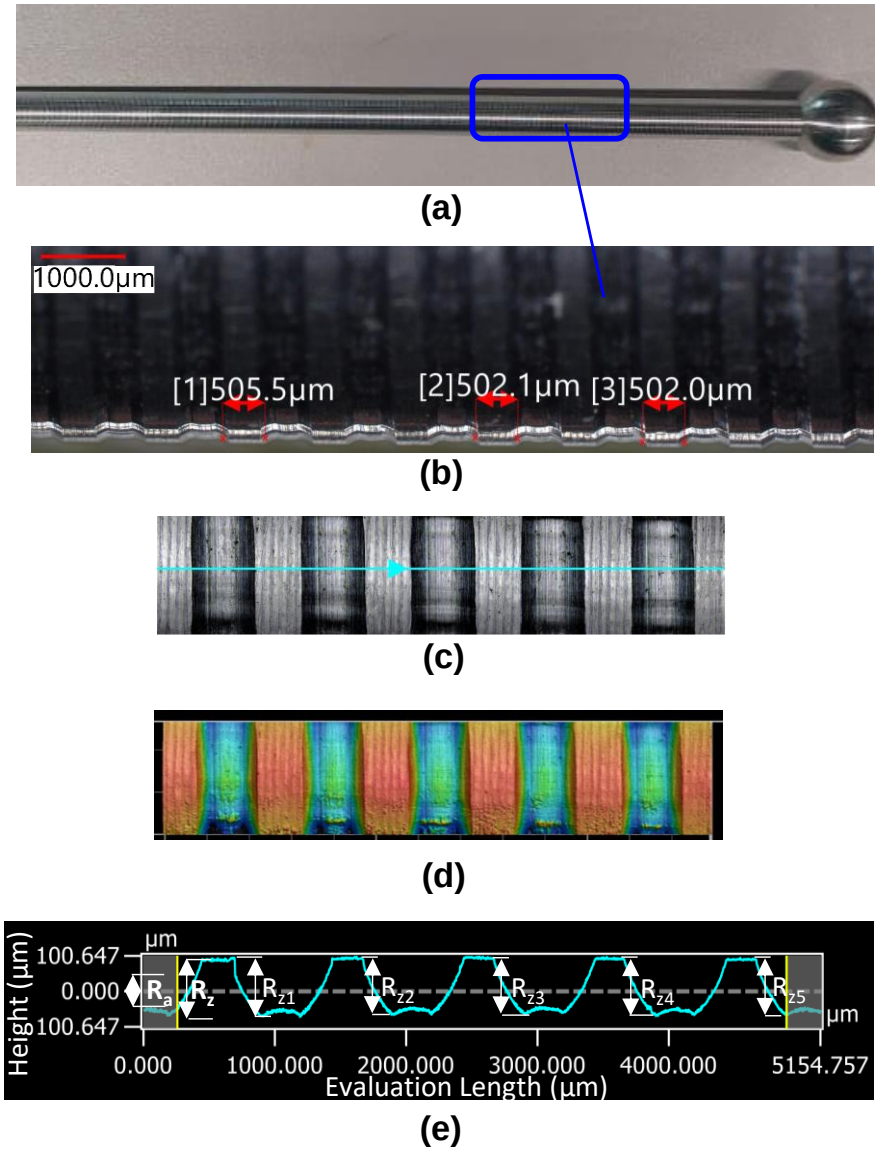

Figure 3.16 An example of a roughness profile for a 750 CLA conductor using a Keyence VK-X200 laser microscope: (a) conductor used, (b) zoomed image measurement for the width of a protrusion of 500 µm, (c) mean surface roughness line and ridges, (d) height image showing peaks in red and valleys in blue and (e) roughness profile over a sampling length of 5,000 µm with R_a and R_z labelled.

3.4 Gas Handling Setup and Procedure

Two different gas carts for handling SF_6 gas and a pre-mixed 20% C_3F_7CN / 80% CO_2 gas mixture were used to avoid the risk of cross contamination. Any new C_3F_7CN/CO_2 and pure CO_2 gas mixtures were filled through direct connection, via a pressure regulator, and assisted using a digital gauge. The detailed equipment and gas handling procedure are discussed in the following sections.

3.4.1 Gas Handling Procedure

Prior to any filling, the vessel was visually inspected and cleaned using isopropyl alcohol (IPA) or ethanol wipes, with any remaining dust inside the vessel removed using a vacuum cleaner. Then, the desired test electrodes were wiped with IPA or ethanol wipes before the final setup. After that, the window was closed and the digital gauge connected, with the vessel vacuumed down to 1 mbar and filled with CO_2 gas above atmospheric pressure for several hours. This was undertaken to ensure the vessel was assembled correctly and had no noticeable leak before vacuuming the vessel down to 1 mbar again. Also, since the CO_2 gas used is dry, it will help absorb any residual moisture. After the preparation step, the designated test gas will be filled in the vessel.

Vacuuming the vessel can be undertaken using a separate vacuum pump and is related to SF_6 gas handling equipment (shown in Figure 3.17) or by a built-in vacuum pump in the C_3F_7CN/CO_2 gas mixture handling cart (shown in Figure 3.18).

SF_6 Gas Handling

A DILO mini-series compact SF_6 gas service cart was used for evacuating air up to 1 mbar for the filling and recovery of SF_6 gas before and after the experiments (shown in Figure 3.17). To fill the vessel, an SF_6 gas cylinder and the vessel were connected to the gas cart at the SF_6 cylinder connection and filling connection, respectively, and by controlling the pressure regulator, the SF_6 gas flowed from the cylinder to the vessel without any need for pumping due to the cylinder pressure being approximately 20 bar. For gas recovery, the vessel was connected to a filter at the recovery location and the pump turned on to push the gas back to the cylinder. The recovery process was completed when the vessel pressure reached below 5 mbar. The digital gauge was used to cross-check the pressure reading.

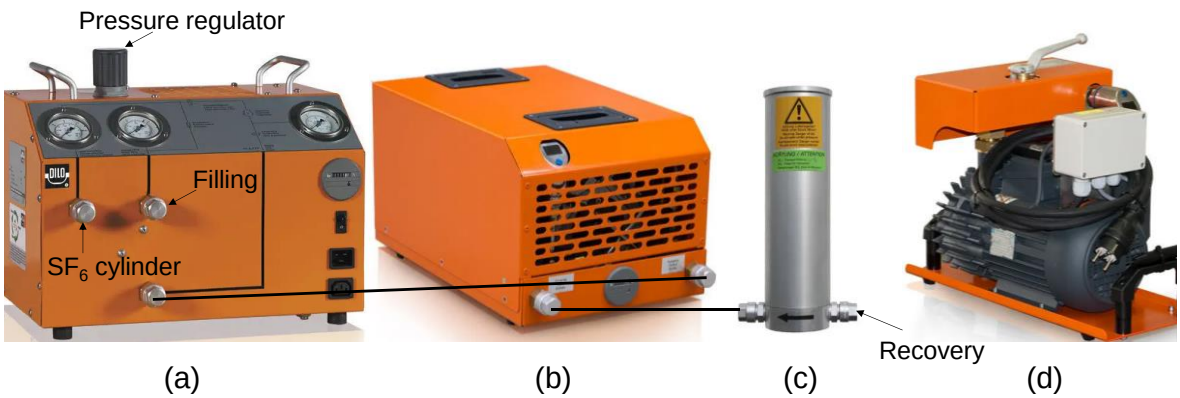

Figure 3.17 DILO mini-series compact SF_6 gas service cart for (a) filling/recovery device, (b) vacuum compressor, (c) filter and (d) vacuum pump for air evacuation.

C_3F_7CN/CO_2 and $C_5F_{10}O/CO_2$ Gas Mixture Handling

A DILO piccolo series gas handling unit was used for evacuation of air down to 1 mbar for the filling and extraction of C_3F_7CN/CO_2 gas mixtures to/from the vessel from/to a storage tank that already had a pre-mixed 20% C_3F_7CN / 80% CO_2 gas mixture (as shown in Figure 3.18).

For the filling or extraction of the gas mixture, the required function was initially chosen from the control unit and the three-way ball valve placed in the required functional position (filling or extraction). During the filling procedure, the flow rate of the gas was controlled via the pressure regulator, while during the recovery, the pressure regulator has to be in a fully open position. When the vessel pressure reaches below 5 mbar, the recovery process was terminated. Also, the pressure reading was cross-checked using the digital gauge. Filling a new C_3F_7CN/CO_2 or $C_5F_{10}O/CO_2$ gas mixture for any of the mixture ratios in the vessel or the storage tank, preparation steps need to be initially performed (digital gauge connection, extraction of air, purging with CO_2 and vacuuming down to 1 mbar), with the gases then filled through direct connection via pressure regulator of C_3F_7CN or $C_5F_{10}O$ and then CO_2 gas bottles based on their partial pressure up to the required final pressure. For example, when filling a 20% C_3F_7CN / 80% CO_2 gas mixture at 5 bar pressure, C_3F_7CN was first filled up to 1 bar, before topping up the CO_2 until it had a final pressure of 5 bar and leaving it for several hours. Then, the final mixture ratio was confirmed via two different commercial gas analysers, which will be discussed in the next section. After the experiment, CO_2 gas was vacuumed and released, with the 20% C_3F_7CN / 80% CO_2 gas mixture recovered to the storage tank. In the case of other mixture ratios and the $C_5F_{10}O/CO_2$ gas mixtures, they were extracted to a waste cylinder to await the final gas disposal process.

(a) (b)

Figure 3.18 20% C_3F_7CN / 80% CO_2 gas mixture handling equipment (a) DILO piccolo series gas handling unit and (b) a storage tank for the pre-mixed gas.

3.4.2 Gas Analysis

The purity and concentrations of the SF_6 gas and C_3F_7CN/CO_2 gas mixture were checked regularly via the use of three different gas analysers (shown in Figure 3.19). A WIKA GA11 gas analyser based on the volume percentage and a DILO C_4 multi-gas analyser based on a mole percentage were used prior to any experiment to confirm the C_3F_7CN/CO_2 mixture ratio. A DILO SF_6 volume percentage measuring device was used to ensure that the SF_6 concentration was higher than 97% because it is the minimum acceptable purity limit for use in insulation applications, as per BS EN/IEC 60480:2019 [137]. The following Table 3.4 shows the measuring ranges and tolerances for each gas analyser.

Table 3.4 Measured gases and tolerances of the used gas analysers.

Gas	Analyser					
	WIKA GA11 (volume %)		**DILO C_4 Multi-gas (mole %)**		**DILO SF_6 (volume %)**	
	Range	**Tolerance**	**Range**	**Tolerance**	**Range**	**Tolerance**
C_3F_7CN	15 - 30%	± 1%	0 - 30%	± 0.2%	-	
O_2	0 - 10%	± 0.3%	0 - 25%	± 0.3%		
CO_2	-		0 - 100%	± 2%		
CO			0 - 500 ppm_v	± 2%		
SF_6			-		0 - 100%	± 0.5%

(a)

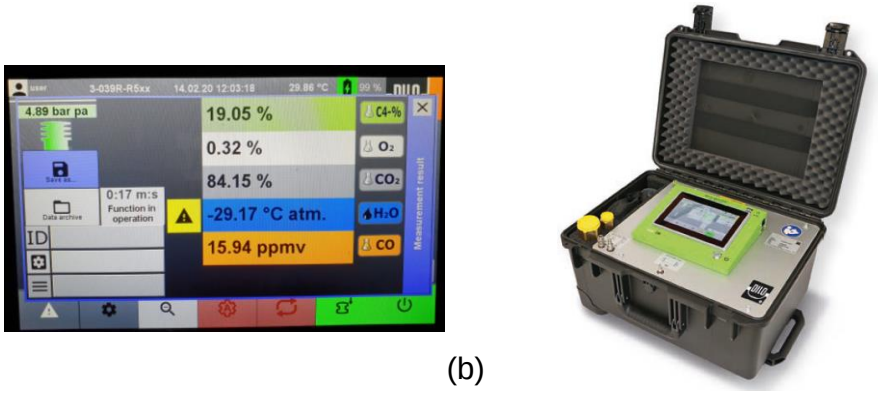

(b)

(c)

Figure 3.19 Measurement examples of the used gas analysers: (a) a WIKA GA11 gas analyser, (b) a DILO C_4 multi-gas analyser and (c) a DILO SF_6 volume percentage gas analyser.

3.4.3 Leakage Detection Instruments

Two commercial gas leak detection devices were used when handling SF_6 and C_3F_7CN (see Figure 3.20). Both devices have the ability to detect a small leak either from the vessel or the gas handling equipment. Ideally, a leak check is performed when the vessel is filled with CO_2 in the preparation step before filling it with any test gas.

(a) (b)

Figure 3.20 Leak detection devices (a) DILO SF_6 and (B) WIKA C_3F_7CN leakage detector devices.

3.5 High Voltage DC Test Setup

DC breakdown tests were performed using a 600 kV, 200 mA HIGHVOLT DC generator (shown in Figure 3.21). The maximum output power of the DC generator is 120 kW with less than a 3% ripple factor and with an automatic voltage regulation and data logging system (HiCOs control and measurement logger). The setup is mounted on a frame base to provide

mobility and has an overall length of about 14 m from the AC transformer up to the voltage divider. Also, the DC voltage polarity can be changed automatically by a motor that controls the diodes in the rectifier column.

The DC voltage generation stages start from the HV AC test transformer, then rectified and smoothed via a rectifier column and a smoothing capacitor, resulting in AC to DC conversion. To protect the DC supply and minimise damage to the test object and electrodes during breakdowns, the output voltage of the smoothing capacitor is connected to an external 6 kΩ current limiting resistor and the system incorporated with a breakdown detection unit located in the earthing of the vessel to ensure a switch-off time of 20-200 ms in the case of a disruptive discharge from the test object. To measure the voltage, a resistive voltage divider (GMR 1200 MΩ / 600 kV) is used to measure the output voltage connected in parallel with the vessel. The DC system is controlled from a control room isolated from the test area by computer-based software (HiCOs) that controls the system voltage, DC polarity, logging of the breakdown data and a motorised earthing system, via a fibre-optic connection (see Figure 3.22).

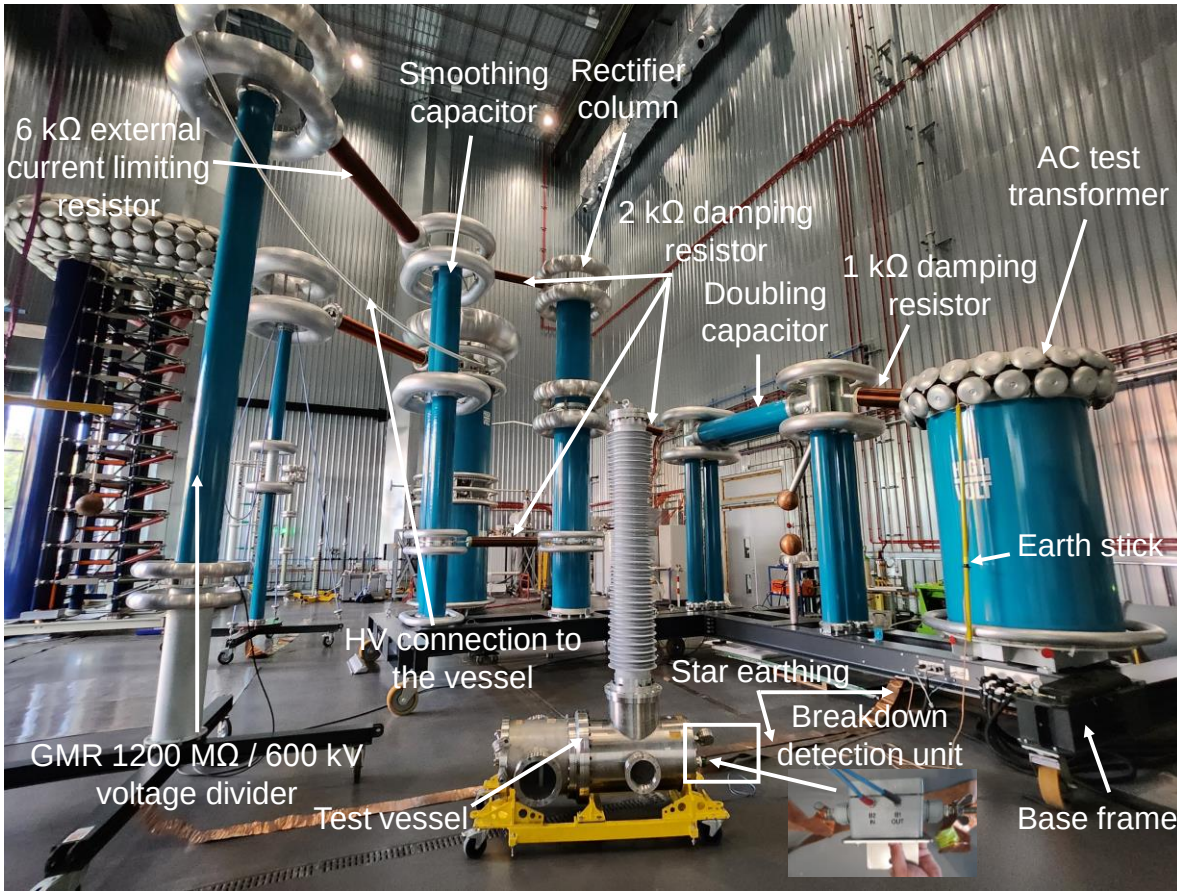

(a)

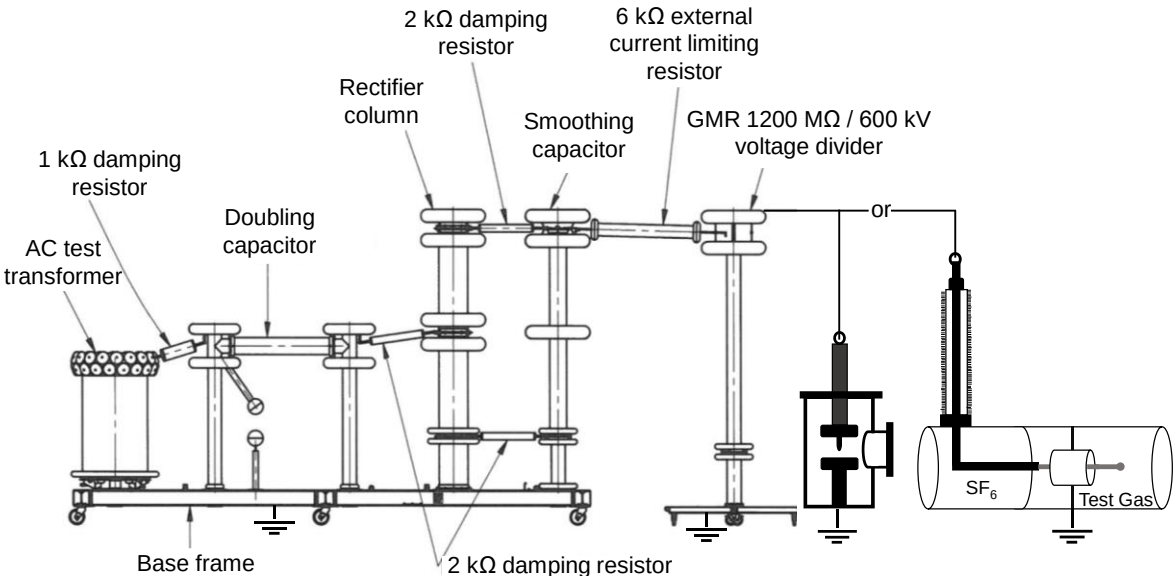

(b)

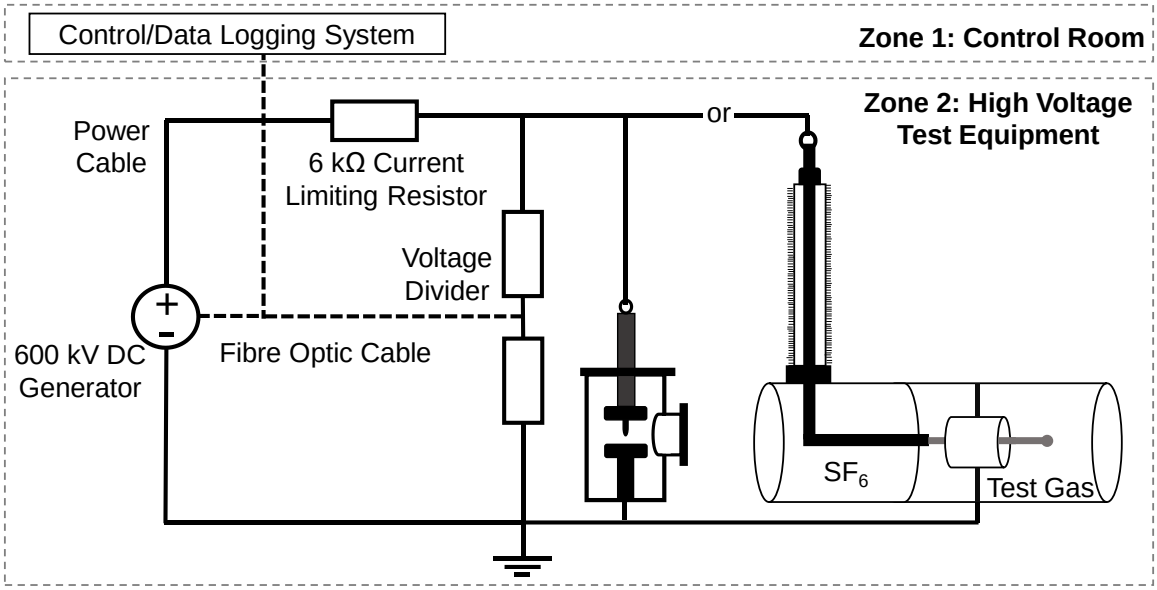

(c)

Figure 3.21 Laboratory setup of the HIGHVOLT DC generator: (a) actual equipment, (b) schematic diagram and (c) equivalent DC circuit.

Figure 3.22 HiCOs computer-based software for controlling the DC generator.

3.6 Experimental Technique and Data Analysis

3.6.1 Experimental Technique

As discussed earlier in the literature review, there are two experimental methods usually used to investigate the DC breakdown characteristics of gases, a multiple level test and a successive discharge test, according to the BS EN 60060-1:2010 standard [98]. Both methods provide almost the same value for $U_{50,}$ as shown in [99].

In this research, all investigations will follow the successive discharge method procedure. Concerning the ramp rate at which the voltage will be increased until disruptive discharge occurs and the time interval between the breakdown event and the next voltage ramp, a comparative investigation will be conducted to determine the effect of waiting time and ramp rate on the breakdown voltage of 20% C_3F_7CN / 80% CO_2 using 25 mm diameter sphere-plane electrodes at a fixed gap of 3 mm (f = 0.85) and pressure of 3 bar. An average value of 15 breakdown events, representing $U_{50,}$ and σ error bars calculated based on Equations 2.27 and 2.28, for a voltage ramp of 1, 2, 5 and 10 kV/s at 2-minute intervals, and a time interval of 1, 2, 4, 6 and 8 minutes at 5 kV/s are shown in Figures 3.23 and 3.24.

From Figures 3.23 and 3.24, the effects of adopting different ramp rates and time intervals show a negligible difference of less than 5% deviation in the U_{50} values. However, the error bars overlapping indicate a comparable breakdown voltage. Therefore, in this research, a voltage ramp of 5 kV/s and 2 minutes waiting time interval will be adopted for all of the experimental work. All tests were conducted at room temperature (≈ 18°C).

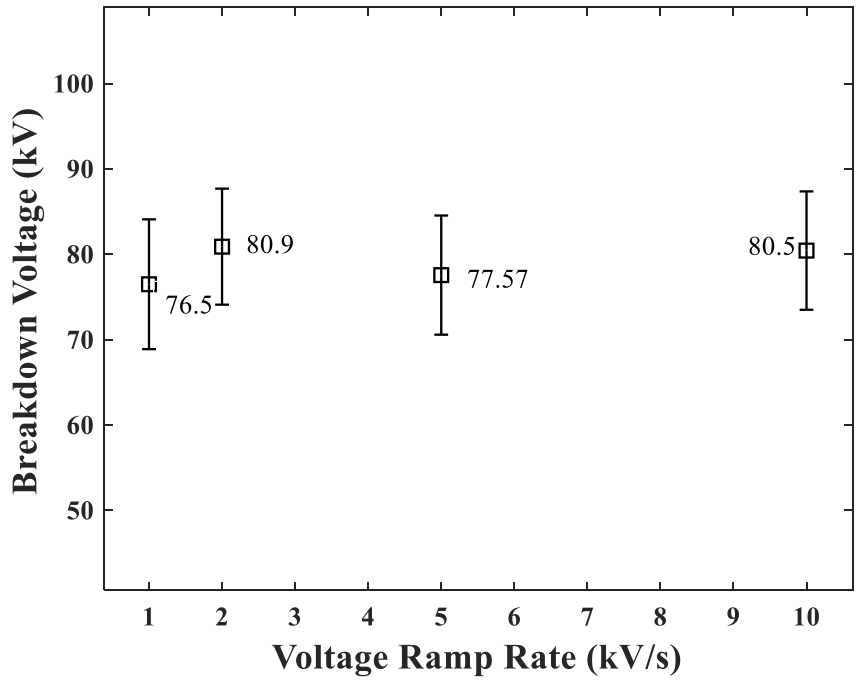

Figure 3.23 Negative DC breakdown voltage of a 20% C_3F_7CN / 80% CO_2 gas mixture using sphere-plane electrodes (25 mm sphere diameter) under 3 bar, a fixed gap of 3 mm and a 2-minute time interval.

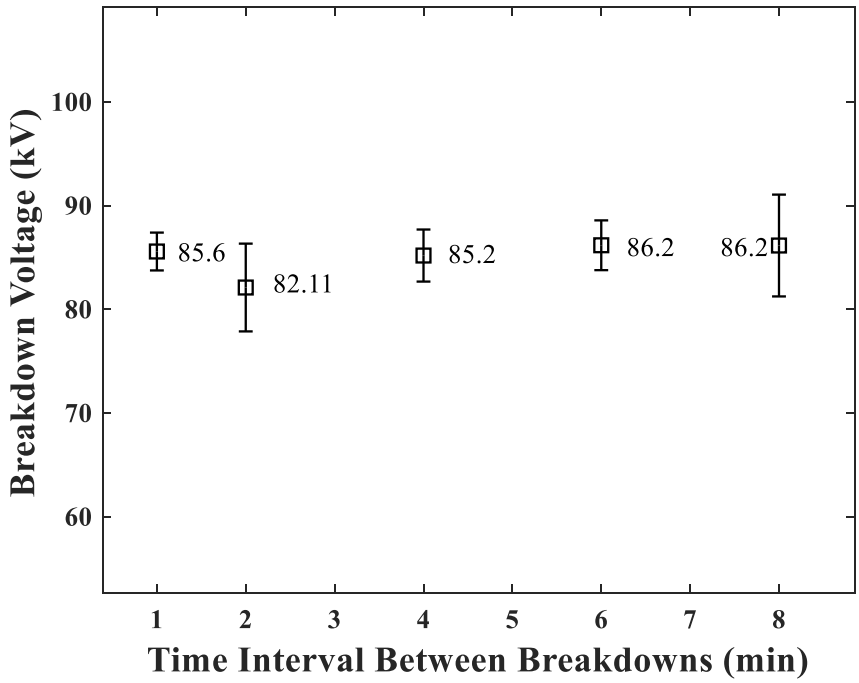

Figure 3.24 Negative DC breakdown voltage of a 20% C_3F_7CN / 80% CO_2 gas mixture using sphere-plane electrodes (25 mm sphere diameter) under 3 bar, a fixed gap of 3 mm and 5 kV/s ramp rate.

3.6.2 Data Analysis

A set of at least 30 breakdowns will be conducted for each test unless specified otherwise. Since breakdown event is a statistical random event, a marginal variation of the breakdown voltage value every breakdown event is expected. Figure 3.25 shows an example of a test data series.

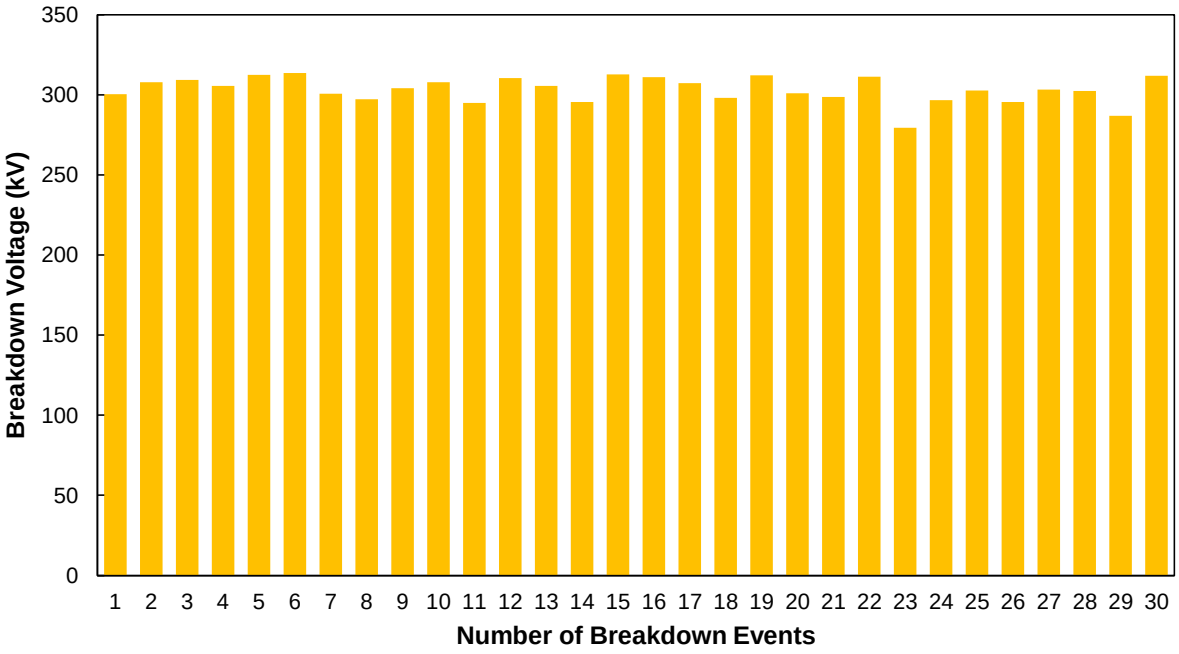

Figure 3.25 Positive DC breakdown voltage of a 20% C_3F_7CN / 80% CO_2 gas mixture using coaxial electrodes (conductor/enclosure diameter of 20/60) under 3 bar pressure.

In order to analyse breakdown data series, 8 data sets were selected randomly from experimental results presented in the next Chapters 4 and 5 that consists of 30 breakdowns each, they will be evaluated based on: (i) Gaussian distribution Z-score analysis with U_{50G} and σ can be calculated using Equations 2.27 and 2.28, (ii) Weibull distribution calculated using derived Equations 3.3 and 3.4 from which the 50% probability of a breakdown (U_{50W}) can be calculated [138], and (iii) a probability distribution with an independent evaluation (assumes a Binomial distribution) presented as a median value (labelled as U_{P50}) with 84.13% and 15.87% percentiles with 75% confidence intervals calculated using Equations 3.5 and 3.6 [52], [139].

$$F = \frac{n - 0.5}{N} \tag{3.3}$$

$$\underset{'\boldsymbol{Y_n}'}{ln(Breakdown\ voltage)} = \underset{'\boldsymbol{Slope}\cdot\boldsymbol{X_n}'}{\frac{1}{B}\ln\left(-\ln(1-F)\right)} + \underset{'\boldsymbol{Y_n}\ \boldsymbol{intercept}'}{ln(\lambda)} \tag{3.4}$$

Where, F is the accumulative probability of breakdown voltage, n is the n^{th} order of the breakdown event, N is the total number of breakdowns, B is the shape parameter, λ is the scale parameter of the Weibull distribution and Y_n and X_n are normalised y-axis and x-axis of a linear equation representation.

$$P\{S_m \le P_{prc}\} = P\{S_{bdn-m+1} > P_{1-prc}\} = 1 - \sum_{j=0}^{m-1}\left(\frac{bdn}{j}\right)prc^j(1-prc)^{bdn-j} \tag{3.5}$$

$$\left(\frac{bdn}{j}\right) = \frac{bdn!}{j!\cdot(bdn-j)!} \tag{3.6}$$

From Equations 3.5 and 3.6, by ordering the breakdown voltages in an ascending order with a list of samples S_i, i=1…bdn, where the total number of breakdowns is bdn, with $1 \le m \le bdn / 2$ and m represents any integer. P_{prc} represents the threshold point where a certain percentage of measurement points fall below, while prc denotes the percentile. P{ } represents the confidence of the percentile. And j is an identifier used for adding up values. As an example of calculation, considering a sample of 30 breakdowns, with 84.13% and 15.87% percentiles with a 75% confidence: $P\{S_m \le P_{0.1587}\} = 0.75$, as a result, $0.75 \le 1 - \sum_{j=0}^{m-1}\left(\frac{30}{j}\right)0.1587^j(1-0.1587)^{30-j}$, the lowest m value at which this condition is satisfied will deliver the 15.87% percentile value, which is equal to 3. While for the 84.13% percentile, it is equal to bdn – m + 1 = 30 – 3 + 1 = 28. In the case if the data is consistent with Gaussian distribution, the median will correspond to the mean (U_{50G}), and the 84.13% and 15.87% percentiles with 75% confidence can be calculated as the difference between U_{50G} and σ [52], [139].

For the example shown in Figure 3.25, the data for the 30 breakdowns were fitted to both Gaussian and Weibull distribution probability plots, with the results shown in Figure 3.26. While Figure 3.27 shows an evaluation of the data set based on the median and 84.13% and 15.87% percentiles with 75% confidence intervals. For the other randomly chosen data sets,

a comparison of the calculated U_{50} or median values and their uncertainty margins are shown in Table 3.5.

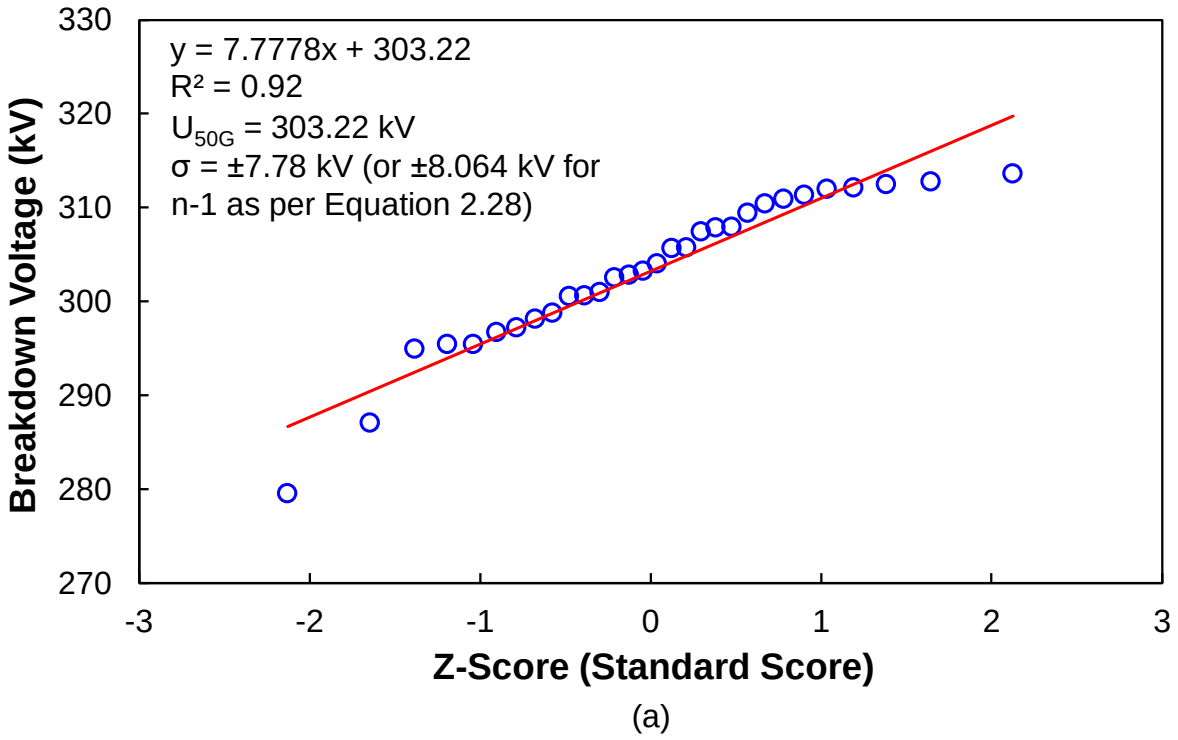

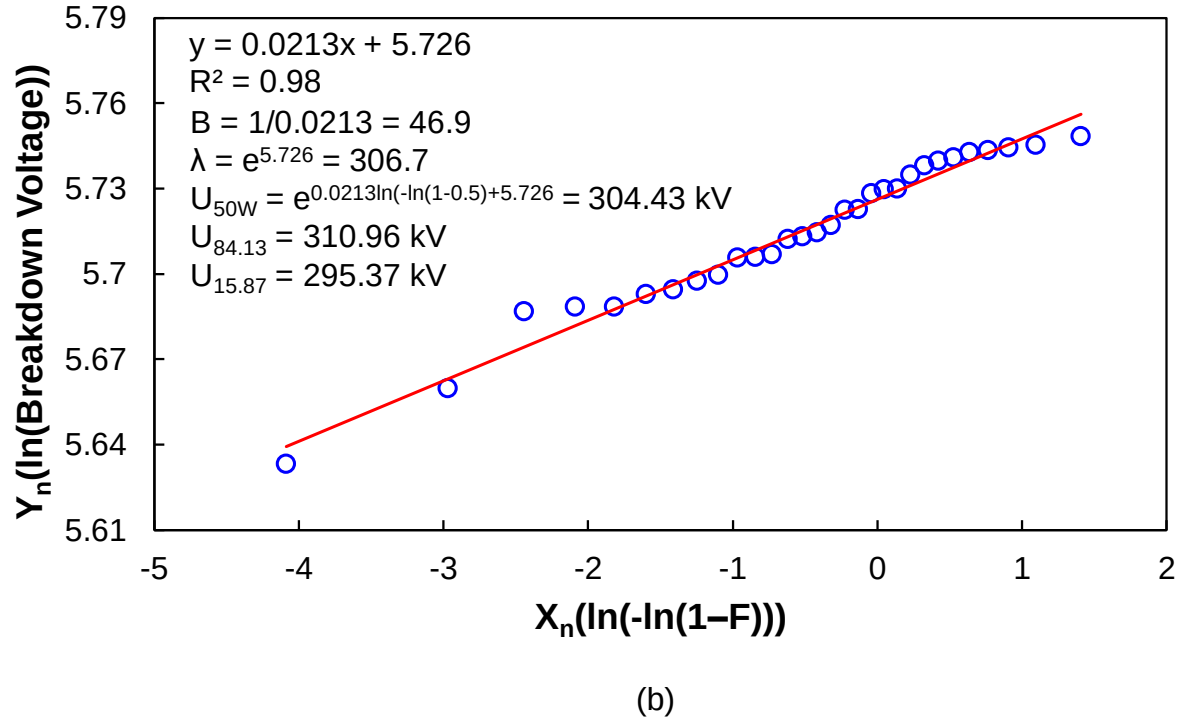

Figure 3.26 Positive DC breakdown voltage of a 20% C_3F_7CN / 80% CO_2 gas mixture using coaxial electrodes (conductor/enclosure diameter of 20/60) under 3 bar pressure, with results fitted to (a) Gaussian distribution and (b) Weibull distribution probability plots. R^2 is the coefficient of determination.

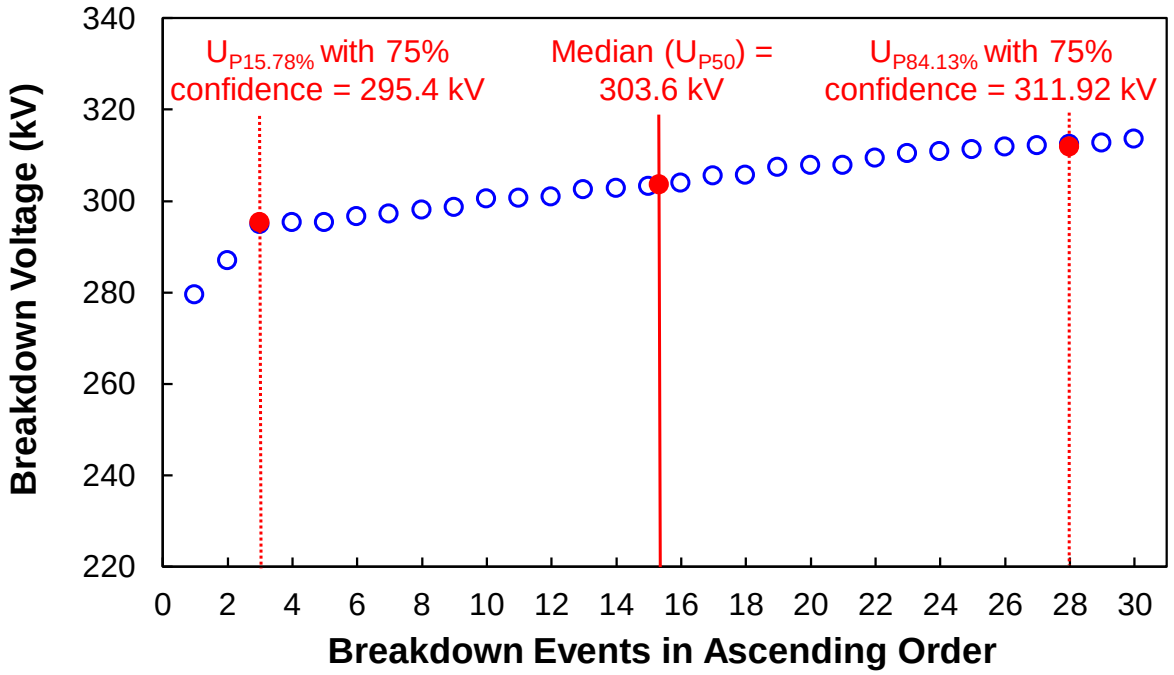

Figure 3.27 Positive DC breakdown voltage of a 20% C_3F_7CN / 80% CO_2 gas mixture using coaxial electrodes (conductor/enclosure diameter of 20/60) under 3 bar pressure, with results in an ascending order and evaluated based on the median labelled as U_{P50}, 84.13% and 15.78% percentiles with 75% confidence.

According to Figure 3.26, the fitted data is consistent with both distributions with a coefficient of determination (R^2) well above 0.85. Therefore, both fittings indicate a good data fit for the 30 data points.

From Table 3.5, there is a negligible difference between the calculated U_{50G} from the Gaussian distribution and both U_{50W} and U_{P50} values of less than 1.1% and 1.5% respectively, and a comparable uncertainty margin calculated from all the approaches. Also, the coefficient of variation obtained from the ratio of the difference between $U_{84.13\%}$ and $U_{15.78\%}$ (or σ) from the mean U_{50} in the case of Gaussian and Weibull distributions (or $U_{P84.13\%}$ and $U_{P15.78\%}$ percentiles with 75% confidence from the median) is around ±10% indicating a relatively low variability in the data with a small uncertainty margin for all the randomly selected data series. This suggests any evaluation method is viable.

Accordingly, the comparison of the DC breakdown characteristics of different tested insulation gases shown in the result figures of the following Chapters 4, 5 and 6 will be based on the U_{50} and σ values representing the average value of breakdowns and error bar respectively, following Gaussian distribution for simplicity, and calculated as per Equations 2.27 and 2.28.

Table 3.5 Comparison of the U_{50G}, U_{50W} and U_{P50} values for 8 randomly selected tests in 20% C_3F_7CN / 80% CO_2.

Test	Gaussian distribution				Weibull distribution			Median and Percentiles with 75% Confidence		Difference (%)	
	U_{50G} (kV)	σ (kV)	$σ/U_{50G}$ (%)	R^2	U_{50W} (kV)	$U_{84.13}$-U_{50W}, $U_{15.87}$-U_{50W} (kV)	R^2	U_{P50} (kV)	$U_{P84.13}$-U_{P50}, $U_{P15.87}$-U_{P50} (kV)	$(U_{50W}-U_{50G})/U_{50G}$	$(U_{P50}-U_{50G})/U_{50G}$
+DC, coaxial ratio 20/60 at 3 bar	303.22	±8.06	2.7	0.92	304.43	+6.5 -9	0.98	303.6	+8.32 -8.2	0.4	0.1
-DC, coaxial ratio 20/60 at 3 bar	238.84	±10.27	4.3	0.93	240.32	+8.4 -11.5	0.97	240.35	+8.88 -11.33	0.6	0.6
+DC, coaxial ratio 10/30 at 5 bar	236.7	±11.21	4.7	0.91	238.34	+9.3 -12.7	0.96	237.1	+12.4 - 8.26	0.7	0.2
+DC, coaxial ratio 10/30 at 1 bar	60.72	±0.87	1.4	0.97	60.86	+0.69 -0.96	0.98	60.88	+0.67 - 1.15	0.2	0.3
+DC, 6.25 mm diameter rod-plane, 25 mm gap and at 5 bar	212.82	±19.71	9.3	0.95	215.19	+16.86 -21.85	0.97	214.6	+16.22 -26.21	1.1	0.8
+DC, 6.25 mm diameter rod-plane, 35 mm gap and at 3 bar	160.31	±10.86	6.8	0.98	161.75	+9.02 -11.99	0.95	162.05	+10.1 - 15.14	0.9	1.1
+DC, 6.25 mm diameter rod-plane, 45 mm gap and at 5 bar	230.5	±18.85	8.2	0.93	232.92	+16.28 -21.3	0.97	233.95	+15.9 - 18.93	1	1.5
+DC, 6.25 mm diameter rod-plane, 45 mm gap and at 1 bar	107	±2.23	2.1	0.97	107.36	+1.85 -2.57	0.89	107.05	+2.33 - 2.66	0.3	0.1

3.7 Summary

This chapter discussed the laboratory test equipment, electrodes, gas handling setup and procedure, and experimental technique used to carry out the investigation on SF_6 and its alternatives under DC voltage. Two different sized pressure vessels were used for the investigations with bushing ratings of 90 and 300 kV_{DC}.

Different types of electrode configurations were designed to examine the DC breakdown characteristics of SF_6 and other alternatives. These were rod-plane and reduced-coaxial electrodes with a range of rod diameters between 3.5-12.5 mm and electrode separations of 5-55 mm, and a coaxial geometries conductor/enclosure with diameters of 8/30, 10/30, 15/30, 15/45 and 20/60 mm, including electrodes with different surface roughness and made of different materials. These were selected to provide a range of field uniformities and electrodes with a practical surface finish and materials typically found in the designs of GILs, GIBs and switches inside ring main units.

A HVDC generator rated up to 600 kV was used to perform the breakdown experiments under both DC polarities. The successive discharge method was used for the DC breakdown test procedure in accordance with the BS EN 60060-1:2010 standard [98]. A voltage ramp of 5 kV/s was used until a breakdown occurred, with a time interval of 2 minutes between successive breakdowns. Voltage ramps and time intervals between 1-10 kV/s and 1-8 minutes were shown to have a negligible effect on the breakdown voltage in the conducted experiment. For the data analysis, an average value and standard deviation (σ) will be calculated for 30 breakdowns for each test to represent a 50% breakdown voltage (U_{50}) and error bar, respectively, as in Equations 2.27 and 2.28.

4 DC BREAKDOWN CHARACTERISTICS OF SF_6 AND ITS ALTERNATIVES IN ROD-PLANE CONFIGURATIONS

4.1 Introduction

This chapter experimentally studies the DC breakdown characteristics of SF_6, CO_2 gases and a 20% C_3F_7CN / 80% CO_2 gas mixture under varying field uniformities using a hemispherical rod-plane configuration with different rod diameters. First, the influence of using different electrode material on the DC ageing test for the 20% C_3F_7CN / 80% CO_2 gas mixture was investigated. 300 breakdown events were applied to the proposed gas mixture to cause clear damage to the used identically sized electrodes, made from stainless steel, aluminium and brass, all with the same gas pressure and gap distance. Also, this investigation examines the changes of the breakdown voltage value over a number of breakdown events to help inform a decision on when to replace the gas mixture and electrodes for future breakdown testing under similar test conditions. Then, a comprehensive study was conducted on the effect of DC polarity on the breakdown characteristics of SF_6, CO_2 gases and a mixture of 20% C_3F_7CN / 80% CO_2 under different gas pressures and field uniformities, achieved via use of three differently sized hemispherical rod diameters and various gap distances. This allows for a comparative evaluation of SF_6 and its proposed alternatives under comparable test conditions covering a wide range of field uniformity (varying gap distance and rod diameter) and gas pressures comparable to the one found in HV equipment.

4.2 The Effect of Repeating Breakdown on Negative DC Breakdown Characteristics of a 20% C_3F_7CN / 80% CO_2 Gas Mixture

This section examines the combined effects of electrode material and electrical ageing by repeating breakdowns on a 20% C_3F_7CN / 80% CO_2 gas mixture at 4.8 bar. Rod-plane electrodes fabricated in stainless steel, aluminium and brass electrodes were experimentally examined by allowing up to 300 breakdowns to determine their breakdown characteristics

under negative DC voltage stress and to generate a sufficient amount of damage on the surface of the electrodes used in the small-scale vessel. The test electrode in this experiment aims to illustrate a small-scale conceptual design of a quasi-uniform field commonly found in gas insulated equipment. This is achieved using a hemisphere 6.25 mm diameter rod-plane electrodes with a gap distance of 3 mm. The gap distance was set using a 3 mm slip gauge. With every electrode material setup, a new (non-tested) 20% C_3F_7CN / 80% CO_2 gas mixture was mixed up to 4.8 bar and analysed before and after each experiment.

4.2.1 Negative DC Breakdown Characteristics

Figure 4.1 shows the breakdown trend of 300 negative DC breakdowns for the tested electrode materials under 4.8 bar. The results in Figure 4.1 demonstrate that stainless steel has a comparatively higher breakdown voltage than aluminium and brass electrodes, with brass exhibiting the lowest performance.

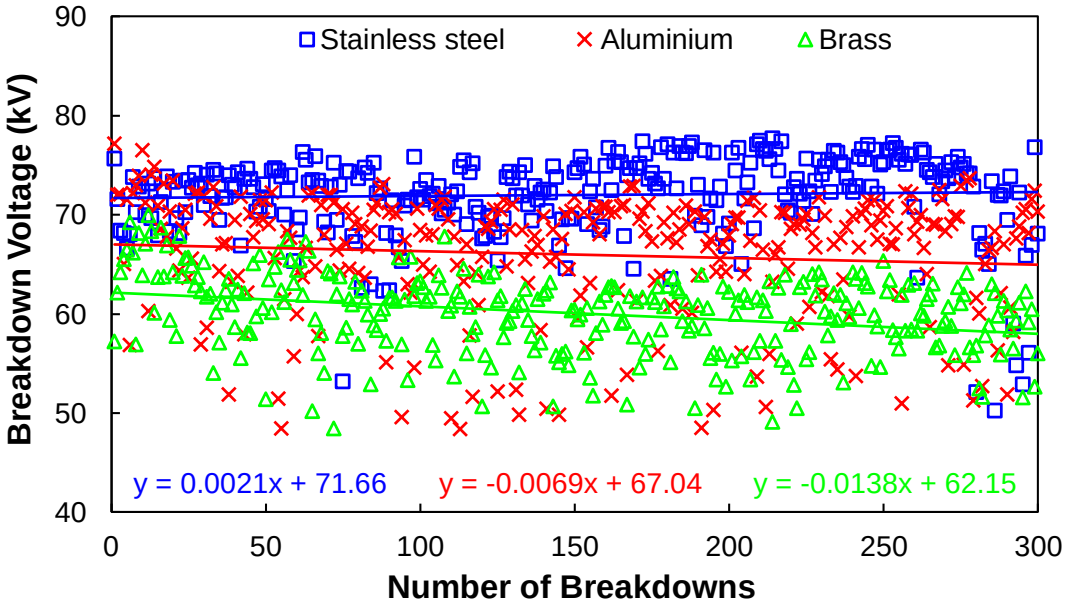

Figure 4.1 Negative DC breakdown characteristics of a 20% C_3F_7CN / 80% CO_2 mixture tested using a rod-plane configuration (6.25 mm rod diameter), for stainless steel, aluminium and brass, a fixed gap of 3 mm and a pressure of 4.8 bar. The straight lines represent the best fit in each case.

Figure 4.2 presents the average voltage of the first and last 20 breakdowns, with Figure 4.3 evaluating the average value for all data sets every 20 breakdowns. As shown in Figure 4.2, the average voltage of the first 20 breakdowns for both aluminium and stainless steel were comparable, with brass being the lowest. This could be a result of the variations in the work function of the electrode materials as it concerns the minimum energy required to de-attach an electron from a solid surface. Therefore, an electrode material with a high work function

will likely have a higher breakdown voltage [107]. Since both aluminium and stainless steel has a comparable work function (see Table 3.1), thus, a similar breakdown voltage performance might be expected for the polished electrodes. Nevertheless, the effect of work function on the breakdown voltage is highly debated in the literature (see Section 2.8.4), as breakdown voltage order does not always follow the highest work function electrode due to the effect of possible oxide layers on some materials [110].

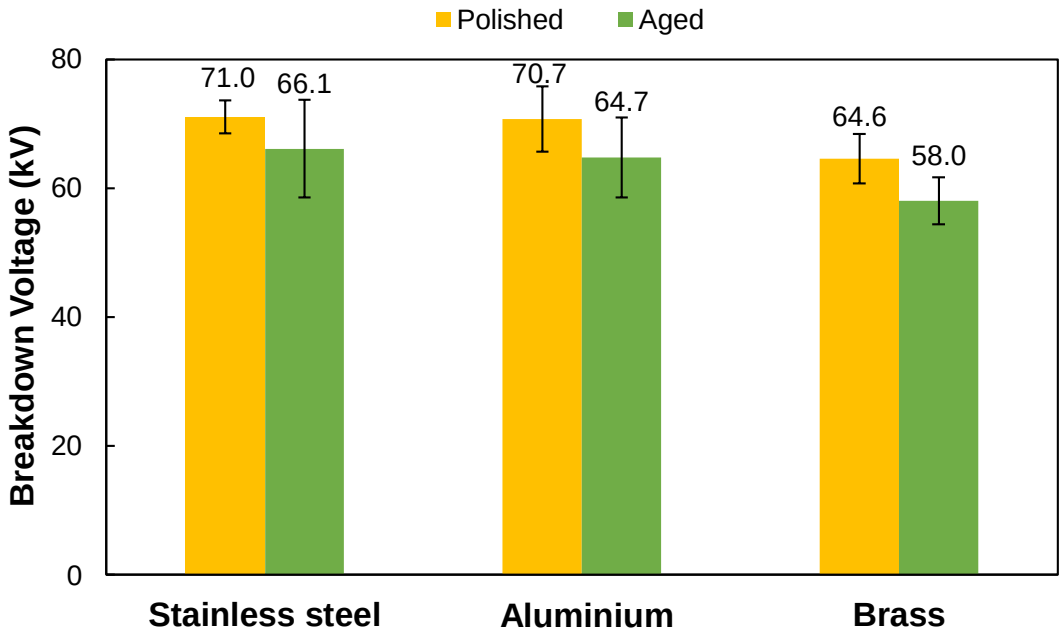

Figure 4.2 First and last 20 breakdowns averaged from the 300 breakdowns for 20% C_3F7CN / 80% CO_2 using stainless steel, aluminium and brass electrodes.

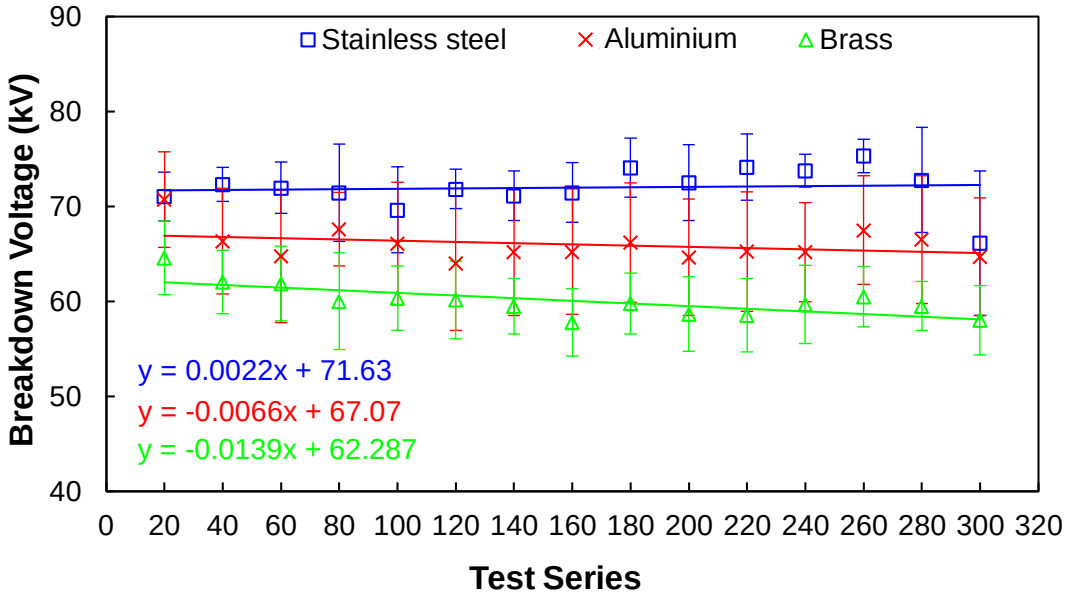

Figure 4.3 Average values from every 20 breakdowns for ageing experiments of 20% C_3F_7CN / 80% CO_2 tested using stainless steel, aluminium and brass electrodes.

Comparing the first and last 20 average breakdowns, all the tested materials show a decreasing trend in the breakdown voltage by a percentage of 6.9%, 8.5% and 10.2% for stainless steel, aluminium and brass, respectively. In Figure 4.3, the breakdown results are depicted as the calculated average of every 20 breakdowns. A gradual declining and scattering data trend can be observed for both the aluminium and brass test configurations with a coefficient of variation around ±6% and ±10% respectively, whereas the breakdown voltage of the stainless steel configuration remained relatively consistent with a coefficient of variation mostly less than ±5% until the final 20 breakdowns. Accordingly, stainless steel rod-plane electrodes will be used in Section 4.3 for characterising SF_6 and its alternative gases under a varying field uniformity.

After the ageing experiment, further investigation was carried on the effect of pressure on the aged electrodes by reducing the gas pressure (Figure 4.4 presents the results for 4.8, 3 and 2 bar for all three tested electrode materials).

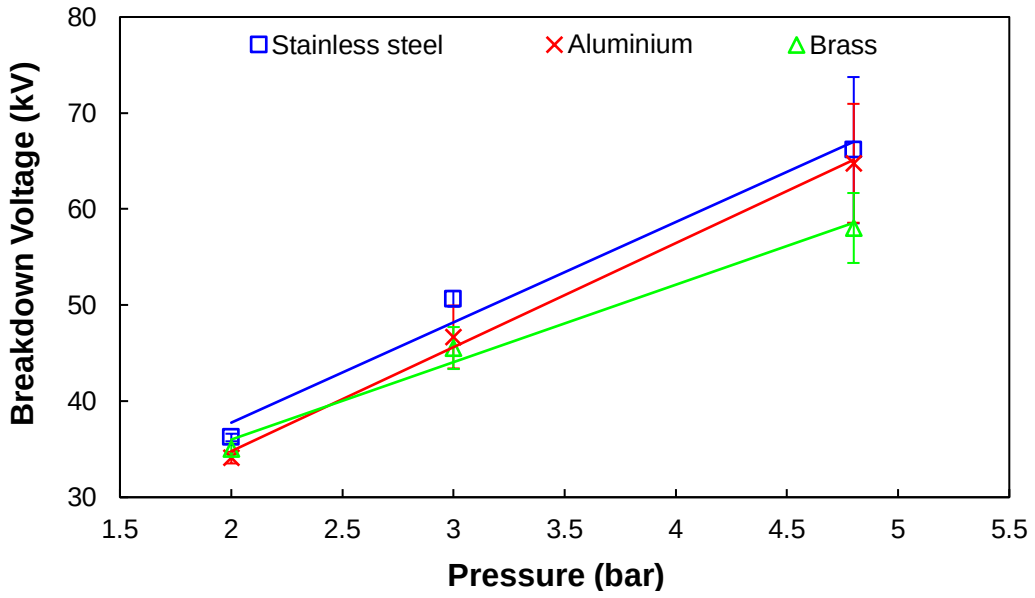

Figure 4.4 Negative DC breakdown for 20% C_3F_7CN / 80% CO_2 tested using a rod-plane configuration (6.25 mm rod diameter), for stainless steel, aluminium and brass, a gap of 3 mm and a pressure of 4.8, 3 and 2 bar.

In [90], it is reported that the effect of electrode surface roughness on the DC breakdown voltage of C_3F_7CN/CO_2 gas mixture is influenced by gas pressure, where the effect of surface roughness is more profound at higher pressures. As shown in Figure 4.4, all materials show comparable breakdown voltages under 2 bar with a greater difference observed in the 4.8 bar results. This accords with conclusions presented in [90]. It also suggested that the effect of electrode material on the breakdown voltage are affected by the gas pressure, with the effect being more visually distinct under higher pressures [107].

4.2.2 Gas Analysis Measurement

Table 4.1 presents the gas analysis for the C_3F_7CN/CO_2 mixture before and after 300 breakdowns under 4.8 bar using a DILO C_4 multi-gas analyser. As shown in Table 4.1, there is no noticeable change in the C_3F_7CN concentration. However, it is clear that the CO content has increased after 300 breakdowns, which is consistent with previously reported literature findings [27]. Note that the stainless steel configuration had a comparatively higher breakdown voltage, leading to higher accumulative discharge energy than aluminium and brass electrodes. This could be the reason why the experiment with the stainless steel configuration had a comparatively higher CO concentration (see Table 4.1).

Table 4.1 Gas analysis using a DILO C_4 multi-gas analyser unit for a C_3F_7CN/CO_2 gas mixture before and after 300 breakdowns under 4.8 bar.

Material	**Gas**	**C_3F_7CN (mole%)**	**CO_2 (mole%)**	**CO (ppmv)**	**O_2 (mole%)**
	Tolerance	± 0.2%	± 2%	± 2%	± 0.3%
Stainless steel	Before	19.4	83.9	12.0	0.3
	After	19.0	84.0	257.9	0.3
Aluminium	Before	18.4	84.0	12.0	0.4
	After	18.6	83.7	232.9	0.2
Brass	Before	19.1	84.2	15.9	0.3
	After	19.1	83.6	213.6	0.2

4.2.3 Electrode Surface Roughness Measurement

Table 4.2 depicts the measured R_a and R_z pre- and post-ageing experiment for all three electrode materials. Based on the results in Table 4.2, the R_z value of stainless steel electrodes increased by at least 5 times, while those of aluminium and brass increased by around 6.5 times after 300 breakdowns. Notably, aluminium exhibited the highest R_z value of 11.57 µm. The stainless steel electrodes had less sustained surface damage than the aluminium and brass electrodes. Despite the comparatively higher breakdown performance found in the stainless steel configuration, there was less surface damage on the stainless steel, most likely attributable to its mechanical and thermal robustness. Aluminium and brass present a deteriorating performance due to their surfaces degrading faster. Overall, the measured C_3F_7CN concentration did not vary significantly after an extensive number of DC breakdowns. The declining trend observed in the breakdown voltage shown in Figure 4.1 was mainly caused by the accumulated surface damage on the tested electrodes rather than

the gas decomposition effect. This accords with [90] where it was found that a rougher electrode surface has a negative effect on the DC breakdown characteristics of a C_3F_7CN/CO_2 gas mixture and it is also pressure dependant.

Table 4.2 Surface roughness measurement using a Jenoptik wave line W5 device before and after 300 breakdowns for stainless steel, aluminium and brass at the centre of the plane electrode.

Material	Polished Electrode		Aged Electrode	
	R_a (µm)	R_z (µm)	R_a (µm)	R_z (µm)
Stainless steel	0.16	1.20	1.32	6.32
Aluminium	0.19	1.81	2.36	11.57
Brass	0.21	1.53	2.11	9.97

4.3 The Effect of DC Polarity and Field Uniformity on the Breakdown of SF_6, CO_2 and the C_3F_7CN/CO_2 Mixture

This section provides an experimental comparative study of various factors related to the DC breakdown voltage of SF_6, CO_2 and a mixture of 20% C_3F_7CN / 80% CO_2 under both DC polarities. Rod-plane configurations made of stainless steel with a range of rod diameters (3.5-12.5 mm) and electrode separations (5-55 mm) were used to provide a wide range of field uniformities. The proposed gases were tested under pressures ranging between 1 and 9 bar. The experimental work in this section was conducted in the large-scale vessel due to the higher voltage range up to 300 kV_{DC} being investigated (bushing limit). Electrode gap distances were set using slip gauges and then adjusted for other gaps using the vessel actuator.

4.3.1 The Effect of Field Uniformity and DC Polarity

Figure 4.5 shows the variation in breakdown voltage with DC polarity for the 20% C_3F_7CN / 80% CO_2 gas mixture and SF_6 as a function of gap distance under 4 bar. As Figure 4.5 presents, increasing the gap distance reduces field uniformity, leading to a transition from a quasi-uniform to a non-uniform electric field (transition from streamer inception to propagation as in Sections 2.5.6 and 2.5.7). For ease of discussion, we define the crossover point as the point at which the breakdown voltage characteristics of each polarity crossover. By increasing the gap distance, before the crossover point, the breakdown voltage of positive DC was higher than that of the negative case, while after the crossover point, it was lower. The determination of the crossover point is within an error margin of ±1 mm with

respect to the gap distance. However, the corresponding f values were not affected since the gap effect starts to saturate in relation to f values, at which point crossover occurs.

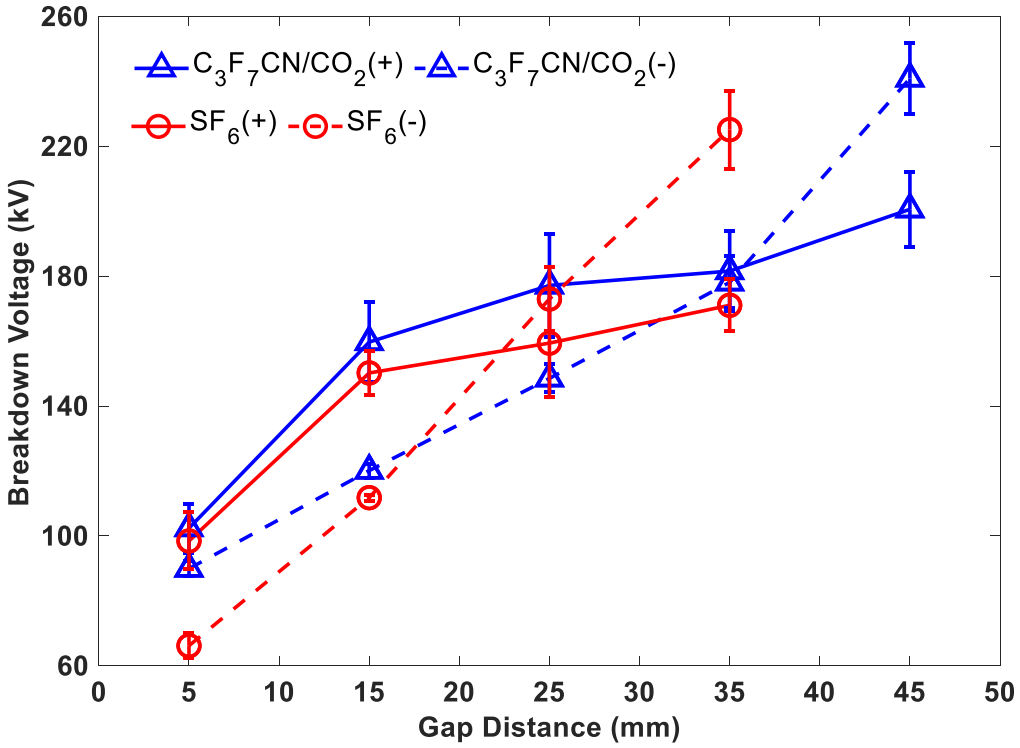

Figure 4.5 Comparison of the breakdown voltage in 20% C_3F_7CN / 80% CO_2 and SF_6 at 4 bar with a 6.25 mm rod. The gap distance to f conversion is presented in Figure 3.9.

A crossover point at ≈22 mm (f of 0.17) was observed for SF_6, whilst it occurred at an increased gap of 35 mm (f of 0.12) for 20% C_3F_7CN / 80% CO_2. For short gaps (d < 22 mm for SF_6 and d < 35 mm for 20% C_3F_7CN / 80% CO_2) and hence quasi-uniform fields (f > 0.17 for SF_6 and f > 0.12 for 20% C_3F_7CN / 80% CO_2), positive breakdown was comparatively higher than the negative equivalent, as the negatively charged electrode can provide an extra source of electrons by the field emissions that will enhance the ionisation process, resulting in a reduction of the breakdown characteristics in the negative case when compared with the positively charged electrode (see Sections 2.5.6 and 2.5.7) [16].

As the gap increases (f decreasing), the electric field becomes highly non-uniform (similar to a point-plane configuration), and in this case, the negative breakdown voltage is higher than the positive breakdown voltage. One of the reasons for this behaviour is, the field required for a stable streamer propagation in the negative case is much higher than the positive one leading to a higher applied voltage is needed to cause a breakdown (refer to streamer propagation in Section 2.5.7) [60].

Comparing both gases, the positive breakdown voltage of 20% C_3F_7CN / 80% CO_2 is always greater than for SF_6. For the negative applied voltage and long gap distances when the field uniformity is highly non-uniform ($f < 0.17$ for SF_6), the breakdown voltage in SF_6 exceeds that of 20% C_3F_7CN / 80% CO_2. Similar characteristics were observed in partial discharge (PD) investigations for non-uniform fields in DC voltages for mixtures of 4%-10% C_3F_7CN with CO_2 [140]. Negative PD inception voltage and AC performance [17] are higher for SF_6 than that of C_3F_7CN and CO_2 mixtures, including the 20% C_3F_7CN ratio, with the opposite behaviour observed for the positive polarity result.

4.3.2 The Effect of Gas Pressure

Figure 4.6 shows the combined effect of pressure, gap distance, gas medium and polarity on the breakdown characteristics of SF_6 and the 20% C_3F_7CN / 80% CO_2 gas mixture. The gas mediums show similar negative DC breakdown trends of a linear increase via the range of gap distances and pressures investigated in this study. For positive DC polarity, breakdown voltages tend to saturate with the gap distance and become lower than their corresponding negative breakdown values. These observed trends suggest a transition in the breakdown mechanism from streamer inception to propagation while the gap distance increases, contributing to the differences observed under both polarities (see Section 2.5.7) [50]. The observed saturation in the positive breakdown voltage with increasing electrode separation is consistent with reports for SF_6 and mixtures with low C_3F_7CN concentrations tested for LI voltage waveforms in [95], [141].

According to Figures 4.5 and 4.6, this saturation behaviour was observed in both gas mediums, with SF_6 saturating at higher f values than the 20% C_3F_7CN / 80% CO_2 gas mixture. Above 1 bar of pressure, crossover for SF_6 appears not to be pressure dependant, occurring at a gap distance of ≈20 mm with f of ≈0.18 for 3-5-bar pressure. A similar f of 0.18 was reported at the crossover point for SF_6 in LI voltage under 7.5 bar pressure [95]. For C_3F_7CN/CO_2, crossovers occurred at gap distances of around 32, 35 and 40 mm, with f values of 0.13, 0.12 and 0.1 corresponding to tests conducted at 3, 4 and 5 bar, respectively. Both gases have a crossover point at a gap distance of 15 mm (f of 0.22) when tested at 1 bar.

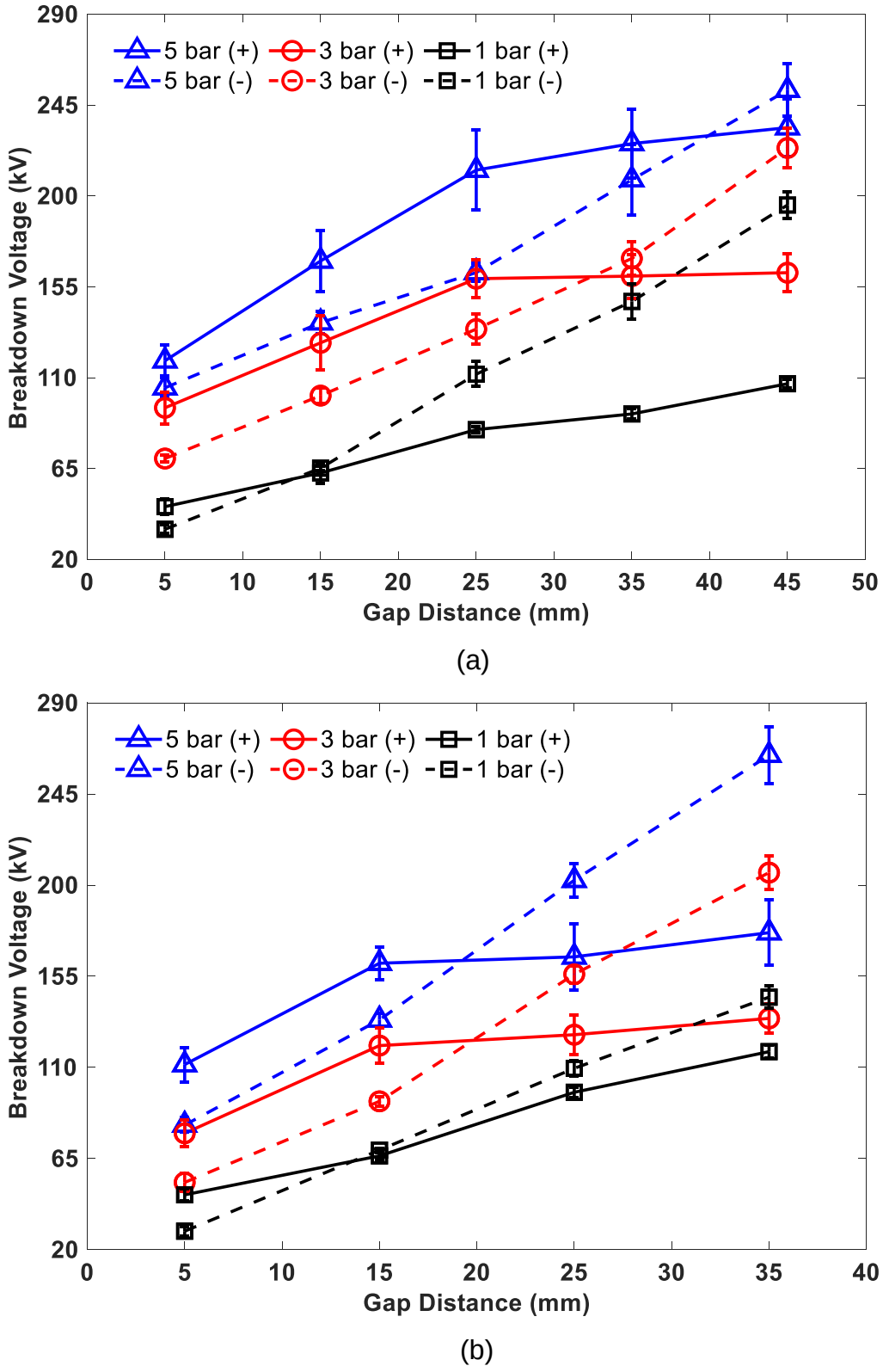

Figure 4.6 Effect of pressure and gap on the breakdown voltage of (a) 20% C_3F_7CN / 80% CO_2 and (b) SF_6 (up to 35 mm due to the bushing limitation) for a 6.25 mm rod.

The dependence of the breakdown voltage on voltage polarity and pressure is influenced by corona discharges (corona stabilised region) under lower pressures. As the pressure increases beyond critical pressure P_c, the corona onset voltage and breakdown voltage are comparable,

as shown in the illustrative Figure 4.7. The transition between these regions may cause a crossover between the breakdown trends of both polarities due to the difference between the behaviour of positive and negative streamers and P_c, at which both corona inception and breakdown voltages coincide [83], [142].

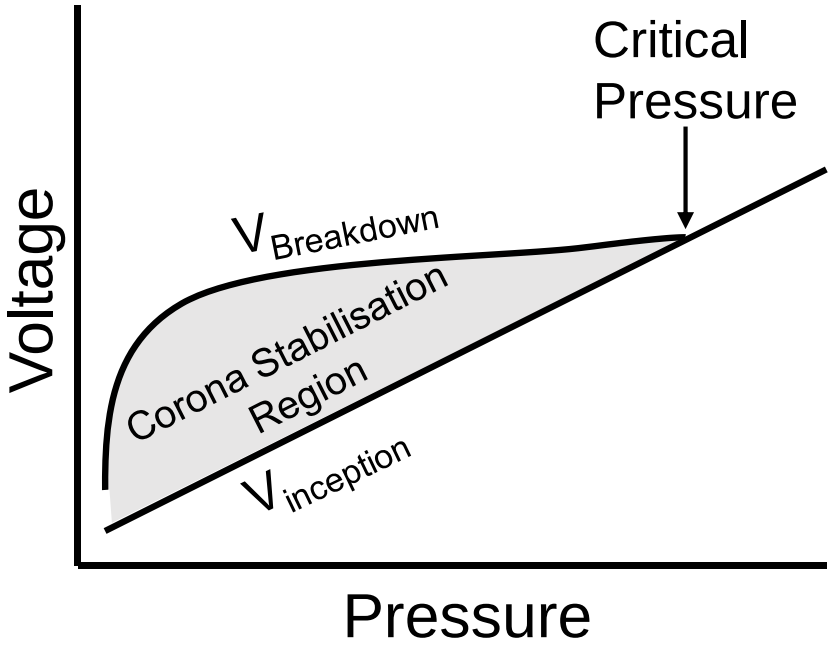

Figure 4.7 Illustration of the corona stabilisation region in the V-p characteristic [83], [142].

Figure 4.8 shows the effect of gas pressure at a fixed gap distance of 25 mm using a 6.25 mm rod-plane electrode in a 20% C_3F_7CN / 80% CO_2 gas mixture. For a gap distance of 25 mm, the f value is equal to 0.15 and being a non-uniform field. At less than 2 bar pressure, the negative breakdown voltage is higher than the positive one, which is reversed under higher pressures. High pressure has significantly increased the positive breakdown voltage and makes the gas less sensitive to field non-uniformity. Similar characteristics were reported for SF_6 in [83], using a 6.3 mm diameter rod-plane with a gap distance of 20 mm.

Both breakdown polarities are influenced by corona stabilisation in a low-pressure region with negative polarity higher than their positive counterpart. The opposite is the case, as the pressure is increasing, with P_c in the positive polarity being lower than the negative case [83], [142]. Figure 4.9 shows the effects of pressure, gap distance and voltage polarity on the breakdown characteristics of CO_2 gas under 2, 3 and 5 bar.

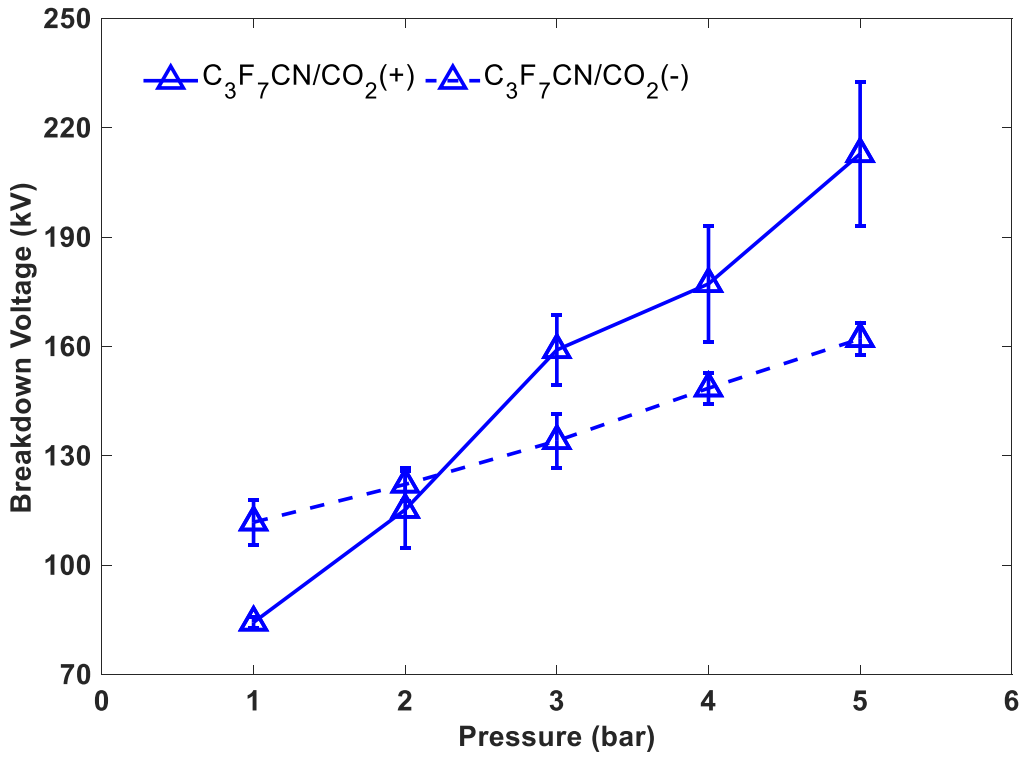

Figure 4.8 Effect of pressure and polarity on breakdown voltage for a 20% C_3F_7CN / 80% CO_2 gas mixture using a 6.25 mm rod at a fixed rod-plane gap of 25 mm.

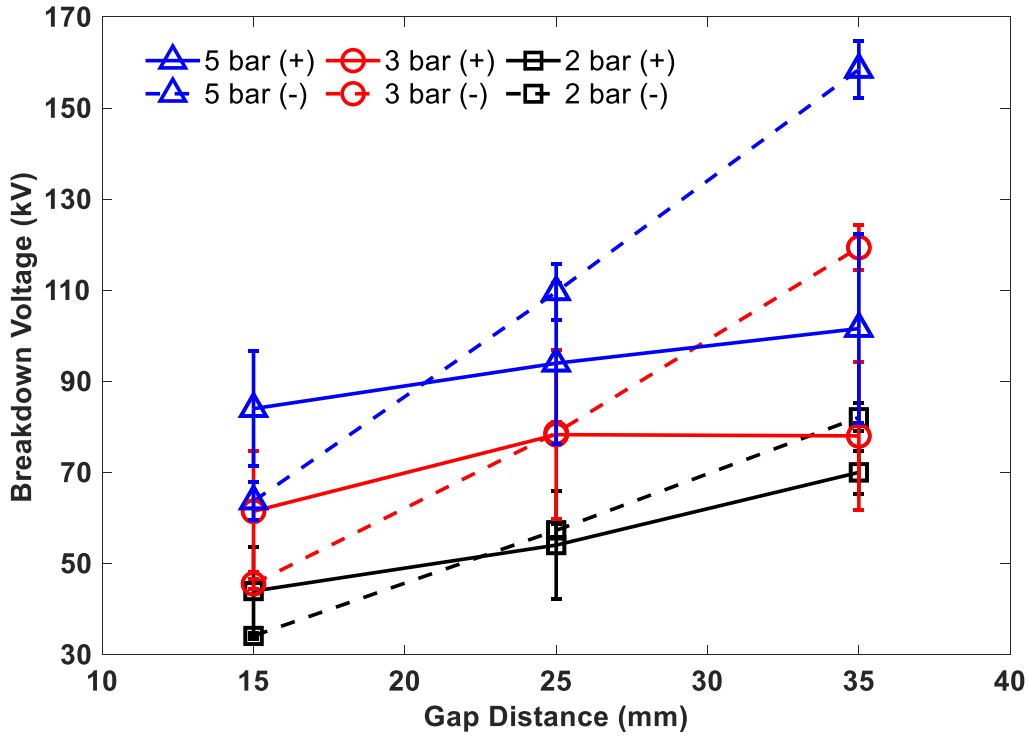

Figure 4.9 Effect of pressure and gap spacing using a 6.25 mm rod diameter in CO_2.

From Figure 4.9, the results show a similar crossover trend when comparing SF_6 and the 20% C_3F_7CN / 80% CO_2 mixture. A significant uncertainty margin is associated with the positive breakdown voltage, making it difficult to define the polarity crossover point.

In [142], the effect of the CO_2 concentration on the positive DC corona stabilisation region with respect to gas pressure for the SF_6/CO_2 gas mixture was reported. It was found that increasing the CO_2 content widens the corona stabilisation region and that higher pressure is required for the corona inception and breakdown voltages to coincide. Hence, the high concentration of CO_2 used in the mixture could be the cause of the positive breakdown voltage saturation occurring at a lower f in the 20% C_3F_7CN / 80% CO_2 mixture than observed in SF_6 under the same conditions. For negative polarity, as the test gap widens (i.e., a non-uniform field), SF_6 has a comparatively higher breakdown voltage than the 20% C_3F_7CN / 80% CO_2 mixture. This can be attributed to CO_2 being a weakly attaching gas, potentially resulting in a higher probability for the detachment of electrons or negative ions [49].

Based on the breakdown voltage results with 6.25 mm rods, Equation 4.1 was used to calculate the pressure normalised maximum electric field strength, E_{max}/p, to quantitatively compare the dielectric performance of different gases. In Figure 4.10, the results were compared against pressure normalised critical electric field strength $(E/p)_{crit}$ obtained from [57], [88] for SF_6 and 20% C_3F_7CN / 80% CO_2 (see Table 6.1 for the used $(E/p)_{crit}$ values).

$$E_{max}/p = \frac{U_{50}}{p \cdot d \cdot f} \tag{4.1}$$

Where U_{50} is the experimentally obtained breakdown voltage, p is the gas pressure, d is the gap distance and f is the field utilisation factor.

Figure 4.10 shows that as pressure increases, E_{max}/p reduces for all gap distances in the 6.25 mm rod configuration until it saturates around $(E/p)_{crit}$ of the gas medium. Note that for SF_6 under negative polarity, E_{max}/p drops slightly below $(E/p)_{crit}$ above 3 bar for the 5 mm and 15 mm gaps with more uniform fields. This is due to the cathode acting as a source of electrons, leading to a greater rate of ionisation and subsequently bringing the breakdown below $(E/p)_{crit}$ [16]. The E_{max}/p value for the 20% C_3F_7CN / 80% CO_2 gas mixture shows a greater ionisation than SF_6 gas, not dropping below $(E/p)_{crit}$ [17].

Figure 4.11 shows the breakdown results as a function of the Pressure·Gap (p·d) criteria. The data points are fitted with power curves to compare the overall dielectric performance of the two gas mediums under both polarities for the 6.25 mm rod with gap spacing in the range of 5 to 55 mm and a pressure range of 1 to 5 bar.

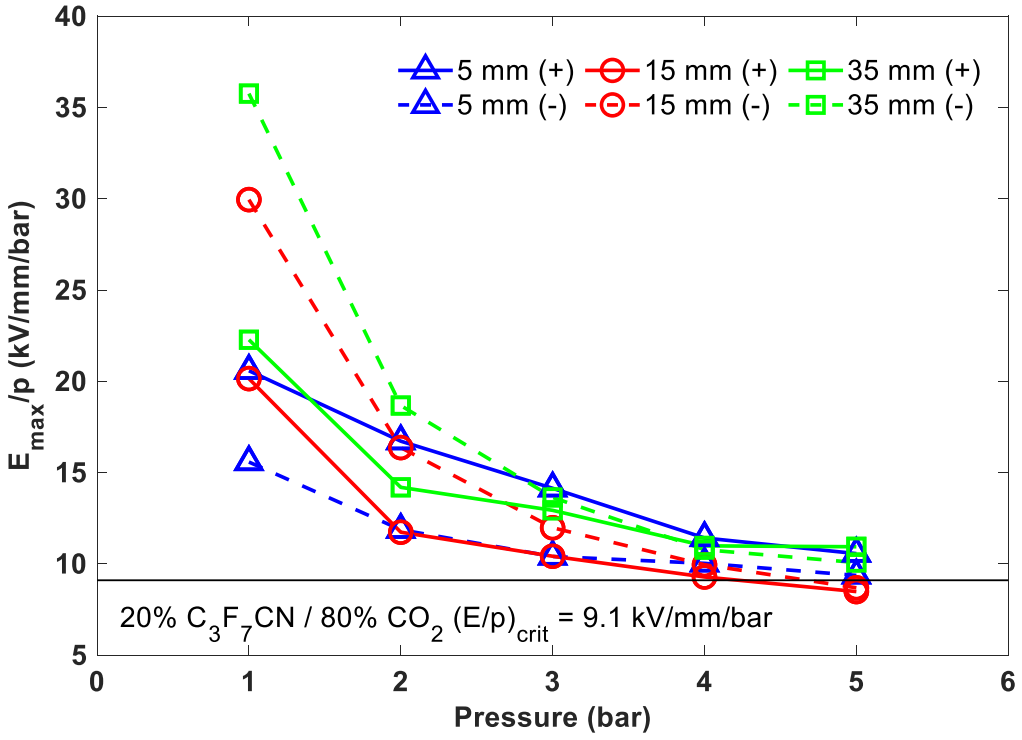

(a)

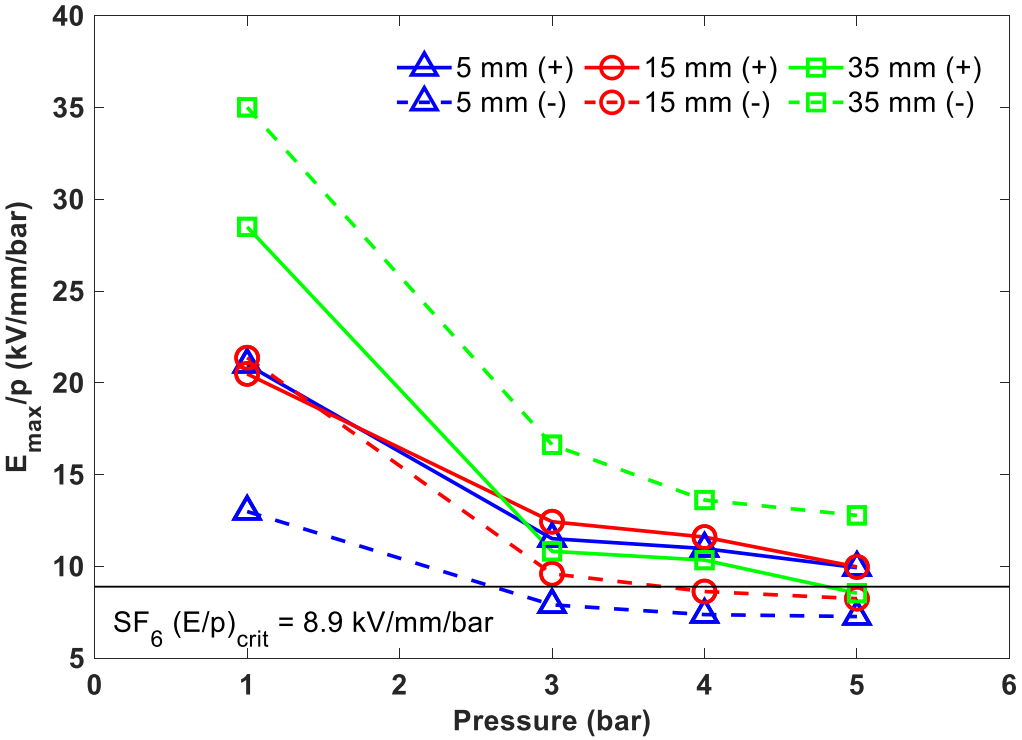

(b)

Figure 4.10 Effect of pressure and gap spacing on E_{max}/p using a 6.25 mm rod-plane configuration for (a) 20% C_3F_7CN / 80% CO_2 and (b) SF_6.

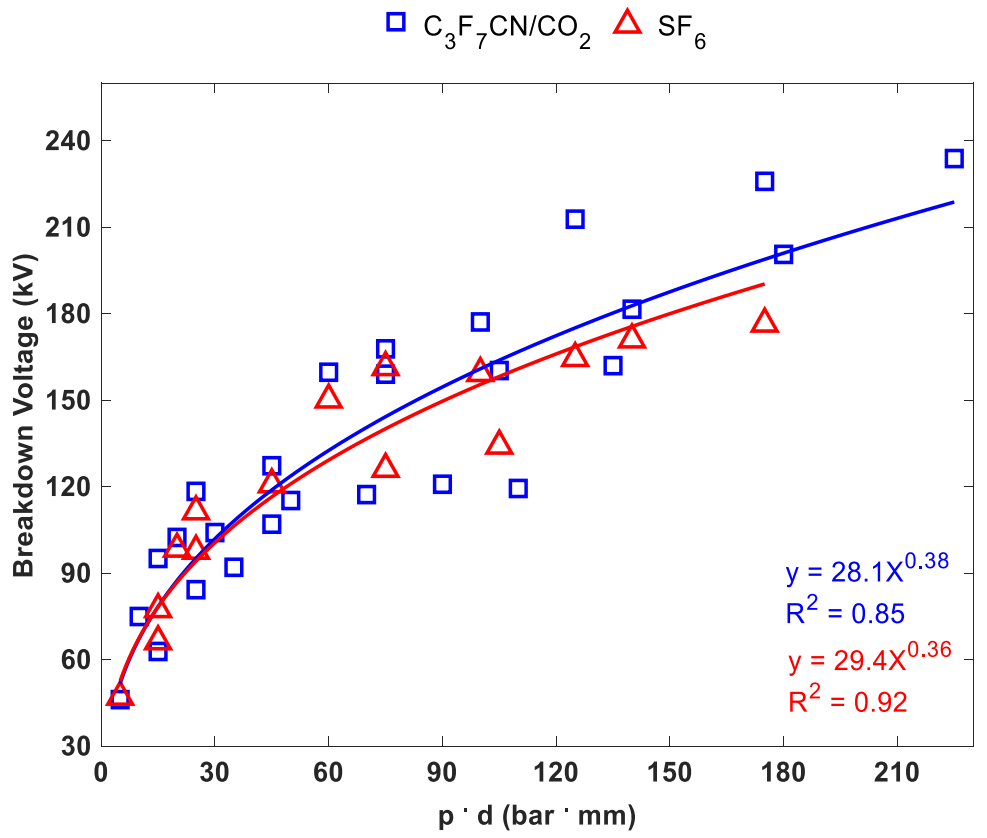

Figure 4.11 Breakdown characteristics as a function of p·d for both 20% C_3F_7CN and 80% CO_2 and SF_6 for a 6.25 mm rod configuration under a pressure range of 1 to 5 bar and a gap range of 5 to 55 mm, and for (a) positive and (b) negative polarities.

For both DC polarities shown in Figure 4.11, SF_6 and the 20% C_3F_7CN / 80% CO_2 gas mixture have a comparable breakdown performance with the 20% C_3F_7CN / 80% CO_2 gas mixture being slightly higher in the positive, which is reversed under a negative applied voltage.

4.3.3 The Effect of Electrode Size

Figure 4.12 compares the polarity crossover points with 3.5 mm, 6.25 mm and 12.5 mm diameter rod electrodes in a 20% C_3F_7CN / 80% CO_2 gas mixture for 2 and 3 bar. Comparing the breakdown results under 2 bar, all electrodes show a polarity crossover point when f reaches 0.16 (shown in Figure 4.12 (a)). This is at gaps of 12, 23 and 45 mm for 3.5 mm, 6.25 mm and 12.5 mm rod-plane electrodes, respectively.

For 3 bar of pressure (see Figure 4.12 (b)), both 3.5 mm and 6.25 mm rods have a polarity crossover point at f equal to 0.13 at 15 mm and 32 mm gaps, respectively, while no polarity crossover point was observed in the case of the 12.5 mm rod at a gap range of 5-45 mm. Extrapolation suggests that polarity crossover might be expected to occur for the 12.5 mm rod at a gap distance of ≈70 mm, where f will be 0.13 (identical to that of 3.5 mm and 6.25 mm rods).

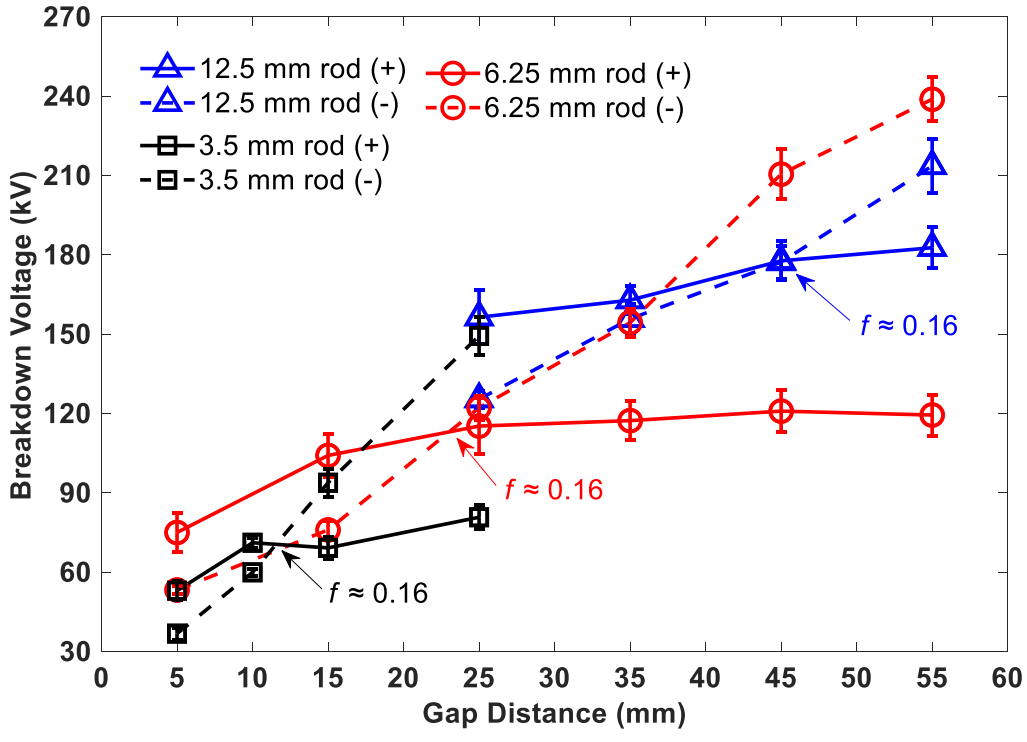

(a)

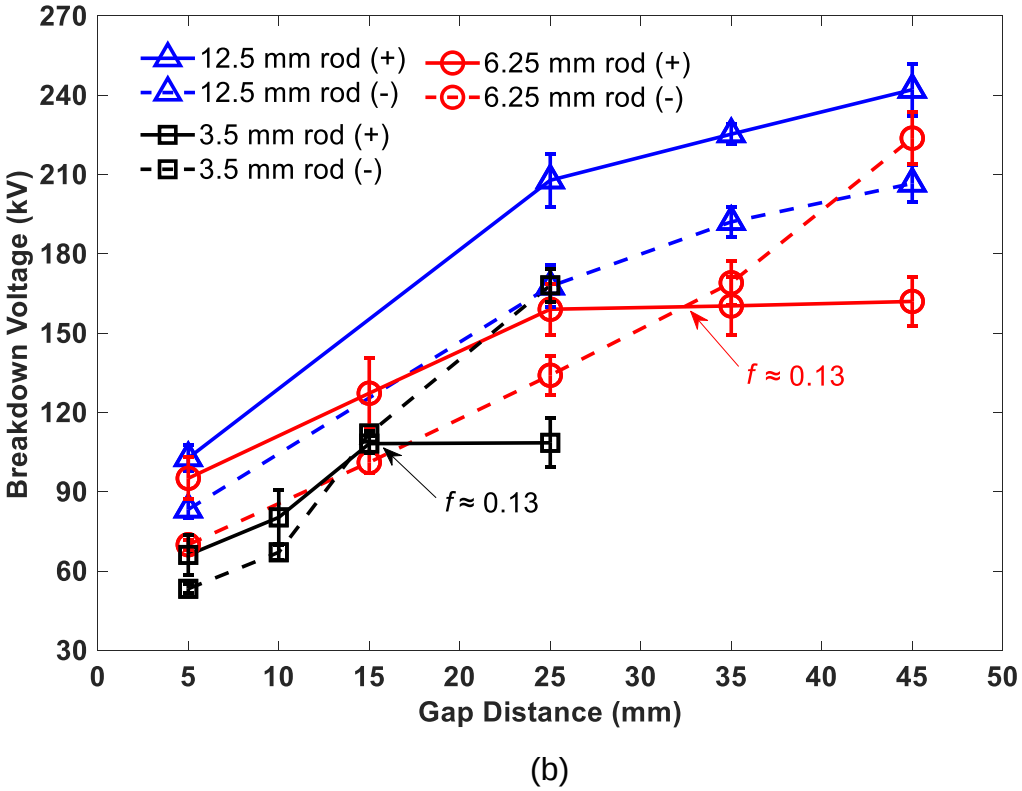

(b)

Figure 4.12 Crossover point trend for rod diameters of 3.5 mm, 6.25 mm and 12.5 mm tested in 20% C_3F_7CN / 80% CO_2 under (a) 2 and (b) 3 bar.

As pressure increases from 2 to 3 bar, polarity crossover occurs at a reduced f value of 0.13. For the 3.5 mm rod, the polarity crossover point shifts from an electrode separation of 12 to 15 mm, while for a 6.25 mm rod, it shifts from 23 to 32 mm. For the 12.5 mm rod, the field uniformity is still quasi-uniform (positive breakdown voltage is higher than the negative) in the case of 3 bar, whilst it is non-uniform in the case of 2 bar pressure where polarity crossover occurs at a gap distance of 45 mm.

Figure 4.13 shows a comparison of the polarity crossover point for the three rod sizes for SF_6 under 3 bar. The effective area of discharge has no influence on the polarity crossover point as it always occurs at f of ≈0.18 for these electrodes. The effect of increasing the electrode diameter below the crossover point is to increase the breakdown voltage for both polarities. For gaps greater than that of the crossover point, a positive breakdown voltage will saturate at higher breakdown voltage values for electrodes with a larger discharge area (higher f), whereas a negative breakdown voltage will increase rapidly with smaller discharge areas (lower f).

Figure 4.14 compares the polarity crossover points in 6.25 mm and 12.5 mm diameters rod-plane electrodes in CO_2 for 7 and 9 bar.

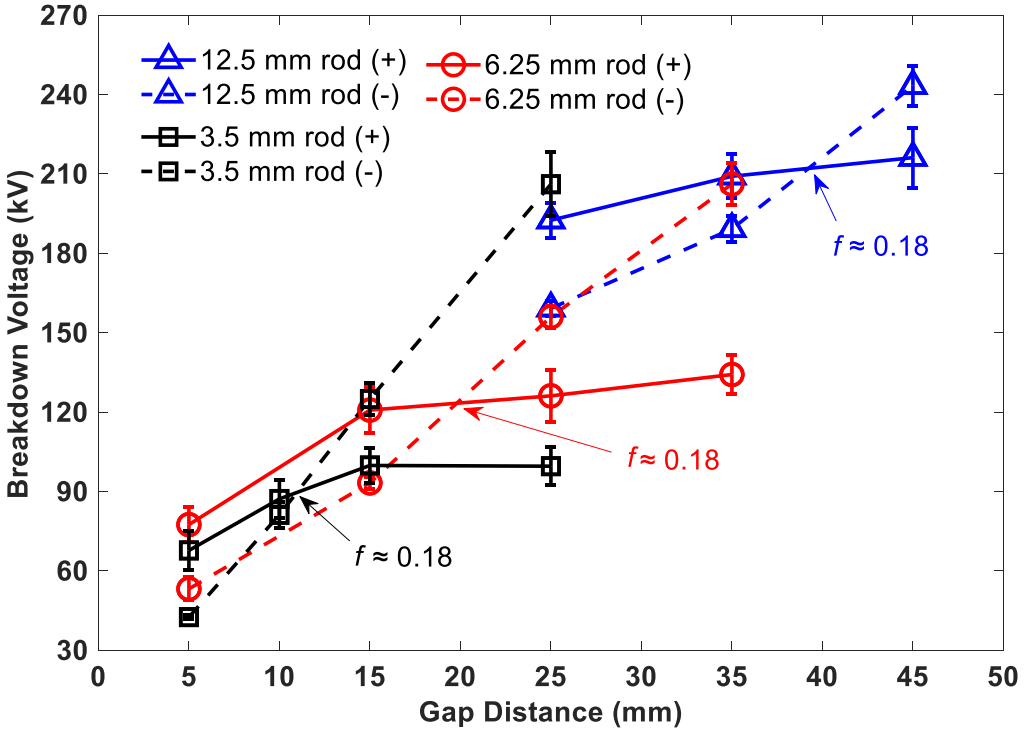

Figure 4.13 Crossover point trend for rod diameters of 3.5 mm, 6.25 mm and 12.5 mm tested in SF_6 under 3 bar.

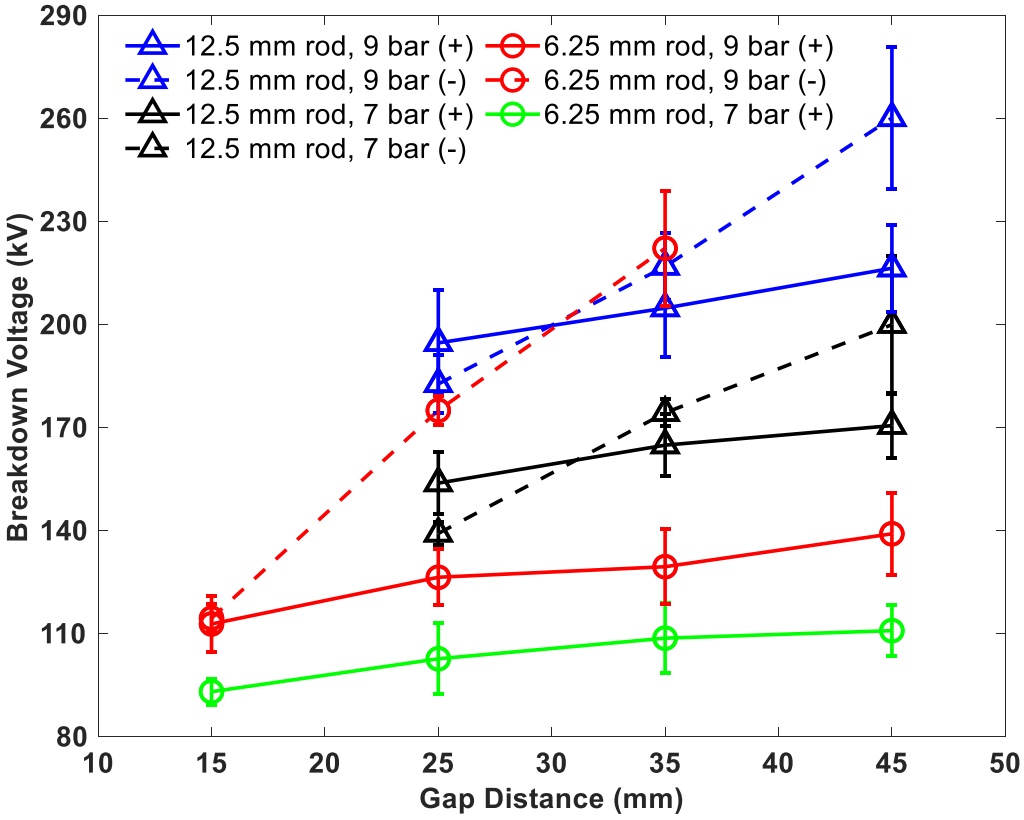

Figure 4.14 Crossover point trend for rod diameters of 6.25 mm and 12.5 mm tested in CO_2 under 7 and 9 bar. Green circle markers are U_{50} results only calculated for 5 breakdowns.

From Figure 4.14, increasing gas pressure beyond 5 bar slightly improved the error bars deviation when compared to the results in Figure 4.9 for lower pressure but it is still significant due to it making the crossover point allocation not accurate enough for comparison. In addition, there was no observed pattern similar to SF_6 or the 20% C_3F_7CN / 80% CO_2 gas mixture at which the polarity crossover point location can be analysed. However, the behaviour of the CO_2 gas remains similar to both SF_6 and 20% C_3F_7CN / 80% CO_2, with the increasing of the gas pressure or rod diameter leading to an increasing positive breakdown voltage that saturates with the increasing gap distance when reaching non-uniform fields. The negative breakdown voltage will increase rapidly with smaller rod diameters (non-uniform fields) or with increasing pressure. Overall, to match the dielectric strength of SF_6 or 20% C_3F_7CN / 80% CO_2, CO_2 needs to be under pressure that is at least 2-3 times higher.

The dependence of the polarity crossover point, at which the f value is considered to identify a non-uniform field, is a function of gas medium and pressure, gap distance and electrode design. It was observed that, in a quasi-uniform field, the positive breakdown voltage is higher than the negative for both gases, and vice versa in non-uniform fields. Figure 4.15 shows the qualitative variation of the polarity crossover point in SF_6 gas and a 20% C_3F_7CN / 80% CO_2 gas mixture.

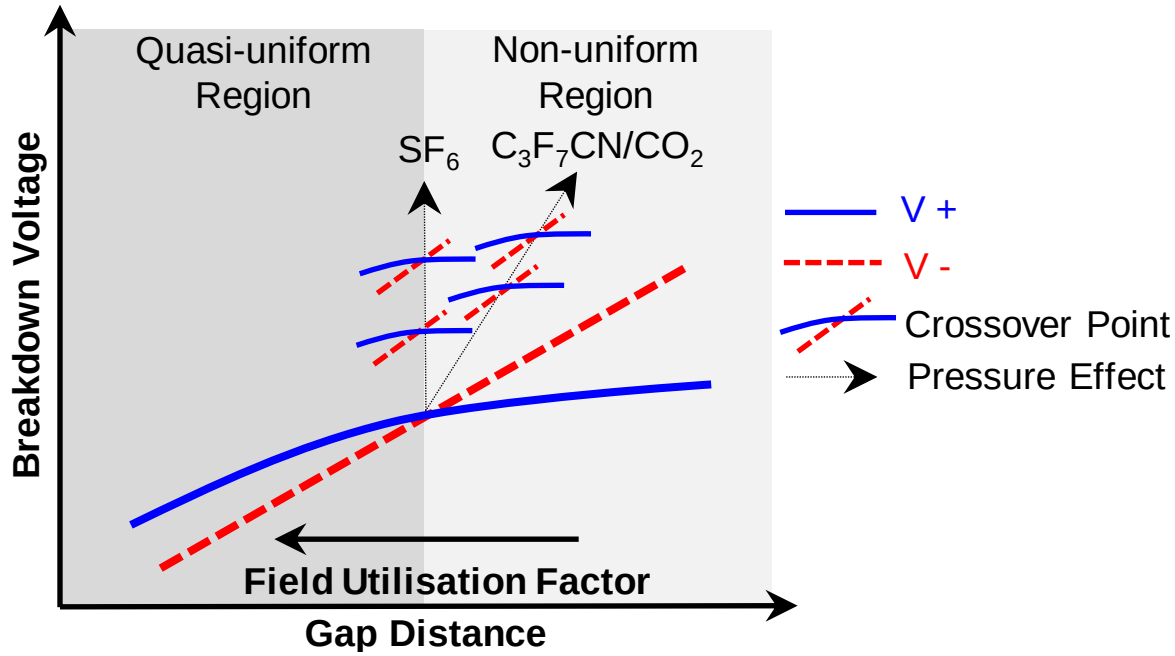

Figure 4.15 Qualitative illustration of the crossover point between both DC polarities due to the influencing factors used in this study.

In the C_3F_7CN/CO_2 mixture (black dotted arrows in Figure 4.15) under high pressure, the value of f becomes less important, with a very low f value (highly non-uniform field) required to cause the negative breakdown voltage to be higher than the positive one, whereas for SF_6, the crossover value of f is pressure independent. Saturation of the positive breakdown voltage and a linear increase of the negative breakdown voltage with an increasing gap (i.e., increasing non-uniformity of the electric field) for all the tested gases (SF_6, CO_2 gases and the 20% C_3F_7CN / 80% CO_2 gas mixture) led to polarity crossover (Figures 4.5 and 4.9). There is a clear indication in the shifting of the crossover point with pressure (>1 bar) for the C_3F_7CN/CO_2 mixture unlike that for SF_6 (see Figure 4.6 and the illustration in Figure 4.15).

Changing the rod diameter will not affect the f at which the polarity crossover point occurs in SF_6 and 20% C_3F_7CN / 80% CO_2 gas mediums (Figures 4.12 and 4.13). It only influences the breakdown voltage value but once the electrode configuration reaches the specific f by controlling the gap distance between them, polarity crossover will occur. For large sized rod electrodes (e.g., the 12.5 mm diameter rod), a long gap separation is required to match the f of small sized rod electrodes (e.g., the 3.5 mm diameter rod).

From a design perspective, the equipment insulation level must be designed to withstand DC voltage polarity, which gives the lowest breakdown voltage. In the case of GIL and busbars with quasi-uniform field geometries, the critical design polarity is negative, giving rise to a lower breakdown voltage than the positive counterpart [16]. For more non-uniform field geometries, as found in switch contacts of ring main units, it is possible that the positive DC breakdown voltage may be lower than the negative DC equivalent [95], [130]. This is dependent on pressure and field uniformity. Hence, the experimentally established crossover points are key to the engineering of the equipment design.

4.4 Summary

This chapter has investigated the DC breakdown characteristics of SF_6, CO_2 and 20% C_3F_7CN / 80% CO_2 gases and mixture in a rod-plane configuration. The effect of different electrode materials on the negative DC breakdown performance of the 20% C_3F_7CN / 80% CO_2 gas mixture over 300 breakdowns were examined and analysed. The results show that stainless steel electrodes attained a higher breakdown voltage and less surface damage when compared with aluminium and brass. In polished electrodes, aluminium matches the

breakdown voltage of stainless steel, with both having a comparable work function. The maximum electrode surface roughness (R_z) values of aluminium and brass were both increased by approximately 6.5 times after 300 negative DC breakdowns. Thus, a decreasing trend for the breakdown voltage was obtained. The measured C_3F_7CN concentration did not vary significantly after an extensive number of DC breakdowns but the CO concentration increased to 200 ppmv. This suggests that the reduction in breakdown performance is less likely to be influenced by gas decomposition and mainly due to the sensitivity of the gas mixture to rougher electrode surfaces.

Furthermore, the effects of DC polarity and field uniformity on the breakdown of SF_6, CO_2 and the C_3F_7CN/CO_2 mixture were investigated and compared. Tests were conducted under both DC polarities to address their influence on the breakdown voltage for each gas under different pressures. The key conclusions are the following:

- Breakdown voltage in negative DC polarity increases with the gap distance for all of the tested gases. However, positive DC polarity tends to saturate as gap distance increases. In SF_6, this saturation starts at a gap separation shorter than that for the 20% C_3F_7CN / 80% CO_2 gas mixture and is not pressure dependant, as is the case for the C_3F_7CN/CO_2 mixture. This identifies the importance of positive DC polarity breakdown in design considerations for gas insulated equipment.

- The effect of DC polarity shows a variation in breakdown voltage that is influenced by field uniformity, pressure and the gas medium. For SF_6 above 1 bar, the breakdown levels under both DC polarities are comparable at f of 0.18. The location of the crossover point for SF_6 is not influenced by gas pressure, whereas the crossover point location in a 20% C_3F_7CN / 80% CO_2 gas mixture is pressure dependant and occurs at a field uniformity that is more non-uniform than that of SF_6.

- The overall breakdown strength of 20% C_3F_7CN / 80% CO_2 is comparable to SF_6 under both polarities, irrespective of field uniformity. Thus, 20% C_3F_7CN / 80% CO_2 can offer a valuable alternative to SF_6 gas in high voltage insulation applications.

5 DC BREAKDOWN CHARACTERISTICS OF SF_6 AND ITS ALTERNATIVES IN COAXIAL CONFIGURATIONS

5.1 Introduction

Coaxial field distribution representing a quasi-uniform field is typically found in GIB and GIL. This chapter experimentally investigates the DC breakdown characteristics of SF_6 and CO_2 gases, and mixtures of 4% $C_5F_{10}O$, 7% C_3F_7CN and 20% C_3F_7CN with CO_2 under both DC polarities in reduced scale coaxial configurations in a large-scale vessel, all of which that have a comparable field utilisation factor to practical GIL or GIB, with conductor/enclosure diameters of 8/30, 10/30, 15/30, 15/45 and 20/60 mm. The conductor surface finish plays an important role in determining the breakdown performance of the gas medium where mirror-finished and polished electrodes represent the best performance and are in agreement with the theoretical gas breakdown criterion values [49]. A practical conductor with a rougher conductor surface finish can lead to an increased possibility of ionisation on the protrusion due to the microscopic surface roughness, resulting in a reduction of the breakdown voltage by a factor ζ [49]. Therefore, the effect of conductor surface roughness will be examined in the 10/30 mm coaxial configuration with a maximum surface roughness (R_z) ranging from 8-121 μm, with the aim of establishing a threshold p·h value for both SF_6 (40-50 bar·μm reported in [49], [112]) and 20% C_3F_7CN / 80% CO_2 to enhance the judgment on the viability of the mixture being a suitable alternative to SF_6 in practical high voltage DC equipment.

5.2 The Effect of the Coaxial Ratio

Figures 5.1 and 5.2 show the effect of using different conductor sizes with a fixed outer enclosure diameter of 8/30, 10/30 and 15/30 mm, which represents corresponding coaxial ratios of 3.75, 3 and 2. Results for both DC polarities and both SF_6 gas, and the 20% C_3F_7CN / 80% CO_2 mixture, show that despite the 8/30 mm coaxial configuration having the longer gap distance or the 15/30 mm coaxial configuration having higher field uniformity, the 10/30 mm coaxial configuration attained the highest breakdown voltage due to it provides the lowest E_{max} (shown in Table 3.2).

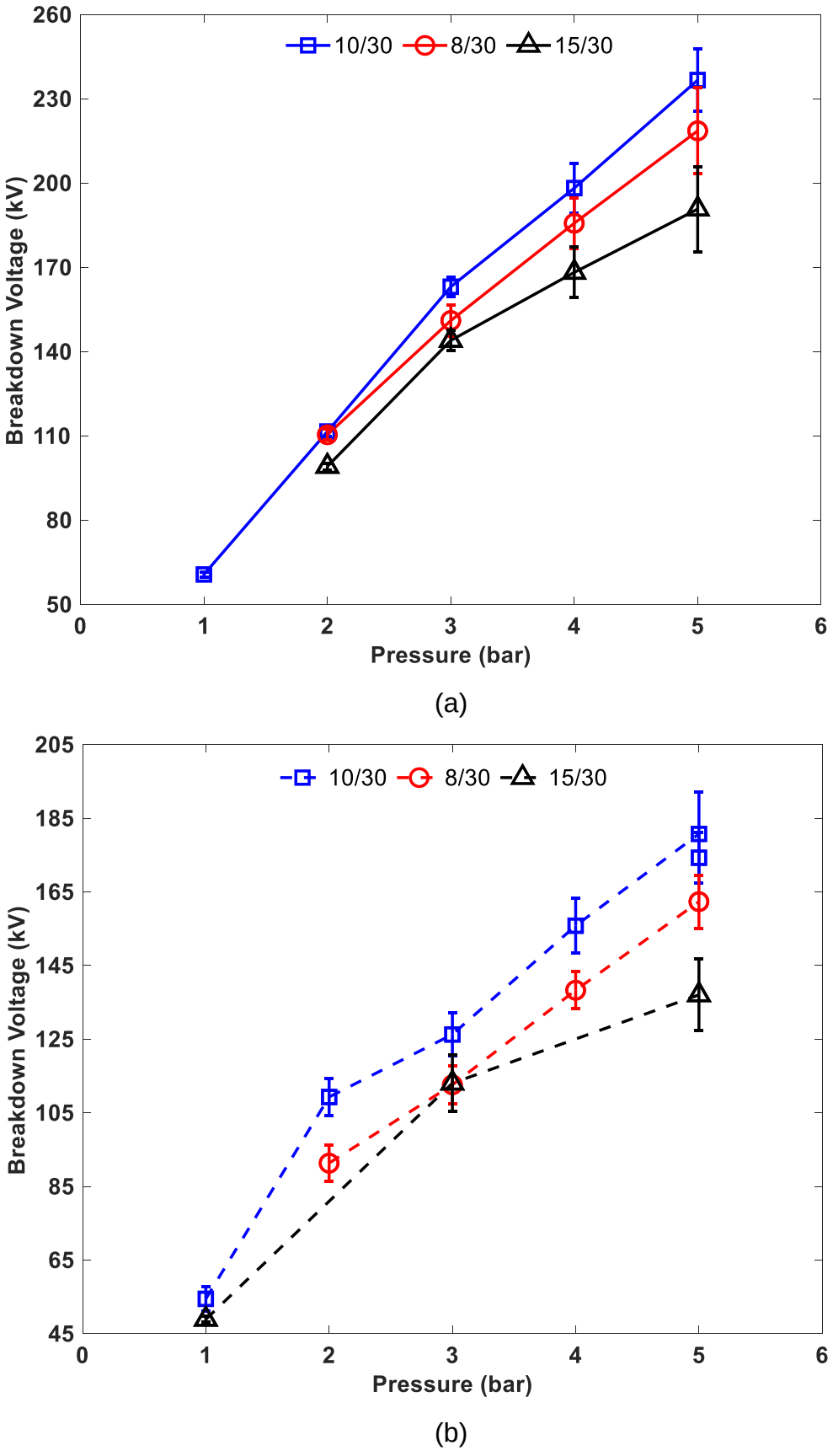

Figure 5.1 Effect of coaxial conductor/enclosure ratio with a fixed inner enclosure of 30 mm diameter on the DC breakdown characteristics of 20% C_3F_7CN / 80% CO_2 for (a) positive and (b) negative DC.

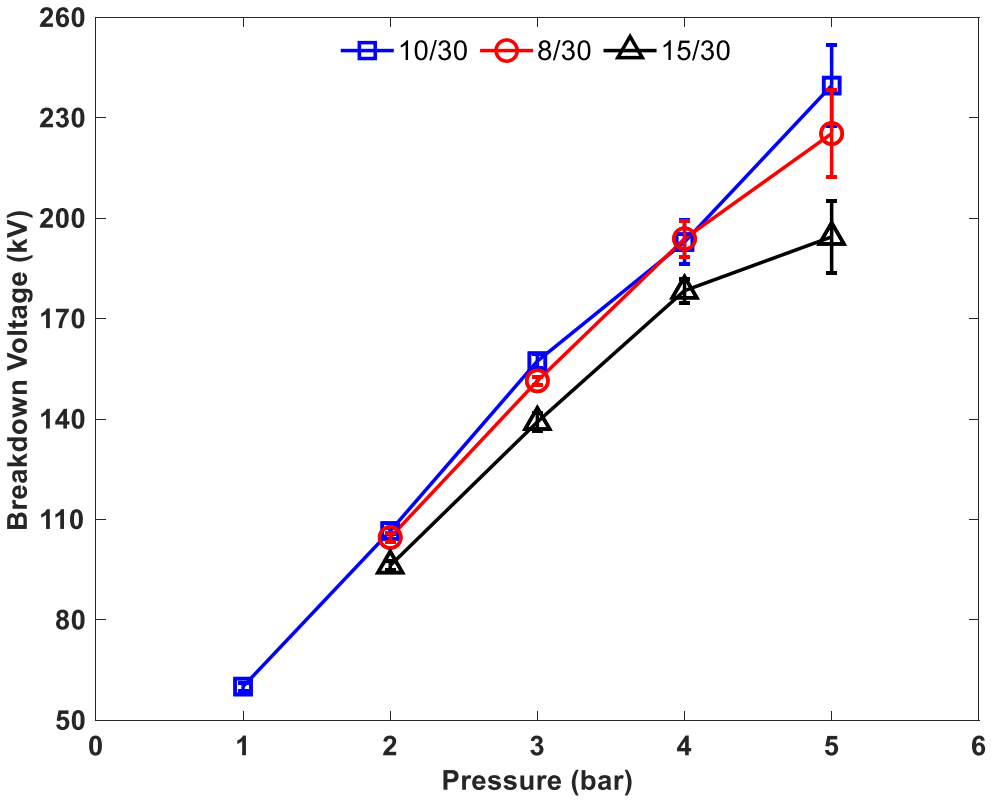

(a)

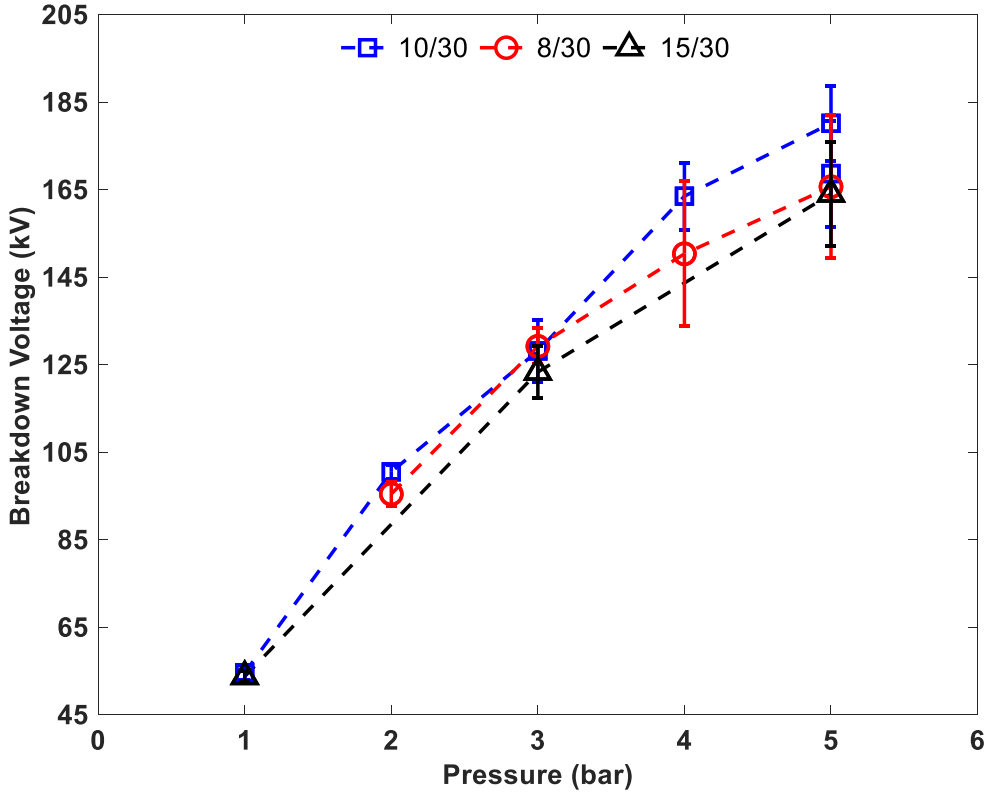

(b)

Figure 5.2 Effect of the coaxial conductor/enclosure ratio with a fixed inner enclosure of 30 mm in diameter on the DC breakdown characteristics of SF_6 for (a) positive and (b) negative DC.

This difference in breakdown voltage is more visible at higher pressures, as shown in Figures 5.1 and 5.2 for the 5 bar results. Therefore, for the subsequent investigations, a coaxial ratio of 3 has been chosen because it provides the highest breakdown voltage out of the three coaxial geometries in this study.

5.3 The Effect of Electrode Material

Figure 5.3 shows the effect of using different electrode materials in a 10/30 coaxial configuration on the breakdown voltage of both DC polarities in 20% C_3F_7CN / 80% CO_2 mixture. Three different combinations were used: (i) both conductor and enclosure are made from Al, (ii) SS conductor with an Al enclosure, and (iii) both conductor and enclosure are made from SS. Results in Figure 5.3 illustrate that for both DC polarities, breakdown voltage values of Al and SS are comparable and within the error bar range. This is consistent with the results detailed in Section 4.2 for the rod-plane configuration (for the first 20 breakdowns average), as both SS and Al having a comparable work function of 4.9 eV and 4.6 eV, respectively (shown earlier in Table 3.1). Therefore, a similar breakdown performance for both materials can be expected [107]. Note that, the effect of oxide layers on some electrode materials could also influence the breakdown performance regardless the work function order as discussed earlier in Section 2.8.4 [110].

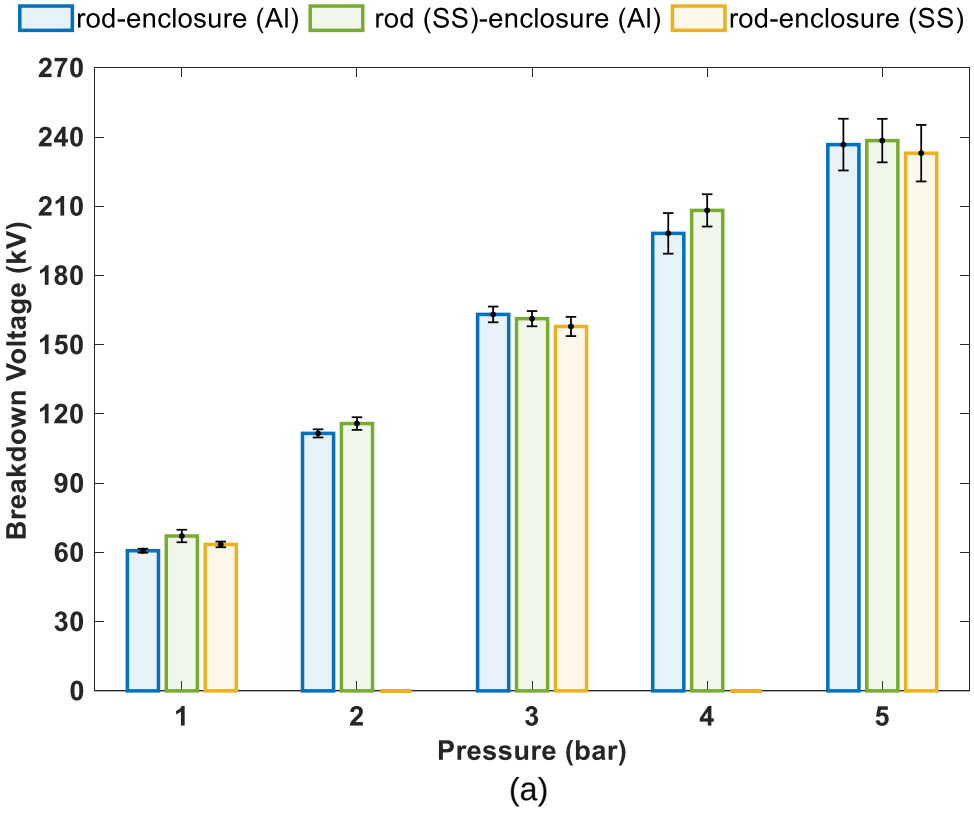

(a)

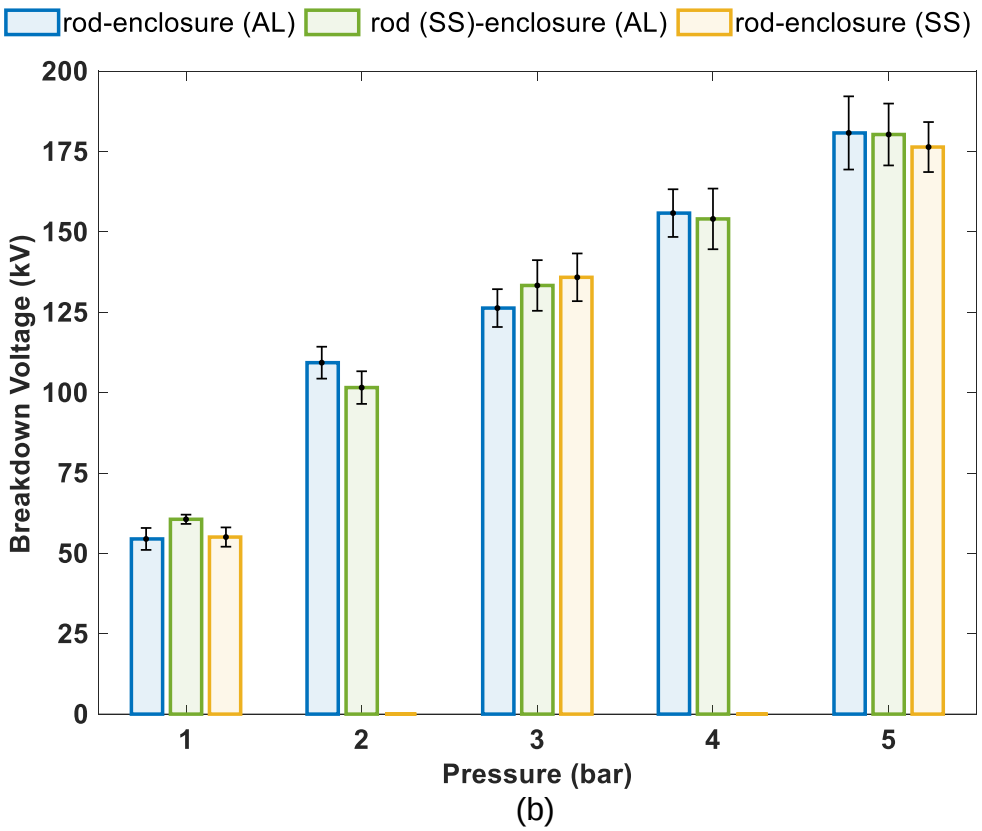

Figure 5.3 Effect of electrode material in a 10/30 mm coaxial configuration for 20% C_3F_7CN / 80% CO_2 for (a) positive and (b) negative DC.

In terms of electrode surface damage, since coaxial geometry was used in this case, material robustness is less likely to have an influence on the breakdown voltage, since the area of the discharge is larger than the one found in a rod-plane configuration, at which the discharges will concentrate at the tip of the rod.

5.4 Comparative Investigation Between SF_6 And Its Alternatives in Coaxial Electrodes

Figures 5.4, 5.5 and 5.6 show the DC breakdown characteristics in different-sized coaxial electrodes with a coaxial ratio of 3, for conductor/enclosure diameters of 10/30, 15/45 and 20/60 mm, respectively, tested for 20% C_3F_7CN / 80% CO_2, 7% C_3F_7CN / 93% CO_2, 4% $C_5F_{10}O$ / 96% CO_2 mixtures, and SF_6 and CO_2 gases under pressure of 1-9 bar. From Figures 5.4, 5.5 and 5.6, all tested gases behave similarly in terms of increasing the gas pressure leading to an increase in the breakdown voltage under both polarities, with negative breakdown polarity being lower than the positive breakdowns. Also, scaling up the coaxial design from 10/30 to 20/60 mm led to a significant increase in the breakdown voltage under both polarities, which is a result of a larger gap distance between the HV and ground

electrodes in the case of the 20/60 mm configuration, while maintaining a similar f factor to the 10/30 configuration (f=0.55).

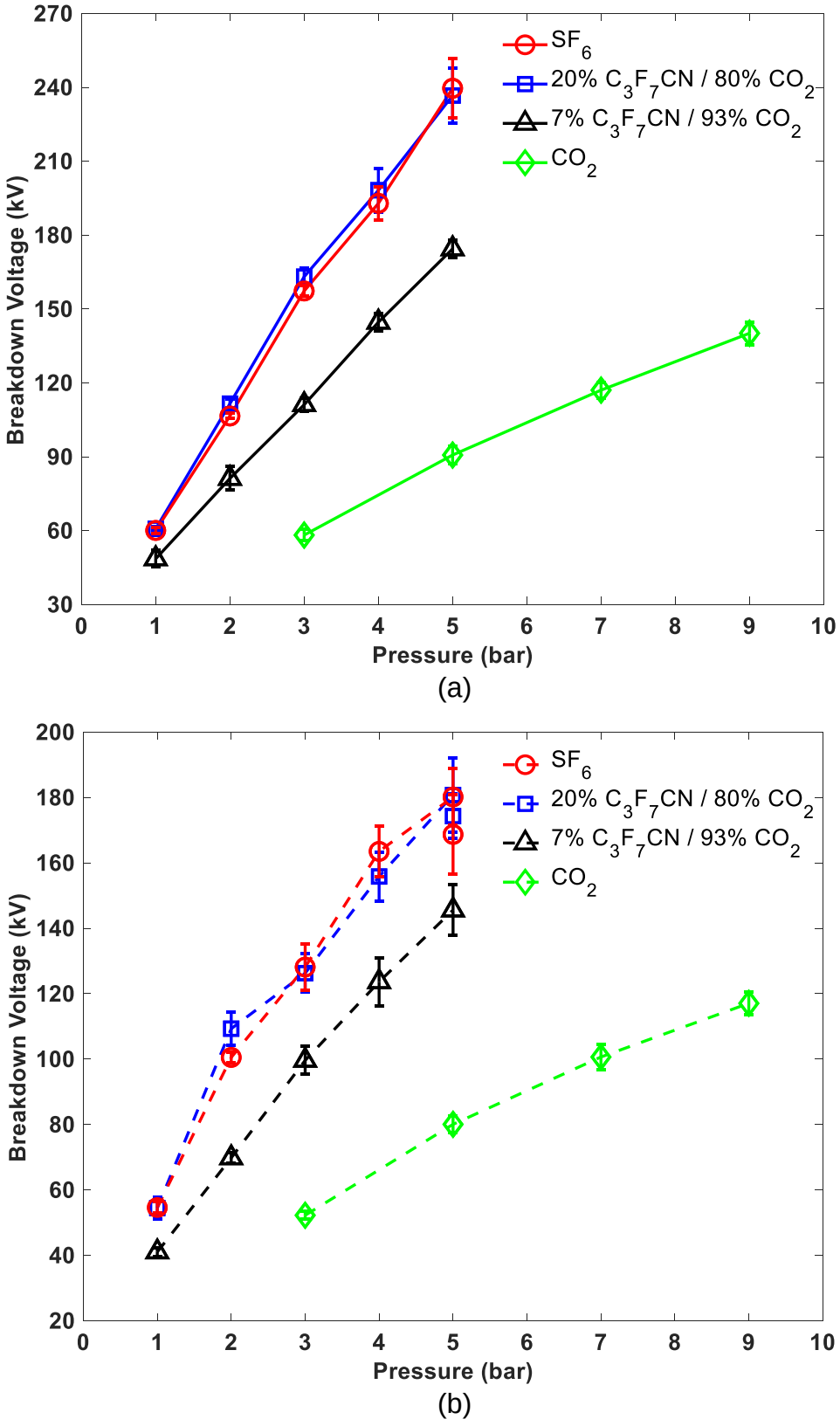

Figure 5.4 Comparison of the DC breakdown characteristics between 20% C_3F_7CN / 80% CO_2, 7% C_3F_7CN / 93% CO_2, SF_6 and CO_2 in 10/30 mm coaxial configuration for (a) positive and (b) negative DC.

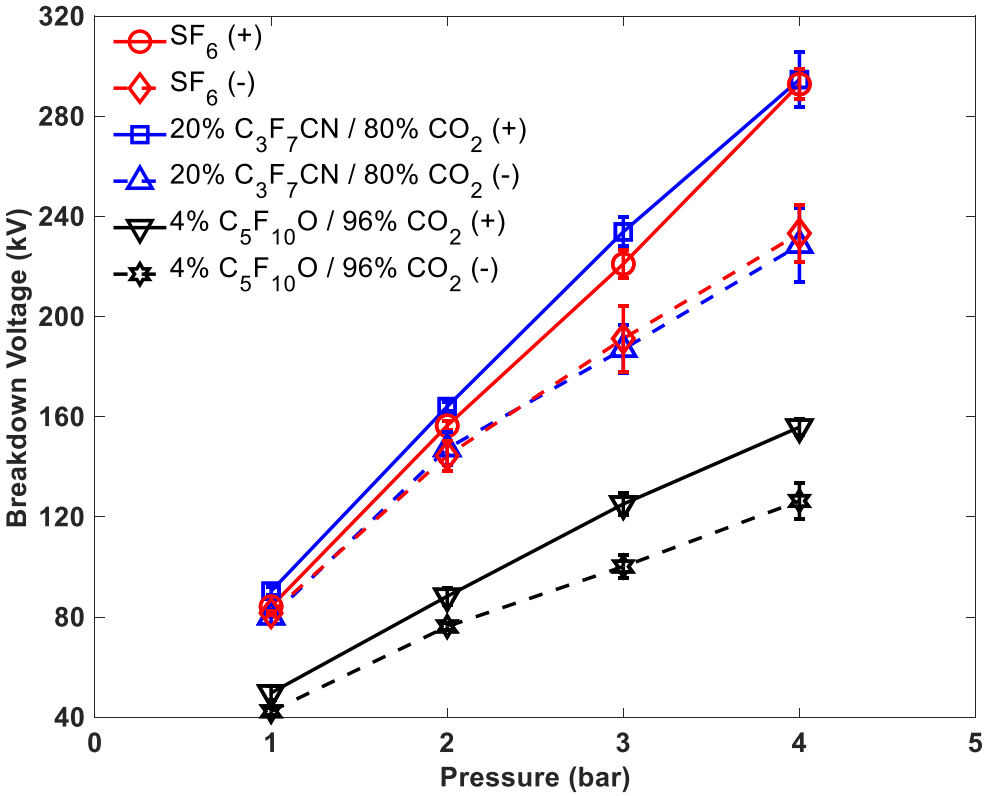

Figure 5.5 Comparison of the DC breakdown characteristics between 20% C_3F_7CN / 80% CO_2, 4% $C_5F_{10}O$ / 96% CO_2 and SF_6 in 15/45 mm coaxial configuration under both DC polarities.

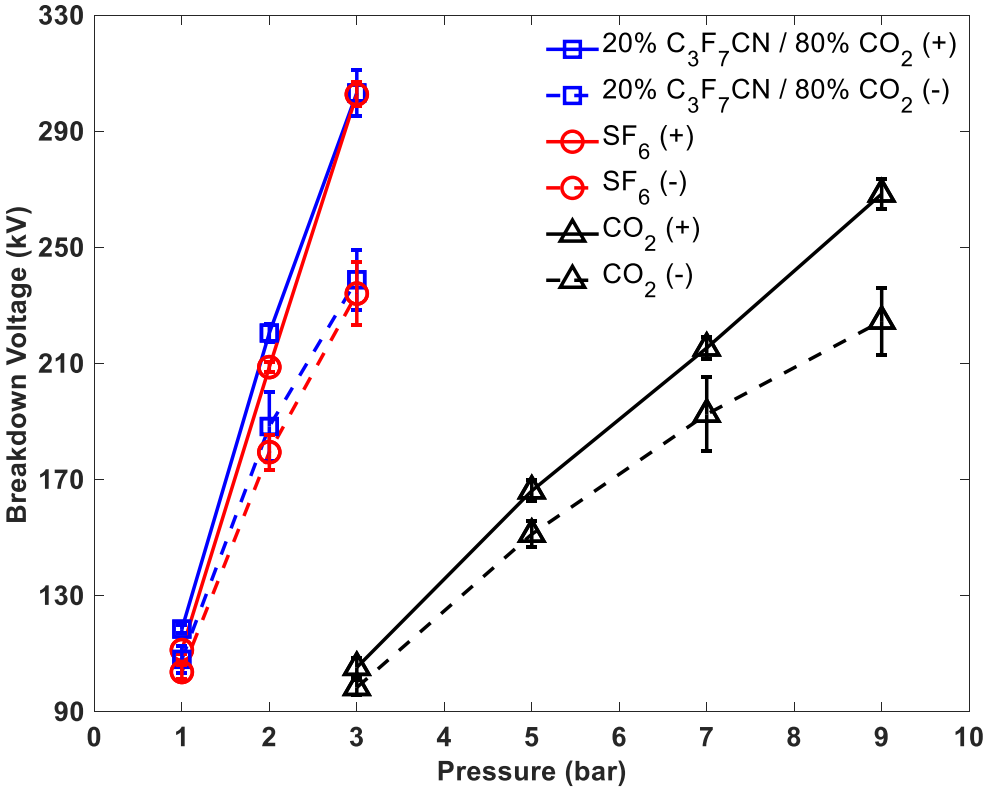

Figure 5.6 Comparison of the DC breakdown characteristics between 20% C_3F_7CN / 80% CO_2, SF_6 and CO_2 in 20/60 mm coaxial configuration under both DC polarities.

Furthermore, since the negative DC breakdowns were always lower than the positive ones in the coaxial configuration, the negatively charged conductor provided an additional source of electrons at which point the electron avalanche can be initiated at a lower electric field when compared to the case in positive DC polarity [13]. Thus, the equipment insulation level must be designed for the lower breakdown voltage polarity.

From the dielectric performance comparison, the 7% C_3F_7CN / 93% CO_2 and 4% $C_5F_{10}O$ / 96% CO_2 mixtures provide a dielectric performance at 75% and 55%, respectively, for SF_6 in the tested pressure range and coaxial geometries shown in Figures 5.4 and 5.5, while CO_2 is around one-third that of SF_6, as shown for both 10/30 and 20/60 coaxial configurations in Figures 5.4 and 5.6. To attain a comparable breakdown performance to SF_6, in the case of the 7% C_3F_7CN concentration, additional pressure needs to be considered in the design of new-build equipment for this mixture by taking into account the boiling point limit and conductor surface roughness sensitivity. For the 4% $C_5F_{10}O$ mixture, increasing the gas pressure to enhance the breakdown strength was not possible in this case due to it having a very high liquefaction temperature [143]. While in CO_2 gas, a larger footprint than that used for SF_6 was needed since only increasing the pressure leads to a non-practical level to match the SF_6 performance, due to the effect of pressure on the breakdown voltage saturating eventually at some point in the high-pressure range. For the breakdown voltage comparison between SF_6 and 20% C_3F_7CN / 80% CO_2, both gases have shown comparable breakdown characteristics in all the investigated coaxial geometries, gas pressures and DC polarities in this study. Thus, a 20% C_3F_7CN / 80% CO_2 gas mixture could technically replace SF_6 from a dielectric breakdown perspective at a comparable working pressure.

5.5 Effect of Conductor Surface Roughness in Coaxial Geometry

To enhance the judgment on the viability of the proposed gas as a one-to-one scenario, further investigation in this section will be conducted on the effect of conductor surface roughness on the breakdown characteristics in coaxial geometry for both gases to evaluate the p·h threshold value at which breakdown voltages start to decline. This will effectively evaluate the 20% C_3F_7CN / 80% CO_2 gas mixture under conditions such as using current SF_6 equipment with their practical surface finishes. Figures 5.7 and 5.8 show the effect of surface roughness on the breakdown characteristics of both DC polarities in 20% C_3F_7CN / 80% CO_2 and SF_6 in a 10/30 mm coaxial configuration at gas pressures of 2, 4 and 5 bar and conductor surface roughness of 8-121.8 µm R_z values.

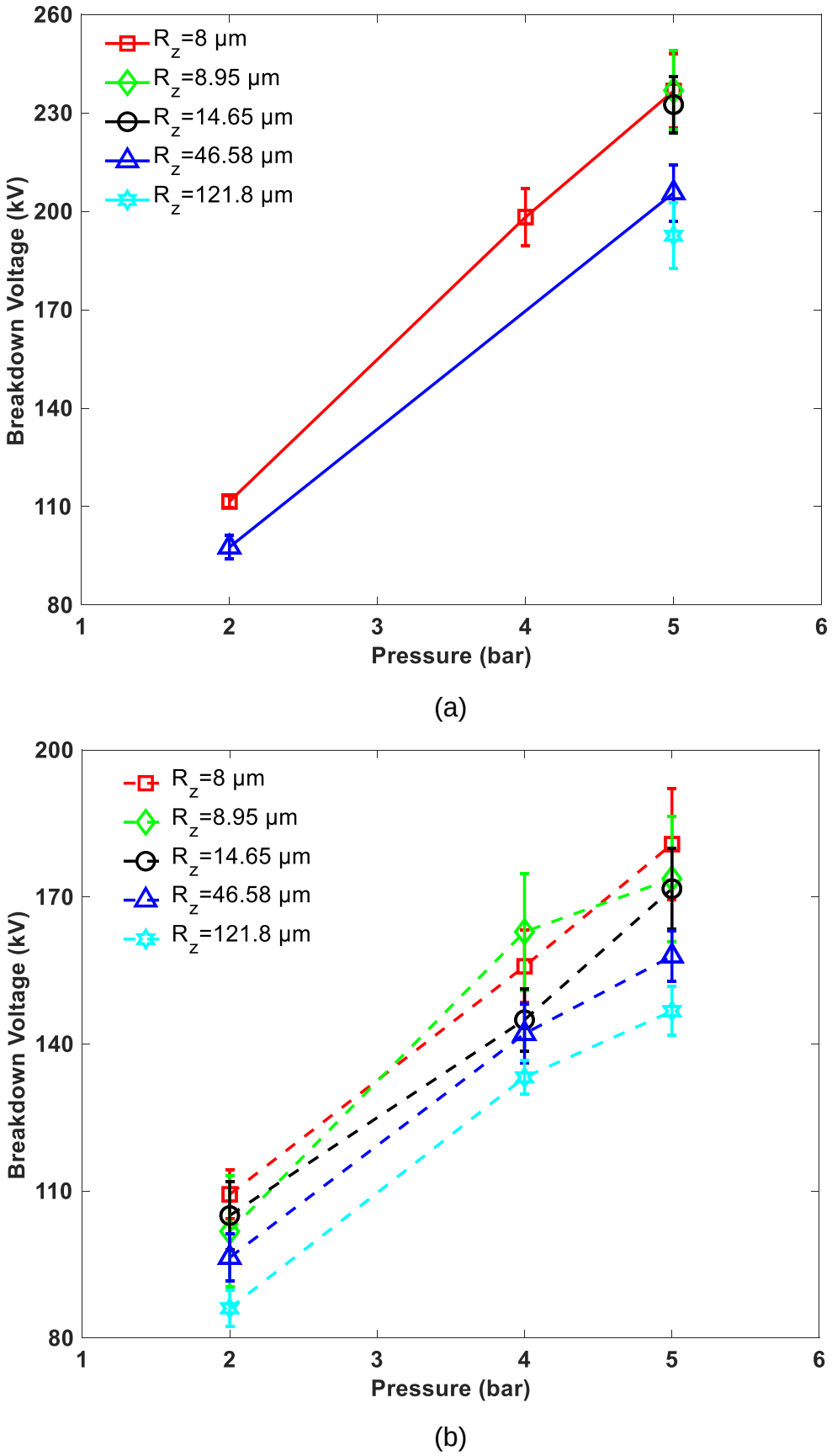

Figure 5.7 DC breakdown characteristics comparison under different conductor surface roughness in a 10/30 coaxial configuration for 20% C_3F_7CN / 80% CO_2 for (a) positive and (b) negative DC polarity.

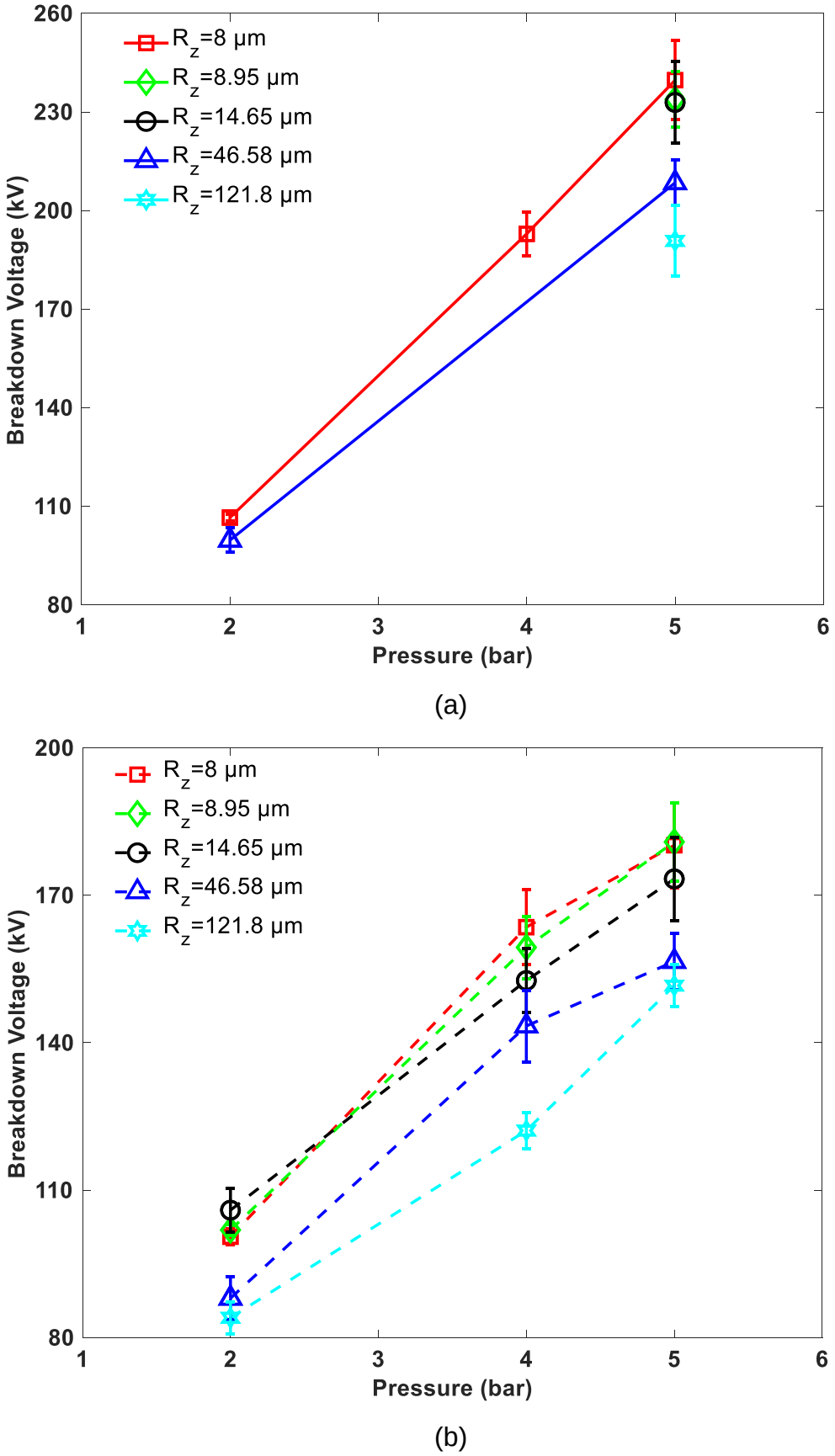

Figure 5.8 DC breakdown characteristics comparison under different conductor surface roughness in a 10/30 coaxial configuration for SF_6 for (a) positive and (b) negative DC polarity.

According to Figures 5.7 and 5.8, the maximum possible breakdown voltage under both DC polarities is attained when the conductor surface roughness is at its minimum in both gases. Conductors with R_z values of 8, 8.95 and 14.65 µm demonstrated a comparable breakdown voltage performance, with 14.65 µm being comparatively lower than the others. While for higher R_z values, such as 46.58 and 121.8 µm, a clear reduction in the breakdown voltage values were observed with the negative DC polarity being more sensitive towards surface roughness than the positive one. These differences in the breakdown voltages are more visible at higher pressures, such as for the 5 bar results. This accords with what was observed in [90] for a 6% C_3F_7CN / 94% CO_2 gas mixture. From the dependency of the breakdown voltage value on the gas pressure and protrusion height, there is a p·h threshold value at which a significant drop on the breakdown voltage can be observed when this is exceeded.

Figure 5.9 presents an evaluation of the effect of p·h values on the breakdown voltage in both 20% C_3F_7CN / 80% CO_2 and SF_6 in all of the tested conductor surface roughness conditions and gas pressures. The results demonstrate that increasing gas pressure resulted in a steeper reduction in breakdown voltage for both SF_6 gas and the C_3F_7CN/CO_2 mixture when tested for a rougher conductor surface. Both gases exhibit similar behaviour in terms of their sensitivity towards the p·h, with a threshold range for both gas candidates around 40-50 bar·µm. The threshold established for SF_6 is consistent with previous reports in [49], [90], [112].

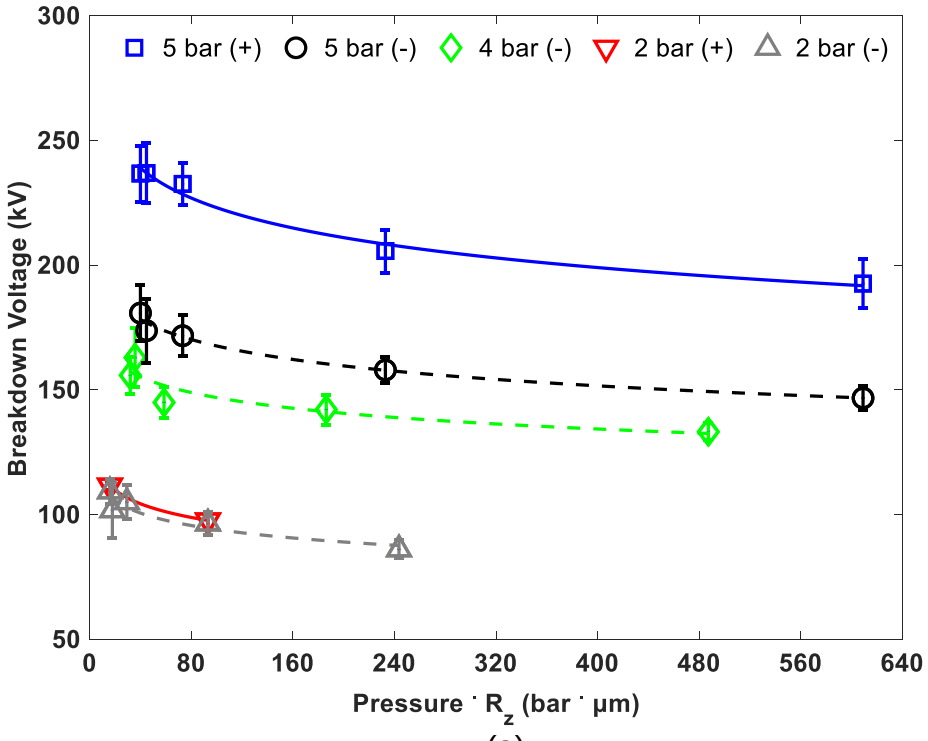

(a)

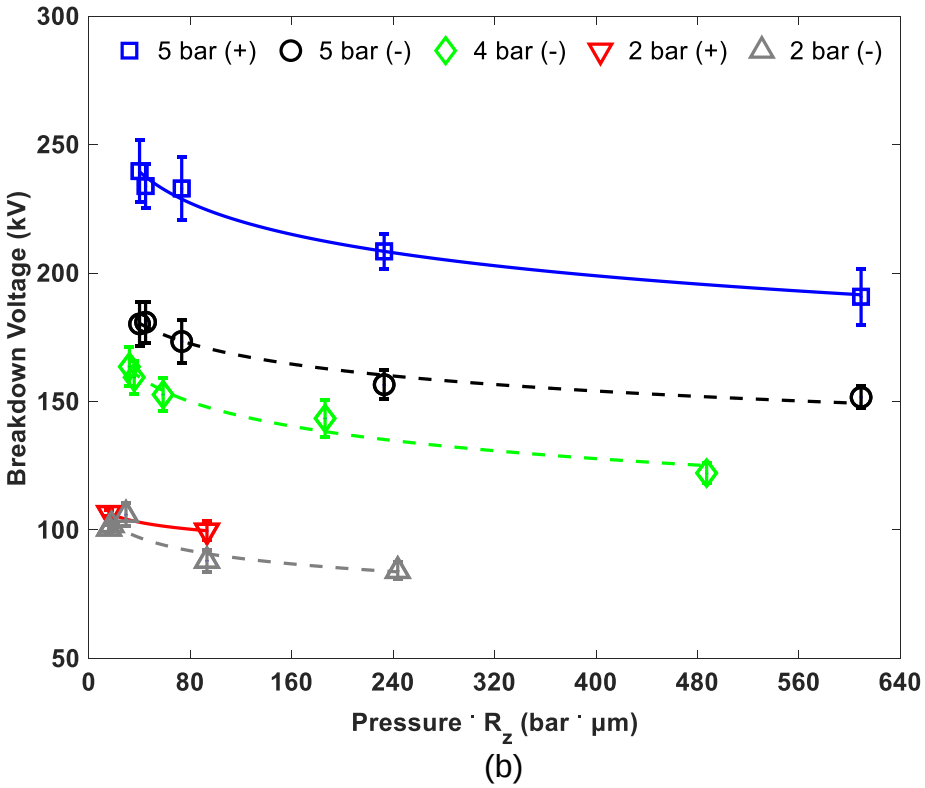

Figure 5.9 DC breakdown characteristics as a function of gas pressure and protrusion height tested in a 10/30 coaxial configuration for (a) 20% C_3F_7CN / 80% CO_2 gas mixture and (b) SF_6 gas.

From the breakdown results tested in this section, E_{max}/p will be calculated and compared against $(E/p)_{crit}$ (see Table 6.1 for the $(E/p)_{crit}$ values used) and shown in Figure 5.10. The following Equation 5.1 was used to calculate the E_{max}/p in coaxial geometry and derived by substituting Equation 3.2 into 4.1 [16].

$$E_{max}/p_{coaxial} = \frac{U_{50}}{p \cdot R_{conductor} \cdot \ln\left(\frac{R_{enclosure}}{R_{conductor}}\right)} \tag{5.1}$$

From the results shown in Figure 5.10, E_{max}/p values for both gases appear to be decreasing whilst the p·h values are increasing. However, before the p·h threshold value, the E_{max}/p changes slowly with p·h and is comparable with $(E/p)_{crit}$. Due to the polarity effect in coaxial geometries discussed earlier in Section 5.4, negative polarity E_{max}/p for 5 and 4 bar pressures are below $(E/p)_{crit}$ regardless of the p·h range, while at 2 bar pressure it is consistent with $(E/p)_{crit}$ as in the positive polarity before the p·h threshold value, since the margins between breakdowns in both polarities are small for this pressure range. This resulting in comparable E_{max}/p characteristics for both DC polarities.

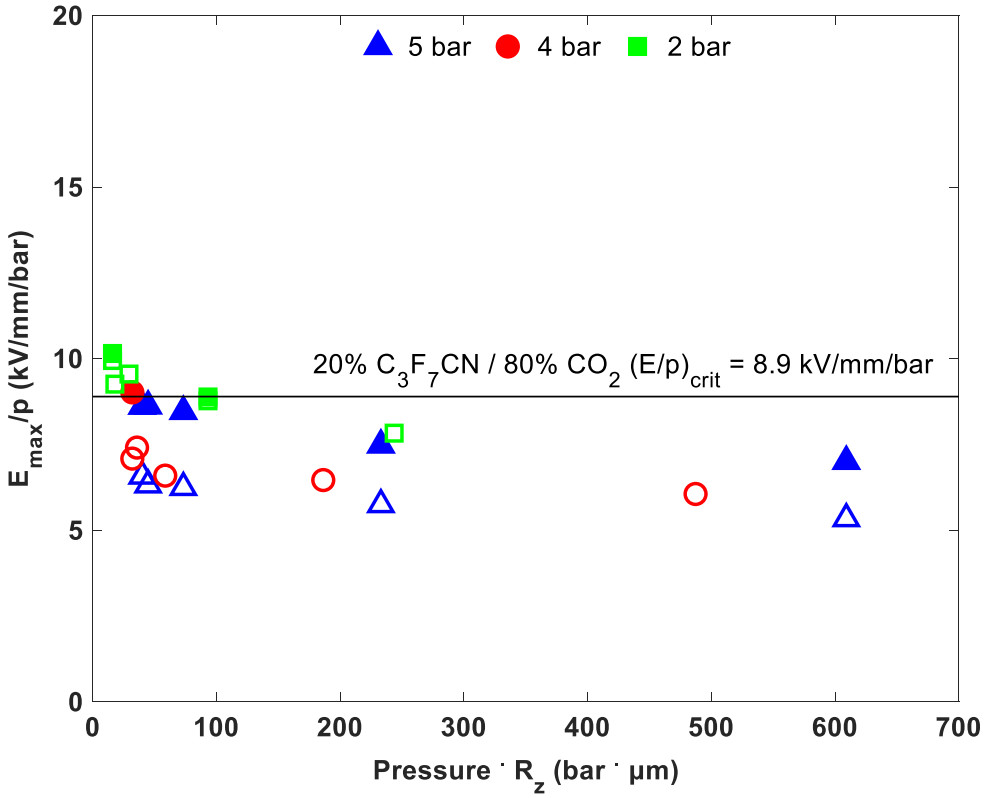

(a)

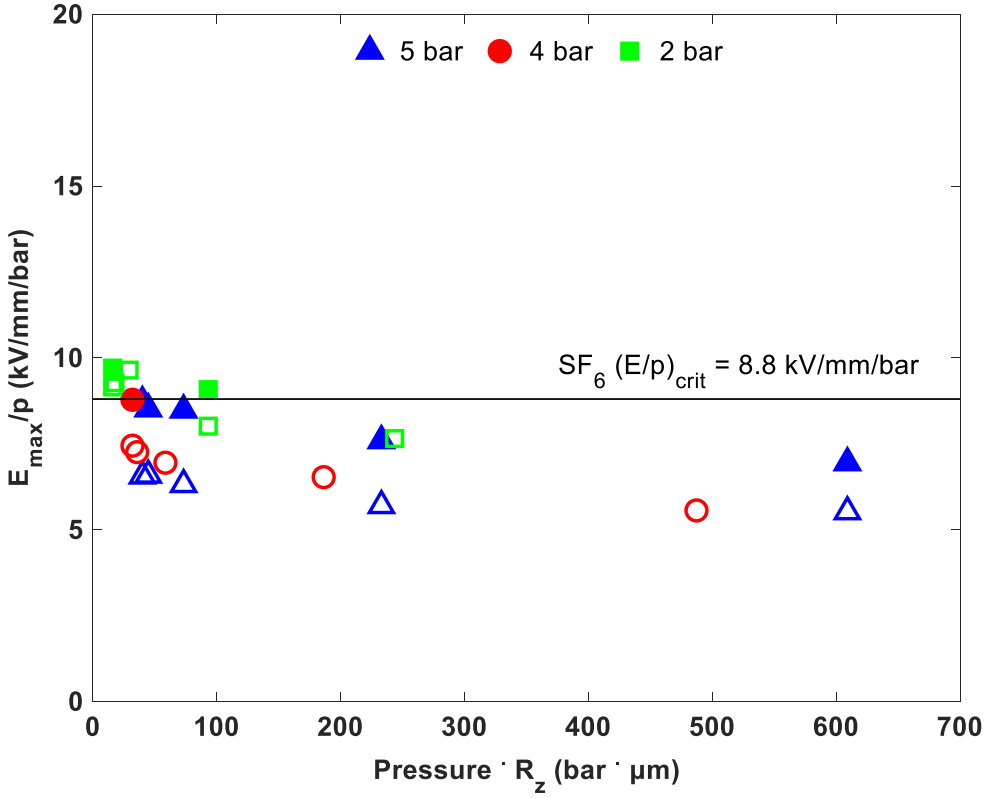

(b)

Figure 5.10 Effect of pressure and protrusion height on E_{max}/p in a 10/30 coaxial configuration for (a) 20% C_3F_7CN / 80% CO_2 and (b) SF_6. Filled markers are positive and unfilled markers are negative E_{max}/p values calculated from breakdown results.

In order to evaluate the p·h threshold value quantitatively from the experimental E_{max}/p for both gases, a mathematical quantity defined as T_p, and calculated based on Equation 5.2, will be used to align both trends of E_{max}/p for SF_6 and the 20% C_3F_7CN / 80% CO_2 mixture at the same scale [118].

$$T_p = \log_{10}\left(\frac{E_{max}/p}{(E/p)_{crit}}\right) \tag{5.2}$$

A suitable criterion for the p·h threshold value of E_{max}/p can be obtained at T_p=-0.05 [118]. This is when the experimental E_{max}/p reaches about 90% of $(E/p)_{crit}$. Based on this definition, the p·h threshold value of the 20% C_3F_7CN / 80% CO_2 gas mixture and SF_6 gas are estimated to be equal to 42.7 bar·µm and 47.4 bar·µm, respectively (illustrated in Figure 5.11). These values fall between 40-50 bar·µm as expected due to this being the established p·h threshold range reported in the literature for SF_6 [49], [90], [112]. There is potential to retrofill 20% C_3F_7CN / 80% CO_2 gas mixture in SF_6 designed equipment without concerns in relation to practical surface finish as it has similar dielectric performance over a range of conductor roughness.

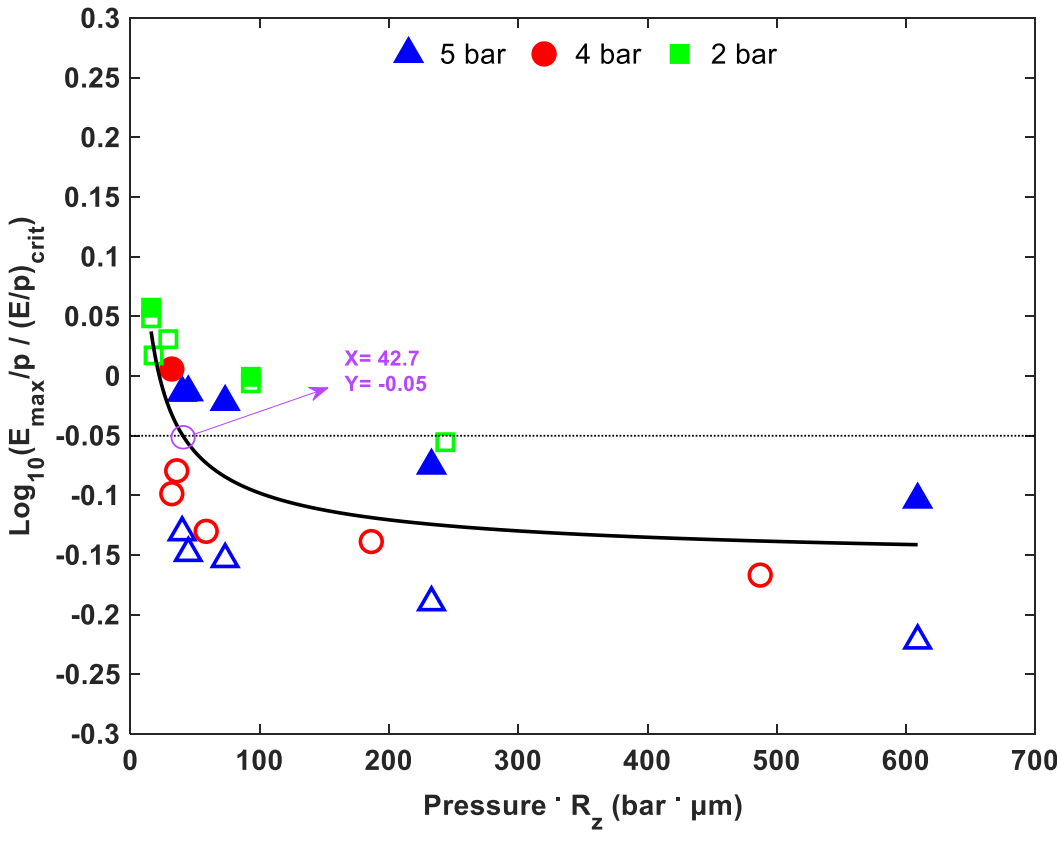

(a)

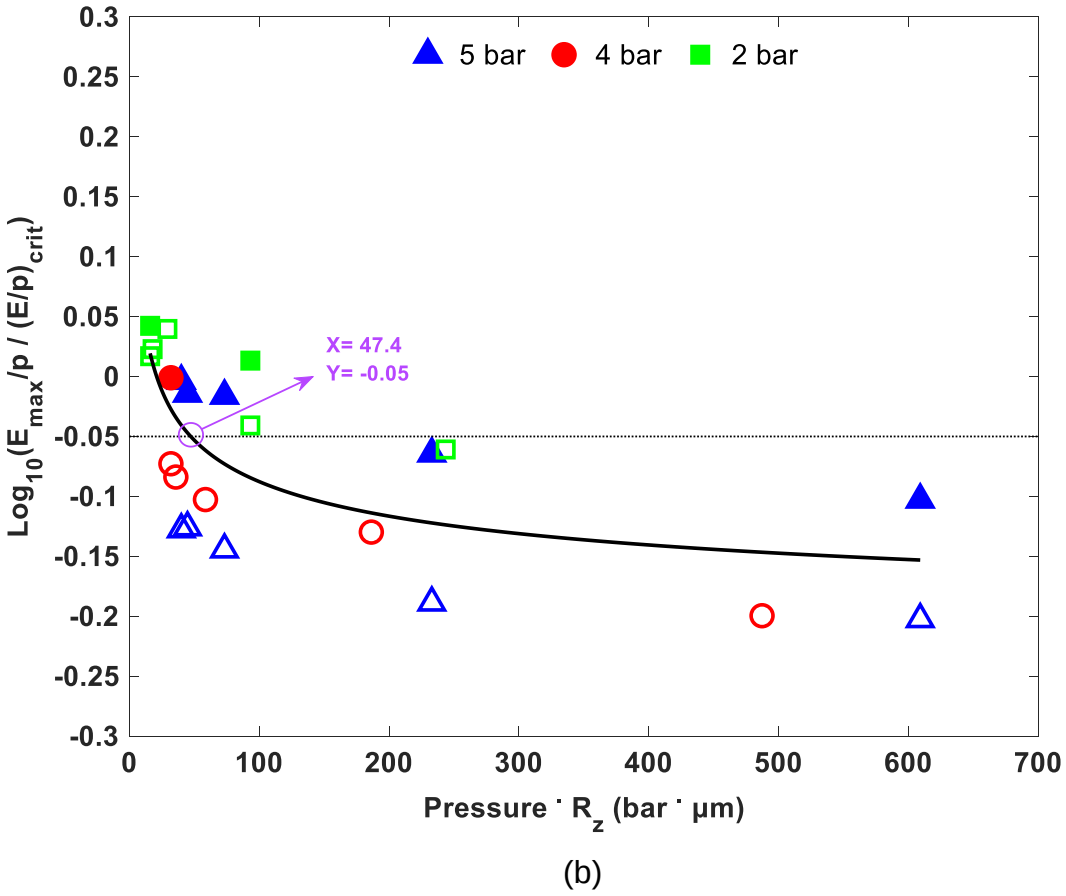

(b)

Figure 5.11 Calculated p·h threshold values of E_{max}/p at a T_p of -0.05 as a threshold criterion in a 10/30 coaxial configuration for (a) 20% C_3F_7CN / 80% CO_2 and (b) SF_6. Filled markers are positive and unfilled markers are negative E_{max}/p values calculated from breakdowns.

5.6 Summary

This chapter has investigated the DC breakdown characteristics in a quasi-uniform field in reduced scale coaxial geometries. Differently sized coaxial geometries were used at conductor/enclosure diameters of 10/30, 15/45 and 20/60 mm representing the optimal ratio and 8/30 and 15/30 mm as a non-optimal ratio. The DC breakdown characteristics of 20% C_3F_7CN / 80% CO_2, 7% C_3F_7CN / 93% CO_2, 4% $C_5F_{10}O$ / 96% CO_2, SF_6 and CO_2 gases were examined under both DC polarities. The effect of conductor surface roughness on the DC breakdown characteristics of 20% C_3F_7CN / 80% CO_2 when compared with SF_6 were examined in 10/30 coaxial geometry with R_z varied from 8-121.8 µm at pressures of up to 5 bar to establish a p·h threshold value for both gases.

The results show that the effect of a coaxial optimal ratio attains a higher breakdown voltage as it provides a lower E_{max} when compared with other ratios in both SF_6 gas and the 20% C_3F_7CN / 80% CO_2 gas mixture, while a negligible difference was observed on the

breakdown voltages at elevated pressure in the 20% C_3F_7CN / 80% CO_2 gas mixture using an AL and SS made enclosure/conductor due to their work functions being comparable.

20% C_3F_7CN / 80% CO_2 gas mixture matches SF_6 gas for a wide range of test conditions, including the conductor surface roughness effect. A common threshold p·h range of 40-50 bar·μm was established for both gases that is consistent with the previously reported value for SF_6 gas, where a significant reduction in the breakdown performance was observed for higher p·h values. This indicates that a 20% C_3F_7CN / 80% CO_2 gas mixture can be retrofilled in existing SF_6 designed equipment without concern about insulation performance reduction due to the practical conductor surface finish.

Low C_3F_7CN concentrations, such as 7%, provides around 75% of the SF_6 dielectric performance that can be mitigated by increasing the gas pressure until it matches the performance of SF_6 by considering the liquefaction temperature and surface roughness sensitivity towards the practical surface finish. While a 4% $C_5F_{10}O$ mixture attains 55% of SF_6's dielectric performance, it is not feasible to increase the gas pressure to enhance the dielectric strength due to the liquefaction temperature limitation for engineering applications. In the case of CO_2, a larger footprint equipment of that used for SF_6 is required since increasing the pressure until it matches the dielectric strength of SF_6 will lead to an impractical pressure level due to the saturation effect.

6 MODELLING OF THE DC BREAKDOWN CHARACTERISTICS OF SF_6 AND ITS ALTERNATIVES

6.1 Introduction

Currently, many alternatives to SF_6 are under investigation, with most of them posing limitations in terms of dielectric strength, toxicity and high boiling point, as detailed in prior Chapter 2. For every gas candidate and mixture ratio, a full experimental investigation set that includes different electrode configurations, surface roughness and gas pressures is required for appropriately characterise the breakdown performance of each candidate gas. This is time and resource intensive experimental approach and impractical for screening every alternative gas or mixture to SF_6.

This chapter aims to develop a generalised modelling approach that can estimate the DC breakdown characteristics of different insulation gases, prior to any experimental work. A simulation based on the streamer inception criterion model has been developed to calculate the streamer inception voltage, which will then be compared to the actual breakdown voltage results obtained experimentally from previous Chapters 4 and 5 under both rod-plane and coaxial electrode configurations. It will take into account gas medium and pressure, electrode design and field uniformity, including different rod-plane diameters, inter electrode gap distance and different size coaxial geometries close to the optimal ratio and conductor surface roughness, as found in practical equipment such as GIB and GIL [13]. This will optimise the selection process of new SF_6 alternatives without having to perform a significant level of experimental activity.

6.2 Streamer Inception Criterion

Streamer mechanism models assume that a fast-moving streamer will be initiated from the head of a single electron avalanche. Highly conductive channels in the gap will be formed from these streamers, which ultimately lead to the breakdown event [144]. Equation 6.1 is a simplified version of Meek's equation and later modified by Pedersen to acquire a semiempirical streamer inception criterion. It is widely accepted that this simplified streamer

inception criterion model is best used to estimate the breakdown voltage where it is a precursor for the breakdown, typically, in quasi-uniform and weakly non-uniform fields regions as increasing the field non-uniformity will cause a transition in the breakdown mechanism from streamer inception to propagation (refer to Section 2.5.7) [56], [57], [60], [145], [146].

$$\int_0^{x_c} \alpha_{eff}(x)dx = K \tag{6.1}$$

where x_c denotes the critical avalanche length at the instant of streamer initiation, α_{eff} is the effective ionisation coefficient at the head of the avalanche (α_{eff} = ionisation coefficient (α) − attachment coefficient (η)) and K is a constant derived from the critical avalanche size (N_c) logarithm. To enable an avalanche to transform into a streamer, N_c values between 10^4-10^8 electrons were reported in the literature, which are associated with K of 9.5-20 (see Section 2.5.6) [24], [48]–[50], [56]–[58]. In this current study, a fixed K value of 10.5 will be used for all gases as it has been widely applied to SF_6 in the literature and provides a generalised modelling approach [56], [57]. In a uniform field, x_c is comparable with the interelectrode gap distance, whereas in a non-uniform field, x_c is the distance at the shortest path from the high-voltage electrode to the point where $\alpha_{eff} = 0$ and it is shorter than the gap distance [56], [146].

As α_{eff} is strongly dependent on the electric field distribution and electrode system used, it can be calculated from the linear approximation between α_{eff}/p and f(E/p), as in Equation 6.2, for a given pressure (p) and gas medium [56], [57], [145], [146], with field dependencies obtained from parameters A and B (B is also known as $(E/p)_{crit}$) for gases and mixtures (as shown in Table 6.1).

$$\frac{\alpha_{eff}(x)}{p} = A\left[\frac{E(x)}{p} - B\right] \; in \; (mm \cdot bar)^{-1} \tag{6.2}$$

The calculation of the A and B parameters shown in Table 6.1 were obtained through the linear regression of the effective ionisation coefficient over E/p experimentally obtained in [57], [85]–[89], [147]–[149] and applied for the streamer inception modelling of this study.

Table 6.1 A, B and K parameters used for streamer calculation [57], [85]–[89], [147]–[149].

Gas	A (kV^{-1})	B or $(E/p)_{crit}$ (kV/mm/bar)			K
		Range	Used		
			Rod-Plane	Coaxial	
7% C_3F_7CN / 93% CO_2	31	5.9-6.8	-	6.4	10.5
20% C_3F_7CN / 80% CO_2	33	8.9-9.1	9.1	8.9	
4% $C_5F_{10}O$ / 96% CO_2	11	3.9-4.2	-	4.2	
HFO1234ze(E)	1.9	5.2		-	
SF_6	27	8.8-8.9	8.9	8.8	
CO_2	12	2.6-2.9	2.9	2.7	

In order to compute the field line data sets of E(x) for the shortest path between the high voltage electrode and ground electrode, FEA was used for the computation of E(x) as detailed in the following, this was done for all the electrode configurations tested earlier in the experimental work of this study.

6.2.1 Rod-Plane Field Line Data Set of E(X)

Three different sized rod-plane electrodes were used in this investigation with diameters of 3.5 mm, 6.25 mm and 12.5 mm respectively. The shortest field line of these electrodes is presented in Figure 6.1. The electrode configurations shown in Figure 6.1 were drawn in COMSOL (similar to Figure 3.8), with the shortest path electric field line data then extracted for all the tested rod diameters and gap distances. Finally, the extracted electric field data sets were used to evaluate the breakdown criterion in Equations 6.1 and 6.2 (see Appendix A.1 for the extracted field line data set of E(x) in the rod-plane configurations).

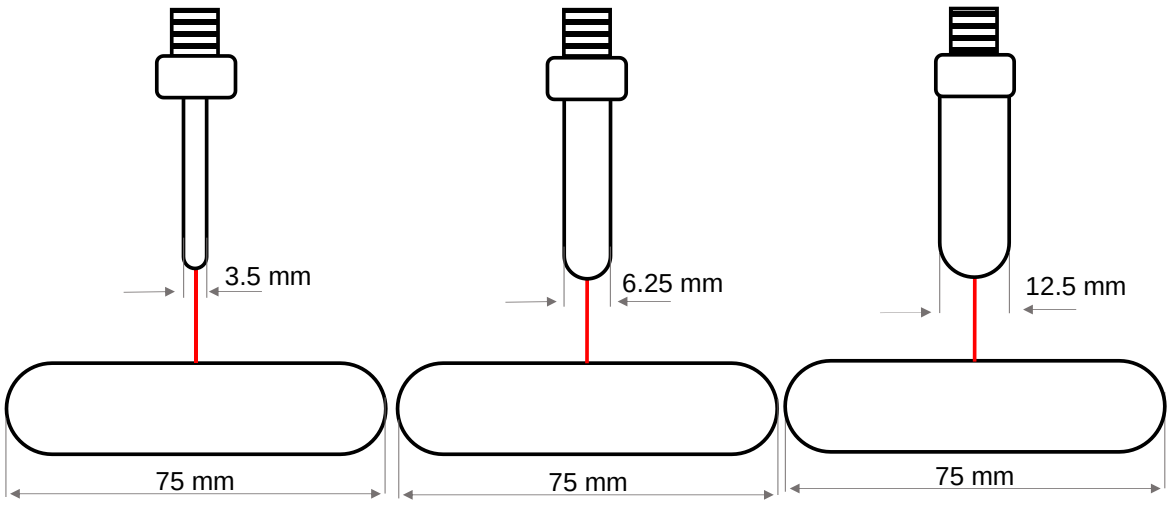

Figure 6.1 Shortest path field line extracted data set drawn in red for the tested rod-plane electrodes.

6.2.2 Single Protrusion Field Line Data Set of E(x) for Coaxial Geometries

FEA was conducted using COMSOL to compute the field line data set of E(x) of the shortest path between conductor and enclosure for the tested coaxial electrodes for a ratio of 1/3 for conductor/enclosure diameters of 10/30, 15/45 and 20/60 mm. This takes into account the surface roughness of the conductor by using a single hemispherical protrusion (shown in Figure 6.2) [112].

The height of the protrusion is equal to the measured R_z values (as in Table 3.3), while the width is set at 500 µm, similar to the one in Figure 3.16 (b) for the R_z of 121.8 µm conductor example. It is adjusted according to the protrusion height for other conductor roughness values. The extracted electric field data sets were used to evaluate the breakdown criterion in Equations 6.1 and 6.2 (see Appendix A.2 for the extracted field line data set of E(x) in the coaxial geometries).

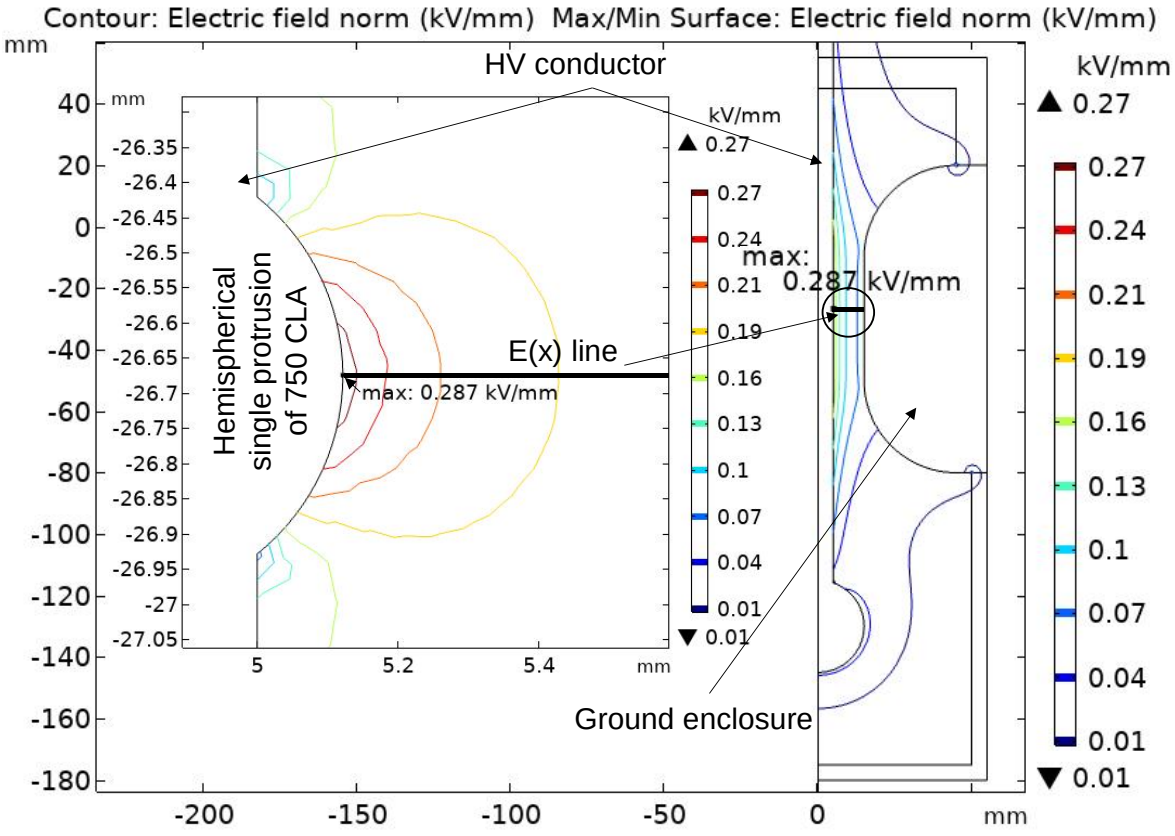

Figure 6.2 COMSOL simulation of a 10/30 mm coaxial configuration with a single hemispherical protrusion on the high-voltage conductor with a R_z of 121.8 µm for the computation of E(x) at 1 kV applied voltage.

The effect of the introduced hemispherical protrusion on the E_{max} values for all the surface roughness values are presented in Table 6.2. Without considering the conductor surface roughness effect, the simulated E_{max} is as low as 0.182 kV/mm, which does not represent the roughness condition in practical equipment. When factoring the surface roughness effect, E_{max} varied from 0.208-0.287 kV/mm for R_z values ranging between 8-121.8 µm for the conductor surface finish. These E_{max} values are used to estimate the effect of conductor surface roughness on the breakdown strength.

Table 6.2 Effect of surface roughness on the E_{max} values obtained from a COMSOL simulation with an applied voltage of 1 kV.

Designed Center Line Average (CLA)	Measured R_z (µm)	E_{max} (kV/mm)
No surface roughness	-	0.182
8 (mirror-finish)	8.00	0.208
16	8.95	0.210
32	14.65	0.217
250	46.58	0.246
750	121.80	0.287

6.2.3 Streamer Criterion Inception Voltage Calculation

Figure 6.3 demonstrates the calculation principle of the streamer criterion in accordance with Equations 6.1 and 6.2. After extracting the field line data set E(x) from COMSOL as in sections 6.2.1 and 6.2.2, E(x) will be scaled and evaluated based on the applied voltage by increasing the voltage value from 1 kV to the point at which it is sufficient to yield an integral's solution over the positive α_{eff} range that is equal to K=10.5, where this voltage is the streamer inception voltage U_i representing the positive breakdown voltage values that will be shown as dotted lines in the result figures in the next Sections 6.3 and 6.4 [50], [52].

If one sees through the definition of the streamer inception criterion, the lowest possible breakdown voltage, or $U_{1\%}$ (representing a 1% probability of breakdown), should be considered in the comparison between the calculated voltage values and the experimentally obtained ones. However, $U_{1\%}$ does not depict the true picture of the minimum breakdown voltage value as it is highly subjected to change with each repetition of the experiment, since breakdown event is a statistical random event. Therefore, the comparison will be based on the experimentally obtained U_{50} values and their error bars representing a central tendency of the observed breakdown voltages within an acceptable uncertainty margin.

A MATLAB code was written to carry out the calculations shown in Appendix B for both the rod-plane and coaxial electrodes configurations. The procedural steps involved in the modelling and calculation of the inception voltage U_i are summarised in the following steps:

1. Draw the electrodes configurations in COMSOL and extract the shortest path field line data set of E(x) at 1 kV.
2. Input A, B, K and p.
3. Define the voltages or scaling factor range (voltage = [1, …, 350]).
4. Multiple the scaling voltage value by the extracted field E(x).
5. For each x value, evaluate if E(x)·voltage/p < B, if yes, α_{eff}=0, otherwise use Equation 6.2 for α_{eff} calculation. Record all the α_{eff} and x values.
6. Evaluate Equation 6.1 and check if the integral is equal or greater than K.
7. If not, repeat from 4 considering the next higher scaling voltage.
8. If yes record the voltage as this voltage is the U_i voltage.

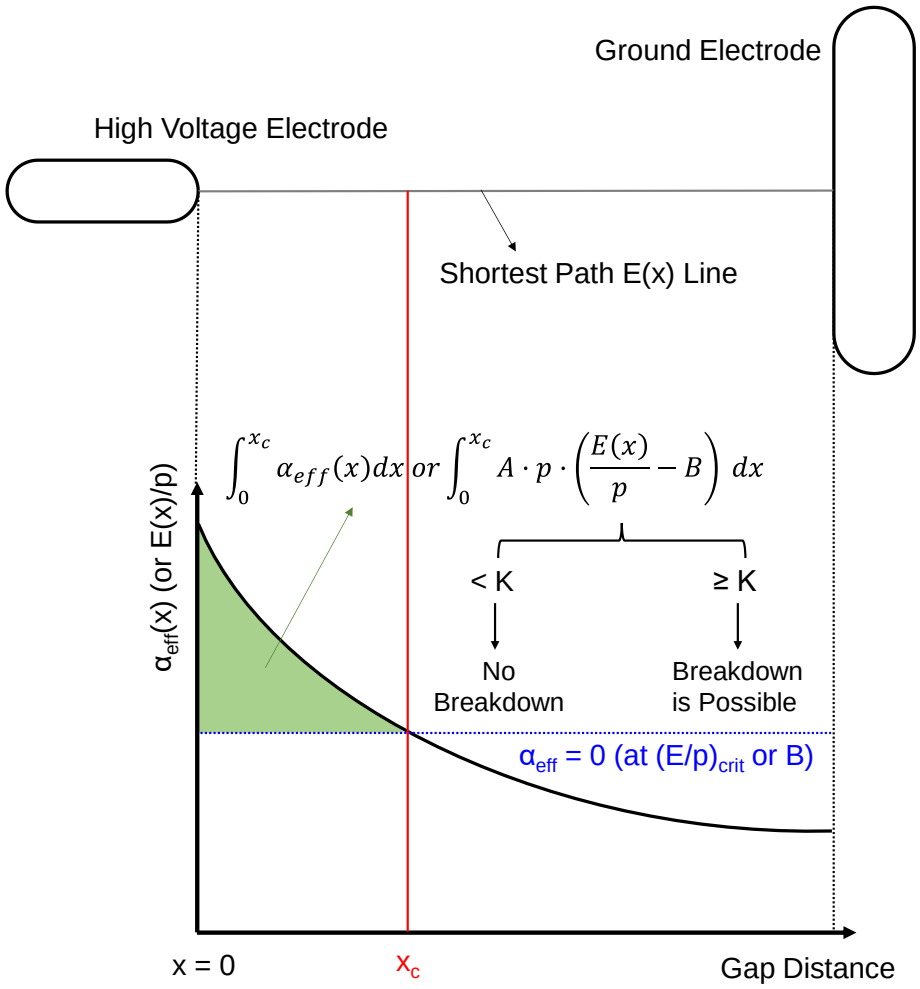

Figure 6.3 Streamer criterion evaluation method by comparing the green area (integration of α_{eff} in the positive region) with the constant K. Breakdown is possible when both are equal [50], [52].

6.3 Inception Voltage Estimation in Rod-Plane Electrodes

In this section, only the positive DC breakdown voltage will be estimated, with the found U_i calculated from Equation 6.1 being compared to the positive DC breakdown voltage obtained experimentally for all of the tested electrode's configurations, gases and mixtures in Chapter 4.

Figures 6.4 and 6.5 show the calculated U_i for all tested rod-plane electrodes, gap distances and pressures shown in Chapter 4 for SF_6. Some equivalent measurements from the literature in [81], [83], [150] are also included in the Figures.

The calculated U_i of SF_6 is close to the breakdown voltage in quasi-uniform fields at an elevated pressure, where the margin between the breakdown voltage and the U_i is at its minimum. For pressures of 2-5 bar and a quasi-uniform field, a reasonable breakdown voltage estimation can be expected due to it is being beyond the corona stabilisation region where both inception voltage and breakdown voltage coincides (see Figure 4.7) [83], [142]. This explains the poor agreement between U_i and breakdown voltage at lower pressures (below 2 bar), and for 3.5 mm rod-plane electrodes, where breakdowns are within the corona stabilisation region and the field is a non-uniform field. Consequently, streamer propagation criterion could be used to determine the breakdown voltage (see Section 2.5.7).

Figure 6.6 shows the calculated U_i for CO_2 gas tested at 7 and 9 bar pressures in 6.25 mm and 12.5 mm diameter rod-plane electrodes. Similar to SF_6, electrode field uniformity and gas pressure are the dominant factors for the accurate estimation of U_i.

This modelling approach was also able to estimate the DC breakdown voltage of HFO1234ze(E) reported in [70] under 2 bar using 25 mm diameter rod-plane electrodes at 10 mm gap distance. The experimentally reported U_{50} value is around 103.6 kV, while the calculated U_i value from the streamer inception criterion is equal to 94.88 kV.

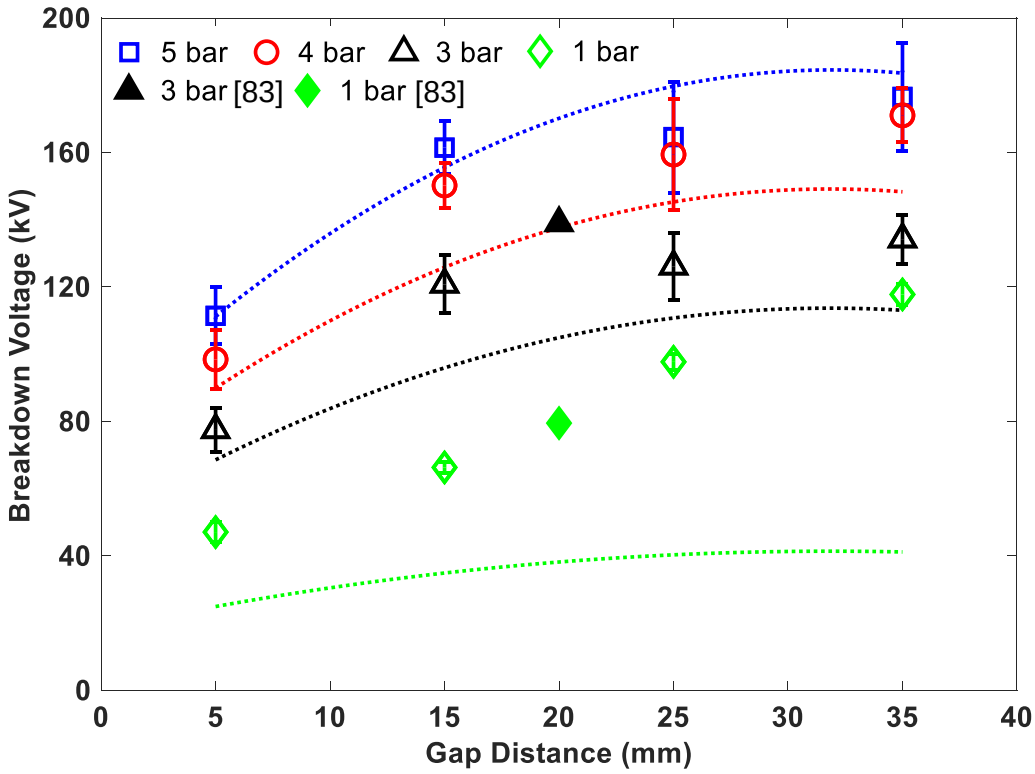

Figure 6.4 SF_6 positive DC breakdown voltage for a rod plane with a 6.25 mm-diameter rod compared to U_i (dashed lines). Filled markers are results from [83] for a 6.3 mm diameter rod-plane under 1 and 3 bar.

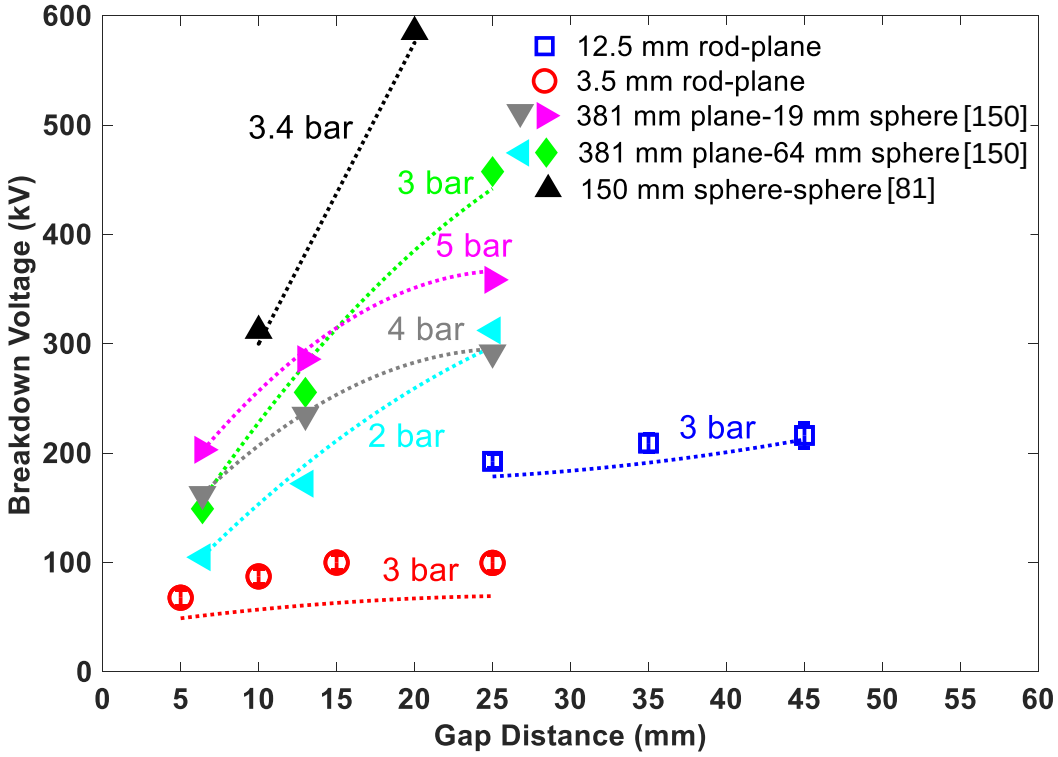

Figure 6.5 SF_6 positive DC breakdown voltage for a rod plane with rod diameters of 12.5 mm and 3.5 mm compared to U_i (dashed lines). Filled markers are results from [150] and [81] for plane-sphere and sphere-sphere configurations.

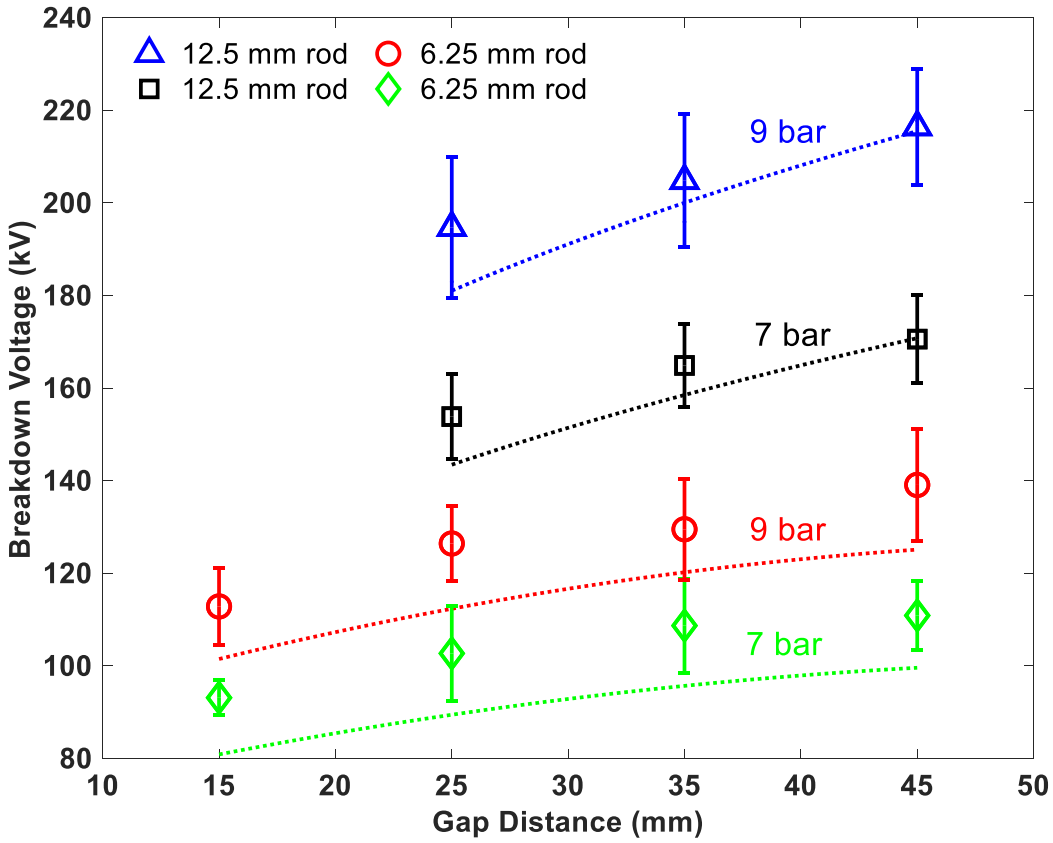

Figure 6.6 CO_2 positive DC breakdown voltage for 12.5 mm and 6.25 mm rod-plane electrodes compared to U_i (dashed lines).

In the case of CO_2 and 20% C_3F_7CN / 80% CO_2 at or below 5 bar pressure, since 80% of the gas mixture is CO_2, a corona stabilisation region wider than that for SF_6 can be expected for both gases [142]. This results in the calculated U_i using a K value of 10.5 being lower than the breakdown voltage in all cases, except for the 6.25 mm rod at 5 bar and 12.5 mm rod at 3 bar in the case of 20% C_3F_7CN / 80% CO_2, where, it should be noted, the calculated results are close to the experimental ones. For a better breakdown voltage estimation of 20% C_3F_7CN / 80% CO_2 and CO_2 at or below 5 bar pressure (assumed to be within the corona stabilisation region), the right-hand side of Equation 6.1 was divided by the f factor corresponding with the electrode design and gap distance as a correction factor that effectively increases the K value, and the breakdown criterion was calculated based on this principle to give a value of $U_{i\_corrected}$. Figures 6.7, 6.8 and 6.9 show the calculated $U_{i\_corrected}$ results for all tested electrodes at 5 bar or below in CO_2 and 20% C_3F_7CN / 80% CO_2, respectively. The results show that $U_{i\_corrected}$ provides a reasonable breakdown voltage estimation in all cases, except for 1 bar, where $U_{i\_corrected}$ is significantly lower than the measured values. This is also observed in SF_6.

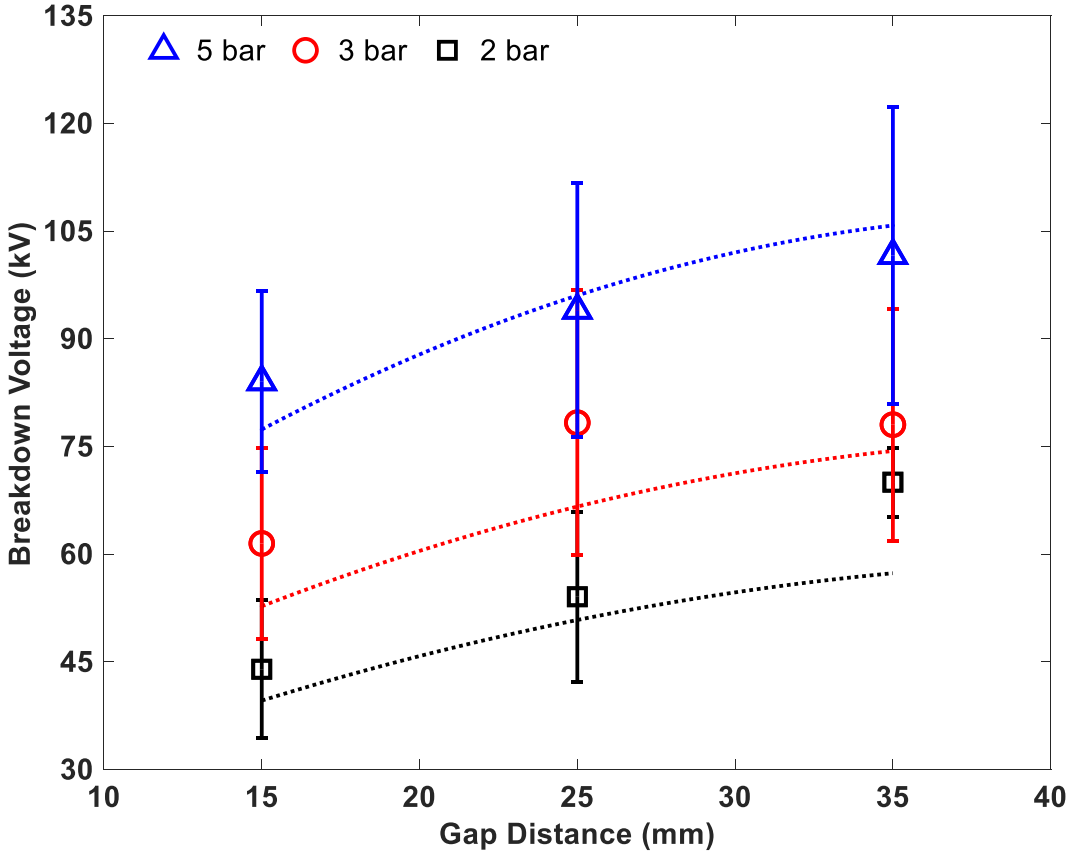

Figure 6.7 CO_2 positive DC breakdown voltage for 6.25 mm rod-plane electrodes compared to $U_{i\_corrected}$ (dashed lines).

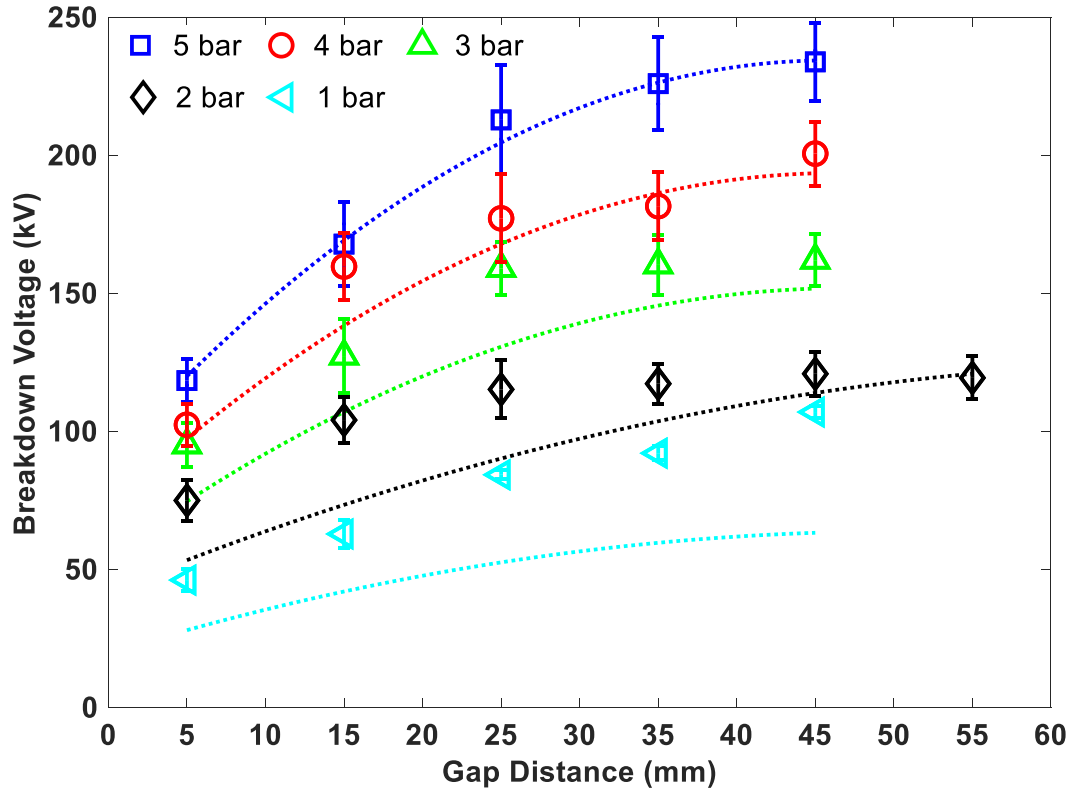

Figure 6.8 20% C_3F_7CN / 80% CO_2 positive DC breakdown voltage for 6.25 mm rod-plane electrodes compared to $U_{i\_corrected}$ (dashed lines).

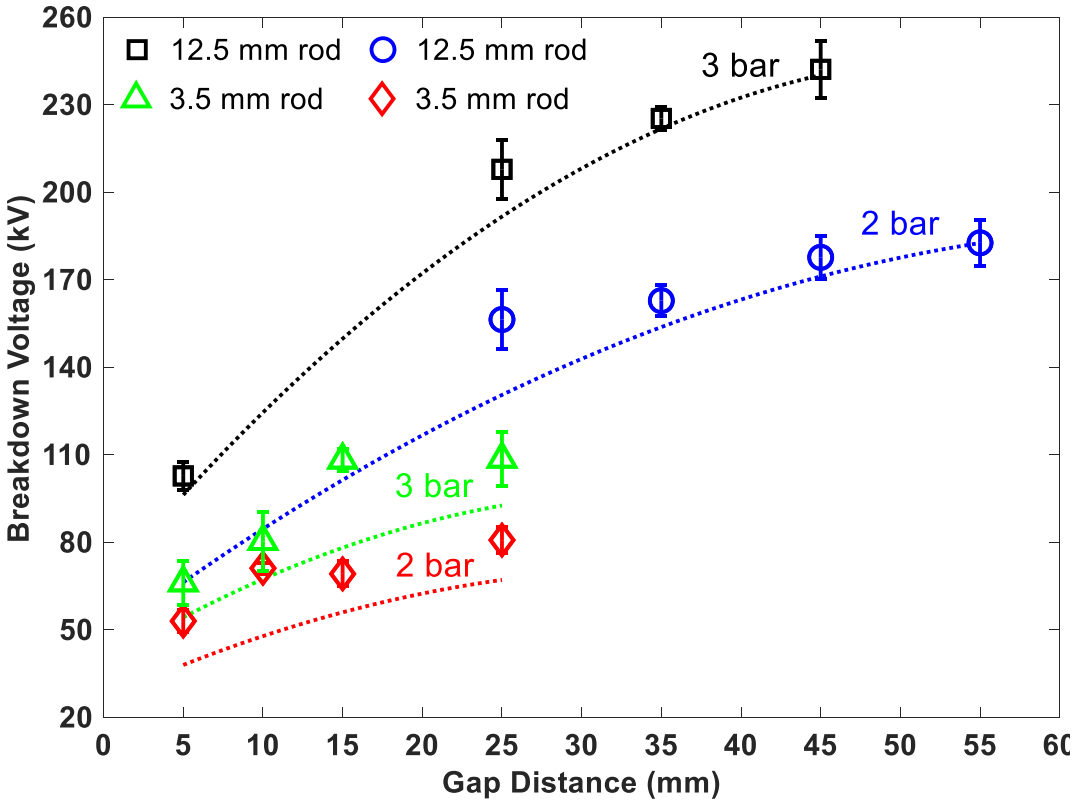

Figure 6.9 20% C_3F_7CN / 80% CO_2 positive DC breakdown voltage for 12.5 mm and 3.5 mm rod-plane electrodes compared to $U_{i\_corrected}$ (dashed lines).

6.4 Inception Voltage Estimation in Coaxial Electrodes

In this section, breakdown in both DC polarities will be estimated, with U_i representing the positive breakdown voltage values, as discussed earlier. In terms of estimating the negative breakdown voltage (U_{neg}), an empirical formula in Equation 6.3 was developed based on the polarity ratio factor (β) between the experimentally obtained positive and negative DC breakdown voltages from Chapter 5. This was achieved using the 10/30 mm coaxial configuration for 20% C_3F_7CN / 80% CO_2 and SF_6. This approach estimates the U_{neg} from the calculated U_i in Equation 6.1, which has been applied for 20% C_3F_7CN / 80% CO_2, 7% C_3F_7CN / 93% CO_2, 4% $C_5F_{10}O$ / 96% CO_2 mixtures and SF_6 gas at a fixed $R_{enclosure}/R_{conductor}$ ratio of 3 for 10/30, 15/45 and 20/60 mm coaxial configurations. At 1 bar pressure, both DC polarities are comparable with β of 1 and, thus, Equation 6.3 was used to calculate the 2-5 bar pressure levels investigated in this current study.

$$U_{neg} = \beta \cdot U_i = -0.2635 \cdot ln(0.0372 \cdot ln(p)) \cdot U_i \tag{6.3}$$

CO_2 gas was found to have a different polarity behaviour than the other tested gases. Therefore, a direct application of the polarity ratio obtained experimentally in a 10/30 mm coaxial configuration was applied to the 20/60 mm coaxial configuration to estimate U_{neg} from U_i calculated using Equation 6.1. This is mainly due to the differences between CO_2 and other tested gases in terms of the wider corona stabilisation region that contributes to the CO_2 polarity behaviour, as well as being a weakly attaching gas in comparison with SF_6, C_3F_7CN and $C_5F_{10}O$ [49], [143].

Figure 6.10 presents a comparison of the experimental and modelled breakdown voltages from Chapter 5. The modelled values are shown as dotted lines obtained from the single protrusion streamer criterion model. This approach was applied to both DC positive and negative polarities for the 20% C_3F_7CN / 80% CO_2 gas mixture shown in Figure 6.10 (a) and (b), SF_6 in Figure 6.10 (c) and (d), and 7% C_3F_7CN / 93% CO_2, 4% $C_5F_{10}O$ / 96% CO_2 mixtures and CO_2 in Figure 6.10 (e) and (f). Figure 6.10 (a), (c) and (e) show that the positive DC breakdowns at 1 bar pressure are comparatively higher than the calculated values. For a pressure range between 3-9 bar for CO_2 and 2-5 bar for other tested gases, the majority of breakdown results are within an uncertainty margin of ±5% against the calculated U_i, including literature results [81] for a 80/200 mm coaxial ratio tested for SF_6, as shown in Figure 6.10 (c). For negative breakdown data shown in Figure 6.10 (b), (d) and (f), by using the pre-determined polarity ratio β factor calculated for the 10/30 coaxial geometry, this allows a reasonable estimation of U_{neg} against experimental data for scaled-up geometries of 15/45 and 20/60 with the same geometrical ratio of 3. The majority of the estimated results from the modelling approach is within ±5% with some results shown to be above ±5% but less than the ±10% presented in the experimental data in this current study. In Figure 6.10 (c), from the breakdown results of the 80/200 mm coaxial configuration reported in [81], despite the geometrical ratio being different to the ratio of 3 used in this current study, the modelled positive breakdown results are comparable with the literature data. A bigger deviation in the modelled negative results can be expected for coaxial geometries that are far apart from the optimal coaxial ratio. A different polarity ratio factor should be experimentally obtained to provide better estimation of those geometries.

Figure 6.11 compares the experimental and calculated breakdown voltage values in the effect of surface roughness on the breakdown characteristics of both DC polarities in SF_6 and 20% C_3F_7CN / 80% CO_2 in a coaxial configuration of 10/30.

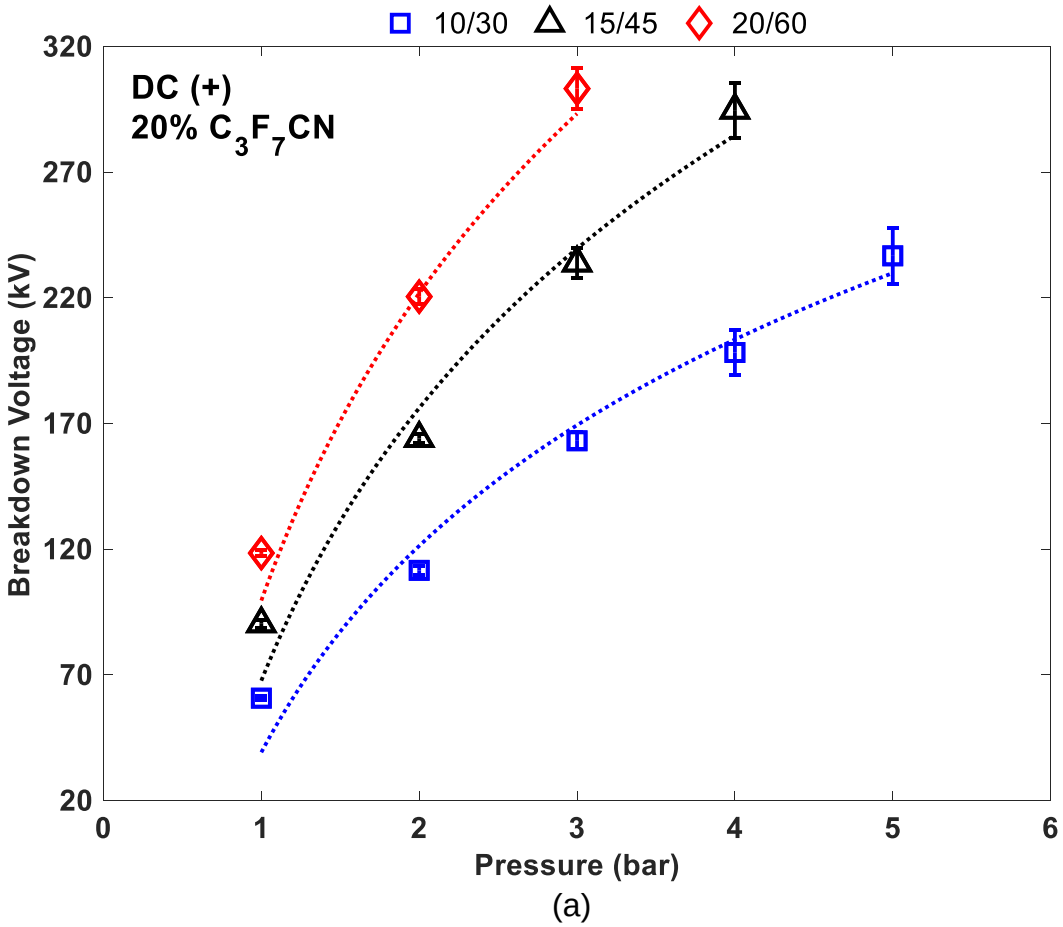
10/30
15/45
20/60
DC (+)
20% C3F7CN
Breakdown Voltage (kV)
Pressure (bar)
320
270
220
170
120
70
20
0
1
2
3
4
5
6

(a)

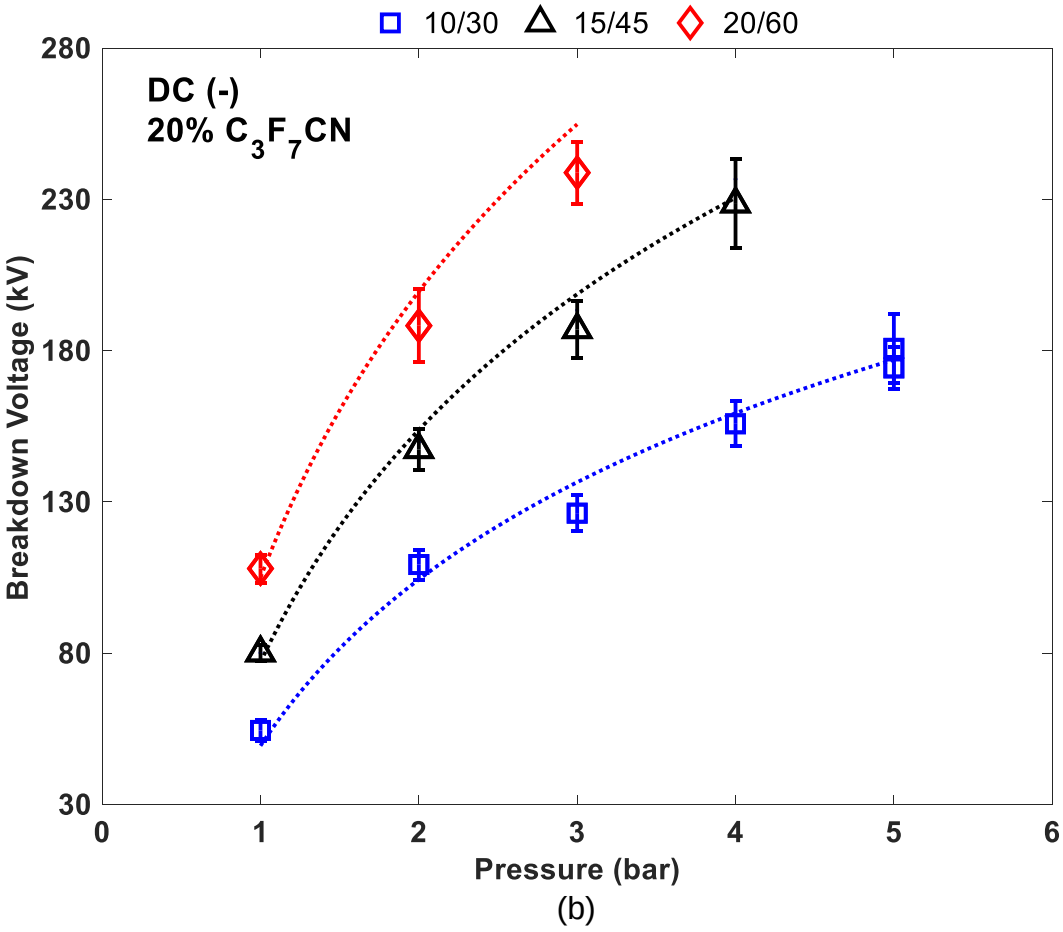
10/30
15/45
20/60
DC (-)
20% C3F7CN
Breakdown Voltage (kV)
Pressure (bar)
280
230
180
130
80
30
0
1
2
3
4
5
6

(b)

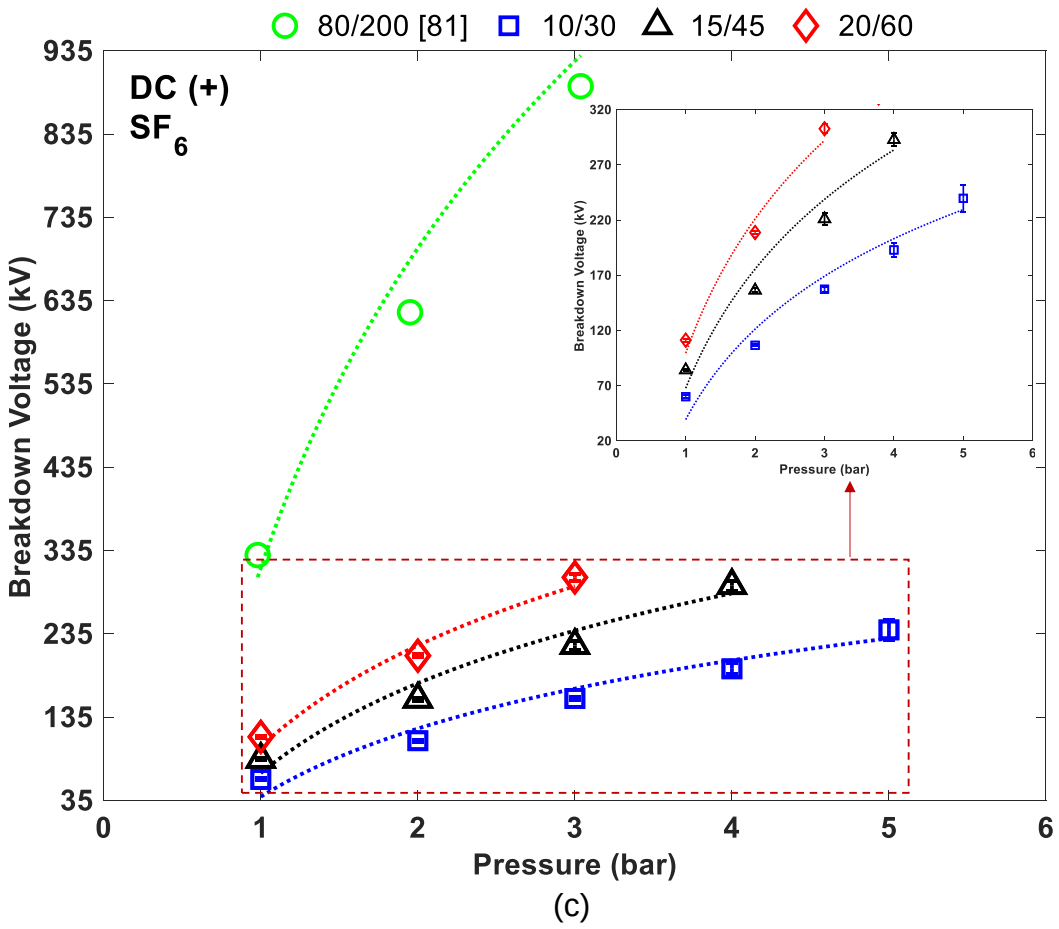
80/200 [81]
10/30
15/45
20/60
DC (+)
SF6
Breakdown Voltage (kV)
Pressure (bar)
935
835
735
635
535
435
335
235
135
35
0
1
2
3
4
5
6
320
270
220
170
120
70
20

(c)

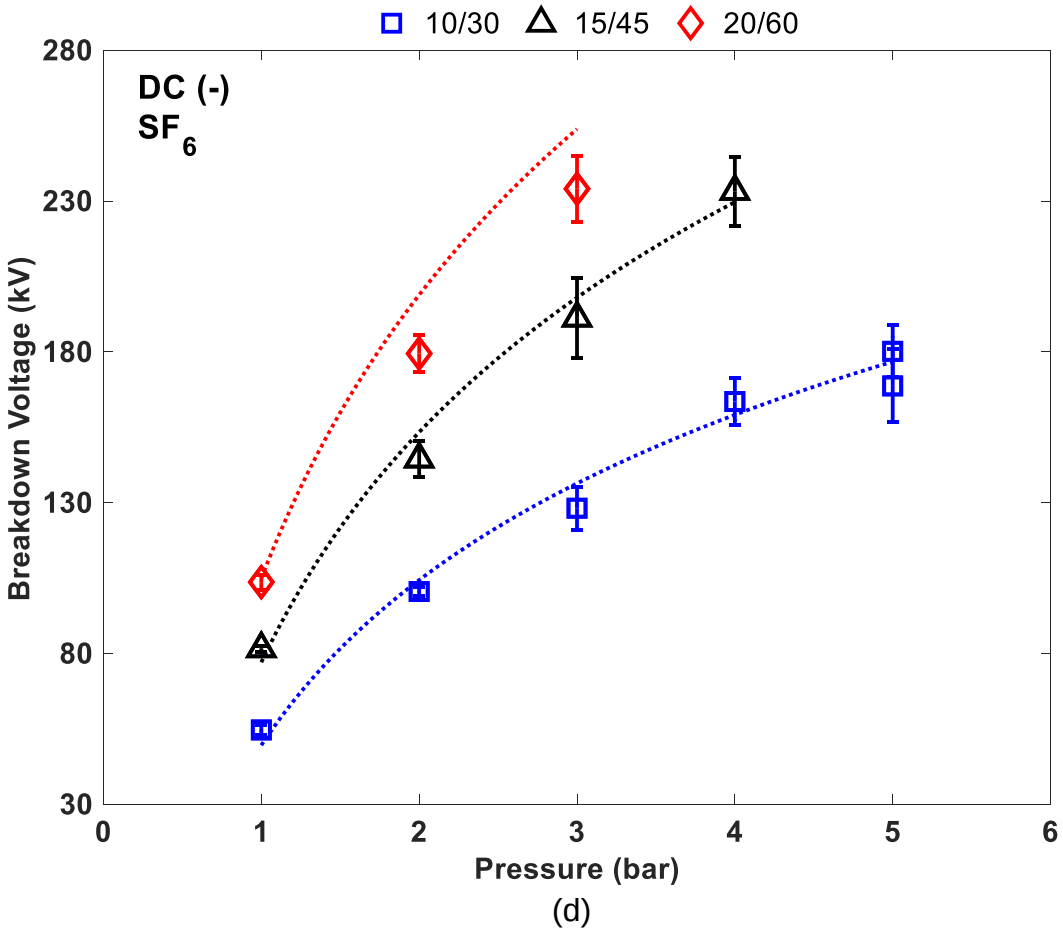
10/30
15/45
20/60
DC (-)
SF6
Breakdown Voltage (kV)
Pressure (bar)
280
230
180
130
80
30
0
1
2
3
4
5
6

(d)

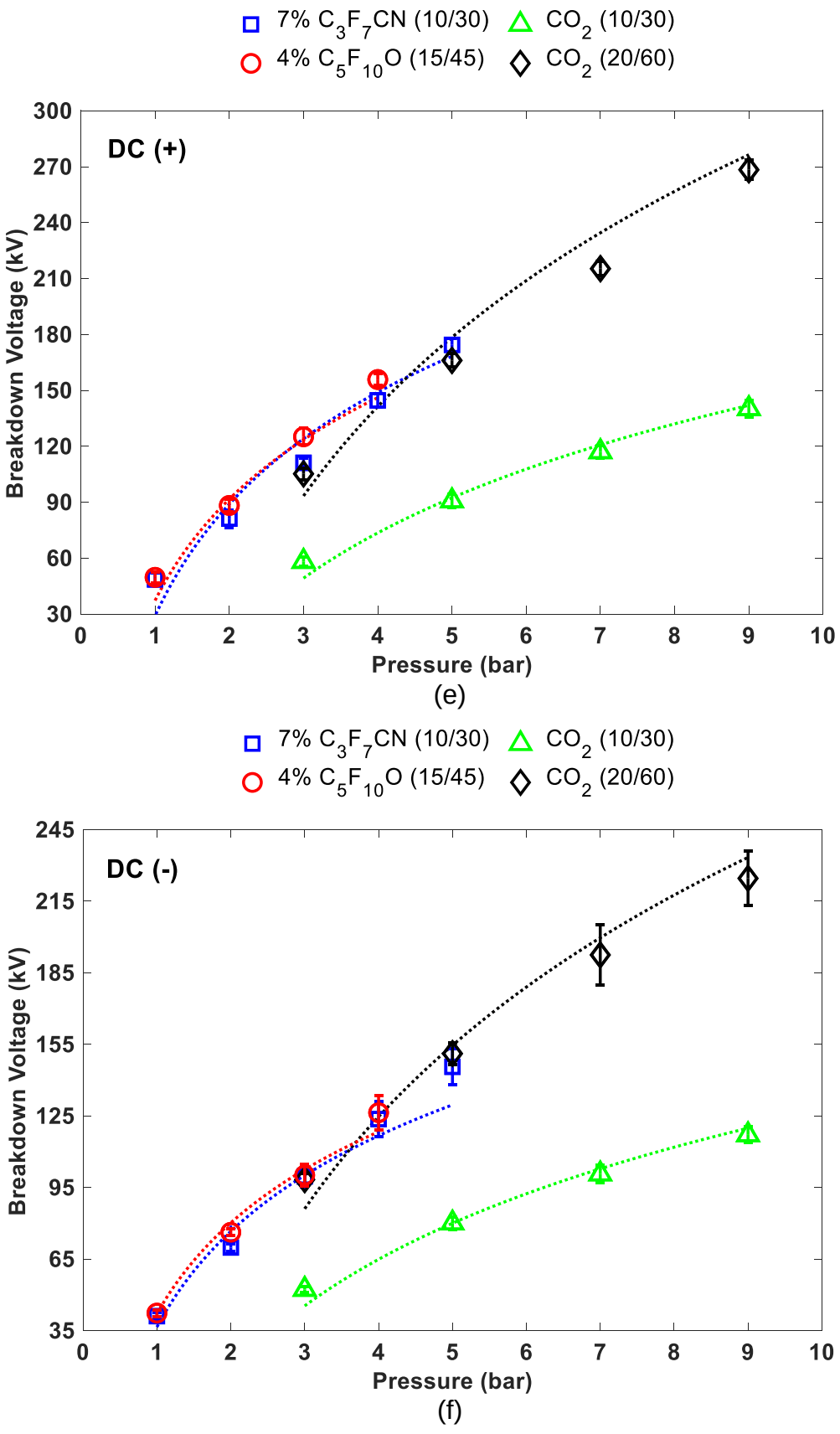

Figure 6.10 Comparison of DC breakdown voltages and modelled results shown in dotted lines for: a 20% C_3F_7CN / 80% CO_2 gas mixture in (a) DC (+) and (b) DC (-); SF_6 in (c) DC (+) and (d) DC (-); and (e) DC (+) and (f) DC (-) show 7% C_3F_7CN / 93% CO_2 and 4% $C_5F_{10}O$ / 96% CO_2 gas mixtures and CO_2 gas tested in different coaxial conductor/enclosure designs.

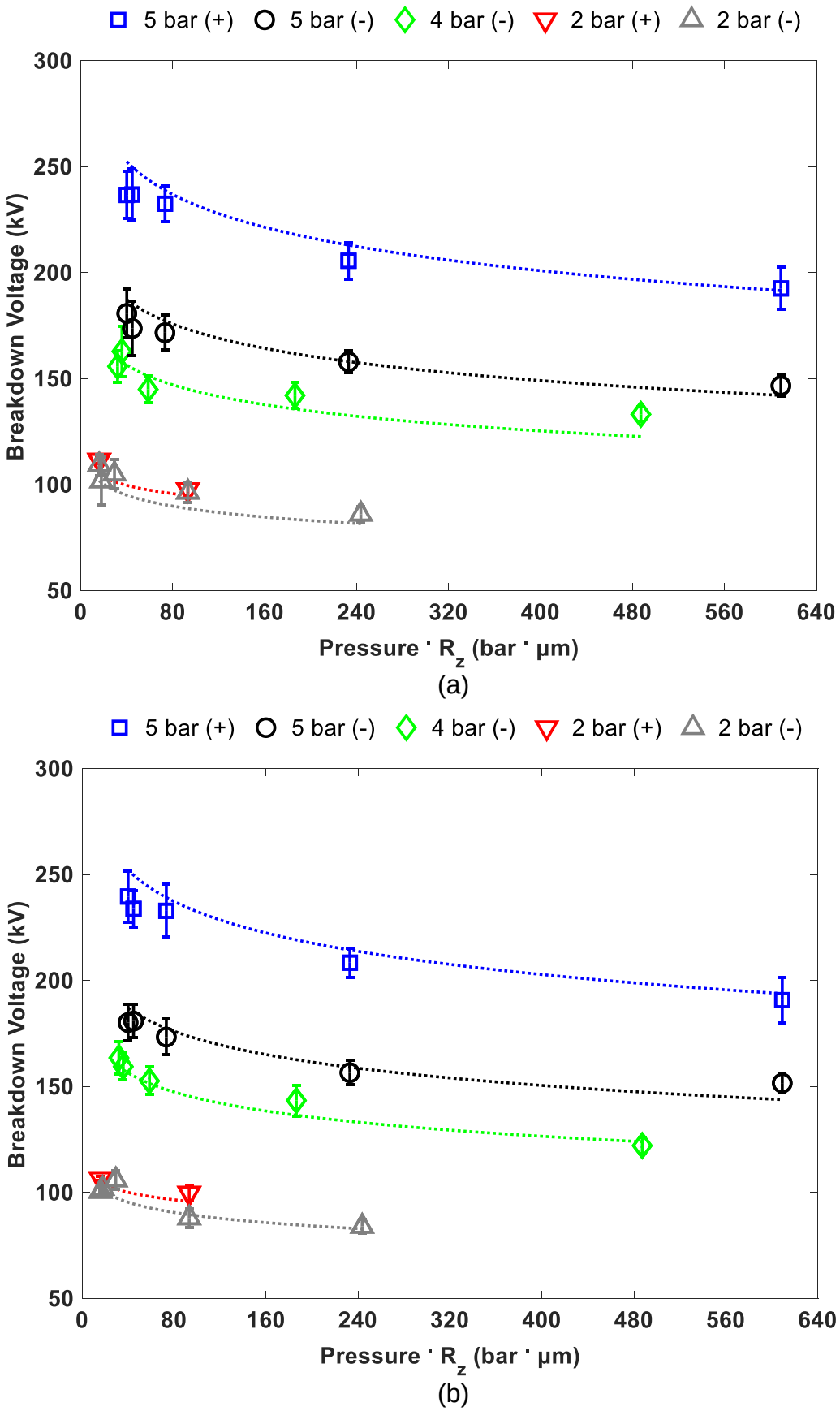

Figure 6.11 Comparison of the experimental and calculated (dotted lines) results in the effect of conductor surface roughness of 10/30 mm coaxial configuration for (a) 20% C_3F_7CN / 80% CO_2 gas mixture and (b) SF_6 over different pressures and DC polarities.

The results in Figure 6.11 demonstrate that the developed single protrusion streamer criterion model is able to estimate the DC breakdown voltages under both polarities for all of the tested conductor surface roughness cases within an uncertainty margin of around ±5%. Accordingly, the applicability of the developed modelling approach is verified.

6.5 Summary

This chapter has provided a comparative study of the experimental and calculated breakdown voltage values tested in Chapters 4 and 5. A mathematical model has been developed based on streamer criterion theory. This model is able to provide an accurate DC breakdown voltage estimate over a wide range of test conditions that is relevant to practical applications, which optimises the selection process of new SF_6 alternatives.

In rod-plane configurations, the mathematical modelling approach was able to estimate the breakdown voltage of HFO1234ze(E) and SF_6 for pressures of 2-5 bar and CO_2 above 5 bar in quasi-uniform and weakly non-uniform fields, whereas in 20% C_3F_7CN / 80% CO_2 and CO_2 below 5 bar pressure, a correction factor was applied to provide a smaller deviation between U_i and the breakdown voltage value that increases the K value, resultant an acceptable estimation of the breakdown voltage for both gases in this case. This is associated with differences between SF_6 and 20% C_3F_7CN / 80% CO_2 and CO_2 in terms of the corona stabilisation region, with a higher pressure being required due to the presence of CO_2 in the mixture that widens the region. Increasing gas pressure beyond the critical pressure at which the inception voltage and breakdown voltage coincide results in an accurate estimation of the breakdown voltage without any correction factor being required.

In the case of coaxial geometries, a single protrusion streamer criterion model was developed that considered the surface roughness of a conductor. DC breakdown characteristics of 20% C_3F_7CN / 80% CO_2, 7% C_3F_7CN / 93% CO_2, 4% $C_5F_{10}O$ / 96% CO_2 gas mixtures and SF_6 and CO_2 gases were compared to the modelled results. The majority of the calculated values from the developed model are within ±5% of the U_{50} values obtained experimentally, which were verified for both DC voltage polarities, coaxial configurations with a geometrical ratio of 3, conductor surface roughness, pressures and gas candidates. This will benefit the experimental characterisation of SF_6 alternatives and the equipment prototyping stage where highly resource intensive experimental investigations are required.

7 CONCLUSION AND FUTURE RESEARCH

7.1 General Conclusions

This thesis has investigated the feasibility of adopting a 20% C_3F_7CN / 80% CO_2 gas mixture as a replacement to SF_6 gas that can be used in gas insulated equipment under DC voltage, due to their shared similarities in terms of physical and chemical properties. Specifically, 20% C_3F_7CN / 80% CO_2 gas mixture can achieve SF_6's dielectric performance at a matching pressure. DC breakdown voltage experimental investigations were conducted on SF_6 as a reference for comparison and on other alternatives, such as CO_2, 4% $C_5F_{10}O$ mixture and mixtures of 7% and 20% C_3F_7CN concentrations, under varying pressures and electrode designs and field uniformities. A mathematical model was developed based on streamer inception criterion that is capable of predicting the DC breakdown voltage under representative conditions. The main conclusions of this work are as follows:

C_3F_7CN and Its Mixtures Breakdown Characteristics Review (Chapter 2):

An extensive review of previous investigations on C_3F_7CN and its mixtures has been presented. The review highlights the importance of greater understanding of C_3F_7CN gas, prior to full deployment in gas-insulated equipment. Findings from the review show that a 20% C_3F_7CN / 80% CO_2 gas mixture has a better dielectric strength when compared to SF_6 gas in uniform and quasi-uniform field configurations. However, in a non-uniform field, SF_6 has higher breakdown voltage than the 20% C_3F_7CN / 80% CO_2 gas mixture. Therefore, special care must be addressed during the design of gas tight equipment filled with the new gas mixture where it is more sensitive to a non-uniform field than SF_6 gas, as well as special consideration given to the corona stabilisation region due to it playing an important role related to this. The initial gas mixture selection was decided upon through a simple trade-off between dielectric performance and liquefaction temperature, dependent on the mixture ratio. Although the use of a lower C_3F_7CN concentration in the mixture with a buffer gas improves the liquefaction temperature limit, it reduces the dielectric performance of the mixture. C_3F_7CN gas is practically a non-toxic gas. Nevertheless, after the gas is exposed to many breakdowns, some of the produced by-products were found to be toxic. Accordingly, it is recommended to avoid contacting and inhaling the aged gas and take adequate eye and respiratory protection when near to these by-products.

Experimental Factors Affecting DC Breakdown Voltage Values (Chapters 2 and 3):

There are many factors that affect the DC breakdown voltage in gases in terms of the experimental procedure, such as the used DC test method, voltage ramp rates, waiting time between breakdowns, mixing time for the gas mixture to be fully homogenous, electrode materials and electrical ageing. These factors have been extensively addressed in prior literature and through preliminary experimental investigations to ensure alignment between theory and practice, and importantly, to adopt a robust experimental procedure. From the literature, in the case of the used DC test method, there was a small difference between the DC breakdown voltage obtained from using a multiple level test and the successive discharge test, producing a negligible difference of 2% in the breakdown voltage. Concerning mixing time, it is recommended to pre-mix the gas in a gas cylinder and recirculate it before conducting any experiment to assure gas homogeneity. Electrode materials have a significant effect on the breakdown voltage. Due to the differences in their work functions and mechanical robustness, where breakdown voltage tends to be high for electrodes with a higher work function. However, oxide layers on certain materials can impact the breakdown voltage order, sometimes not following the expected order based solely on the work function. Moreover, electrical ageing produces a drop in the breakdown voltage after exposing the setup to numerous breakdown events, primarily due to electrode surface damage rather than gas aging.

The DC investigation followed the successive discharge method according to the BS EN 60060-1:2010 standard, in which the voltage is increased in 5 kV/s until breakdown occurs, with a waiting time of 2 minutes between breakdown being adopted. An investigation was conducted on the effect of adopting different ramp rates and waiting times. Voltage ramps and time intervals between 1-10 kV/s and 1-8 minutes were shown to have a negligible effect on the breakdown voltage. For the data analysis, a Gaussian distribution was adopted, with the average value and standard deviation (σ) calculated for 30 breakdowns (unless specified otherwise) representing 50% probability of breakdown voltage (U_{50}) and error bar respectively shown in the results figures. A comparison with other statistical techniques, such as the Weibull distribution, was also presented for several data sets. The analysis results show a negligible difference between the U_{50} values calculated based on the Gaussian distribution and those obtained from other distributions.

DC Breakdown Characteristics in Rod-Plane Electrodes (Chapter 4):

A preliminary investigation was conducted on the effect of different electrode materials on the breakdown performance of the 20% C_3F_7CN / 80% CO_2 gas mixture over 300 breakdowns under negative DC. Three sets of 6.25 mm diameter rod-plane electrodes manufactured in stainless steel, aluminium and brass were tested for a fixed gap distance of 3 mm and pressure of 4.8 bar. All electrodes were fabricated with R_a and R_z equal to 0.2 μm and less than 2 μm, respectively. It was measured using a JENOPTIK W5 surface roughness measurement device before and after each experiment. In addition, a DILO C_4 multi-gas analyser unit was used to analyse the gas inside the vessel prior and post each experiment. It provided the concentrations of C_3F_7CN, CO_2, CO, O_2 and humidity. The results show that stainless steel has the highest breakdown voltage and the lowest change in surface roughness over the 300 breakdowns when compared to aluminium and brass that is related to their work functions and mechanical robustness. Worth noting that, aluminium electrodes attain a similar breakdown performance with the stainless steel one for the first 20 breakdowns (polished electrodes) as both have a comparable work function. The post-testing gas analyses showed a negligible reduction in the C_3F_7CN content after 300 breakdowns.

An experimental study was conducted in regard to the effects of DC polarity and field uniformity on the breakdown characteristics of SF_6, CO_2 and a 20% C_3F_7CN/ 80% CO_2 gas mixture. Rod-plane geometries with a range of rod diameters (3.5-12.5 mm) and electrode separations (5-55 mm) were used to provide different degrees of field uniformity. SF_6 and CO_2 gases, and the 20% C_3F_7CN / 80% CO_2 gas mixture were tested under pressures ranging between 1 and 9 bar. Breakdown voltages under both polarities rise linearly with gap distance in quasi-uniform fields, with the positive being higher. Increasingly non-uniform fields lead to saturation in the case of a positive breakdown voltage, while in the negative polarity case, the breakdown voltage increases linearly (transition from streamer inception to propagation). As a result, the two polarities' breakdown voltage magnitudes crossover as field non-uniformity increases. The value at which the negative value exceeds the positive is dependent on the field uniformity, pressure and gas medium. This value is at f of 0.18 in the case of SF_6 gas, while it is pressure dependant in the case of the 20% C_3F_7CN / 80% CO_2 gas mixture.

DC Breakdown Characteristics in Reduced-Scale Coaxial Electrodes (Chapter 5):

The DC breakdown characteristics of SF_6, CO_2 and mixtures of 7% and 20 % C_3F_7CN and 4% $C_5F_{10}O$ ratios were also experimentally investigated in reduced scale coaxial geometries under varying pressure, representing gas insulated lines, matching the design concept and consistent with their f values adopted across modern industries (at the coaxial optimal ratio).

Differently sized coaxial electrodes with conductor/enclosure diameters of 8/30, 10/30, 15/30, 15/45 and 20/60 mm were used to conduct a comparative analysis. The effect of conductor surface roughness and electrode material were also examined in the 10/30 mm coaxial configuration with R_z ranging from 8-121 μm. The results show that at the coaxial optimal ratio (1/3 conductor/enclosure diameters), the highest breakdown voltage can be attained, when compared to the 8/30 and 15/30 mm coaxial configurations.

7% C_3F_7CN / 93% CO_2 provides an average of 75% of the dielectric performance of SF_6, while 4% $C_5F_{10}CO$ / 96% CO_2 attains 55% and CO_2 is around one-third of SF_6 for the tested pressure range and geometries. To be comparable with SF_6, in the case of the 7% C_3F_7CN concentration, additional pressure needs to be considered in the newly designed equipment for this mixture that takes into account boiling point limits and surface roughness sensitivity. However, increasing the gas pressure is not feasible in the case of the 4% $C_5F_{10}O$ mixture due to the liquefaction temperature limitation. CO_2 requires a larger footprint than SF_6 because increasing the pressure will only lead to a non-practical level.

The 20% C_3F_7CN / 80% CO_2 gas mixture is comparable with SF_6's dielectric strength and surface roughness effect under a wide range of test conditions. Both gases show a common p·h range threshold of 40-50 bar·μm, with increasing the p·h beyond threshold significantly reducing the breakdown performance of both gases. Overall, the 20% C_3F_7CN / 80% CO_2 gas mixture could be retrofilled in existing SF_6 designed equipment without concern of about the equipment's practical surface finish that can lead to a reduction in the insulation performance.

A Mathematical Model for Accurately Estimating The DC Breakdown Voltage Based On The Streamer Criterion Theory (Chapter 6):

A generalised modelling approach, based on a streamer criterion, was developed that is capable of estimating the DC breakdown characteristics of different insulation gases prior to any experimental work that considers gas medium and pressure, electrode design (rod-plane

or coaxial at a ratio of 3) and conductor surface roughness. This model can provide an accurate estimation of the DC breakdown voltage and covers a wide range of test conditions related to practical applications. Thus, it optimises the future selection process of new SF_6 alternatives for DC breakdown performance under representative conditions.

7.2 Future Research

The work presented in this thesis shows the potential of adopting a 20% C_3F_7CN / 80% CO_2 gas mixture under a DC field as a valuable alternative to the SF_6 gas after comparing the DC breakdown characteristics of both polarities under different field uniformities and pressures. The following future research would further accelerate the development of an environmentally friendly DC-GIL for the future.

7.2.1 Large-Scale GIL Demonstrator Withstand and Long-Term Energisation Investigations

To fully verify the feasibility of adopting the proposed gas mixture as an alternative to SF_6 gas, large-scale high voltage testing is required. This could be achieved by using a demonstrator GIL. It is not appropriate to perform breakdown investigations on this equipment due to the damage that would be caused to the demonstrator. Instead, withstand investigations and partial discharge inspection should be used as criteria to assess the behaviour of the C_3F_7CN/CO_2 gas mixture in comparison with SF_6. Then, via long-term energisation, it could be connected to an actual power network. The first step could be to scale up the design of the small-scale coaxial several times until it reaches the demonstrator GIL design. During the scaling process, the developed single protrusion streamer criterion model could be used to reduce the testing required for this evaluation and to cross-check the model's validity for large scale equipment.

7.2.2 DC Partial Discharge Characterisation

The first failure phase associated with gas insulators that leads to breakdown is partial discharge. Therefore, a comparison between the DC PD characteristics of SF_6 gas and a C_3F_7CN/CO_2 gas mixture is highly recommended. This could be achieved via use of both methods, apparent charge and ultra-high frequency measurement techniques using artificial pre-designed defects and protrusions on both conductor and enclosure that mimic what is typically found in an actual GIL. This would enhance the judgment on the 20% C_3F_7CN /

80% CO_2 gas mixture being a suitable alternative to SF_6 gas. It is also worth comparing the experimentally measured PD inception voltages with the calculated streamer inception voltages from the developed single protrusion streamer criterion model and measure the effect of electrode design on the size of the corona stabilisation region between both gases, including the effect of using high concentrations of CO_2 gas in the proposed mixture.

7.2.3 Characterisation of Natural Origin Gases as an Alternative to SF_6

These gases attract attention due to their very low GWP. However, they can only achieve one-third of SF_6's dielectric strength at a comparable pressure. This results in a much higher operating pressure above 10 bar and a larger equipment footprint than that of SF_6 if these gases are utilised at a voltage level of 400 kV or above. A comparative study is required to characterise the natural origin gases with SF_6 gas at which both dielectric strengths can be comparable. This can be done under different field uniformities including the practical equipment range, that also covers the effect of surface roughness on the breakdown voltage at this high-pressure level and establish a p·h threshold value, to assure the practical surface finish design requirement for these gases. It would also be useful to study the feasibility of operating at such a high pressure range from a maintenance and cost perspective, concerning the leakage rate and the sealing of the equipment to maintain the pressure level.

REFERENCES

[1] J. Reichl, M. Schmidthaler, and F. Schneider, “The value of supply security: The costs of power outages to Austrian households, firms and the public sector,” Johannes Kepler University, Linz, 2013. doi: 10.1016/j.eneco.2012.08.044.

[2] T. Magier, M. Tenzer, and H. Koch, “Direct Current Gas-Insulated Transmission Lines,” *IEEE Trans. Power Deliv.*, vol. 33, no. 1, pp. 440–446, Feb. 2018, doi: 10.1109/TPWRD.2017.2716182.

[3] H. Koch, *Gas Insulated Transmission Lines - GIL*. Tampa: Wiley-IEEE Press, 2008.

[4] Grid Tech Team, “Applications for High-Voltage Direct Current Transmission Technologies,” *US Dept of Energy Workshop: Applications of HVDC Technologies*. Department of Energy United States of America, pp. 1–20, 2013, [Online]. Available: https://energy.gov/sites/prod/files/2015/11/f27/Applications of HVDC Technologies - Summary FINAL.pdf.

[5] M. Kosse *et al.*, “Overview of development, design, testing and application of compact gas-insulated DC systems up to ± 550 kV,” *Glob. Energy Interconnect.*, vol. 2, no. 6, pp. 567–577, Dec. 2019, doi: 10.1016/j.gloei.2020.01.011.

[6] C. Franck, A. Chachereau, and J. Pachin, “SF_6-Free Gas-Insulated Switchgear: Current Status and Future Trends,” *IEEE Electr. Insul. Mag.*, vol. 37, no. 1, pp. 7–16, Jan. 2021, doi: 10.1109/MEI.2021.9290463.

[7] S. Smith *et al.*, “The Earth’s Energy Budget, Climate Feedbacks and Climate Sensitivity Supplementary Material,” *in IPCC AR6*, SM7 2021.

[8] “Inventory of U.S. greenhouse gas emissions and sinks: 1990-2009,” *Federal Register*, vol. 76, no. 36. Agency, United States Environmental Protection, p. 10026, 2011, [Online]. Available: https://www.epa.gov/sites/production/files/2018-01/documents/2018_complete_report.pdf.

[9] D. Koch, “SF_6 properties, and use in MV and HV switchgear,” *Cahier Technique Schneider Electric*, no. 188. p. 22, 2003, [Online]. Available: http://www.schneider-electric.com.

[10] A. Beroual and A. Haddad, “Recent advances in the quest for a new insulation gas with a low impact on the environment to replace Sulfur Hexafluoride (SF_6) gas in

high-voltage power network applications," *Energies*, vol. 10, no. 8, pp. 1216–1236, 2017, doi: 10.3390/en10081216.

[11] L. Chen *et al.*, "CF_3I Gas Mixtures: Breakdown Characteristics and Potential for Electrical Insulation," *IEEE Trans. Power Deliv.*, vol. 32, no. 2, pp. 1089–1097, 2017, doi: 10.1109/TPWRD.2016.2602259.

[12] T. Rokunohe *et al.*, "Development of SF_6-free 72.5 kV GIS," *IEEE Trans. Power Deliv.*, vol. 22, no. 3, pp. 1869–1876, Jul. 2007, doi: 10.1109/TPWRD.2007.899273.

[13] L. Loizou *et al.*, "Technical Viability of Retro-Filling C_3F_7CN/CO_2 Gas Mixtures in SF_6-Designed Gas Insulated Lines and Busbars at Transmission Voltages," *IEEE Trans. Power Deliv.*, vol. 35, no. 5, pp. 2394–2402, Oct. 2020, doi: 10.1109/TPWRD.2020.2967582.

[14] 3M Electronics Materials Solutions Division, "3M™ Novec™ 4710 Insulating Gas," *Technical Data Sheet*. 3M, pp. 1–4, 2015, [Online]. Available: http://multimedia.3m.com/mws/media/1132124O/3m-novec-4710-insulating-gas.pdf.

[15] L. Loizou, L. Chen, and Q. Liu, "Breakdown Characteristics of C_3F_7CN/CO_2 Gas Mixtures in Rod-Plane Gaps," in *2018 IEEE International Conference on High Voltage Engineering and Application (ICHVE)*, Sep. 2018, pp. 1–4, doi: 10.1109/ICHVE.2018.8641943.

[16] L. Loizou *et al.*, "Lightning impulse breakdown characteristics of SF_6 and 20% C_3F_7CN / 80% CO_2 mixture under weakly non-uniform electric fields," *IEEE Trans. Dielectr. Electr. Insul.*, vol. 27, no. 3, pp. 848–856, Jun. 2020, doi: 10.1109/TDEI.2020.008762.

[17] B. Zhang, N. Uzelac, and Y. Cao, "Fluoronitrile/CO_2 mixture as an eco-friendly alternative to SF_6 for medium voltage switchgears," *IEEE Trans. Dielectr. Electr. Insul.*, vol. 25, no. 4, pp. 1340–1350, Aug. 2018, doi: 10.1109/TDEI.2018.007146.

[18] L. Maksoud *et al.*, "Dynamitron® SF_6-FREE Project: The Assessment of g^3 Applicability," in *MATPOST*, pp. 1-4, 2019.

[19] S. Wilke *et al.*, "Zero Emission F-gas-free 420 kV GIS for a Net Zero Carbon Future," Cigre A3/B3 Colloquium, PS1, Birmingham, 2023.

[20] "EU legislation to control F-gases." https://climate.ec.europa.eu/eu-action/fluorinated-greenhouse-gases/eu-legislation-control-f-gases_en#tab-0-0

(accessed Jul. 11, 2023).

[21] "Fluorinated gases (F gases) - GOV.UK." https://www.gov.uk/guidance/fluorinated-gases-f-gases#sulphur-hexafluoride (accessed Jul. 11, 2023).

[22] IEEE, *C37.123-2016 - IEEE Guide for Specifications for High-Voltage Gas-Insulated Substations Rated 52 kV and Above*. IEEE, 2016.

[23] ABB, "Gas-insulated switchgear (GIS) 72.5 - 1200 kV." ABB, p. 1, 2018, [Online]. Available: new.abb.com/high-voltage/gis.

[24] W. Koos and K. Holtzhausen, *High Voltage Engineering Practice and Theory*. Stellenbosch, (South) Africa: Univ. Stellenbosch, 2008.

[25] D. Tzelepis *et al.*, "Voltage and current measuring technologies for high voltage direct current supergrids: A technology review identifying the options for protection, fault location and automation applications," *IEEE Access*, vol. 8, pp. 203398–203428, 2020, doi: 10.1109/ACCESS.2020.3035905.

[26] I. Iddrissu *et al.*, "Negative DC Breakdown Characteristics of C_3F_7CN / CO_2 Gas Mixture for Application in High Voltage Accelerators," *IEEE Trans. Dielectr. Electr. Insul.*, vol. 28, no. 3, pp. 946–954, Jun. 2021, doi: 10.1109/TDEI.2021.009376.

[27] I. Iddrissu *et al.*, "Gas Decomposition and Electrode Degradation Characteristics of a 20% C_3F_7CN and 80% CO_2 Gas Mixture for High Voltage Accelerator," *High Volt.*, pp. 1–10, 2021.

[28] K. Elnaddab, *Evaluation of Gas Insulated Lines (GIL) for Long Distance HVAC Power Transfer*. December, Cardiff: Cardiff University, 2014.

[29] L. Chen, *Investigation on the Feasibility of Trifluoroiodomethane (CF_3I) for Application in Gas-Insulated Lines*. August, Cardiff: Cardiff Univirsity, 2015.

[30] "Gas-Insulated Tranmission Lines for Rated Voltages of 72.5 kV and above," International Electrotechnical Commission IEC 61640, 1998.

[31] "Gas-insulated transmission lines." SIEMENS, 2018, [Online]. Available: https://www.siemens.com/global/en/home/products/energy/high-voltage/power-transmission-lines/gas-insulated-lines.html.

[32] W. Holaus, "Pressurized Air Cables - a new technology for sustainable energy transmission 12 kV - 420 kV," in *VDE High Voltage Technology; 4. ETG-Symposium*, 2022, pp. 1–6.

[33] "Hivoduct High Voltage Technology." https://www.hivoduct.com/Home/ (accessed Feb. 13, 2024).

[34] C. Neumann *et al.*, "Basic phenomena in gas-insulated HVDC systems and adequate dielectric testing," *CIGRE-IEC Conference on EHV and UHV (AC & DC)*, D1: Materials and emerging test techniques, Hokkaido, 2019.

[35] W. Jian *et al.*, "Motion analysis of the particle in DC GIL considering the random collisions and gaseous resistance," in *Proceedings of the IEEE International Conference on Properties and Applications of Dielectric Materials*, Jul. 2015, vol. 2015-Octob, pp. 480–483, doi: 10.1109/ICPADM.2015.7295313.

[36] Cigré Working Group D1.03, "Gas Insulated Systems for HVDC: DC Stress at DC and AC Systems," CIGRE, Paris, 2012.

[37] L. Zavattoni, *Conduction phenomena through gas and insulating solids in HVDC Gas Insulated Substations, and consequences on electric field distribution*. Grenoble: Universite De Grenoble, 2014.

[38] W. Zhiyuan *et al.*, "Three dimensional simulating and experimental study on the influential factors of the effectiveness of the DC-GIL particle trap," in *ICEMPE 2017 - 1st International Conference on Electrical Materials and Power Equipment*, 2017, pp. 544–547, doi: 10.1109/ICEMPE.2017.7982199.

[39] M. Ouyang, M. Baker, and T. Garrity, "Novel Design Concepts of a Compressed Gas HVDC Transmission Line," *IEEE Power Eng. Rev.*, vol. PER-2, no. 7, pp. 57–58, 1982, doi: 10.1109/MPER.1982.5521101.

[40] T. Hasegawa *et al.*, "Development of insulation structure and enhancement of insulation reliability of 500 KV de GIS," *IEEE Power Eng. Rev.*, vol. 17, no. 1, p. 46, 1997, doi: 10.1109/MPER.1997.560684.

[41] M. Tenzer, H. Koch, and D. Imamovic, "Underground transmission lines for high power AC and DC transmission," in *2016 IEEE/PES Transmission and Distribution Conference and Exposition (T&D)*, May 2016, vol. 2016-July, pp. 1–4, doi: 10.1109/TDC.2016.7519942.

[42] T. Hasegawa *et al.*, "DC dielectric characteristics and conception of insulation design for DC GIS," *IEEE Power Eng. Rev.*, vol. 16, no. 10, p. 50, 1996, doi: 10.1109/MPER.1996.4311018.

[43] Z. Jia *et al.*, "Flashover characteristics along the epoxy resin insulator under DC

voltage in SF_6 gas," in *Proceedings - 2012 International Conference on Computer Distributed Control and Intelligent Environmental Monitoring, CDCIEM 2012*, Mar. 2012, pp. 338–342, doi: 10.1109/CDCIEM.2012.87.

[44] H. Fujinami *et al.*, "Mechanism and Effect of DC Charge Accumulation on SF_6 Gas Insulated Spacers," *IEEE Power Eng. Rev.*, vol. 9, no. 7, p. 62, 1989, doi: 10.1109/MPER.1989.4310816.

[45] E. Volpov, "Dielectric strength coordination and generalized spacer design rules for HVAC/DC SF_6 gas insulated systems," *IEEE Trans. Dielectr. Electr. Insul.*, vol. 11, no. 6, pp. 949–963, 2004, doi: 10.1109/TDEI.2004.1387818.

[46] M. Hallas *et al.*, "Commissioning and Service Experience with a ±550 kV DC GIL conducted in Frame of a CIGRE Prototype Installation Test," *IEEE Trans. Power Deliv.*, pp. 1–11, 2023, doi: 10.1109/TPWRD.2023.3263722.

[47] H. Koch *et al.*, "High power underground transmission for HV DC," *CIGRE Sess. 46*, vol. 2016-Augus, no. Ccc, 2016.

[48] N. Malik, A. Al-Arainy, and M. Qureshi, *Electrical Insulation in Power Systems*. Taylor & Francis, 1998.

[49] A. Haddad and D. Warne, *Advances in High Voltage Engineering*. IET, 2004.

[50] A. Küchler, *High Voltage Engineering*. Berlin, Heidelberg: Springer Berlin Heidelberg, 2018.

[51] M. Kamarudin, *Gas Mixtures on the Breakdown Characteristics in Uniform and Non-Uniform Field Configurations*. June, Cardiff: Cardiff University, 2013.

[52] J. Pachin *et al.*, "Design criteria for experiments to measure the breakdown voltage of insulating gases in uniform electric fields," CIGRE D1.67, 2021. doi: https://doi.org/10.3929/ethz-b-000518539.

[53] E. Kuffel, W. Zaengl, and J. Kuffel, *High Voltage Engineering Fundamentals*, 2nd Editio. Oxford, UK: Butterworth-Heinemann, 2000.

[54] N. Malik and A. Qureshi, "A review of electrical breakdown in mixtures of SF_6 and other gases," *IEEE Trans. Electr. Insul.*, vol. EI-14, no. 1, pp. 1–13, 1979, doi: 10.1109/TEI.1979.298198.

[55] R. Aroara and W. Mosch, *High Voltage and Electrical Insulation Engineering*. Hoboken, New Jersey: John Wiley & Sons, Inc., 2011.

[56] W. Zaengl and K. Petcharaks, "Application of Streamer Breakdown Criterion for Inhomogeneous Fields in Dry Air and SF_6," in *Gaseous Dielectrics VII*, no. 1, Boston, MA: Springer US, 1994, pp. 153–159.

[57] N. Malik, "Streamer Breakdown Criterion for Compressed Gases," *IEEE Trans. Electr. Insul.*, vol. EI-16, no. 5, pp. 463–467, Oct. 1981, doi: 10.1109/TEI.1981.298444.

[58] S. Kumar *et al.*, "Electrical Breakdown Study in CO_2 and CO_2-O_2 Mixtures in AC, DC and Pulsed Electric Fields at 0.1–1 MPa Pressure," *IEEE Trans. Dielectr. Electr. Insul.*, vol. 28, no. 1, pp. 158–166, Feb. 2021, doi: 10.1109/TDEI.2020.009115.

[59] F. Mauseth, J. Jorstad, and A. Pedersen, "Streamer inception and propagation for air insulated rod-plane gaps with barriers," in *2012 Annual Report Conference on Electrical Insulation and Dielectric Phenomena*, Oct. 2012, pp. 739–732, doi: 10.1109/CEIDP.2012.6378884.

[60] A. Pedersen *et al.*, "Streamer inception and propagation models for designing air insulated power devices," in *2009 IEEE Conference on Electrical Insulation and Dielectric Phenomena*, Aug. 2009, pp. 604–607, doi: 10.1109/CEIDP.2009.5377740.

[61] "Sulfur Hexafluoride," *Definitions*. World of Chemicals, 2020, doi: 10.32388/zybv84.

[62] T. Olsen, "Use of SF_6 Gas in Medium Voltage Switchgear," no. 53. SIEMENS, pp. 1–3, 2005, [Online]. Available: https://www.energy.siemens.com/us/pool/us/services/power-transmission-distribution/medium-voltage-product-services/tech-topics-application-notes/techtopics53rev0.pdf.

[63] S. Meijer, J. Smit, and A. Girodet, "Comparison of the breakdown strength of N_2, CO_2 and SF_6 using the extended up-and-down method," in *Proceedings of the IEEE International Conference on Properties and Applications of Dielectric Materials*, Jun. 2006, pp. 653–656, doi: 10.1109/ICPADM.2006.284262.

[64] C. Scott *et al.*, "F-gas-free Natural-Origin Gases, for MV GIS, to manage your sustainable grid," Cigre A3/B3 Colloquium, Birmingham, 2023.

[65] T. Koike *et al.*,, "Development of SF_6-Free 72/84kV GIS Using Synthetic Air as an Alternative to SF_6," Cigre A3/B3 Colloquium, PS1, Birmingham, 2023.

[66] T. Uchii *et al.*, "High-Voltage Switchgear Technology Applying CO_2/O_2 Natural-

Origin Gas Mixture as an Alternative Insulating and Interrupting Medium to SF_6," Cigre A3/B3 Colloquium, PS1, Birmingham, 2023.

[67] T. Barbe *et al.*, "Dual-gas concept and design compatibility between SF_6 & SF_6-free GIS products," Cigre A3/B3 Colloquium, PS2, Birmingham, 2023.

[68] Siemens, "Gas-insulated switchgear from 72.5 to 550 kV," 2016. Accessed: Jul. 20, 2023. [Online]. Available: https://assets.siemens-energy.com/siemens/assets/api/uuid:c8dd938d-f50c-4fbe-89de-4efde3ecd7fe/gas-insulated-switchgear-72-550kv-en.pdf?ste_sid=32c28e1fcb79bd3b958794537d29a841.

[69] T. Rokunohe *et al.*, "Development of 72-kV high-pressure air-insulated GIS with vacuum circuit breaker," *Electr. Eng. Japan*, vol. 157, no. 4, pp. 13–23, Dec. 2006, doi: 10.1002/eej.20451.

[70] P. Ranjan *et al.*, "Anomalous First Breakdown Behavior for HFO1234ze(E)," *IEEE Trans. Dielectr. Electr. Insul.*, vol. 28, no. 5, pp. 1620–1627, Oct. 2021, doi: 10.1109/TDEI.2021.009676.

[71] P. Simka and N. Ranjan, "Dielectric Strength of C5 Perfluoroketone," in *19th International Symposium on High Voltage Engineering*, 2015, pp. 23–28.

[72] 3M Electronics Materials Solutions Division, "3M™ Novec™ 5110 Insulating Gas." 3M, pp. 1–4, 2017, [Online]. Available: http://multimedia.3m.com/mws/media/1132123O/3m-novec-5110-insulating-gas.pdf.

[73] Y. Kieffel and F. Biquez, "SF_6 alternative development for high voltage switchgears," CIGRE, Paris, 2014. doi: 10.1109/ICACACT.2014.7223577.

[74] J. Owens, "Greenhouse Gas Emission Reductions in Power Equipment Through Use of a Sustainable Alternative to SF_6," in *Proceedings of the IEEE Power Engineering Society Transmission and Distribution Conference*, 2018, vol. 2018-April, doi: 10.1109/TDC.2018.8440337.

[75] Michael Eves *et al.*, "SF_6 Alternatives A Literature Review on SF_6 Gas Alternatives for use on the Distribution Network," *West. Power Distrib. Innov.*, vol. 1, pp. 9–10, 2018.

[76] G. Chen *et al.*, "Research progress on environmental-friendly insulating gases for HVDC gas-insulated transmission lines," *CSEE J. Power Energy Syst.*, vol. 7, no. 3,

pp. 510–529, 2019, doi: 10.17775/CSEEJPES.2019.01060.

[77] R. Sinnott, *Coulson & Richardsons Chemical Engineering Design*, vol. 6, no. 4. Butterworth-Heinemann, 2005.

[78] IEC 62271-203:2011, "High-voltage switchgear and controlgear - Gas-insulated metal-enclosed switchgear for rated voltages above 52 kV," 2011.

[79] L. Loizou, L. Chen, and Q. Liu, "A Comparative Study on the Breakdown Characteristics of SF_6 and 20% C_3F_7CN / 80% CO_2 Gas Mixture in a Coaxial Configuration," in *2019 IEEE Conference on Electrical Insulation and Dielectric Phenomena (CEIDP)*, Oct. 2019, pp. 234–237, doi: 10.1109/CEIDP47102.2019.9009877.

[80] L. Loizou, L. Chen, and Q. Liu, "Breakdown Characteristics of C_3F_7CN/CO_2 Gas Mixtures in Rod-Plane Gaps," 2018, doi: 10.1109/ICHVE.2018.8641943.

[81] S. Menju and K. Takahashi, "DC dielectric strength of a SF_6 gas insulated system," *IEEE Trans. Power Appar. Syst.*, vol. PAS-97, no. 1, pp. 217–224, 1978, doi: 10.1109/TPAS.1978.354472.

[82] A. Beroual and M. Coulibaly, "Experimental investigation of breakdown voltage of CO_2, N_2 and SF_6 gases, and CO_2-SF_6 and N_2-SF_6 mixtures under different voltage waveforms," in *2016 IEEE International Power Modulator and High Voltage Conference (IPMHVC)*, Jul. 2016, vol. 11, no. 4, pp. 292–295, doi: 10.1109/IPMHVC.2016.8012898.

[83] N. Malik and A. Qureshi, "The Influence of Voltage Polarity and Field Non-Uniformity on the Breakdown Behavior of Rod-Plane Gaps Filled with SF_6," *IEEE Trans. Electr. Insul.*, vol. EI-14, no. 6, pp. 327–333, Dec. 1979, doi: 10.1109/TEI.1979.298188.

[84] C. Works and T. Dakin, "Dielectric breakdown of sulfur hexafluoride in nonuniform fields," *Trans. Am. Inst. Electr. Eng. Part I Commun. Electron.*, vol. 72, no. 5, pp. 682–689, 2013, doi: 10.1109/tce.1953.6371946.

[85] H. Nechmi *et al.*, "Fluoronitriles / CO_2 gas mixture as an eco-friendly alternative candidate to SF_6 in high voltage insulation systems," in *2016 IEEE Conference on Electrical Insulation and Dielectric Phenomena (CEIDP)*, Oct. 2016, vol. 2016-Decem, pp. 384–387, doi: 10.1109/CEIDP.2016.7785493.

[86] D. Xiao, *Gas Discharge and Gas Insulation*. Springer, Berlin, Heidelberg, 2016.

[87] Y. Long *et al.*, “Measurement of Ionization and Attachment Coefficients in C_4F_7N/CO_2 Gas Mixture as Substitute Gas to SF_6,” *IEEE Access*, vol. 8, pp. 76790–76795, 2020, doi: 10.1109/ACCESS.2020.2990301.

[88] H. Nechmi *et al.*, “Effective ionization coefficients and limiting field strength of fluoronitriles-CO_2 mixtures,” *IEEE Trans. Dielectr. Electr. Insul.*, vol. 24, no. 2, pp. 886–892, 2017, doi: 10.1109/TDEI.2017.006538.

[89] A. Chachereau, A. Hösl, and C. Franck, “Electrical insulation properties of the perfluoronitrile C_4F_7N,” *J. Phys. D. Appl. Phys.*, vol. 51, no. 49, 2018, doi: 10.1088/1361-6463/aae458.

[90] X. Ai *et al.*, “The effect of electrode surface roughness on the breakdown characteristics of C_3F_7CN/CO_2 gas mixtures,” *Int. J. Electr. Power Energy Syst.*, vol. 118, no. March 2019, p. 105751, 2020, doi: 10.1016/j.ijepes.2019.105751.

[91] Y. Tu *et al.*, “Insulation Characteristics of Fluoronitriles / CO_2 Gas Mixture under DC Electric Field,” *IEEE Trans. Dielectr. Electr. Insul.*, vol. 25, no. 4, pp. 1324–1331, 2018.

[92] C. Wang *et al.*, “Characteristics of C_3F_7CN/CO_2 as an alternative to SF_6 in HVDC-GIL systems,” *IEEE Trans. Dielectr. Electr. Insul.*, vol. 25, no. 4, pp. 1351–1356, Aug. 2018, doi: 10.1109/TDEI.2018.007494.

[93] A. Hopf *et al.*, “Dielectric strength of SF_6 substitutes, alternative insulation gases and PFC-gas-mixtures,” in *2017 IEEE Electrical Insulation Conference, EIC 2017*, 2017, pp. 209–212, doi: 10.1109/EIC.2017.8004635.

[94] A. Beroual, U. Khaled, and M. Coulibaly, “Experimental investigation of the breakdown voltage of CO_2, N_2, and SF_6 gases, and CO_2-SF_6 and N_2-SF_6 mixtures under different voltage waveforms,” *Energies*, vol. 11, no. 4, pp. 1–12, 2018, doi: 10.3390/en11040902.

[95] H. Nechmi *et al.*, “Fluoronitriles/CO_2 gas mixture as promising substitute to SF_6 for insulation in high voltage applications,” *IEEE Trans. Dielectr. Electr. Insul.*, vol. 23, no. 5, pp. 2587–2593, Oct. 2016, doi: 10.1109/TDEI.2016.7736816.

[96] F. Sadaoui and A. Beroual, “Influence of polarity on breakdown voltage of gases in divergent electric field under lightning impulse voltages,” *ICHVE 2012 - 2012 Int. Conf. High Volt. Eng. Appl.*, no. August 2017, pp. 496–499, 2012, doi: 10.1109/ICHVE.2012.6357035.

[97] U. Riechert *et al.*, “Compact gas-insulated systems for high voltage direct current transmission: Design and testing,” in *Proceedings of the IEEE Power Engineering Society Transmission and Distribution Conference*, 2016, vol. 2016-July, doi: 10.1109/TDC.2016.7520069.

[98] IEC 60060-1, “High-voltage test techniques Part 1 : General definitions and test requirements,” *Eur. Stand.*, vol. 2010, pp. 1–78, 2010.

[99] S. Phontusa and S. Chotigo, “Comparison of DC breakdown voltage between multiple level test and successive discharge test methods,” in *5th International Conference on Electrical Engineering/Electronics, Computer, Telecommunications and Information Technology, ECTI-CON 2008*, 2008, vol. 2, pp. 913–916, doi: 10.1109/ECTICON.2008.4600579.

[100] IEC 60243-1:1998, *Electrical strength of insulating materials — Test methods Part 1: Tests at power frequencies*. International Standard, 1999.

[101] M. Ngoc *et al.*, “Electrical breakdown of CF_3I and CF_3I-N_2 gas mixtures,” in *Annual Report - Conference on Electrical Insulation and Dielectric Phenomena, CEIDP*, Aug. 2009, pp. 557–560, doi: 10.1109/CEIDP.2009.5377861.

[102] O. Lesaint *et al.*, “A Study of Breakdown Properties of HFO Gas under DC and Impulse Voltage,” in *Annual Report - Conference on Electrical Insulation and Dielectric Phenomena, CEIDP*, 2018, vol. 2018-Octob, pp. 606–609, doi: 10.1109/CEIDP.2018.8544877.

[103] J. Key and D. Ball, *Introductory Chemistry- 1st Canadian Edition*. Victoria: BCcampus, 2014.

[104] L. Niemeyer, “Cigre Guide for SF_6 Gas Mixtures. Application and Handling in Electric Power Equipment,” ABB Corporate Research Centre, Baden, 1998.

[105] S. Ohtsuka *et al.*, “Insulation Properties of CO_2/N_2 Gas Mixture with a Small Amount of SF_6,” *Gaseous Dielectr. IX*, vol. sec. 5, pp. 295–300, 2001, doi: 10.1007/978-1-4615-0583-9_40.

[106] S. Ohtsuka *et al.*, “Insulation properties of a CO_2/N_2 50% SF_6 gas mixture in a nonuniform field,” *Electr. Eng. Japan (English Transl. Denki Gakkai Ronbunshi)*, vol. 140, no. 3, pp. 34–43, 2002, doi: 10.1002/eej.10019.

[107] H. Sharifpanah, A. Gholami, and S. Jamali, “Effect of electrode material on the breakdown voltage of SF_6-N_2 and SF_6-CO_2 mixtures in a weakly non-uniform electric

field," in *IEEE 2nd International Power and Energy Conference (PECon)*, 2008, pp. 1532–1534, doi: 10.1109/PECON.2008.4762714.

[108] W. Opydo and J. Opydo, "Comparative analysis of vacuum and SF_6 as high voltage insulations," in *Proceedings of the 3rd International Conference on Properties and Applications of Dielectric Materials*, 1992, pp. 396–399, doi: 10.1109/icpadm.1991.172081.

[109] S. Gossel and C. Leu, "Electrical Breakdown of Short Spark Gaps with Several Electrode Materials in Atmospheric Air at AC (50 Hz) And Ramp Voltage (10 kV/μs)," in *The 19th International Symposium on High Voltage Engineering*, 2015, pp. 23–28.

[110] A. Cookson, "Electrical breakdown for uniform fields in compressed gases," *Proc. Inst. Electr. Eng.*, vol. 117, p. 269, 1970.

[111] P. Cornette, D. Costa, and P. Marcus, "DFT Modelling of Cu Segregation in Al-Cu Alloys Covered by an Ultrathin Oxide Film and Possible Links with Passivity," *Metals (Basel).*, vol. 7, no. 9, p. 366, Sep. 2017, doi: 10.3390/met7090366.

[112] A. Pedersen, "The effect of surface roughness on breakdown in SF_6," *IEEE Trans. Power Appar. Syst.*, vol. 94, no. 5, pp. 1749–1754, 1975, doi: 10.1109/T-PAS.1975.32019.

[113] Y. Oiu *et al.*, "Effect of electrode surface roughness on breakdown of SF_6 gas insulation," in *Conference Record of the 1988 IEEE International Symposium on Electrical Insulation*, pp. 93–96, doi: 10.1109/ELINSL.1988.13875.

[114] O. Farish, O. Ibrahim, and B. Crichton, "Effect of electrode surface roughness on breakdown in nitrogen/SF_6 mixtures," *Proc. Inst. Electr. Eng.*, vol. 123, no. 10, p. 1047, 1976, doi: 10.1049/piee.1976.0233.

[115] I. McAllister, "The influence of electrode macroscopic curvature upon surface roughness effects in compressed SF_6," *Arch. für Elektrotechnik*, vol. 62, no. 1, pp. 43–49, Jan. 1980, doi: 10.1007/BF01578116.

[116] Y. Qiu and I. Chalmers, "Effect of electrode surface roughness on breakdown in SF_6-N_2 and SF_6-CO_2 gas mixtures," *J. Phys. D. Appl. Phys.*, vol. 26, no. 11, pp. 1928–1932, Nov. 1993, doi: 10.1088/0022-3727/26/11/014.

[117] W. Boeck, R. Graf, and M. Finkel, "Effect of surface roughness and curvature on streamer inception and breakdown of N_2SF_6 mixtures," in *Proceedings of the IEEE*

International Conference on Properties and Applications of Dielectric Materials, 2003, vol. 2, pp. 543–546, doi: 10.1109/ICPADM.2003.1218474.

[118] Y. Zheng *et al.*, " Influence of conductor surface roughness on insulation performance of C_4F_7N/CO_2 mixed gas ," *IEEE Trans. Dielectr. Electr. Insul.*, vol. 26, no. 3, pp. 922–929, 2019, doi: 10.1109/tdei.2019.007871.

[119] Y. Zhou *et al.*, "Comparison of Decomposition By-products of C_4F_7N/CO_2 Mixed Gas under AC Discharge Breakdown and Partial Discharge," in *2019 5th International Conference on Electric Power Equipment - Switching Technology (ICEPE-ST)*, Oct. 2019, pp. 82–85, doi: 10.1109/ICEPE-ST.2019.8928835.

[120] B. Zhang *et al.*, "Decomposition characteristics of C_4F_7N/CO_2 mixture under AC discharge breakdown," *AIP Adv.*, vol. 9, no. 11, p. 115212, Nov. 2019, doi: 10.1063/1.5115588.

[121] L. Christophorou and J. Olthoff, *Gaseous Dielectrics VIII*. Berlin: Springer Science & Business Media, 1998.

[122] Greenhouse Gas Protocol, "Global Warming Potential Values," 2015. Accessed: Apr. 30, 2020. [Online]. Available: https://www.ghgprotocol.org/sites/default/files/ghgp/Global-Warming-Potential-Values %28Feb 16 2016%29_1.pdf.

[123] J. Daniel and S. Solomon, "On the climate forcing of carbon monoxide," *J. Geophys. Res. Atmos.*, vol. 103, no. D11, pp. 13249–13260, Jun. 1998, doi: 10.1029/98JD00822.

[124] S. Alliance, "Acute Toxicity - Inhalation," *Society for Chemical Hazard Communication*, 2018. https://www.schc.org/assets/docs/ghs_info_sheets/acute_toxicity_inhalation_2017_07.pdf (accessed Aug. 07, 2023).

[125] Y. Li *et al.*, "Study on the thermal decomposition characteristics of C_4F_7N–CO_2 mixture as eco-friendly gas-insulating medium," *High Volt.*, vol. 5, no. 1, pp. 46–52, Feb. 2020, doi: 10.1049/hve.2019.0032.

[126] "Introduction Cylinder Information Gas and Gas Mixture Shipping Classifications." Accessed: Apr. 30, 2020. [Online]. Available: https://www.mathesongas.com/pdfs/litcenter/Shipping-Classification.pdf.

[127] J. Owens *et al.*, "Recent Development of Two Alternative Gases to SF_6 for High

Voltage Electrical Power Applications," *Energies*, vol. 14, no. 16, p. 5051, Aug. 2021, doi: 10.3390/en14165051.

[128] Y. Li *et al.*, "Assessment on the toxicity and application risk of C_4F_7N: A new SF_6 alternative gas," *J. Hazard. Mater.*, vol. 368, no. 299, pp. 653–660, Apr. 2019, doi: 10.1016/j.jhazmat.2019.01.100.

[129] A. Carles *et al.*, "Heptafluoroisobutyronitrile (C_4F_7N), a gas used for insulating and arc quenching in electrical switchgear, is neurotoxic in the mouse brain," *Toxicology*, vol. 480, no. September, p. 153319, Oct. 2022, doi: 10.1016/j.tox.2022.153319.

[130] P. Widger, H. Griffiths, and A. Haddad, "Insulation strength of CF_3I-CO_2 gas mixtures as an alternative to SF_6 in MV switch disconnectors," *IEEE Trans. Dielectr. Electr. Insul.*, vol. 25, no. 1, pp. 330–338, Feb. 2018, doi: 10.1109/TDEI.2018.006932.

[131] Y. Liu *et al.*, "Study on Breakdown Probability of Multimaterial Electrodes in EDM," *Adv. Mater. Sci. Eng.*, vol. 2018, pp. 1–8, 2018, doi: 10.1155/2018/2961879.

[132] Azo, "Material Science | News | Materials Engineering | News," *AZoNetwork*, 2019. https://www.azom.com/ (accessed Jun. 02, 2021).

[133] N. Barrett *et al.*, "Microscopic work function anisotropy and surface chemistry of 316L stainless steel using photoelectron emission microscopy," *J. Electron Spectros. Relat. Phenomena*, vol. 195, pp. 117–124, Aug. 2014, doi: 10.1016/j.elspec.2014.05.015.

[134] "ISO - ISO 4287:1997 - Geometrical Product Specifications (GPS) — Surface texture: Profile method — Terms, definitions and surface texture parameters." https://www.iso.org/standard/10132.html (accessed Mar. 29, 2023).

[135] L. Chen *et al.*, "Potential of CF_3I gas mixture as an insulation medium in gas-insulated equipment," in *2015 IEEE Conference on Electrical Insulation and Dielectric Phenomena (CEIDP)*, Oct. 2015, vol. 2015-Decem, pp. 868–871, doi: 10.1109/CEIDP.2015.7352013.

[136] CGIT Westboro, "Compressed Gas Insulated Transmission Bus Systems Worldwide Experience List," 2012. [Online]. Available: www.cgit-westboro.com.

[137] IEC 60480:2019, "Guidelines for the checking and treatment of sulphur hexafluoride (SF_6) taken from electrical equipment and specification for its re-use," British Standandard Institutions, 2019.

[138] D. Montgomery and G. Runger, *Applied Statistics and Probability for Engineers*, Third Edit. John Wiley & Sons, Inc., 2014.

[139] H. Schmid and A. Huber, "Measuring a Small Number of Samples, and the 3v Fallacy: Shedding Light on Confidence and Error Intervals," *IEEE Solid-State Circuits Mag.*, vol. 6, no. 2, pp. 52–58, 2014, doi: 10.1109/MSSC.2014.2313714.

[140] C. Toigo *et al.*, "Partial discharge behavior of protrusion on high voltage conductor in GIS/GIL under high voltage direct current: Comparison of SF_6 and SF_6 alternative gases," *IEEE Trans. Dielectr. Electr. Insul.*, vol. 27, no. 1, pp. 140–147, Feb. 2020, doi: 10.1109/TDEI.2019.008358.

[141] T. Zhang *et al.*, "Insulation properties of C_4F_7N/CO_2 mixtures under lightning impulse," *IEEE Trans. Dielectr. Electr. Insul.*, vol. 27, no. 1, pp. 181–188, Feb. 2020, doi: 10.1109/TDEI.2019.008378.

[142] N. Malik, A. Qureshi, and Y. Safar, "DC Voltage Breakdown of SF_6-Air and SF_6-CO_2 Mixtures in Rod-Plane Gaps," *IEEE Trans. Electr. Insul.*, vol. EI-18, no. 6, pp. 629–636, Dec. 1983, doi: 10.1109/TEI.1983.298701.

[143] F. Zeng *et al.*, "Breakdown Characteristics of Eco-Friendly Gas $C_5F_{10}O/CO_2$ Under Switching Impulse in Nonuniform Electric Field," *IEEE Trans. Dielectr. Electr. Insul.*, vol. 29, no. 3, pp. 866–873, Jun. 2022, doi: 10.1109/TDEI.2022.3168334.

[144] N. Malik and A. Qureshi, "Breakdown mechanisms in sulphur-hexafluoride," *IIEEE Trans. Electr. Insul.*, vol. E1-13, no. 3, pp. 135–145, 1978, doi: 10.1109/TEI.1978.298121.

[145] N. Malik and A. Qureshi, "Calculation of discharge inception voltages in SF_6-N_2 mixtures," *IEEE Trans. Electr. Insul.*, vol. EI-14, no. 2, pp. 70–76, Apr. 1979, doi: 10.1109/TEI.1979.298158.

[146] K. Petcharaks, "Applicability of the streamer breakdown criterion to inhomogenous gas gaps," 1995, doi: 10.3929/ETHZ-A-001507778.

[147] A. Chachereau, A. Hösl, and C. Franck, "Electrical insulation properties of the perfluoroketone $C_5F_{10}O$," *J. Phys. D. Appl. Phys.*, vol. 51, no. 33, p. 335204, Aug. 2018, doi: 10.1088/1361-6463/aad174.

[148] A. Chachereau, M. Rabie, and C. Franck, "Electron swarm parameters of the hydrofluoroolefine HFO1234ze," *Plasma Sources Sci. Technol.*, vol. 25, p. 1, 2016.

[149] "ETHZ database." www.lxcat.net/ETHZ (accessed Nov. 06, 2022).

[150] S. Philp, "Compressed Gas Insulation in the Million-Volt Range: A Comparison or SF_6 with N_2 and CO_2," *IEEE Trans. Power Appar. Syst.*, vol. 82, no. 66, pp. 356–359, Jun. 1963, doi: 10.1109/TPAS.1963.291364.

APPENDIX A: EXTRACTED FIELD LINE DATA SET OF E(X) FROM COMSOL SIMULATION

A.1 Rod-Plane Configurations

Table A.1 Field line data set of E(x) with x is the distance away from the high voltage electrode, for 3.5 mm diameter rod-plane electrodes at 1 kV applied voltage (mesh size: 0.0005 mm minimum element size and 0.5 mm maximum element size).

5 mm Gap		10 mm Gap		15 mm Gap		25 mm Gap	
x (mm)	E(x) (kV/mm)	x (mm)	E(x) (kV/mm)	x (mm)	E(x) (kV/mm)	x (mm)	E(x) (kV/mm)
0	0.631643	0	0.522348	0	0.494158	0	0.439629
0.054075	0.610541	0.061449	0.502307	0.07058	0.472277	0.08278	0.416557
0.108151	0.589444	0.122899	0.482272	0.141159	0.450404	0.16556	0.393497
0.162226	0.568353	0.184348	0.462242	0.211739	0.428539	0.248341	0.370452
0.216302	0.54727	0.245798	0.44222	0.282318	0.406683	0.331121	0.347426
0.270377	0.526194	0.307247	0.422205	0.352898	0.384839	0.413901	0.324423
0.324452	0.505127	0.368696	0.4022	0.423477	0.363008	0.496681	0.30257
0.378528	0.48407	0.430146	0.382205	0.494057	0.342316	0.579461	0.289514
0.432603	0.463024	0.491595	0.363407	0.564636	0.329638	0.662242	0.27534
0.486678	0.443464	0.553044	0.352002	0.635216	0.315841	0.745022	0.261172
0.540754	0.431831	0.614494	0.339418	0.705795	0.302051	0.827802	0.247011
0.594829	0.418729	0.675943	0.326838	0.776375	0.288269	0.910582	0.232859
0.648905	0.405631	0.737393	0.314264	0.846955	0.274495	0.993362	0.218826
0.70298	0.392539	0.798842	0.301697	0.917534	0.260731	1.076143	0.209526
0.757055	0.379452	0.860291	0.289136	0.988114	0.247545	1.158923	0.200121
0.811131	0.36637	0.921741	0.276584	1.058693	0.239072	1.241703	0.190719
0.865206	0.353296	0.98319	0.264594	1.129273	0.230035	1.324483	0.181321
0.919282	0.340229	1.044639	0.256891	1.199852	0.221002	1.407263	0.171928
0.973357	0.327849	1.106089	0.248637	1.270432	0.211972	1.490044	0.162796
1.027432	0.319937	1.167538	0.240385	1.341011	0.202946	1.572824	0.156758
1.081508	0.311348	1.228988	0.232136	1.411591	0.193925	1.655604	0.150466
1.135583	0.302761	1.290437	0.223889	1.482171	0.185152	1.738384	0.144176
1.189658	0.294177	1.351886	0.215646	1.55275	0.179235	1.821164	0.137889
1.243734	0.285595	1.413336	0.207407	1.62333	0.173077	1.903945	0.131604
1.297809	0.277016	1.474785	0.199439	1.693909	0.166921	1.986725	0.125475
1.351885	0.26844	1.536234	0.194071	1.764489	0.160767	2.069505	0.121391
1.40596	0.259868	1.597684	0.188436	1.835068	0.154615	2.152285	0.117156
1.460035	0.251645	1.659133	0.182804	1.905648	0.148465	2.235065	0.112922
1.514111	0.246146	1.720583	0.177172	1.976227	0.142497	2.317846	0.108689
1.568186	0.240302	1.782032	0.171543	2.046807	0.138469	2.400626	0.104457
1.622261	0.23446	1.843481	0.165914	2.117386	0.134262	2.483406	0.100309
1.676337	0.228619	1.904931	0.160288	2.187966	0.130056	2.566186	0.09741
1.730412	0.222779	1.96638	0.154849	2.258546	0.125851	2.648966	0.094428
1.784488	0.216941	2.027829	0.151194	2.329125	0.121647	2.731747	0.091447
1.838563	0.211105	2.089279	0.147354	2.399705	0.117444	2.814527	0.088466
1.892638	0.20527	2.150728	0.143515	2.470284	0.113359	2.897307	0.085485
1.946714	0.199663	2.212178	0.139676	2.540864	0.110588	2.980087	0.082555
2.000789	0.195948	2.273627	0.135838	2.611443	0.1077	3.062867	0.080431
2.054865	0.192009	2.335076	0.132001	2.682023	0.104814	3.145648	0.078257
2.10894	0.18807	2.396526	0.128165	2.752602	0.101927	3.228428	0.076084
2.163015	0.184132	2.457975	0.124454	2.823182	0.099042	3.311208	0.07391
2.217091	0.180194	2.519425	0.121959	2.893762	0.096156	3.393988	0.071738
2.271166	0.176258	2.580874	0.11934	2.964341	0.093332	3.476768	0.069596
2.325241	0.172322	2.642323	0.116721	3.034921	0.091315	3.559549	0.068005
2.379317	0.168387	2.703773	0.114103	3.1055	0.089239	3.642329	0.066382
2.433392	0.164613	2.765222	0.111485	3.17608	0.087163	3.725109	0.064759
2.487466	0.162175	2.826671	0.108867	3.246659	0.085088	3.807889	0.063136
2.541539	0.159576	2.888121	0.10625	3.317239	0.083012	3.890669	0.061514

2.595612	0.156977	2.94957	0.103696	3.387818	0.080937	3.97345	0.05991
2.649686	0.154379	3.01102	0.101891	3.458398	0.078897	4.05623	0.058681
2.703759	0.151781	3.072469	0.100022	3.528977	0.077382	4.13901	0.057433
2.757832	0.149184	3.133918	0.098154	3.599557	0.075833	4.22179	0.056184
2.811906	0.146587	3.195368	0.096285	3.670137	0.074284	4.304571	0.054936
2.865979	0.14399	3.256817	0.094417	3.740716	0.072736	4.387351	0.053688
2.920052	0.141478	3.318266	0.092549	3.811296	0.071187	4.470131	0.052452
2.973788	0.139819	3.379716	0.090681	3.881875	0.069639	4.552911	0.05148
3.027524	0.138076	3.441165	0.08885	3.952455	0.068111	4.635691	0.050496
3.081259	0.136333	3.502615	0.087505	4.023034	0.066943	4.718472	0.049512
3.134995	0.134591	3.564064	0.086124	4.093614	0.065753	4.801252	0.048528
3.188731	0.132848	3.625513	0.084743	4.164193	0.064564	4.884032	0.047544
3.242467	0.131106	3.686963	0.083362	4.234773	0.063374	4.966812	0.046568
3.296202	0.129364	3.748412	0.081981	4.305352	0.062185	5.049592	0.045785
3.349938	0.127622	3.809861	0.0806	4.375932	0.060996	5.132373	0.044993
3.403674	0.125925	3.871311	0.079219	4.446512	0.05982	5.215153	0.044202
3.454275	0.124803	3.93276	0.077861	4.517091	0.058898	5.297933	0.04341
3.504876	0.123636	3.99421	0.076834	4.587671	0.057963	5.380713	0.042619
3.555477	0.12247	4.055659	0.075785	4.65825	0.057028	5.463493	0.041833
3.606078	0.121303	4.117108	0.074737	4.72883	0.056093	5.546274	0.041191
3.656679	0.120137	4.178558	0.073688	4.799409	0.055157	5.629054	0.040543
3.70728	0.118971	4.240007	0.072639	4.869989	0.054222	5.711834	0.039896
3.757881	0.117804	4.301456	0.071591	4.940568	0.053296	5.794614	0.039248
3.808482	0.116638	4.362906	0.070542	5.011148	0.052556	5.877394	0.038601
3.859083	0.115496	4.424355	0.069508	5.081728	0.051806	5.960175	0.037957
3.905087	0.114773	4.485805	0.068709	5.152307	0.051056	6.042955	0.037424
3.951091	0.114026	4.547254	0.067897	5.222887	0.050307	6.125735	0.036886
3.997094	0.113279	4.608703	0.067084	5.293466	0.049557	6.208515	0.036349
4.043098	0.112533	4.670153	0.066271	5.364046	0.048807	6.291295	0.035811
4.089102	0.111786	4.731602	0.065458	5.434625	0.048064	6.374076	0.035274
4.135105	0.11104	4.793052	0.064645	5.505205	0.04746	6.456856	0.034739
4.181109	0.110293	4.854501	0.063832	5.575784	0.046849	6.539636	0.03429
4.227113	0.109547	4.91595	0.063029	5.646364	0.046239	6.622416	0.033839
4.273116	0.108806	4.9774	0.062398	5.716943	0.045628	6.705196	0.033387
4.315011	0.108394	5.038849	0.061758	5.787523	0.045018	6.787977	0.032935
4.356905	0.107977	5.100298	0.061118	5.858103	0.044407	6.870757	0.032483
4.398799	0.107559	5.161748	0.060478	5.928682	0.043801	6.953537	0.032034
4.440694	0.107142	5.223197	0.059838	5.999262	0.043302	7.036317	0.031652
4.482588	0.106724	5.284647	0.059199	6.069841	0.042798	7.119097	0.031269
4.524482	0.106307	5.346096	0.058559	6.140421	0.042295	7.201878	0.030885
4.566377	0.105889	5.407545	0.057925	6.211	0.041791	7.284658	0.030501
4.608271	0.105472	5.468995	0.057422	6.28158	0.041287	7.367438	0.030118
4.650165	0.105066	5.530444	0.056913	6.352159	0.040783	7.450218	0.029736
4.689036	0.104939	5.591893	0.056403	6.422739	0.040283	7.532998	0.029408
4.727906	0.1048	5.653343	0.055894	6.493319	0.039866	7.615779	0.029079
4.766777	0.104662	5.714792	0.055385	6.563898	0.039445	7.698559	0.02875
4.805647	0.104523	5.776242	0.054875	6.634478	0.039025	7.781339	0.028421
4.844518	0.104384	5.837691	0.054366	6.705057	0.038605	7.864119	0.028092
4.883388	0.104245	5.89914	0.053861	6.775637	0.038185	7.946899	0.027765
4.922259	0.104106	5.96059	0.053458	6.846216	0.037764	8.02968	0.027482
4.961129	0.103968	6.022039	0.05305	6.916796	0.037347	8.11246	0.027197
5	0.103829	6.083488	0.052641	6.987375	0.036995	8.19524	0.026913
-	-	6.144938	0.052233	7.057955	0.036641	8.27802	0.026629
-	-	6.206387	0.051825	7.128534	0.036288	8.3608	0.026344
-	-	6.267837	0.051417	7.199114	0.035934	8.443581	0.026061
-	-	6.329286	0.051009	7.269694	0.03558	8.526361	0.025814
-	-	6.390735	0.050604	7.340273	0.035226	8.609141	0.025567
-	-	6.452185	0.05028	7.410853	0.034874	8.691921	0.025319
-	-	6.513634	0.049952	7.481432	0.034576	8.774701	0.025072
-	-	6.575083	0.049624	7.552012	0.034276	8.857482	0.024824
-	-	6.636533	0.049297	7.622591	0.033976	8.940262	0.024578
-	-	6.697982	0.048969	7.693171	0.033676	9.023042	0.024362
-	-	6.759432	0.048642	7.76375	0.033376	9.105822	0.024145
-	-	6.820881	0.048314	7.83433	0.033076	9.188602	0.023928
-	-	6.88233	0.047989	7.904909	0.032778	9.271383	0.023711
-	-	6.94378	0.047729	7.975489	0.032523	9.354163	0.023494
-	-	7.005229	0.047467	8.046069	0.032267	9.436943	0.023278
-	-	7.066679	0.047205	8.116648	0.032012	9.519723	0.023088
-	-	7.128128	0.046943	8.187228	0.031756	9.602503	0.022897
-	-	7.189577	0.046681	8.257807	0.0315	9.685284	0.022706
-	-	7.251027	0.046419	8.328387	0.031244	9.768064	0.022515
-	-	7.312476	0.046157	8.398966	0.030989	9.850844	0.022324
-	-	7.373925	0.045896	8.469546	0.030771	9.933624	0.022133

-	-	7.435375	0.045691	8.540125	0.030552	10.0164	0.021965
-	-	7.496824	0.045483	8.610705	0.030333	10.09918	0.021796
-	-	7.558274	0.045276	8.681285	0.030114	10.18196	0.021626
-	-	7.619723	0.045068	8.751864	0.029895	10.26475	0.021457
-	-	7.681172	0.044861	8.822444	0.029676	10.34753	0.021288
-	-	7.742622	0.044653	8.893023	0.029458	10.43031	0.02112
-	-	7.804071	0.044446	8.963603	0.02927	10.51309	0.02097
-	-	7.86552	0.04424	9.034182	0.029082	10.59587	0.020819
-	-	7.926959	0.044081	9.104762	0.028894	10.67865	0.020669
-	-	7.988398	0.04392	9.175341	0.028706	10.76143	0.020519
-	-	8.049836	0.043759	9.245921	0.028518	10.84421	0.020368
-	-	8.111275	0.043599	9.3165	0.02833	10.92699	0.020219
-	-	8.172713	0.043438	9.38708	0.028142	11.00977	0.020085
-	-	8.234152	0.043277	9.45766	0.027981	11.09255	0.019951
-	-	8.29559	0.043116	9.528239	0.027819	11.17533	0.019816
-	-	8.357029	0.042957	9.598819	0.027658	11.25811	0.019682
-	-	8.415571	0.042838	9.669398	0.027496	11.34089	0.019548
-	-	8.474113	0.042718	9.739978	0.027334	11.42367	0.019414
-	-	8.532655	0.042598	9.810557	0.027172	11.50645	0.019294
-	-	8.591198	0.042479	9.881137	0.027011	11.58923	0.019174
-	-	8.64974	0.042359	9.951716	0.026873	11.67201	0.019054
-	-	8.708282	0.042239	10.0223	0.026734	11.75479	0.018934
-	-	8.766824	0.042119	10.09288	0.026595	11.83757	0.018814
-	-	8.825366	0.042	10.16346	0.026456	11.92035	0.018694
-	-	8.878867	0.041918	10.23403	0.026317	12.00313	0.018586
-	-	8.932368	0.041835	10.30461	0.026178	12.08591	0.018478
-	-	8.985869	0.041752	10.37519	0.026039	12.16869	0.018371
-	-	9.039369	0.041669	10.44577	0.02592	12.25147	0.018263
-	-	9.09287	0.041587	10.51635	0.025801	12.33425	0.018155
-	-	9.146371	0.041504	10.58693	0.025682	12.41703	0.018047
-	-	9.199872	0.041421	10.65751	0.025563	12.49981	0.01795
-	-	9.253372	0.041338	10.72809	0.025443	12.58259	0.017853
-	-	9.30206	0.04129	10.79867	0.025324	12.66537	0.017756
-	-	9.350748	0.041241	10.86925	0.025205	12.74815	0.017659
-	-	9.399436	0.041193	10.93983	0.025104	12.83093	0.017562
-	-	9.448124	0.041144	11.01041	0.025002	12.91371	0.017465
-	-	9.496812	0.041095	11.08099	0.024901	12.99649	0.017377
-	-	9.5455	0.041047	11.15157	0.024799	13.07927	0.017289
-	-	9.594188	0.040998	11.22215	0.024697	13.16205	0.017202
-	-	9.642876	0.04095	11.29273	0.024596	13.24483	0.017114
-	-	9.687516	0.040935	11.36331	0.024494	13.32761	0.017026
-	-	9.732157	0.040918	11.43389	0.024409	13.41039	0.016939
-	-	9.776797	0.040902	11.50447	0.024323	13.49317	0.01686
-	-	9.821438	0.040885	11.57505	0.024236	13.57595	0.016781
-	-	9.866078	0.040868	11.64563	0.02415	13.65873	0.016701
-	-	9.910719	0.040852	11.71621	0.024064	13.74151	0.016622
-	-	9.955359	0.040835	11.78678	0.023978	13.82429	0.016543
-	-	10	0.040819	11.85736	0.023892	13.90707	0.016464
-	-	-	-	11.92794	0.023821	13.98985	0.016392
-	-	-	-	11.99852	0.023749	14.07263	0.01632
-	-	-	-	12.0691	0.023677	14.15541	0.016249
-	-	-	-	12.13968	0.023605	14.23819	0.016177
-	-	-	-	12.21026	0.023533	14.32097	0.016105
-	-	-	-	12.28084	0.023461	14.40376	0.016034
-	-	-	-	12.35142	0.023389	14.48654	0.015969
-	-	-	-	12.422	0.02333	14.56932	0.015904
-	-	-	-	12.49258	0.023271	14.6521	0.015839
-	-	-	-	12.56316	0.023212	14.73488	0.015774
-	-	-	-	12.63374	0.023153	14.81766	0.015709
-	-	-	-	12.70432	0.023094	14.90044	0.015644
-	-	-	-	12.7749	0.023035	14.98322	0.015585
-	-	-	-	12.84548	0.022976	15.066	0.015526
-	-	-	-	12.91605	0.022929	15.14878	0.015467
-	-	-	-	12.98662	0.022882	15.23156	0.015408
-	-	-	-	13.0572	0.022835	15.31434	0.015349
-	-	-	-	13.12777	0.022788	15.39712	0.01529
-	-	-	-	13.19834	0.022741	15.4799	0.015236
-	-	-	-	13.26892	0.022694	15.56268	0.015183
-	-	-	-	13.33949	0.022646	15.64546	0.015129
-	-	-	-	13.40697	0.022611	15.72824	0.015076
-	-	-	-	13.47444	0.022575	15.81102	0.015022
-	-	-	-	13.54192	0.022539	15.8938	0.014969
-	-	-	-	13.6094	0.022503	15.97658	0.01492

-	-	-	-	13.67687	0.022467	16.05936	0.014872
-	-	-	-	13.74435	0.022431	16.14214	0.014823
-	-	-	-	13.81183	0.022395	16.22492	0.014774
-	-	-	-	13.87372	0.02237	16.3077	0.014726
-	-	-	-	13.93562	0.022345	16.39048	0.014677
-	-	-	-	13.99751	0.022319	16.47326	0.014633
-	-	-	-	14.0594	0.022294	16.55604	0.014589
-	-	-	-	14.1213	0.022269	16.63882	0.014545
-	-	-	-	14.18319	0.022244	16.7216	0.014501
-	-	-	-	14.24508	0.022218	16.80438	0.014457
-	-	-	-	14.30146	0.022203	16.88716	0.014413
-	-	-	-	14.35784	0.022188	16.96994	0.014373
-	-	-	-	14.41422	0.022173	17.05272	0.014333
-	-	-	-	14.47059	0.022158	17.1355	0.014293
-	-	-	-	14.52697	0.022143	17.21828	0.014253
-	-	-	-	14.58335	0.022128	17.30106	0.014213
-	-	-	-	14.63973	0.022114	17.38384	0.014173
-	-	-	-	14.69119	0.022109	17.46662	0.014137
-	-	-	-	14.74266	0.022103	17.5494	0.014101
-	-	-	-	14.79413	0.022098	17.63218	0.014064
-	-	-	-	14.8456	0.022093	17.71496	0.014028
-	-	-	-	14.89706	0.022088	17.79774	0.013992
-	-	-	-	14.94853	0.022083	17.88052	0.013956
-	-	-	-	15	0.022078	17.9633	0.013923
-	-	-	-	-	-	18.04608	0.01389
-	-	-	-	-	-	18.12886	0.013858
-	-	-	-	-	-	18.21164	0.013825
-	-	-	-	-	-	18.29442	0.013792
-	-	-	-	-	-	18.3772	0.013759
-	-	-	-	-	-	18.45999	0.01373
-	-	-	-	-	-	18.54277	0.0137
-	-	-	-	-	-	18.62555	0.013671
-	-	-	-	-	-	18.70833	0.013641
-	-	-	-	-	-	18.79111	0.013612
-	-	-	-	-	-	18.87389	0.013582
-	-	-	-	-	-	18.95667	0.013556
-	-	-	-	-	-	19.03945	0.013529
-	-	-	-	-	-	19.12223	0.013502
-	-	-	-	-	-	19.20501	0.013476
-	-	-	-	-	-	19.28779	0.013449
-	-	-	-	-	-	19.37057	0.013423
-	-	-	-	-	-	19.45335	0.013399
-	-	-	-	-	-	19.53613	0.013375
-	-	-	-	-	-	19.61891	0.013351
-	-	-	-	-	-	19.70169	0.013328
-	-	-	-	-	-	19.78447	0.013304
-	-	-	-	-	-	19.86725	0.01328
-	-	-	-	-	-	19.95003	0.013259
-	-	-	-	-	-	20.03281	0.013238
-	-	-	-	-	-	20.11559	0.013217
-	-	-	-	-	-	20.19837	0.013195
-	-	-	-	-	-	20.28115	0.013174
-	-	-	-	-	-	20.36393	0.013153
-	-	-	-	-	-	20.44671	0.013134
-	-	-	-	-	-	20.52949	0.013116
-	-	-	-	-	-	20.61227	0.013097
-	-	-	-	-	-	20.69505	0.013078
-	-	-	-	-	-	20.77783	0.013059
-	-	-	-	-	-	20.86061	0.013041
-	-	-	-	-	-	20.94339	0.013024
-	-	-	-	-	-	21.02617	0.013008
-	-	-	-	-	-	21.10895	0.012991
-	-	-	-	-	-	21.19173	0.012975
-	-	-	-	-	-	21.27451	0.012958
-	-	-	-	-	-	21.35729	0.012942
-	-	-	-	-	-	21.44007	0.012928
-	-	-	-	-	-	21.52285	0.012913
-	-	-	-	-	-	21.60563	0.012899
-	-	-	-	-	-	21.68841	0.012885
-	-	-	-	-	-	21.77119	0.012871
-	-	-	-	-	-	21.85397	0.012856
-	-	-	-	-	-	21.93675	0.012844
-	-	-	-	-	-	22.01953	0.012832

-	-	-	-	-	-	22.10231	0.01282
-	-	-	-	-	-	22.18509	0.012808
-	-	-	-	-	-	22.26787	0.012796
-	-	-	-	-	-	22.35064	0.012784
-	-	-	-	-	-	22.4325	0.012773
-	-	-	-	-	-	22.51436	0.012763
-	-	-	-	-	-	22.59622	0.012753
-	-	-	-	-	-	22.67808	0.012743
-	-	-	-	-	-	22.75994	0.012733
-	-	-	-	-	-	22.8418	0.012723
-	-	-	-	-	-	22.92225	0.012714
-	-	-	-	-	-	23.00271	0.012706
-	-	-	-	-	-	23.08317	0.012698
-	-	-	-	-	-	23.16362	0.01269
-	-	-	-	-	-	23.24408	0.012682
-	-	-	-	-	-	23.32453	0.012673
-	-	-	-	-	-	23.40308	0.012667
-	-	-	-	-	-	23.48164	0.012661
-	-	-	-	-	-	23.56019	0.012654
-	-	-	-	-	-	23.63874	0.012648
-	-	-	-	-	-	23.71729	0.012642
-	-	-	-	-	-	23.79584	0.012635
-	-	-	-	-	-	23.86935	0.012631
-	-	-	-	-	-	23.94287	0.012626
-	-	-	-	-	-	24.01638	0.012622
-	-	-	-	-	-	24.08989	0.012618
-	-	-	-	-	-	24.1634	0.012613
-	-	-	-	-	-	24.23691	0.012609
-	-	-	-	-	-	24.30352	0.012606
-	-	-	-	-	-	24.37013	0.012603
-	-	-	-	-	-	24.43674	0.012601
-	-	-	-	-	-	24.50335	0.012598
-	-	-	-	-	-	24.56996	0.012595
-	-	-	-	-	-	24.63657	0.012592
-	-	-	-	-	-	24.69714	0.012592
-	-	-	-	-	-	24.75772	0.012591
-	-	-	-	-	-	24.81829	0.012590
-	-	-	-	-	-	24.87886	0.012589
-	-	-	-	-	-	24.93943	0.012588
-	-	-	-	-	-	25	0.012587

Table A.2 Field line data set of E(x) with x is the distance away from the high voltage electrode, for 6.25 mm diameter rod-plane electrodes at 1 kV applied voltage (mesh size: 0.0005 mm minimum element size and 0.5 mm maximum element size).

5 mm Gap		**15 mm Gap**		**25 mm Gap**		**35 mm Gap**		**45 mm Gap**		**55 mm Gap**	
x (mm)	**E(x) (kV/mm)**	**x (mm)**	**E(x) (kV/mm)**	**x (mm)**	**E(x) (kV/mm)**	**x (mm)**	**E(x) (kV/mm)**	**x (mm)**	**E(x) (kV/mm)**	**x (mm)**	**E(x) (kV/mm)**
0	0.440578	0	0.028069	0	0.274074	0	0.265167	0	0.249183	0	0.235527
0.06	0.428552	0.07	0.028075	0.08	0.262645	0.08	0.254135	0.08	0.238802	0.10	0.223755
0.11	0.416528	0.14	0.028081	0.17	0.251219	0.17	0.243106	0.17	0.228424	0.20	0.211987
0.17	0.404506	0.21	0.028088	0.25	0.239795	0.25	0.232079	0.25	0.218048	0.30	0.200223
0.22	0.392487	0.29	0.028094	0.33	0.228374	0.33	0.221056	0.33	0.207675	0.40	0.188462
0.28	0.380469	0.36	0.028100	0.42	0.216956	0.42	0.210036	0.42	0.197305	0.50	0.176614
0.33	0.368454	0.43	0.028106	0.50	0.205527	0.50	0.198889	0.50	0.186846	0.60	0.168673
0.39	0.356442	0.50	0.028112	0.58	0.197939	0.58	0.191404	0.58	0.179835	0.70	0.160826
0.44	0.344433	0.57	0.028130	0.67	0.190369	0.67	0.184051	0.67	0.172919	0.80	0.152981
0.50	0.332411	0.64	0.028149	0.75	0.182801	0.75	0.176700	0.75	0.166004	0.90	0.145138
0.56	0.324676	0.71	0.028167	0.83	0.175234	0.83	0.169351	0.83	0.159090	1.00	0.137630
0.61	0.316960	0.79	0.028185	0.92	0.167670	0.92	0.162004	0.92	0.152179	1.10	0.132526
0.67	0.309244	0.86	0.028203	1.00	0.160480	1.00	0.155009	1.00	0.145615	1.20	0.127092
0.72	0.301530	0.93	0.028222	1.08	0.155629	1.08	0.150265	1.08	0.141170	1.30	0.121659
0.78	0.293818	1.00	0.028240	1.17	0.150408	1.17	0.145173	1.17	0.136380	1.40	0.116228
0.83	0.286107	1.07	0.028271	1.25	0.145187	1.25	0.140081	1.25	0.131591	1.50	0.110872
0.89	0.278397	1.14	0.028301	1.33	0.139968	1.33	0.134991	1.33	0.126804	1.60	0.107105
0.94	0.270689	1.21	0.028332	1.42	0.134751	1.42	0.129902	1.42	0.122017	1.70	0.103265
1.00	0.263621	1.29	0.028363	1.50	0.129625	1.50	0.124907	1.50	0.117316	1.80	0.099425
1.06	0.259114	1.36	0.028393	1.58	0.126031	1.58	0.121398	1.58	0.114013	1.90	0.095586
1.11	0.253971	1.43	0.028424	1.67	0.122347	1.67	0.117796	1.67	0.110627	2.00	0.091789
1.17	0.248828	1.50	0.028455	1.75	0.118663	1.75	0.114195	1.75	0.107242	2.10	0.088966
1.22	0.243687	1.57	0.028498	1.83	0.114980	1.83	0.110594	1.83	0.103857	2.20	0.086100
1.28	0.238546	1.64	0.028542	1.92	0.111298	1.92	0.106994	1.92	0.100473	2.30	0.083236

1.33	0.233406	1.71	0.028586	2.00	0.107666	2.00	0.103442	2.00	0.097133	2.40	0.080371
1.39	0.228268	1.79	0.028629	2.08	0.104974	2.08	0.100805	2.08	0.094651	2.50	0.077537
1.44	0.223130	1.86	0.028673	2.17	0.102232	2.17	0.098120	2.17	0.092127	2.60	0.075374
1.50	0.218145	1.93	0.028717	2.25	0.099489	2.25	0.095436	2.25	0.089602	2.70	0.073181
1.56	0.214826	2.00	0.028760	2.33	0.096748	2.33	0.092752	2.33	0.087078	2.80	0.070989
1.61	0.211358	2.07	0.028817	2.42	0.094006	2.42	0.090068	2.42	0.084554	2.90	0.068797
1.67	0.207889	2.14	0.028874	2.50	0.091301	2.50	0.087418	2.50	0.082062	3.00	0.066624
1.72	0.204421	2.21	0.028931	2.58	0.089245	2.58	0.085397	2.58	0.080161	3.10	0.064926
1.78	0.200953	2.29	0.028989	2.67	0.087152	2.67	0.083343	2.67	0.078229	3.20	0.063208
1.83	0.197486	2.36	0.029046	2.75	0.085060	2.75	0.081290	2.75	0.076297	3.30	0.061491
1.89	0.194018	2.43	0.029103	2.83	0.082967	2.83	0.079236	2.83	0.074365	3.40	0.059773
1.94	0.190552	2.50	0.029160	2.92	0.080875	2.92	0.077183	2.92	0.072434	3.50	0.058069
2.00	0.187162	2.57	0.029231	3.00	0.078805	3.00	0.075152	3.00	0.070523	3.60	0.056709
2.06	0.184798	2.64	0.029303	3.08	0.077192	3.08	0.073565	3.08	0.069030	3.70	0.055335
2.11	0.182357	2.71	0.029375	3.17	0.075556	3.17	0.071957	3.17	0.067516	3.80	0.053963
2.17	0.179916	2.79	0.029446	3.25	0.073921	3.25	0.070349	3.25	0.066003	3.90	0.052590
2.22	0.177476	2.86	0.029518	3.33	0.072285	3.33	0.068741	3.33	0.064490	4.00	0.051226
2.28	0.175036	2.93	0.029589	3.42	0.070649	3.42	0.067133	3.42	0.062977	4.10	0.050118
2.33	0.172596	3.00	0.029661	3.50	0.069029	3.50	0.065539	3.50	0.061477	4.20	0.049001
2.39	0.170156	3.07	0.029748	3.58	0.067739	3.58	0.064269	3.58	0.060281	4.30	0.047884
2.44	0.167717	3.14	0.029835	3.67	0.066434	3.67	0.062984	3.67	0.059072	4.40	0.046768
2.50	0.165329	3.21	0.029922	3.75	0.065130	3.75	0.061698	3.75	0.057862	4.50	0.045657
2.56	0.163660	3.29	0.030009	3.83	0.063825	3.83	0.060413	3.83	0.056653	4.60	0.044741
2.61	0.161939	3.36	0.030096	3.92	0.062520	3.92	0.059128	3.92	0.055443	4.70	0.043820
2.67	0.160219	3.43	0.030183	4.00	0.061226	4.00	0.057853	4.00	0.054243	4.80	0.042898
2.72	0.158498	3.50	0.030270	4.08	0.060177	4.08	0.056819	4.08	0.053269	4.90	0.041976
2.78	0.156778	3.57	0.030373	4.17	0.059119	4.17	0.055774	4.17	0.052285	5.00	0.041059
2.83	0.155057	3.64	0.030477	4.25	0.058060	4.25	0.054729	4.25	0.051302	5.10	0.040292
2.89	0.153337	3.71	0.030581	4.33	0.057001	4.33	0.053684	4.33	0.050318	5.20	0.039522
2.94	0.151617	3.79	0.030685	4.42	0.055943	4.42	0.052640	4.42	0.049335	5.30	0.038751
3.00	0.149929	3.86	0.030789	4.50	0.054891	4.50	0.051602	4.50	0.048358	5.40	0.037980
3.06	0.148768	3.93	0.030893	4.58	0.054027	4.58	0.050747	4.58	0.047552	5.50	0.037213
3.11	0.147575	4.00	0.030997	4.67	0.053155	4.67	0.049885	4.67	0.046740	5.60	0.036564
3.17	0.146383	4.07	0.031119	4.75	0.052283	4.75	0.049023	4.75	0.045929	5.70	0.035912
3.22	0.145190	4.14	0.031242	4.83	0.051411	4.83	0.048161	4.83	0.045117	5.80	0.035260
3.28	0.143998	4.21	0.031364	4.92	0.050539	4.92	0.047299	4.92	0.044305	5.90	0.034608
3.33	0.142805	4.29	0.031487	5.00	0.049673	5.00	0.046443	5.00	0.043498	6.00	0.033959
3.39	0.141613	4.36	0.031609	5.08	0.048951	5.08	0.045727	5.08	0.042824	6.10	0.033404
3.44	0.140421	4.43	0.031732	5.17	0.048223	5.17	0.045007	5.17	0.042145	6.20	0.032847
3.50	0.139247	4.50	0.031854	5.25	0.047496	5.25	0.044286	5.25	0.041467	6.30	0.032291
3.56	0.138482	4.57	0.031997	5.33	0.046769	5.33	0.043566	5.33	0.040788	6.40	0.031734
3.61	0.137699	4.64	0.032140	5.42	0.046042	5.42	0.042846	5.42	0.040109	6.50	0.031179
3.67	0.136916	4.71	0.032283	5.50	0.045318	5.50	0.042129	5.50	0.039434	6.60	0.030701
3.72	0.136132	4.79	0.032427	5.58	0.044709	5.58	0.041524	5.58	0.038863	6.70	0.030221
3.78	0.135349	4.86	0.032570	5.67	0.044095	5.67	0.040915	5.67	0.038289	6.80	0.029741
3.83	0.134566	4.93	0.032713	5.75	0.043482	5.75	0.040306	5.75	0.037716	6.90	0.029261
3.89	0.133783	5.00	0.032856	5.83	0.042869	5.83	0.039697	5.83	0.037142	7.00	0.028783
3.94	0.133000	5.07	0.033022	5.92	0.042255	5.92	0.039088	5.92	0.036568	7.10	0.028367
4.00	0.132225	5.14	0.033189	6.00	0.041645	6.00	0.038482	6.00	0.035997	7.20	0.027951
4.06	0.131789	5.21	0.033355	6.08	0.041125	6.08	0.037965	6.08	0.035509	7.30	0.027534
4.11	0.131346	5.29	0.033522	6.17	0.040603	6.17	0.037446	6.17	0.035019	7.40	0.027117
4.17	0.130902	5.36	0.033689	6.25	0.040080	6.25	0.036926	6.25	0.034529	7.50	0.026701
4.22	0.130459	5.43	0.033855	6.33	0.039558	6.33	0.036406	6.33	0.034039	7.60	0.026338
4.28	0.130015	5.50	0.034021	6.42	0.039035	6.42	0.035887	6.42	0.033548	7.70	0.025973
4.33	0.129572	5.57	0.034214	6.50	0.038515	6.50	0.035369	6.50	0.033060	7.80	0.025609
4.39	0.129129	5.64	0.034407	6.58	0.038068	6.58	0.034924	6.58	0.032640	7.90	0.025244
4.44	0.128686	5.71	0.034600	6.67	0.037619	6.67	0.034476	6.67	0.032218	8.00	0.024880
4.50	0.128250	5.79	0.034793	6.75	0.037171	6.75	0.034028	6.75	0.031796	8.10	0.024560
4.56	0.128108	5.86	0.034986	6.83	0.036722	6.83	0.033581	6.83	0.031373	8.20	0.024240
4.61	0.127960	5.93	0.035180	6.92	0.036273	6.92	0.033133	6.92	0.030951	8.30	0.023919
4.67	0.127812	6.00	0.035372	7.00	0.035826	7.00	0.032688	7.00	0.030530	8.40	0.023598
4.72	0.127663	6.07	0.035595	7.08	0.035439	7.08	0.032301	7.08	0.030165	8.50	0.023277
4.78	0.127515	6.14	0.035819	7.17	0.035050	7.17	0.031912	7.17	0.029799	8.60	0.022994
4.83	0.127367	6.21	0.036042	7.25	0.034662	7.25	0.031524	7.25	0.029432	8.70	0.022710
4.89	0.127219	6.29	0.036266	7.33	0.034273	7.33	0.031136	7.33	0.029065	8.80	0.022426
4.94	0.127071	6.36	0.036490	7.42	0.033885	7.42	0.030747	7.42	0.028699	8.90	0.022142
5	0.126922	6.43	0.036714	7.50	0.033498	7.50	0.030360	7.50	0.028333	9.00	0.021858
-	-	6.50	0.036936	7.58	0.033160	7.58	0.030022	7.58	0.028014	9.10	0.021606
-	-	6.57	0.037195	7.67	0.032822	7.67	0.029683	7.67	0.027693	9.20	0.021353
-	-	6.64	0.037454	7.75	0.032483	7.75	0.029344	7.75	0.027372	9.30	0.021100
-	-	6.71	0.037713	7.83	0.032144	7.83	0.029004	7.83	0.027052	9.40	0.020847
-	-	6.79	0.037972	7.92	0.031806	7.92	0.028665	7.92	0.026731	9.50	0.020595
-	-	6.86	0.038231	8.00	0.031468	8.00	0.028326	8.00	0.026411	9.60	0.020369

-	-	6.93	0.038490	8.08	0.031173	8.08	0.028029	8.08	0.026130	9.70	0.020143
-	-	7.00	0.038748	8.17	0.030876	8.17	0.027731	8.17	0.025848	9.80	0.019917
-	-	7.07	0.039048	8.25	0.030579	8.25	0.027432	8.25	0.025566	9.90	0.019691
-	-	7.14	0.039349	8.33	0.030282	8.33	0.027134	8.33	0.025284	10.00	0.019465
-	-	7.21	0.039650	8.42	0.029985	8.42	0.026835	8.42	0.025002	10.10	0.019262
-	-	7.29	0.039950	8.50	0.029689	8.50	0.026538	8.50	0.024720	10.20	0.019059
-	-	7.36	0.040251	8.58	0.029428	8.58	0.026275	8.58	0.024471	10.30	0.018856
-	-	7.43	0.040552	8.67	0.029166	8.67	0.026011	8.67	0.024222	10.40	0.018653
-	-	7.50	0.040851	8.75	0.028905	8.75	0.025747	8.75	0.023972	10.50	0.018451
-	-	7.57	0.041200	8.83	0.028643	8.83	0.025483	8.83	0.023722	10.60	0.018268
-	-	7.64	0.041550	8.92	0.028381	8.92	0.025219	8.92	0.023473	10.70	0.018085
-	-	7.71	0.041900	9.00	0.028120	9.00	0.024956	9.00	0.023224	10.80	0.017902
-	-	7.79	0.042251	9.08	0.027889	9.08	0.024722	9.08	0.023002	10.90	0.017719
-	-	7.86	0.042601	9.17	0.027658	9.17	0.024488	9.17	0.022780	11.00	0.017536
-	-	7.93	0.042951	9.25	0.027426	9.25	0.024253	9.25	0.022558	11.10	0.017371
-	-	8.00	0.043299	9.33	0.027194	9.33	0.024019	9.33	0.022336	11.20	0.017205
-	-	8.07	0.043707	9.42	0.026962	9.42	0.023784	9.42	0.022114	11.30	0.017039
-	-	8.14	0.044117	9.50	0.026731	9.50	0.023550	9.50	0.021892	11.40	0.016874
-	-	8.21	0.044526	9.58	0.026526	9.58	0.023341	9.58	0.021694	11.50	0.016708
-	-	8.29	0.044936	9.67	0.026320	9.67	0.023132	9.67	0.021495	11.60	0.016558
-	-	8.36	0.045345	9.75	0.026113	9.75	0.022923	9.75	0.021297	11.70	0.016408
-	-	8.43	0.045755	9.83	0.025907	9.83	0.022713	9.83	0.021098	11.80	0.016257
-	-	8.50	0.046162	9.92	0.025701	9.92	0.022504	9.92	0.020900	11.90	0.016107
-	-	8.57	0.046641	10.00	0.025496	10.00	0.022295	10.00	0.020702	12.00	0.015957
-	-	8.64	0.047123	10.08	0.025312	10.08	0.022108	10.08	0.020524	12.10	0.015820
-	-	8.71	0.047604	10.17	0.025128	10.17	0.021920	10.17	0.020346	12.20	0.015683
-	-	8.79	0.048086	10.25	0.024944	10.25	0.021732	10.25	0.020168	12.30	0.015546
-	-	8.86	0.048568	10.33	0.024760	10.33	0.021545	10.33	0.019990	12.40	0.015409
-	-	8.93	0.049049	10.42	0.024576	10.42	0.021357	10.42	0.019811	12.50	0.015273
-	-	9.00	0.049528	10.50	0.024392	10.50	0.021170	10.50	0.019634	12.60	0.015148
-	-	9.07	0.050095	10.58	0.024228	10.58	0.021001	10.58	0.019473	12.70	0.015023
-	-	9.14	0.050665	10.67	0.024063	10.67	0.020832	10.67	0.019313	12.80	0.014898
-	-	9.21	0.051235	10.75	0.023898	10.75	0.020663	10.75	0.019152	12.90	0.014773
-	-	9.29	0.051806	10.83	0.023733	10.83	0.020494	10.83	0.018992	13.00	0.014648
-	-	9.36	0.052376	10.92	0.023569	10.92	0.020325	10.92	0.018831	13.10	0.014534
-	-	9.43	0.052946	11.00	0.023404	11.00	0.020157	11.00	0.018671	13.20	0.014419
-	-	9.50	0.053512	11.08	0.023256	11.08	0.020005	11.08	0.018526	13.30	0.014305
-	-	9.57	0.054189	11.17	0.023108	11.17	0.019852	11.17	0.018381	13.40	0.014190
-	-	9.64	0.054870	11.25	0.022960	11.25	0.019700	11.25	0.018236	13.50	0.014076
-	-	9.71	0.055551	11.33	0.022812	11.33	0.019547	11.33	0.018091	13.60	0.013971
-	-	9.79	0.056232	11.42	0.022664	11.42	0.019395	11.42	0.017946	13.70	0.013866
-	-	9.86	0.056914	11.50	0.022516	11.50	0.019242	11.50	0.017801	13.80	0.013761
-	-	9.93	0.057595	11.58	0.022383	11.58	0.019104	11.58	0.017669	13.90	0.013656
-	-	10.00	0.058270	11.67	0.022250	11.67	0.018966	11.67	0.017538	14.00	0.013551
-	-	10.07	0.059086	11.75	0.022116	11.75	0.018828	11.75	0.017406	14.10	0.013454
-	-	10.14	0.059907	11.83	0.021983	11.83	0.018690	11.83	0.017274	14.20	0.013358
-	-	10.21	0.060729	11.92	0.021850	11.92	0.018552	11.92	0.017143	14.30	0.013261
-	-	10.29	0.061550	12.00	0.021716	12.00	0.018414	12.00	0.017011	14.40	0.013164
-	-	10.36	0.062372	12.08	0.021596	12.08	0.018289	12.08	0.016891	14.50	0.013068
-	-	10.43	0.063193	12.17	0.021476	12.17	0.018163	12.17	0.016772	14.60	0.012979
-	-	10.50	0.064007	12.25	0.021355	12.25	0.018038	12.25	0.016652	14.70	0.012890
-	-	10.57	0.065001	12.33	0.021235	12.33	0.017912	12.33	0.016532	14.80	0.012801
-	-	10.64	0.066004	12.42	0.021115	12.42	0.017787	12.42	0.016412	14.90	0.012712
-	-	10.71	0.067007	12.50	0.020994	12.50	0.017661	12.50	0.016293	15.00	0.012623
-	-	10.79	0.068009	12.58	0.020886	12.58	0.017547	12.58	0.016183	15.10	0.012541
-	-	10.86	0.069012	12.67	0.020777	12.67	0.017433	12.67	0.016074	15.20	0.012458
-	-	10.93	0.070015	12.75	0.020668	12.75	0.017319	12.75	0.015965	15.30	0.012376
-	-	11.00	0.071006	12.83	0.020559	12.83	0.017204	12.83	0.015856	15.40	0.012294
-	-	11.07	0.072236	12.92	0.020450	12.92	0.017090	12.92	0.015746	15.50	0.012212
-	-	11.14	0.073477	13.00	0.020341	13.00	0.016976	13.00	0.015637	15.60	0.012136
-	-	11.21	0.074718	13.08	0.020243	13.08	0.016872	13.08	0.015537	15.70	0.012060
-	-	11.29	0.075959	13.17	0.020144	13.17	0.016767	13.17	0.015437	15.80	0.011983
-	-	11.36	0.077200	13.25	0.020045	13.25	0.016663	13.25	0.015337	15.90	0.011907
-	-	11.43	0.078442	13.33	0.019947	13.33	0.016559	13.33	0.015237	16.00	0.011831
-	-	11.50	0.079666	13.42	0.019848	13.42	0.016454	13.42	0.015137	16.10	0.011761
-	-	11.57	0.081211	13.50	0.019750	13.50	0.016350	13.50	0.015037	16.20	0.011690
-	-	11.64	0.082772	13.58	0.019660	13.58	0.016255	13.58	0.014946	16.30	0.011620
-	-	11.71	0.084334	13.67	0.019571	13.67	0.016159	13.67	0.014854	16.40	0.011550
-	-	11.79	0.085896	13.75	0.019481	13.75	0.016064	13.75	0.014763	16.50	0.011479
-	-	11.86	0.087458	13.83	0.019392	13.83	0.015968	13.83	0.014671	16.60	0.011414
-	-	11.93	0.089020	13.92	0.019302	13.92	0.015873	13.92	0.014579	16.70	0.011348
-	-	12.00	0.090556	14.00	0.019213	14.00	0.015778	14.00	0.014488	16.80	0.011283
-	-	12.07	0.092535	14.08	0.019132	14.08	0.015690	14.08	0.014404	16.90	0.011217

-	-	12.14	0.094539	14.17	0.019050	14.17	0.015603	14.17	0.014319	17.00	0.011152
-	-	12.21	0.096544	14.25	0.018969	14.25	0.015515	14.25	0.014235	17.10	0.011091
-	-	12.29	0.098549	14.33	0.018888	14.33	0.015428	14.33	0.014151	17.20	0.011031
-	-	12.36	0.100553	14.42	0.018807	14.42	0.015340	14.42	0.014067	17.30	0.010970
-	-	12.43	0.102558	14.50	0.018725	14.50	0.015253	14.50	0.013983	17.40	0.010909
-	-	12.50	0.104524	14.58	0.018652	14.58	0.015173	14.58	0.013905	17.50	0.010848
-	-	12.57	0.107117	14.67	0.018578	14.67	0.015092	14.67	0.013828	17.60	0.010792
-	-	12.64	0.109749	14.75	0.018504	14.75	0.015012	14.75	0.013750	17.70	0.010735
-	-	12.71	0.112381	14.83	0.018430	14.83	0.014932	14.83	0.013673	17.80	0.010679
-	-	12.79	0.115014	14.92	0.018356	14.92	0.014851	14.92	0.013595	17.90	0.010622
-	-	12.86	0.117647	15.00	0.018283	15.00	0.014771	15.00	0.013518	18.00	0.010565
-	-	12.93	0.120280	15.08	0.018216	15.08	0.014697	15.08	0.013446	18.10	0.010513
-	-	13.00	0.122858	15.17	0.018148	15.17	0.014623	15.17	0.013375	18.20	0.010460
-	-	13.07	0.126347	15.25	0.018081	15.25	0.014549	15.25	0.013303	18.30	0.010407
-	-	13.14	0.129893	15.33	0.018014	15.33	0.014475	15.33	0.013232	18.40	0.010355
-	-	13.21	0.133439	15.42	0.017947	15.42	0.014402	15.42	0.013160	18.50	0.010302
-	-	13.29	0.136985	15.50	0.017880	15.50	0.014328	15.50	0.013089	18.60	0.010253
-	-	13.36	0.140532	15.58	0.017819	15.58	0.014260	15.58	0.013023	18.70	0.010204
-	-	13.43	0.144079	15.67	0.017758	15.67	0.014192	15.67	0.012957	18.80	0.010155
-	-	13.50	0.147525	15.75	0.017697	15.75	0.014124	15.75	0.012891	18.90	0.010106
-	-	13.57	0.152462	15.83	0.017636	15.83	0.014056	15.83	0.012825	19.00	0.010056
-	-	13.64	0.157502	15.92	0.017575	15.92	0.013988	15.92	0.012759	19.10	0.010011
-	-	13.71	0.162543	16.00	0.017514	16.00	0.013920	16.00	0.012693	19.20	0.009965
-	-	13.79	0.167586	16.08	0.017459	16.08	0.013857	16.08	0.012632	19.30	0.009919
-	-	13.86	0.172629	16.17	0.017403	16.17	0.013794	16.17	0.012571	19.40	0.009873
-	-	13.93	0.177674	16.25	0.017348	16.25	0.013731	16.25	0.012510	19.50	0.009827
-	-	14.00	0.182285	16.33	0.017292	16.33	0.013669	16.33	0.012449	19.60	0.009784
-	-	14.07	0.189167	16.42	0.017237	16.42	0.013606	16.42	0.012388	19.70	0.009741
-	-	14.14	0.196486	16.50	0.017182	16.50	0.013543	16.50	0.012327	19.80	0.009698
-	-	14.21	0.203807	16.58	0.017131	16.58	0.013485	16.58	0.012270	19.90	0.009656
-	-	14.29	0.211130	16.67	0.017081	16.67	0.013427	16.67	0.012213	20.00	0.009613
-	-	14.36	0.218454	16.75	0.017031	16.75	0.013369	16.75	0.012157	20.10	0.009573
-	-	14.43	0.225779	16.83	0.016980	16.83	0.013311	16.83	0.012100	20.20	0.009533
-	-	14.50	0.233174	16.92	0.016930	16.92	0.013253	16.92	0.012044	20.30	0.009492
-	-	14.57	0.244298	17.00	0.016880	17.00	0.013196	17.00	0.011987	20.40	0.009452
-	-	14.64	0.255356	17.08	0.016834	17.08	0.013142	17.08	0.011935	20.50	0.009412
-	-	14.71	0.266418	17.17	0.016789	17.17	0.013088	17.17	0.011882	20.60	0.009375
-	-	14.79	0.277482	17.25	0.016743	17.25	0.013035	17.25	0.011830	20.70	0.009337
-	-	14.86	0.288549	17.33	0.016697	17.33	0.012981	17.33	0.011777	20.80	0.009300
-	-	14.93	0.299619	17.42	0.016652	17.42	0.012928	17.42	0.011725	20.90	0.009262
-	-	15	0.310690	17.50	0.016606	17.50	0.012874	17.50	0.011672	21.00	0.009225
-	-	-	-	17.58	0.016565	17.58	0.012825	17.58	0.011624	21.10	0.009190
-	-	-	-	17.67	0.016524	17.67	0.012775	17.67	0.011575	21.20	0.009154
-	-	-	-	17.75	0.016482	17.75	0.012726	17.75	0.011526	21.30	0.009119
-	-	-	-	17.83	0.016441	17.83	0.012676	17.83	0.011477	21.40	0.009084
-	-	-	-	17.92	0.016400	17.92	0.012627	17.92	0.011429	21.50	0.009049
-	-	-	-	18.00	0.016358	18.00	0.012577	18.00	0.011380	21.60	0.009016
-	-	-	-	18.08	0.016321	18.08	0.012531	18.08	0.011335	21.70	0.008983
-	-	-	-	18.17	0.016284	18.17	0.012485	18.17	0.011289	21.80	0.008950
-	-	-	-	18.25	0.016247	18.25	0.012440	18.25	0.011244	21.90	0.008917
-	-	-	-	18.33	0.016209	18.33	0.012394	18.33	0.011199	22.00	0.008884
-	-	-	-	18.42	0.016172	18.42	0.012348	18.42	0.011154	22.10	0.008853
-	-	-	-	18.50	0.016135	18.50	0.012302	18.50	0.011108	22.20	0.008823
-	-	-	-	18.58	0.016101	18.58	0.012260	18.58	0.011066	22.30	0.008792
-	-	-	-	18.67	0.016068	18.67	0.012217	18.67	0.011024	22.40	0.008761
-	-	-	-	18.75	0.016034	18.75	0.012175	18.75	0.010982	22.50	0.008730
-	-	-	-	18.83	0.016001	18.83	0.012132	18.83	0.010940	22.60	0.008701
-	-	-	-	18.92	0.015967	18.92	0.012090	18.92	0.010897	22.70	0.008672
-	-	-	-	19.00	0.015933	19.00	0.012047	19.00	0.010855	22.80	0.008643
-	-	-	-	19.08	0.015903	19.08	0.012008	19.08	0.010816	22.90	0.008614
-	-	-	-	19.17	0.015873	19.17	0.011969	19.17	0.010777	23.00	0.008585
-	-	-	-	19.25	0.015843	19.25	0.011929	19.25	0.010738	23.10	0.008558
-	-	-	-	19.33	0.015813	19.33	0.011890	19.33	0.010698	23.20	0.008531
-	-	-	-	19.42	0.015783	19.42	0.011850	19.42	0.010659	23.30	0.008504
-	-	-	-	19.50	0.015753	19.50	0.011811	19.50	0.010620	23.40	0.008476
-	-	-	-	19.58	0.015726	19.58	0.011775	19.58	0.010583	23.50	0.008449
-	-	-	-	19.67	0.015699	19.67	0.011738	19.67	0.010547	23.60	0.008424
-	-	-	-	19.75	0.015673	19.75	0.011702	19.75	0.010510	23.70	0.008398
-	-	-	-	19.83	0.015646	19.83	0.011665	19.83	0.010474	23.80	0.008373
-	-	-	-	19.92	0.015619	19.92	0.011629	19.92	0.010437	23.90	0.008347
-	-	-	-	20.00	0.015592	20.00	0.011592	20.00	0.010400	24.00	0.008322
-	-	-	-	20.08	0.015569	20.08	0.011558	20.08	0.010366	24.10	0.008298
-	-	-	-	20.17	0.015545	20.17	0.011525	20.17	0.010332	24.20	0.008274

-	-	-	-	20.25	0.015521	20.25	0.011491	20.25	0.010298	24.30	0.008250
-	-	-	-	20.33	0.015497	20.33	0.011457	20.33	0.010264	24.40	0.008226
-	-	-	-	20.42	0.015474	20.42	0.011423	20.42	0.010230	24.50	0.008202
-	-	-	-	20.50	0.015450	20.50	0.011389	20.50	0.010196	24.60	0.008179
-	-	-	-	20.58	0.015429	20.58	0.011358	20.58	0.010164	24.70	0.008157
-	-	-	-	20.67	0.015408	20.67	0.011326	20.67	0.010132	24.80	0.008134
-	-	-	-	20.75	0.015387	20.75	0.011295	20.75	0.010100	24.90	0.008112
-	-	-	-	20.83	0.015367	20.83	0.011264	20.83	0.010069	25.00	0.008089
-	-	-	-	20.92	0.015346	20.92	0.011232	20.92	0.010037	25.10	0.008068
-	-	-	-	21.00	0.015325	21.00	0.011201	21.00	0.010005	25.20	0.008047
-	-	-	-	21.08	0.015307	21.08	0.011172	21.08	0.009975	25.30	0.008026
-	-	-	-	21.17	0.015289	21.17	0.011143	21.17	0.009946	25.40	0.008005
-	-	-	-	21.25	0.015271	21.25	0.011114	21.25	0.009916	25.50	0.007984
-	-	-	-	21.33	0.015253	21.33	0.011084	21.33	0.009886	25.60	0.007964
-	-	-	-	21.42	0.015235	21.42	0.011055	21.42	0.009856	25.70	0.007944
-	-	-	-	21.50	0.015217	21.50	0.011026	21.50	0.009827	25.80	0.007924
-	-	-	-	21.58	0.015201	21.58	0.010999	21.58	0.009799	25.90	0.007904
-	-	-	-	21.67	0.015186	21.67	0.010972	21.67	0.009771	26.00	0.007885
-	-	-	-	21.75	0.015170	21.75	0.010945	21.75	0.009744	26.10	0.007866
-	-	-	-	21.83	0.015155	21.83	0.010918	21.83	0.009716	26.20	0.007847
-	-	-	-	21.92	0.015140	21.92	0.010891	21.92	0.009688	26.30	0.007829
-	-	-	-	22.00	0.015124	22.00	0.010864	22.00	0.009660	26.40	0.007810
-	-	-	-	22.08	0.015111	22.08	0.010839	22.08	0.009634	26.50	0.007791
-	-	-	-	22.17	0.015098	22.17	0.010814	22.17	0.009609	26.60	0.007774
-	-	-	-	22.25	0.015086	22.25	0.010789	22.25	0.009583	26.70	0.007756
-	-	-	-	22.33	0.015073	22.33	0.010764	22.33	0.009557	26.80	0.007739
-	-	-	-	22.42	0.015060	22.42	0.010739	22.42	0.009531	26.90	0.007721
-	-	-	-	22.50	0.015047	22.50	0.010714	22.50	0.009505	27.00	0.007704
-	-	-	-	22.58	0.015037	22.58	0.010691	22.58	0.009481	27.10	0.007687
-	-	-	-	22.67	0.015026	22.67	0.010668	22.67	0.009457	27.20	0.007671
-	-	-	-	22.75	0.015016	22.75	0.010645	22.75	0.009432	27.30	0.007655
-	-	-	-	22.83	0.015005	22.83	0.010621	22.83	0.009408	27.40	0.007638
-	-	-	-	22.92	0.014995	22.92	0.010598	22.92	0.009384	27.50	0.007622
-	-	-	-	23.00	0.014984	23.00	0.010575	23.00	0.009360	27.60	0.007606
-	-	-	-	23.08	0.014976	23.08	0.010554	23.08	0.009337	27.70	0.007591
-	-	-	-	23.17	0.014968	23.17	0.010532	23.17	0.009314	27.80	0.007576
-	-	-	-	23.25	0.014960	23.25	0.010511	23.25	0.009292	27.90	0.007560
-	-	-	-	23.33	0.014952	23.33	0.010489	23.33	0.009269	28.00	0.007545
-	-	-	-	23.42	0.014944	23.42	0.010468	23.42	0.009247	28.10	0.007530
-	-	-	-	23.50	0.014936	23.50	0.010446	23.50	0.009224	28.20	0.007516
-	-	-	-	23.58	0.014931	23.58	0.010426	23.58	0.009203	28.30	0.007501
-	-	-	-	23.67	0.014925	23.67	0.010406	23.67	0.009182	28.40	0.007487
-	-	-	-	23.75	0.014919	23.75	0.010386	23.75	0.009161	28.50	0.007472
-	-	-	-	23.83	0.014913	23.83	0.010366	23.83	0.009140	28.60	0.007459
-	-	-	-	23.92	0.014908	23.92	0.010347	23.92	0.009118	28.70	0.007445
-	-	-	-	24.00	0.014902	24.00	0.010327	24.00	0.009097	28.80	0.007432
-	-	-	-	24.08	0.014899	24.08	0.010308	24.08	0.009078	28.90	0.007418
-	-	-	-	24.17	0.014895	24.17	0.010290	24.17	0.009058	29.00	0.007405
-	-	-	-	24.25	0.014892	24.25	0.010271	24.25	0.009038	29.10	0.007392
-	-	-	-	24.33	0.014888	24.33	0.010253	24.33	0.009018	29.20	0.007379
-	-	-	-	24.42	0.014885	24.42	0.010235	24.42	0.008999	29.30	0.007367
-	-	-	-	24.50	0.014882	24.50	0.010216	24.50	0.008979	29.40	0.007354
-	-	-	-	24.58	0.014881	24.58	0.010199	24.58	0.008960	29.50	0.007341
-	-	-	-	24.67	0.014879	24.67	0.010182	24.67	0.008942	29.60	0.007329
-	-	-	-	24.75	0.014878	24.75	0.010165	24.75	0.008924	29.70	0.007317
-	-	-	-	24.83	0.014877	24.83	0.010148	24.83	0.008905	29.80	0.007306
-	-	-	-	24.92	0.014876	24.92	0.010131	24.92	0.008887	29.90	0.007294
-	-	-	-	25	0.014875	25.00	0.010114	25.00	0.008868	30.00	0.007282
-	-	-	-	-	-	25.08	0.010099	25.08	0.008851	30.10	0.007271
-	-	-	-	-	-	25.17	0.010083	25.17	0.008834	30.20	0.007260
-	-	-	-	-	-	25.25	0.010067	25.25	0.008817	30.30	0.007248
-	-	-	-	-	-	25.33	0.010051	25.33	0.008799	30.40	0.007237
-	-	-	-	-	-	25.42	0.010036	25.42	0.008782	30.50	0.007226
-	-	-	-	-	-	25.50	0.010020	25.50	0.008765	30.60	0.007216
-	-	-	-	-	-	25.58	0.010006	25.58	0.008749	30.70	0.007205
-	-	-	-	-	-	25.67	0.009991	25.67	0.008733	30.80	0.007195
-	-	-	-	-	-	25.75	0.009977	25.75	0.008717	30.90	0.007185
-	-	-	-	-	-	25.83	0.009962	25.83	0.008701	31.00	0.007174
-	-	-	-	-	-	25.92	0.009948	25.92	0.008685	31.10	0.007165
-	-	-	-	-	-	26.00	0.009933	26.00	0.008668	31.20	0.007155
-	-	-	-	-	-	26.08	0.009920	26.08	0.008653	31.30	0.007145
-	-	-	-	-	-	26.17	0.009907	26.17	0.008638	31.40	0.007135
-	-	-	-	-	-	26.25	0.009893	26.25	0.008623	31.50	0.007126

-	-	-	-	-	-	26.33	0.009880	26.33	0.008608	31.60	0.007117
-	-	-	-	-	-	26.42	0.009867	26.42	0.008593	31.70	0.007108
-	-	-	-	-	-	26.50	0.009853	26.50	0.008578	31.80	0.007099
-	-	-	-	-	-	26.58	0.009841	26.58	0.008564	31.90	0.007090
-	-	-	-	-	-	26.67	0.009829	26.67	0.008550	32.00	0.007081
-	-	-	-	-	-	26.75	0.009817	26.75	0.008536	32.10	0.007072
-	-	-	-	-	-	26.83	0.009805	26.83	0.008522	32.20	0.007064
-	-	-	-	-	-	26.92	0.009792	26.92	0.008508	32.30	0.007055
-	-	-	-	-	-	27.00	0.009780	27.00	0.008494	32.40	0.007047
-	-	-	-	-	-	27.08	0.009769	27.08	0.008481	32.50	0.007038
-	-	-	-	-	-	27.17	0.009758	27.17	0.008468	32.60	0.007031
-	-	-	-	-	-	27.25	0.009747	27.25	0.008455	32.70	0.007023
-	-	-	-	-	-	27.33	0.009735	27.33	0.008442	32.80	0.007015
-	-	-	-	-	-	27.42	0.009724	27.42	0.008429	32.90	0.007007
-	-	-	-	-	-	27.50	0.009713	27.50	0.008416	33.00	0.006999
-	-	-	-	-	-	27.58	0.009703	27.58	0.008404	33.10	0.006992
-	-	-	-	-	-	27.67	0.009693	27.67	0.008392	33.20	0.006985
-	-	-	-	-	-	27.75	0.009682	27.75	0.008380	33.30	0.006977
-	-	-	-	-	-	27.83	0.009672	27.83	0.008367	33.40	0.006970
-	-	-	-	-	-	27.92	0.009662	27.92	0.008355	33.50	0.006963
-	-	-	-	-	-	28.00	0.009652	28.00	0.008343	33.60	0.006956
-	-	-	-	-	-	28.08	0.009642	28.08	0.008332	33.70	0.006949
-	-	-	-	-	-	28.17	0.009633	28.17	0.008321	33.80	0.006943
-	-	-	-	-	-	28.25	0.009624	28.25	0.008309	33.90	0.006936
-	-	-	-	-	-	28.33	0.009615	28.33	0.008298	34.00	0.006929
-	-	-	-	-	-	28.42	0.009605	28.42	0.008287	34.10	0.006923
-	-	-	-	-	-	28.50	0.009596	28.50	0.008275	34.20	0.006917
-	-	-	-	-	-	28.58	0.009588	28.58	0.008265	34.30	0.006911
-	-	-	-	-	-	28.67	0.009579	28.67	0.008254	34.40	0.006904
-	-	-	-	-	-	28.75	0.009571	28.75	0.008244	34.50	0.006898
-	-	-	-	-	-	28.83	0.009562	28.83	0.008233	34.60	0.006892
-	-	-	-	-	-	28.92	0.009554	28.92	0.008223	34.70	0.006887
-	-	-	-	-	-	29.00	0.009545	29.00	0.008212	34.80	0.006881
-	-	-	-	-	-	29.08	0.009538	29.08	0.008202	34.90	0.006875
-	-	-	-	-	-	29.17	0.009530	29.17	0.008193	35.00	0.006870
-	-	-	-	-	-	29.25	0.009523	29.25	0.008183	35.10	0.006864
-	-	-	-	-	-	29.33	0.009515	29.33	0.008173	35.20	0.006859
-	-	-	-	-	-	29.42	0.009507	29.42	0.008163	35.30	0.006854
-	-	-	-	-	-	29.50	0.009500	29.50	0.008153	35.40	0.006848
-	-	-	-	-	-	29.58	0.009493	29.58	0.008144	35.50	0.006843
-	-	-	-	-	-	29.67	0.009486	29.67	0.008135	35.60	0.006838
-	-	-	-	-	-	29.75	0.009479	29.75	0.008126	35.70	0.006834
-	-	-	-	-	-	29.83	0.009473	29.83	0.008117	35.80	0.006829
-	-	-	-	-	-	29.92	0.009466	29.92	0.008108	35.90	0.006824
-	-	-	-	-	-	30.00	0.009459	30.00	0.008099	36.00	0.006819
-	-	-	-	-	-	30.08	0.009453	30.08	0.008090	36.10	0.006815
-	-	-	-	-	-	30.17	0.009447	30.17	0.008082	36.20	0.006810
-	-	-	-	-	-	30.25	0.009441	30.25	0.008074	36.30	0.006806
-	-	-	-	-	-	30.33	0.009435	30.33	0.008065	36.40	0.006801
-	-	-	-	-	-	30.42	0.009429	30.42	0.008057	36.50	0.006797
-	-	-	-	-	-	30.50	0.009423	30.50	0.008048	36.60	0.006793
-	-	-	-	-	-	30.58	0.009417	30.58	0.008041	36.70	0.006789
-	-	-	-	-	-	30.67	0.009412	30.67	0.008033	36.80	0.006785
-	-	-	-	-	-	30.75	0.009407	30.75	0.008025	36.90	0.006781
-	-	-	-	-	-	30.83	0.009401	30.83	0.008017	37.00	0.006777
-	-	-	-	-	-	30.92	0.009396	30.92	0.008009	37.10	0.006773
-	-	-	-	-	-	31.00	0.009391	31.00	0.008002	37.20	0.006770
-	-	-	-	-	-	31.08	0.009386	31.08	0.007994	37.30	0.006766
-	-	-	-	-	-	31.17	0.009381	31.17	0.007987	37.40	0.006762
-	-	-	-	-	-	31.25	0.009377	31.25	0.007980	37.50	0.006759
-	-	-	-	-	-	31.33	0.009372	31.33	0.007973	37.60	0.006755
-	-	-	-	-	-	31.42	0.009367	31.42	0.007966	37.70	0.006752
-	-	-	-	-	-	31.50	0.009363	31.50	0.007958	37.80	0.006749
-	-	-	-	-	-	31.58	0.009359	31.58	0.007952	37.90	0.006746
-	-	-	-	-	-	31.67	0.009355	31.67	0.007945	38.00	0.006742
-	-	-	-	-	-	31.75	0.009351	31.75	0.007938	38.10	0.006739
-	-	-	-	-	-	31.83	0.009347	31.83	0.007932	38.20	0.006736
-	-	-	-	-	-	31.92	0.009343	31.92	0.007925	38.30	0.006734
-	-	-	-	-	-	32.00	0.009339	32.00	0.007918	38.40	0.006731
-	-	-	-	-	-	32.08	0.009336	32.08	0.007912	38.50	0.006728
-	-	-	-	-	-	32.17	0.009332	32.17	0.007906	38.60	0.006725
-	-	-	-	-	-	32.25	0.009329	32.25	0.007900	38.70	0.006722
-	-	-	-	-	-	32.33	0.009326	32.33	0.007894	38.80	0.006720

-	-	-	-	-	-	32.42	0.009322	32.42	0.007888	38.90	0.006717
-	-	-	-	-	-	32.50	0.009319	32.50	0.007881	39.00	0.006715
-	-	-	-	-	-	32.58	0.009316	32.58	0.007876	39.10	0.006712
-	-	-	-	-	-	32.67	0.009314	32.67	0.007870	39.20	0.006710
-	-	-	-	-	-	32.75	0.009311	32.75	0.007865	39.30	0.006708
-	-	-	-	-	-	32.83	0.009308	32.83	0.007859	39.40	0.006705
-	-	-	-	-	-	32.92	0.009305	32.92	0.007853	39.50	0.006703
-	-	-	-	-	-	33.00	0.009303	33.00	0.007848	39.60	0.006701
-	-	-	-	-	-	33.08	0.009301	33.08	0.007842	39.70	0.006699
-	-	-	-	-	-	33.17	0.009299	33.17	0.007837	39.80	0.006697
-	-	-	-	-	-	33.25	0.009296	33.25	0.007832	39.90	0.006695
-	-	-	-	-	-	33.33	0.009294	33.33	0.007827	40.00	0.006693
-	-	-	-	-	-	33.42	0.009292	33.42	0.007822	40.10	0.006691
-	-	-	-	-	-	33.50	0.009290	33.50	0.007816	40.20	0.006689
-	-	-	-	-	-	33.58	0.009289	33.58	0.007812	40.30	0.006687
-	-	-	-	-	-	33.67	0.009287	33.67	0.007807	40.40	0.006686
-	-	-	-	-	-	33.75	0.009286	33.75	0.007802	40.50	0.006684
-	-	-	-	-	-	33.83	0.009284	33.83	0.007797	40.60	0.006682
-	-	-	-	-	-	33.92	0.009283	33.92	0.007793	40.70	0.006682
-	-	-	-	-	-	34.00	0.009281	34.00	0.007788	40.80	0.006682
-	-	-	-	-	-	34.08	0.009280	34.08	0.007783	40.90	0.006682
-	-	-	-	-	-	34.17	0.009280	34.17	0.007779	41.00	0.006682
-	-	-	-	-	-	34.25	0.009279	34.25	0.007775	41.10	0.006682
-	-	-	-	-	-	34.33	0.009278	34.33	0.007770	41.20	0.006682
-	-	-	-	-	-	34.42	0.009277	34.42	0.007766	41.30	0.006682
-	-	-	-	-	-	34.50	0.009276	34.50	0.007762	41.40	0.006682
-	-	-	-	-	-	34.58	0.009276	34.58	0.007758	41.50	0.006682
-	-	-	-	-	-	34.67	0.009275	34.67	0.007754	41.60	0.006681
-	-	-	-	-	-	34.75	0.009275	34.75	0.007750	41.70	0.006681
-	-	-	-	-	-	34.83	0.009275	34.83	0.007746	41.80	0.006681
-	-	-	-	-	-	34.92	0.009275	34.92	0.007742	41.90	0.006681
-	-	-	-	-	-	35	0.009274	35.00	0.007738	42.00	0.006681
-	-	-	-	-	-	-	-	35.08	0.007734	42.10	0.006681
-	-	-	-	-	-	-	-	35.17	0.007730	42.20	0.006681
-	-	-	-	-	-	-	-	35.25	0.007727	42.30	0.006681
-	-	-	-	-	-	-	-	35.33	0.007723	42.40	0.006680
-	-	-	-	-	-	-	-	35.42	0.007720	42.50	0.006680
-	-	-	-	-	-	-	-	35.50	0.007716	42.60	0.006680
-	-	-	-	-	-	-	-	35.58	0.007713	42.70	0.006680
-	-	-	-	-	-	-	-	35.67	0.007709	42.80	0.006680
-	-	-	-	-	-	-	-	35.75	0.007706	42.90	0.006679
-	-	-	-	-	-	-	-	35.83	0.007703	43.00	0.006679
-	-	-	-	-	-	-	-	35.92	0.007699	43.10	0.006679
-	-	-	-	-	-	-	-	36.00	0.007696	43.20	0.006679
-	-	-	-	-	-	-	-	36.08	0.007693	43.30	0.006678
-	-	-	-	-	-	-	-	36.17	0.007690	43.40	0.006678
-	-	-	-	-	-	-	-	36.25	0.007687	43.50	0.006678
-	-	-	-	-	-	-	-	36.33	0.007684	43.60	0.006678
-	-	-	-	-	-	-	-	36.42	0.007681	43.70	0.006678
-	-	-	-	-	-	-	-	36.50	0.007678	43.80	0.006677
-	-	-	-	-	-	-	-	36.58	0.007676	43.90	0.006677
-	-	-	-	-	-	-	-	36.67	0.007673	44.00	0.006677
-	-	-	-	-	-	-	-	36.75	0.007670	44.10	0.006676
-	-	-	-	-	-	-	-	36.83	0.007667	44.20	0.006676
-	-	-	-	-	-	-	-	36.92	0.007665	44.30	0.006676
-	-	-	-	-	-	-	-	37.00	0.007662	44.40	0.006675
-	-	-	-	-	-	-	-	37.08	0.007660	44.50	0.006675
-	-	-	-	-	-	-	-	37.17	0.007657	44.60	0.006675
-	-	-	-	-	-	-	-	37.25	0.007655	44.70	0.006675
-	-	-	-	-	-	-	-	37.33	0.007652	44.80	0.006674
-	-	-	-	-	-	-	-	37.42	0.007650	44.90	0.006674
-	-	-	-	-	-	-	-	37.50	0.007647	45.00	0.006674
-	-	-	-	-	-	-	-	37.58	0.007645	45.10	0.006674
-	-	-	-	-	-	-	-	37.67	0.007643	45.20	0.006673
-	-	-	-	-	-	-	-	37.75	0.007641	45.30	0.006673
-	-	-	-	-	-	-	-	37.83	0.007639	45.40	0.006673
-	-	-	-	-	-	-	-	37.92	0.007636	45.50	0.006672
-	-	-	-	-	-	-	-	38.00	0.007634	45.60	0.006672
-	-	-	-	-	-	-	-	38.08	0.007632	45.70	0.006671
-	-	-	-	-	-	-	-	38.17	0.007630	45.80	0.006671
-	-	-	-	-	-	-	-	38.25	0.007628	45.90	0.006671
-	-	-	-	-	-	-	-	38.33	0.007627	46.00	0.006671
-	-	-	-	-	-	-	-	38.42	0.007625	46.10	0.006670

-	-	-	-	-	-	-	-	38.50	0.007623	46.20	0.006670
-	-	-	-	-	-	-	-	38.58	0.007621	46.30	0.006670
-	-	-	-	-	-	-	-	38.67	0.007619	46.40	0.006669
-	-	-	-	-	-	-	-	38.75	0.007617	46.50	0.006669
-	-	-	-	-	-	-	-	38.83	0.007616	46.60	0.006669
-	-	-	-	-	-	-	-	38.92	0.007614	46.70	0.006668
-	-	-	-	-	-	-	-	39.00	0.007612	46.80	0.006668
-	-	-	-	-	-	-	-	39.08	0.007611	46.90	0.006668
-	-	-	-	-	-	-	-	39.17	0.007609	47.00	0.006667
-	-	-	-	-	-	-	-	39.25	0.007608	47.10	0.006667
-	-	-	-	-	-	-	-	39.33	0.007606	47.20	0.006667
-	-	-	-	-	-	-	-	39.42	0.007604	47.30	0.006666
-	-	-	-	-	-	-	-	39.50	0.007603	47.40	0.006666
-	-	-	-	-	-	-	-	39.58	0.007602	47.50	0.006666
-	-	-	-	-	-	-	-	39.67	0.007600	47.60	0.006666
-	-	-	-	-	-	-	-	39.75	0.007599	47.70	0.006665
-	-	-	-	-	-	-	-	39.83	0.007598	47.80	0.006665
-	-	-	-	-	-	-	-	39.92	0.007596	47.90	0.006665
-	-	-	-	-	-	-	-	40.00	0.007595	48.00	0.006664
-	-	-	-	-	-	-	-	40.08	0.007594	48.10	0.006664
-	-	-	-	-	-	-	-	40.17	0.007592	48.20	0.006664
-	-	-	-	-	-	-	-	40.25	0.007591	48.30	0.006663
-	-	-	-	-	-	-	-	40.33	0.007590	48.40	0.006663
-	-	-	-	-	-	-	-	40.42	0.007589	48.50	0.006663
-	-	-	-	-	-	-	-	40.50	0.007588	48.60	0.006662
-	-	-	-	-	-	-	-	40.58	0.007587	48.70	0.006662
-	-	-	-	-	-	-	-	40.67	0.007586	48.80	0.006662
-	-	-	-	-	-	-	-	40.75	0.007585	48.90	0.006661
-	-	-	-	-	-	-	-	40.83	0.007584	49.00	0.006661
-	-	-	-	-	-	-	-	40.92	0.007583	49.10	0.006661
-	-	-	-	-	-	-	-	41.00	0.007582	49.20	0.006661
-	-	-	-	-	-	-	-	41.08	0.007581	49.30	0.006660
-	-	-	-	-	-	-	-	41.17	0.007580	49.40	0.006660
-	-	-	-	-	-	-	-	41.25	0.007579	49.50	0.006660
-	-	-	-	-	-	-	-	41.33	0.007578	49.60	0.006660
-	-	-	-	-	-	-	-	41.42	0.007577	49.70	0.006659
-	-	-	-	-	-	-	-	41.50	0.007576	49.80	0.006659
-	-	-	-	-	-	-	-	41.58	0.007576	49.90	0.006659
-	-	-	-	-	-	-	-	41.67	0.007575	50.00	0.006658
-	-	-	-	-	-	-	-	41.75	0.007574	50.10	0.006658
-	-	-	-	-	-	-	-	41.83	0.007573	50.20	0.006658
-	-	-	-	-	-	-	-	41.92	0.007573	50.30	0.006658
-	-	-	-	-	-	-	-	42.00	0.007572	50.40	0.006658
-	-	-	-	-	-	-	-	42.08	0.007571	50.50	0.006657
-	-	-	-	-	-	-	-	42.17	0.007571	50.60	0.006657
-	-	-	-	-	-	-	-	42.25	0.007570	50.70	0.006657
-	-	-	-	-	-	-	-	42.33	0.007569	50.80	0.006657
-	-	-	-	-	-	-	-	42.42	0.007569	50.90	0.006656
-	-	-	-	-	-	-	-	42.50	0.007568	51.00	0.006656
-	-	-	-	-	-	-	-	42.58	0.007568	51.10	0.006656
-	-	-	-	-	-	-	-	42.67	0.007567	51.20	0.006656
-	-	-	-	-	-	-	-	42.75	0.007567	51.30	0.006656
-	-	-	-	-	-	-	-	42.83	0.007566	51.40	0.006655
-	-	-	-	-	-	-	-	42.92	0.007566	51.50	0.006655
-	-	-	-	-	-	-	-	43.00	0.007565	51.60	0.006655
-	-	-	-	-	-	-	-	43.08	0.007565	51.70	0.006655
-	-	-	-	-	-	-	-	43.17	0.007564	51.80	0.006655
-	-	-	-	-	-	-	-	43.25	0.007564	51.90	0.006654
-	-	-	-	-	-	-	-	43.33	0.007564	52.00	0.006654
-	-	-	-	-	-	-	-	43.42	0.007563	52.10	0.006654
-	-	-	-	-	-	-	-	43.50	0.007563	52.20	0.006654
-	-	-	-	-	-	-	-	43.58	0.007563	52.30	0.006654
-	-	-	-	-	-	-	-	43.67	0.007562	52.40	0.006654
-	-	-	-	-	-	-	-	43.75	0.007562	52.50	0.006654
-	-	-	-	-	-	-	-	43.83	0.007562	52.60	0.006653
-	-	-	-	-	-	-	-	43.92	0.007562	52.70	0.006653
-	-	-	-	-	-	-	-	44.00	0.007561	52.80	0.006653
-	-	-	-	-	-	-	-	44.08	0.007561	52.90	0.006653
-	-	-	-	-	-	-	-	44.17	0.007561	53.00	0.006653
-	-	-	-	-	-	-	-	44.25	0.007561	53.10	0.006653
-	-	-	-	-	-	-	-	44.33	0.007561	53.20	0.006653
-	-	-	-	-	-	-	-	44.42	0.007561	53.30	0.006653
-	-	-	-	-	-	-	-	44.50	0.007560	53.40	0.006653

-	-	-	-	-	-	-	-	44.58	0.007560	53.50	0.006652
-	-	-	-	-	-	-	-	44.67	0.007560	53.60	0.006652
-	-	-	-	-	-	-	-	44.75	0.007560	53.70	0.006652
-	-	-	-	-	-	-	-	44.83	0.007560	53.80	0.006652
-	-	-	-	-	-	-	-	44.92	0.007560	53.90	0.006652
-	-	-	-	-	-	-	-	45	0.007560	54.00	0.006652
-	-	-	-	-	-	-	-	-	-	54.10	0.006652
-	-	-	-	-	-	-	-	-	-	54.20	0.006652
-	-	-	-	-	-	-	-	-	-	54.30	0.006652
-	-	-	-	-	-	-	-	-	-	54.40	0.006652
-	-	-	-	-	-	-	-	-	-	54.50	0.006652
-	-	-	-	-	-	-	-	-	-	54.60	0.006652
-	-	-	-	-	-	-	-	-	-	54.70	0.006652
-	-	-	-	-	-	-	-	-	-	54.80	0.006652
-	-	-	-	-	-	-	-	-	-	54.90	0.006652
-	-	-	-	-	-	-	-	-	-	55	0.006652

Table A.3 Field line data set of E(x) with x is the distance away from the high voltage electrode, for 12.5 mm diameter rod-plane electrodes at 1 kV applied voltage (mesh size: 0.0005 mm minimum element size and 0.5 mm maximum element size).

5 mm Gap		**25 mm Gap**		**35 mm Gap**		**45 mm Gap**		**55 mm Gap**	
x (mm)	**E(x) (kV/mm)**	**x (mm)**	**E(x) (kV/mm)**	**x (mm)**	**E(x) (kV/mm)**	**x (mm)**	**E(x) (kV/mm)**	**x (mm)**	**E(x) (kV/mm)**
0	0.316369	0	0.163589	0	0.152808	0	0.137504	0	0.127657
0.055556	0.311547	0.083333	0.159738	0.083333	0.149205	0.083333	0.134263	0.1	0.124047
0.111111	0.306725	0.166667	0.155887	0.166667	0.145603	0.166667	0.131023	0.2	0.120436
0.166667	0.301904	0.25	0.152037	0.25	0.142	0.25	0.127782	0.3	0.116826
0.222222	0.297083	0.333333	0.148187	0.333333	0.138397	0.333333	0.124542	0.4	0.113216
0.277778	0.292262	0.416667	0.144337	0.416667	0.134795	0.416667	0.121302	0.5	0.10963
0.333333	0.287441	0.5	0.14052	0.5	0.131221	0.5	0.118088	0.6	0.106773
0.388889	0.282621	0.583333	0.137491	0.583333	0.128375	0.583333	0.115529	0.7	0.103894
0.444444	0.277801	0.666667	0.13443	0.666667	0.1255	0.666667	0.112945	0.8	0.101015
0.5	0.27306	0.75	0.131369	0.75	0.122625	0.75	0.110362	0.9	0.098136
0.555556	0.269515	0.833333	0.128308	0.833333	0.119751	0.833333	0.107778	1	0.095283
0.611111	0.265892	0.916667	0.125247	0.916667	0.116877	0.916667	0.105195	1.1	0.092991
0.666667	0.262269	1	0.122219	1	0.114033	1	0.102639	1.2	0.090674
0.722222	0.258646	1.083333	0.119795	1.083333	0.111749	1.083333	0.100587	1.3	0.088358
0.777778	0.255023	1.166667	0.117338	1.166667	0.109435	1.166667	0.098509	1.4	0.086041
0.833333	0.251401	1.25	0.114882	1.25	0.107122	1.25	0.09643	1.5	0.083741
0.888889	0.247778	1.333333	0.112426	1.333333	0.104808	1.333333	0.094352	1.6	0.081863
0.944444	0.244156	1.416667	0.10997	1.416667	0.102494	1.416667	0.092274	1.7	0.079969
1	0.240609	1.5	0.107535	1.5	0.1002	1.5	0.090213	1.8	0.078075
1.055556	0.237948	1.583333	0.105552	1.583333	0.098327	1.583333	0.088532	1.9	0.076181
1.111111	0.235214	1.666667	0.103549	1.666667	0.096434	1.666667	0.086832	2	0.074298
1.166667	0.232479	1.75	0.101545	1.75	0.094542	1.75	0.085133	2.1	0.07274
1.222222	0.229744	1.833333	0.099542	1.833333	0.092649	1.833333	0.083434	2.2	0.071171
1.277778	0.22701	1.916667	0.097538	1.916667	0.090757	1.916667	0.081735	2.3	0.069603
1.333333	0.224275	2	0.095548	2	0.088877	2	0.080048	2.4	0.068035
1.388889	0.221541	2.083333	0.093907	2.083333	0.087322	2.083333	0.078653	2.5	0.066474
1.444444	0.218807	2.166667	0.092252	2.166667	0.085755	2.166667	0.077246	2.6	0.065168
1.5	0.216117	2.25	0.090598	2.25	0.084187	2.25	0.075839	2.7	0.063854
1.555556	0.214077	2.333333	0.088943	2.333333	0.08262	2.333333	0.074433	2.8	0.06254
1.611111	0.211994	2.416667	0.087289	2.416667	0.081053	2.416667	0.073026	2.9	0.061226
1.666667	0.20991	2.5	0.085643	2.5	0.079495	2.5	0.071628	3	0.059918
1.722222	0.207827	2.583333	0.08427	2.583333	0.07819	2.583333	0.070458	3.1	0.058812
1.777778	0.205743	2.666667	0.082887	2.666667	0.076877	2.666667	0.06928	3.2	0.0577
1.833333	0.20366	2.75	0.081503	2.75	0.075563	2.75	0.068102	3.3	0.056588
1.888889	0.201577	2.833333	0.08012	2.833333	0.07425	2.833333	0.066924	3.4	0.055476
1.944444	0.199493	2.916667	0.078737	2.916667	0.072937	2.916667	0.065746	3.5	0.054369
2	0.197441	3	0.077362	3	0.071631	3	0.064574	3.6	0.053424
2.055556	0.195889	3.083333	0.076201	3.083333	0.070526	3.083333	0.063583	3.7	0.052474
2.111111	0.194306	3.166667	0.075033	3.166667	0.069414	3.166667	0.062586	3.8	0.051525
2.166667	0.192724	3.25	0.073866	3.25	0.068303	3.25	0.061589	3.9	0.050575
2.222222	0.191141	3.333333	0.072698	3.333333	0.067191	3.333333	0.060592	4	0.049629
2.277778	0.189558	3.416667	0.07153	3.416667	0.06608	3.416667	0.059596	4.1	0.048815
2.333333	0.187976	3.5	0.070368	3.5	0.064974	3.5	0.058603	4.2	0.047998
2.388889	0.186393	3.583333	0.069378	3.583333	0.06403	3.583333	0.057757	4.3	0.04718
2.444444	0.184811	3.666667	0.068384	3.666667	0.06308	3.666667	0.056906	4.4	0.046363
2.5	0.183247	3.75	0.067389	3.75	0.062131	3.75	0.056055	4.5	0.045548
2.555556	0.182078	3.833333	0.066394	3.833333	0.061182	3.833333	0.055204	4.6	0.044842
2.611111	0.180891	3.916667	0.065399	3.916667	0.060233	3.916667	0.054353	4.7	0.044133

2.666667	0.179704	4	0.064409	4	0.059288	4	0.053505	4.8	0.043424
2.722222	0.178517	4.083333	0.063558	4.083333	0.058475	4.083333	0.052776	4.9	0.042715
2.777778	0.17733	4.166667	0.062704	4.166667	0.057658	4.166667	0.052044	5	0.042008
2.833333	0.176143	4.25	0.06185	4.25	0.056841	4.25	0.051311	5.1	0.041391
2.888889	0.174956	4.333333	0.060995	4.333333	0.056024	4.333333	0.050579	5.2	0.040773
2.944444	0.173769	4.416667	0.060141	4.416667	0.055207	4.416667	0.049846	5.3	0.040154
3	0.172595	4.5	0.05929	4.5	0.054393	4.5	0.049116	5.4	0.039535
3.055556	0.171745	4.583333	0.058554	4.583333	0.053688	4.583333	0.048484	5.5	0.038918
3.111111	0.170883	4.666667	0.057815	4.666667	0.05298	4.666667	0.047849	5.6	0.038376
3.166667	0.17002	4.75	0.057076	4.75	0.052271	4.75	0.047214	5.7	0.037832
3.222222	0.169158	4.833333	0.056337	4.833333	0.051563	4.833333	0.046579	5.8	0.037289
3.277778	0.168296	4.916667	0.055598	4.916667	0.050855	4.916667	0.045944	5.9	0.036745
3.333333	0.167433	5	0.054861	5	0.050149	5	0.045311	6	0.036203
3.388889	0.166571	5.083333	0.05422	5.083333	0.049533	5.083333	0.044758	6.1	0.035724
3.444444	0.165709	5.166667	0.053577	5.166667	0.048915	5.166667	0.044204	6.2	0.035244
3.5	0.164854	5.25	0.052933	5.25	0.048297	5.25	0.04365	6.3	0.034764
3.555556	0.164276	5.333333	0.05229	5.333333	0.047678	5.333333	0.043095	6.4	0.034284
3.611111	0.16369	5.416667	0.051647	5.416667	0.04706	5.416667	0.042541	6.5	0.033805
3.666667	0.163104	5.5	0.051005	5.5	0.046444	5.5	0.041988	6.6	0.03338
3.722222	0.162518	5.583333	0.050443	5.583333	0.045903	5.583333	0.041503	6.7	0.032954
3.777778	0.161933	5.666667	0.04988	5.666667	0.04536	5.666667	0.041017	6.8	0.032528
3.833333	0.161347	5.75	0.049316	5.75	0.044818	5.75	0.04053	6.9	0.032101
3.888889	0.160761	5.833333	0.048753	5.833333	0.044275	5.833333	0.040043	7	0.031676
3.944444	0.160176	5.916667	0.048189	5.916667	0.043732	5.916667	0.039556	7.1	0.031297
4	0.159593	6	0.047627	6	0.043191	6	0.039071	7.2	0.030917
4.055556	0.159256	6.083333	0.047133	6.083333	0.042714	6.083333	0.038643	7.3	0.030537
4.111111	0.158917	6.166667	0.046637	6.166667	0.042235	6.166667	0.038213	7.4	0.030157
4.166667	0.158578	6.25	0.04614	6.25	0.041756	6.25	0.037783	7.5	0.029778
4.222222	0.158239	6.333333	0.045644	6.333333	0.041277	6.333333	0.037353	7.6	0.029438
4.277778	0.157899	6.416667	0.045148	6.416667	0.040798	6.416667	0.036924	7.7	0.029098
4.333333	0.15756	6.5	0.044653	6.5	0.04032	6.5	0.036495	7.8	0.028757
4.388889	0.157221	6.583333	0.044215	6.583333	0.039896	6.583333	0.036115	7.9	0.028417
4.444444	0.156882	6.666667	0.043777	6.666667	0.039471	6.666667	0.035733	8	0.028077
4.5	0.156548	6.75	0.043338	6.75	0.039046	6.75	0.035352	8.1	0.027772
4.555556	0.156438	6.833333	0.042899	6.833333	0.038621	6.833333	0.034971	8.2	0.027466
4.611111	0.156323	6.916667	0.04246	6.916667	0.038196	6.916667	0.034589	8.3	0.02716
4.666667	0.156209	7	0.042022	7	0.037772	7	0.034209	8.4	0.026854
4.722222	0.156094	7.083333	0.041633	7.083333	0.037395	7.083333	0.03387	8.5	0.026549
4.777778	0.15598	7.166667	0.041243	7.166667	0.037016	7.166667	0.03353	8.6	0.026273
4.833333	0.155866	7.25	0.040853	7.25	0.036638	7.25	0.03319	8.7	0.025997
4.888889	0.155751	7.333333	0.040462	7.333333	0.036259	7.333333	0.03285	8.8	0.025721
4.944444	0.155637	7.416667	0.040072	7.416667	0.03588	7.416667	0.03251	8.9	0.025445
5	0.155522	7.5	0.039683	7.5	0.035503	7.5	0.032171	9	0.025169
-	-	7.583333	0.039336	7.583333	0.035165	7.583333	0.031867	9.1	0.024919
-	-	7.666667	0.038988	7.666667	0.034826	7.666667	0.031563	9.2	0.02467
-	-	7.75	0.03864	7.75	0.034487	7.75	0.031258	9.3	0.02442
-	-	7.833333	0.038292	7.833333	0.034148	7.833333	0.030954	9.4	0.02417
-	-	7.916667	0.037944	7.916667	0.03381	7.916667	0.03065	9.5	0.02392
-	-	8	0.037597	8	0.033472	8	0.030346	9.6	0.023693
-	-	8.083333	0.037286	8.083333	0.033168	8.083333	0.030073	9.7	0.023466
-	-	8.166667	0.036975	8.166667	0.032864	8.166667	0.0298	9.8	0.023239
-	-	8.25	0.036663	8.25	0.032559	8.25	0.029526	9.9	0.023012
-	-	8.333333	0.036351	8.333333	0.032255	8.333333	0.029253	10	0.022785
-	-	8.416667	0.03604	8.416667	0.031951	8.416667	0.028979	10.1	0.022579
-	-	8.5	0.035729	8.5	0.031647	8.5	0.028706	10.2	0.022372
-	-	8.583333	0.03545	8.583333	0.031374	8.583333	0.02846	10.3	0.022165
-	-	8.666667	0.03517	8.666667	0.031099	8.666667	0.028213	10.4	0.021959
-	-	8.75	0.03489	8.75	0.030825	8.75	0.027966	10.5	0.021752
-	-	8.833333	0.03461	8.833333	0.030551	8.833333	0.02772	10.6	0.021563
-	-	8.916667	0.034331	8.916667	0.030277	8.916667	0.027473	10.7	0.021375
-	-	9	0.034051	9	0.030003	9	0.027227	10.8	0.021186
-	-	9.083333	0.0338	9.083333	0.029756	9.083333	0.027004	10.9	0.020997
-	-	9.166667	0.033548	9.166667	0.029508	9.166667	0.026781	11	0.020808
-	-	9.25	0.033296	9.25	0.02926	9.25	0.026558	11.1	0.020635
-	-	9.333333	0.033043	9.333333	0.029012	9.333333	0.026334	11.2	0.020463
-	-	9.416667	0.032791	9.416667	0.028764	9.416667	0.026111	11.3	0.02029
-	-	9.5	0.03254	9.5	0.028516	9.5	0.025888	11.4	0.020117
-	-	9.583333	0.032313	9.583333	0.028292	9.583333	0.025686	11.5	0.019944
-	-	9.666667	0.032085	9.666667	0.028067	9.666667	0.025483	11.6	0.019786
-	-	9.75	0.031857	9.75	0.027842	9.75	0.025281	11.7	0.019627
-	-	9.833333	0.03163	9.833333	0.027617	9.833333	0.025078	11.8	0.019468
-	-	9.916667	0.031402	9.916667	0.027393	9.916667	0.024875	11.9	0.01931
-	-	10	0.031175	10	0.027168	10	0.024673	12	0.019151

-	-	10.08333	0.030969	10.08333	0.026964	10.08333	0.024489	12.1	0.019005
-	-	10.16667	0.030763	10.16667	0.02676	10.16667	0.024305	12.2	0.018859
-	-	10.25	0.030557	10.25	0.026555	10.25	0.02412	12.3	0.018713
-	-	10.33333	0.030351	10.33333	0.026351	10.33333	0.023936	12.4	0.018567
-	-	10.41667	0.030144	10.41667	0.026146	10.41667	0.023751	12.5	0.018422
-	-	10.5	0.029939	10.5	0.025942	10.5	0.023567	12.6	0.018287
-	-	10.58333	0.029752	10.58333	0.025756	10.58333	0.023399	12.7	0.018153
-	-	10.66667	0.029565	10.66667	0.02557	10.66667	0.023231	12.8	0.018018
-	-	10.75	0.029378	10.75	0.025383	10.75	0.023062	12.9	0.017884
-	-	10.83333	0.029191	10.83333	0.025197	10.83333	0.022894	13	0.01775
-	-	10.91667	0.029004	10.91667	0.025011	10.91667	0.022726	13.1	0.017626
-	-	11	0.028817	11	0.024825	11	0.022557	13.2	0.017501
-	-	11.08333	0.028648	11.08333	0.024655	11.08333	0.022404	13.3	0.017377
-	-	11.16667	0.028478	11.16667	0.024484	11.16667	0.02225	13.4	0.017253
-	-	11.25	0.028308	11.25	0.024314	11.25	0.022096	13.5	0.017129
-	-	11.33333	0.028138	11.33333	0.024144	11.33333	0.021942	13.6	0.017014
-	-	11.41667	0.027968	11.41667	0.023973	11.41667	0.021788	13.7	0.016899
-	-	11.5	0.027798	11.5	0.023803	11.5	0.021634	13.8	0.016785
-	-	11.58333	0.027644	11.58333	0.023648	11.58333	0.021493	13.9	0.01667
-	-	11.66667	0.027489	11.66667	0.023492	11.66667	0.021352	14	0.016555
-	-	11.75	0.027334	11.75	0.023336	11.75	0.02121	14.1	0.016449
-	-	11.83333	0.02718	11.83333	0.02318	11.83333	0.021069	14.2	0.016342
-	-	11.91667	0.027025	11.91667	0.023024	11.91667	0.020928	14.3	0.016236
-	-	12	0.026871	12	0.022868	12	0.020787	14.4	0.01613
-	-	12.08333	0.02673	12.08333	0.022726	12.08333	0.020657	14.5	0.016023
-	-	12.16667	0.026589	12.16667	0.022583	12.16667	0.020528	14.6	0.015925
-	-	12.25	0.026448	12.25	0.02244	12.25	0.020398	14.7	0.015826
-	-	12.33333	0.026307	12.33333	0.022297	12.33333	0.020268	14.8	0.015727
-	-	12.41667	0.026166	12.41667	0.022154	12.41667	0.020138	14.9	0.015629
-	-	12.5	0.026025	12.5	0.022011	12.5	0.020009	15	0.01553
-	-	12.58333	0.025896	12.58333	0.021879	12.58333	0.01989	15.1	0.015438
-	-	12.66667	0.025768	12.66667	0.021748	12.66667	0.01977	15.2	0.015347
-	-	12.75	0.025639	12.75	0.021617	12.75	0.019651	15.3	0.015255
-	-	12.83333	0.02551	12.83333	0.021485	12.83333	0.019531	15.4	0.015163
-	-	12.91667	0.025382	12.91667	0.021354	12.91667	0.019412	15.5	0.015072
-	-	13	0.025253	13	0.021222	13	0.019292	15.6	0.014986
-	-	13.08333	0.025136	13.08333	0.021102	13.08333	0.019182	15.7	0.014901
-	-	13.16667	0.025018	13.16667	0.020981	13.16667	0.019072	15.8	0.014816
-	-	13.25	0.024901	13.25	0.02086	13.25	0.018962	15.9	0.01473
-	-	13.33333	0.024783	13.33333	0.020739	13.33333	0.018852	16	0.014645
-	-	13.41667	0.024665	13.41667	0.020618	13.41667	0.018742	16.1	0.014566
-	-	13.5	0.024548	13.5	0.020497	13.5	0.018632	16.2	0.014486
-	-	13.58333	0.024441	13.58333	0.020385	13.58333	0.01853	16.3	0.014407
-	-	13.66667	0.024333	13.66667	0.020274	13.66667	0.018428	16.4	0.014327
-	-	13.75	0.024226	13.75	0.020162	13.75	0.018326	16.5	0.014248
-	-	13.83333	0.024118	13.83333	0.020051	13.83333	0.018225	16.6	0.014174
-	-	13.91667	0.024011	13.91667	0.019939	13.91667	0.018123	16.7	0.0141
-	-	14	0.023904	14	0.019828	14	0.018021	16.8	0.014026
-	-	14.08333	0.023806	14.08333	0.019725	14.08333	0.017927	16.9	0.013952
-	-	14.16667	0.023707	14.16667	0.019622	14.16667	0.017833	17	0.013878
-	-	14.25	0.023609	14.25	0.019519	14.25	0.017739	17.1	0.013808
-	-	14.33333	0.023511	14.33333	0.019416	14.33333	0.017645	17.2	0.013739
-	-	14.41667	0.023413	14.41667	0.019313	14.41667	0.017551	17.3	0.01367
-	-	14.5	0.023315	14.5	0.01921	14.5	0.017456	17.4	0.013601
-	-	14.58333	0.023225	14.58333	0.019115	14.58333	0.017369	17.5	0.013532
-	-	14.66667	0.023135	14.66667	0.01902	14.66667	0.017282	17.6	0.013467
-	-	14.75	0.023045	14.75	0.018925	14.75	0.017195	17.7	0.013402
-	-	14.83333	0.022955	14.83333	0.018829	14.83333	0.017108	17.8	0.013338
-	-	14.91667	0.022865	14.91667	0.018734	14.91667	0.01702	17.9	0.013273
-	-	15	0.022776	15	0.018639	15	0.016933	18	0.013208
-	-	15.08333	0.022694	15.08333	0.018551	15.08333	0.016852	18.1	0.013148
-	-	15.16667	0.022612	15.16667	0.018463	15.16667	0.016771	18.2	0.013088
-	-	15.25	0.022529	15.25	0.018375	15.25	0.01669	18.3	0.013027
-	-	15.33333	0.022447	15.33333	0.018287	15.33333	0.016609	18.4	0.012967
-	-	15.41667	0.022365	15.41667	0.018199	15.41667	0.016529	18.5	0.012906
-	-	15.5	0.022283	15.5	0.018111	15.5	0.016448	18.6	0.01285
-	-	15.58333	0.022208	15.58333	0.018029	15.58333	0.016373	18.7	0.012793
-	-	15.66667	0.022133	15.66667	0.017948	15.66667	0.016297	18.8	0.012736
-	-	15.75	0.022058	15.75	0.017866	15.75	0.016222	18.9	0.01268
-	-	15.83333	0.021983	15.83333	0.017785	15.83333	0.016147	19	0.012623
-	-	15.91667	0.021908	15.91667	0.017703	15.91667	0.016072	19.1	0.01257
-	-	16	0.021833	16	0.017622	16	0.015997	19.2	0.012517
-	-	16.08333	0.021764	16.08333	0.017546	16.08333	0.015927	19.3	0.012464

-	-	16.16667	0.021696	16.16667	0.01747	16.16667	0.015857	19.4	0.012411
-	-	16.25	0.021627	16.25	0.017395	16.25	0.015787	19.5	0.012358
-	-	16.33333	0.021559	16.33333	0.017319	16.33333	0.015717	19.6	0.012308
-	-	16.41667	0.02149	16.41667	0.017243	16.41667	0.015647	19.7	0.012259
-	-	16.5	0.021422	16.5	0.017168	16.5	0.015577	19.8	0.012209
-	-	16.58333	0.021359	16.58333	0.017098	16.58333	0.015512	19.9	0.012159
-	-	16.66667	0.021297	16.66667	0.017028	16.66667	0.015447	20	0.01211
-	-	16.75	0.021234	16.75	0.016957	16.75	0.015382	20.1	0.012063
-	-	16.83333	0.021172	16.83333	0.016887	16.83333	0.015317	20.2	0.012016
-	-	16.91667	0.021109	16.91667	0.016817	16.91667	0.015252	20.3	0.01197
-	-	17	0.021047	17	0.016747	17	0.015187	20.4	0.011923
-	-	17.08333	0.02099	17.08333	0.016682	17.08333	0.015127	20.5	0.011876
-	-	17.16667	0.020933	17.16667	0.016617	17.16667	0.015066	20.6	0.011833
-	-	17.25	0.020876	17.25	0.016552	17.25	0.015005	20.7	0.011789
-	-	17.33333	0.020819	17.33333	0.016486	17.33333	0.014945	20.8	0.011745
-	-	17.41667	0.020762	17.41667	0.016421	17.41667	0.014884	20.9	0.011701
-	-	17.5	0.020705	17.5	0.016356	17.5	0.014823	21	0.011658
-	-	17.58333	0.020654	17.58333	0.016296	17.58333	0.014767	21.1	0.011617
-	-	17.66667	0.020602	17.66667	0.016235	17.66667	0.01471	21.2	0.011576
-	-	17.75	0.02055	17.75	0.016175	17.75	0.014654	21.3	0.011534
-	-	17.83333	0.020498	17.83333	0.016114	17.83333	0.014597	21.4	0.011493
-	-	17.91667	0.020447	17.91667	0.016054	17.91667	0.014541	21.5	0.011452
-	-	18	0.020395	18	0.015993	18	0.014484	21.6	0.011414
-	-	18.08333	0.020348	18.08333	0.015937	18.08333	0.014432	21.7	0.011375
-	-	18.16667	0.020301	18.16667	0.015881	18.16667	0.014379	21.8	0.011336
-	-	18.25	0.020254	18.25	0.015824	18.25	0.014326	21.9	0.011298
-	-	18.33333	0.020208	18.33333	0.015768	18.33333	0.014273	22	0.011259
-	-	18.41667	0.020161	18.41667	0.015712	18.41667	0.014221	22.1	0.011223
-	-	18.5	0.020114	18.5	0.015656	18.5	0.014168	22.2	0.011187
-	-	18.58333	0.020072	18.58333	0.015603	18.58333	0.014119	22.3	0.01115
-	-	18.66667	0.020029	18.66667	0.015551	18.66667	0.01407	22.4	0.011114
-	-	18.75	0.019987	18.75	0.015499	18.75	0.01402	22.5	0.011078
-	-	18.83333	0.019945	18.83333	0.015446	18.83333	0.013971	22.6	0.011044
-	-	18.91667	0.019902	18.91667	0.015394	18.91667	0.013922	22.7	0.01101
-	-	19	0.01986	19	0.015342	19	0.013873	22.8	0.010976
-	-	19.08333	0.019822	19.08333	0.015293	19.08333	0.013827	22.9	0.010941
-	-	19.16667	0.019784	19.16667	0.015245	19.16667	0.013781	23	0.010907
-	-	19.25	0.019746	19.25	0.015196	19.25	0.013735	23.1	0.010875
-	-	19.33333	0.019708	19.33333	0.015147	19.33333	0.013689	23.2	0.010843
-	-	19.41667	0.01967	19.41667	0.015099	19.41667	0.013643	23.3	0.010811
-	-	19.5	0.019632	19.5	0.01505	19.5	0.013597	23.4	0.010779
-	-	19.58333	0.019598	19.58333	0.015005	19.58333	0.013554	23.5	0.010747
-	-	19.66667	0.019564	19.66667	0.01496	19.66667	0.013511	23.6	0.010717
-	-	19.75	0.01953	19.75	0.014914	19.75	0.013468	23.7	0.010687
-	-	19.83333	0.019496	19.83333	0.014869	19.83333	0.013425	23.8	0.010657
-	-	19.91667	0.019462	19.91667	0.014824	19.91667	0.013382	23.9	0.010627
-	-	20	0.019428	20	0.014779	20	0.013339	24	0.010596
-	-	20.08333	0.019398	20.08333	0.014737	20.08333	0.013298	24.1	0.010568
-	-	20.16667	0.019367	20.16667	0.014694	20.16667	0.013258	24.2	0.01054
-	-	20.25	0.019337	20.25	0.014652	20.25	0.013218	24.3	0.010511
-	-	20.33333	0.019307	20.33333	0.01461	20.33333	0.013178	24.4	0.010483
-	-	20.41667	0.019277	20.41667	0.014568	20.41667	0.013138	24.5	0.010455
-	-	20.5	0.019247	20.5	0.014526	20.5	0.013097	24.6	0.010428
-	-	20.58333	0.01922	20.58333	0.014487	20.58333	0.01306	24.7	0.010401
-	-	20.66667	0.019194	20.66667	0.014448	20.66667	0.013022	24.8	0.010375
-	-	20.75	0.019167	20.75	0.014409	20.75	0.012985	24.9	0.010348
-	-	20.83333	0.019141	20.83333	0.01437	20.83333	0.012947	25	0.010321
-	-	20.91667	0.019114	20.91667	0.01433	20.91667	0.012909	25.1	0.010296
-	-	21	0.019088	21	0.014291	21	0.012872	25.2	0.010271
-	-	21.08333	0.019064	21.08333	0.014255	21.08333	0.012837	25.3	0.010246
-	-	21.16667	0.019041	21.16667	0.014218	21.16667	0.012801	25.4	0.010221
-	-	21.25	0.019018	21.25	0.014182	21.25	0.012766	25.5	0.010196
-	-	21.33333	0.018995	21.33333	0.014146	21.33333	0.012731	25.6	0.010172
-	-	21.41667	0.018972	21.41667	0.014109	21.41667	0.012696	25.7	0.010149
-	-	21.5	0.018949	21.5	0.014073	21.5	0.012661	25.8	0.010125
-	-	21.58333	0.018929	21.58333	0.014039	21.58333	0.012628	25.9	0.010102
-	-	21.66667	0.01891	21.66667	0.014005	21.66667	0.012595	26	0.010078
-	-	21.75	0.01889	21.75	0.013971	21.75	0.012562	26.1	0.010056
-	-	21.83333	0.01887	21.83333	0.013937	21.83333	0.012529	26.2	0.010034
-	-	21.91667	0.018851	21.91667	0.013904	21.91667	0.012496	26.3	0.010012
-	-	22	0.018831	22	0.01387	22	0.012463	26.4	0.009989
-	-	22.08333	0.018814	22.08333	0.013838	22.08333	0.012432	26.5	0.009967
-	-	22.16667	0.018798	22.16667	0.013807	22.16667	0.012401	26.6	0.009946

-	-	22.25	0.018781	22.25	0.013775	22.25	0.012371	26.7	0.009926
-	-	22.33333	0.018765	22.33333	0.013744	22.33333	0.01234	26.8	0.009905
-	-	22.41667	0.018749	22.41667	0.013712	22.41667	0.012309	26.9	0.009884
-	-	22.5	0.018732	22.5	0.013681	22.5	0.012278	27	0.009863
-	-	22.58333	0.018719	22.58333	0.013652	22.58333	0.012249	27.1	0.009844
-	-	22.66667	0.018705	22.66667	0.013622	22.66667	0.01222	27.2	0.009824
-	-	22.75	0.018692	22.75	0.013593	22.75	0.012192	27.3	0.009804
-	-	22.83333	0.018679	22.83333	0.013564	22.83333	0.012163	27.4	0.009785
-	-	22.91667	0.018665	22.91667	0.013535	22.91667	0.012134	27.5	0.009765
-	-	23	0.018652	23	0.013505	23	0.012105	27.6	0.009747
-	-	23.08333	0.018642	23.08333	0.013478	23.08333	0.012078	27.7	0.009728
-	-	23.16667	0.018631	23.16667	0.013451	23.16667	0.012051	27.8	0.00971
-	-	23.25	0.018621	23.25	0.013424	23.25	0.012024	27.9	0.009692
-	-	23.33333	0.018611	23.33333	0.013397	23.33333	0.011997	28	0.009673
-	-	23.41667	0.0186	23.41667	0.01337	23.41667	0.01197	28.1	0.009656
-	-	23.5	0.01859	23.5	0.013343	23.5	0.011943	28.2	0.009639
-	-	23.58333	0.018583	23.58333	0.013317	23.58333	0.011918	28.3	0.009622
-	-	23.66667	0.018575	23.66667	0.013292	23.66667	0.011893	28.4	0.009604
-	-	23.75	0.018568	23.75	0.013267	23.75	0.011867	28.5	0.009587
-	-	23.83333	0.018561	23.83333	0.013242	23.83333	0.011842	28.6	0.009571
-	-	23.91667	0.018553	23.91667	0.013217	23.91667	0.011817	28.7	0.009555
-	-	24	0.018546	24	0.013192	24	0.011792	28.8	0.009539
-	-	24.08333	0.018542	24.08333	0.013168	24.08333	0.011768	28.9	0.009522
-	-	24.16667	0.018537	24.16667	0.013145	24.16667	0.011744	29	0.009506
-	-	24.25	0.018533	24.25	0.013122	24.25	0.011721	29.1	0.009491
-	-	24.33333	0.018529	24.33333	0.013098	24.33333	0.011697	29.2	0.009476
-	-	24.41667	0.018524	24.41667	0.013075	24.41667	0.011673	29.3	0.009461
-	-	24.5	0.01852	24.5	0.013052	24.5	0.01165	29.4	0.009446
-	-	24.58333	0.018518	24.58333	0.01303	24.58333	0.011628	29.5	0.00943
-	-	24.66667	0.018517	24.66667	0.013008	24.66667	0.011606	29.6	0.009416
-	-	24.75	0.018515	24.75	0.012987	24.75	0.011584	29.7	0.009402
-	-	24.83333	0.018514	24.83333	0.012965	24.83333	0.011561	29.8	0.009388
-	-	24.91667	0.018512	24.91667	0.012944	24.91667	0.011539	29.9	0.009374
-	-	25	0.018511	25	0.012922	25	0.011517	30	0.00936
-	-	-	-	25.08333	0.012902	25.08333	0.011497	30.1	0.009346
-	-	-	-	25.16667	0.012882	25.16667	0.011476	30.2	0.009333
-	-	-	-	25.25	0.012862	25.25	0.011455	30.3	0.00932
-	-	-	-	25.33333	0.012842	25.33333	0.011435	30.4	0.009306
-	-	-	-	25.41667	0.012822	25.41667	0.011414	30.5	0.009293
-	-	-	-	25.5	0.012802	25.5	0.011393	30.6	0.009281
-	-	-	-	25.58333	0.012784	25.58333	0.011374	30.7	0.009268
-	-	-	-	25.66667	0.012765	25.66667	0.011355	30.8	0.009256
-	-	-	-	25.75	0.012747	25.75	0.011335	30.9	0.009244
-	-	-	-	25.83333	0.012728	25.83333	0.011316	31	0.009231
-	-	-	-	25.91667	0.01271	25.91667	0.011297	31.1	0.00922
-	-	-	-	26	0.012691	26	0.011277	31.2	0.009208
-	-	-	-	26.08333	0.012674	26.08333	0.011259	31.3	0.009196
-	-	-	-	26.16667	0.012657	26.16667	0.011241	31.4	0.009185
-	-	-	-	26.25	0.01264	26.25	0.011223	31.5	0.009173
-	-	-	-	26.33333	0.012623	26.33333	0.011205	31.6	0.009162
-	-	-	-	26.41667	0.012606	26.41667	0.011187	31.7	0.009152
-	-	-	-	26.5	0.012589	26.5	0.011169	31.8	0.009141
-	-	-	-	26.58333	0.012574	26.58333	0.011153	31.9	0.00913
-	-	-	-	26.66667	0.012558	26.66667	0.011136	32	0.009119
-	-	-	-	26.75	0.012543	26.75	0.011119	32.1	0.009109
-	-	-	-	26.83333	0.012527	26.83333	0.011102	32.2	0.009099
-	-	-	-	26.91667	0.012511	26.91667	0.011085	32.3	0.009089
-	-	-	-	27	0.012496	27	0.011068	32.4	0.009079
-	-	-	-	27.08333	0.012481	27.08333	0.011053	32.5	0.009069
-	-	-	-	27.16667	0.012467	27.16667	0.011037	32.6	0.00906
-	-	-	-	27.25	0.012453	27.25	0.011021	32.7	0.00905
-	-	-	-	27.33333	0.012438	27.33333	0.011006	32.8	0.009041
-	-	-	-	27.41667	0.012424	27.41667	0.01099	32.9	0.009032
-	-	-	-	27.5	0.01241	27.5	0.010974	33	0.009022
-	-	-	-	27.58333	0.012397	27.58333	0.01096	33.1	0.009014
-	-	-	-	27.66667	0.012384	27.66667	0.010945	33.2	0.009005
-	-	-	-	27.75	0.01237	27.75	0.01093	33.3	0.008997
-	-	-	-	27.83333	0.012357	27.83333	0.010916	33.4	0.008988
-	-	-	-	27.91667	0.012344	27.91667	0.010901	33.5	0.008979
-	-	-	-	28	0.012331	28	0.010886	33.6	0.008971
-	-	-	-	28.08333	0.012319	28.08333	0.010873	33.7	0.008963
-	-	-	-	28.16667	0.012307	28.16667	0.010859	33.8	0.008955
-	-	-	-	28.25	0.012295	28.25	0.010846	33.9	0.008947

-	-	-	-	28.33333	0.012283	28.33333	0.010832	34	0.008939
-	-	-	-	28.41667	0.012271	28.41667	0.010818	34.1	0.008932
-	-	-	-	28.5	0.012259	28.5	0.010805	34.2	0.008925
-	-	-	-	28.58333	0.012249	28.58333	0.010792	34.3	0.008917
-	-	-	-	28.66667	0.012238	28.66667	0.010779	34.4	0.00891
-	-	-	-	28.75	0.012227	28.75	0.010767	34.5	0.008902
-	-	-	-	28.83333	0.012216	28.83333	0.010754	34.6	0.008896
-	-	-	-	28.91667	0.012205	28.91667	0.010741	34.7	0.008889
-	-	-	-	29	0.012194	29	0.010729	34.8	0.008882
-	-	-	-	29.08333	0.012185	29.08333	0.010717	34.9	0.008875
-	-	-	-	29.16667	0.012175	29.16667	0.010705	35	0.008869
-	-	-	-	29.25	0.012165	29.25	0.010693	35.1	0.008862
-	-	-	-	29.33333	0.012155	29.33333	0.010682	35.2	0.008856
-	-	-	-	29.41667	0.012146	29.41667	0.01067	35.3	0.00885
-	-	-	-	29.5	0.012136	29.5	0.010658	35.4	0.008844
-	-	-	-	29.58333	0.012127	29.58333	0.010647	35.5	0.008837
-	-	-	-	29.66667	0.012118	29.66667	0.010636	35.6	0.008832
-	-	-	-	29.75	0.012109	29.75	0.010625	35.7	0.008826
-	-	-	-	29.83333	0.012101	29.83333	0.010614	35.8	0.00882
-	-	-	-	29.91667	0.012092	29.91667	0.010604	35.9	0.008815
-	-	-	-	30	0.012083	30	0.010593	36	0.008809
-	-	-	-	30.08333	0.012075	30.08333	0.010582	36.1	0.008804
-	-	-	-	30.16667	0.012067	30.16667	0.010572	36.2	0.008799
-	-	-	-	30.25	0.01206	30.25	0.010562	36.3	0.008793
-	-	-	-	30.33333	0.012052	30.33333	0.010552	36.4	0.008788
-	-	-	-	30.41667	0.012044	30.41667	0.010542	36.5	0.008783
-	-	-	-	30.5	0.012036	30.5	0.010532	36.6	0.008778
-	-	-	-	30.58333	0.012029	30.58333	0.010522	36.7	0.008774
-	-	-	-	30.66667	0.012022	30.66667	0.010513	36.8	0.008769
-	-	-	-	30.75	0.012016	30.75	0.010504	36.9	0.008764
-	-	-	-	30.83333	0.012009	30.83333	0.010494	37	0.00876
-	-	-	-	30.91667	0.012002	30.91667	0.010485	37.1	0.008755
-	-	-	-	31	0.011995	31	0.010476	37.2	0.008751
-	-	-	-	31.08333	0.011989	31.08333	0.010467	37.3	0.008747
-	-	-	-	31.16667	0.011983	31.16667	0.010458	37.4	0.008743
-	-	-	-	31.25	0.011977	31.25	0.01045	37.5	0.008738
-	-	-	-	31.33333	0.011971	31.33333	0.010441	37.6	0.008735
-	-	-	-	31.41667	0.011965	31.41667	0.010432	37.7	0.008731
-	-	-	-	31.5	0.011959	31.5	0.010424	37.8	0.008727
-	-	-	-	31.58333	0.011954	31.58333	0.010416	37.9	0.008723
-	-	-	-	31.66667	0.011949	31.66667	0.010408	38	0.008719
-	-	-	-	31.75	0.011943	31.75	0.0104	38.1	0.008716
-	-	-	-	31.83333	0.011938	31.83333	0.010392	38.2	0.008713
-	-	-	-	31.91667	0.011933	31.91667	0.010384	38.3	0.008709
-	-	-	-	32	0.011928	32	0.010376	38.4	0.008706
-	-	-	-	32.08333	0.011924	32.08333	0.010368	38.5	0.008703
-	-	-	-	32.16667	0.011919	32.16667	0.010361	38.6	0.0087
-	-	-	-	32.25	0.011915	32.25	0.010354	38.7	0.008697
-	-	-	-	32.33333	0.011911	32.33333	0.010346	38.8	0.008694
-	-	-	-	32.41667	0.011907	32.41667	0.010339	38.9	0.008691
-	-	-	-	32.5	0.011902	32.5	0.010332	39	0.008688
-	-	-	-	32.58333	0.011899	32.58333	0.010325	39.1	0.008685
-	-	-	-	32.66667	0.011895	32.66667	0.010318	39.2	0.008682
-	-	-	-	32.75	0.011892	32.75	0.010311	39.3	0.00868
-	-	-	-	32.83333	0.011888	32.83333	0.010305	39.4	0.008677
-	-	-	-	32.91667	0.011885	32.91667	0.010298	39.5	0.008674
-	-	-	-	33	0.011881	33	0.010291	39.6	0.008672
-	-	-	-	33.08333	0.011879	33.08333	0.010285	39.7	0.008671
-	-	-	-	33.16667	0.011876	33.16667	0.010279	39.8	0.008671
-	-	-	-	33.25	0.011873	33.25	0.010272	39.9	0.008671
-	-	-	-	33.33333	0.01187	33.33333	0.010266	40	0.008671
-	-	-	-	33.41667	0.011868	33.41667	0.01026	40.1	0.008671
-	-	-	-	33.5	0.011865	33.5	0.010254	40.2	0.008671
-	-	-	-	33.58333	0.011863	33.58333	0.010248	40.3	0.008671
-	-	-	-	33.66667	0.011861	33.66667	0.010242	40.4	0.008671
-	-	-	-	33.75	0.011859	33.75	0.010237	40.5	0.008671
-	-	-	-	33.83333	0.011857	33.83333	0.010231	40.6	0.008671
-	-	-	-	33.91667	0.011856	33.91667	0.010225	40.7	0.008671
-	-	-	-	34	0.011854	34	0.01022	40.8	0.00867
-	-	-	-	34.08333	0.011852	34.08333	0.010214	40.9	0.00867
-	-	-	-	34.16667	0.011851	34.16667	0.010209	41	0.00867
-	-	-	-	34.25	0.01185	34.25	0.010204	41.1	0.00867
-	-	-	-	34.33333	0.011849	34.33333	0.010199	41.2	0.00867

-	-	-	-	34.41667	0.011848	34.41667	0.010194	41.3	0.008669
-	-	-	-	34.5	0.011847	34.5	0.010189	41.4	0.008669
-	-	-	-	34.58333	0.011846	34.58333	0.010184	41.5	0.008669
-	-	-	-	34.66667	0.011846	34.66667	0.010179	41.6	0.008669
-	-	-	-	34.75	0.011846	34.75	0.010174	41.7	0.008668
-	-	-	-	34.83333	0.011845	34.83333	0.01017	41.8	0.008668
-	-	-	-	34.91667	0.011845	34.91667	0.010165	41.9	0.008668
-	-	-	-	35	0.011844	35	0.01016	42	0.008668
-	-	-	-	-	-	35.08333	0.010156	42.1	0.008667
-	-	-	-	-	-	35.16667	0.010152	42.2	0.008667
-	-	-	-	-	-	35.25	0.010147	42.3	0.008666
-	-	-	-	-	-	35.33333	0.010143	42.4	0.008666
-	-	-	-	-	-	35.41667	0.010139	42.5	0.008666
-	-	-	-	-	-	35.5	0.010134	42.6	0.008665
-	-	-	-	-	-	35.58333	0.01013	42.7	0.008665
-	-	-	-	-	-	35.66667	0.010127	42.8	0.008665
-	-	-	-	-	-	35.75	0.010123	42.9	0.008664
-	-	-	-	-	-	35.83333	0.010119	43	0.008664
-	-	-	-	-	-	35.91667	0.010115	43.1	0.008663
-	-	-	-	-	-	36	0.010111	43.2	0.008663
-	-	-	-	-	-	36.08333	0.010107	43.3	0.008663
-	-	-	-	-	-	36.16667	0.010104	43.4	0.008662
-	-	-	-	-	-	36.25	0.0101	43.5	0.008662
-	-	-	-	-	-	36.33333	0.010097	43.6	0.008661
-	-	-	-	-	-	36.41667	0.010093	43.7	0.008661
-	-	-	-	-	-	36.5	0.01009	43.8	0.00866
-	-	-	-	-	-	36.58333	0.010087	43.9	0.00866
-	-	-	-	-	-	36.66667	0.010083	44	0.008659
-	-	-	-	-	-	36.75	0.01008	44.1	0.008659
-	-	-	-	-	-	36.83333	0.010077	44.2	0.008659
-	-	-	-	-	-	36.91667	0.010074	44.3	0.008658
-	-	-	-	-	-	37	0.010071	44.4	0.008657
-	-	-	-	-	-	37.08333	0.010068	44.5	0.008657
-	-	-	-	-	-	37.16667	0.010065	44.6	0.008657
-	-	-	-	-	-	37.25	0.010062	44.7	0.008656
-	-	-	-	-	-	37.33333	0.010059	44.8	0.008656
-	-	-	-	-	-	37.41667	0.010056	44.9	0.008655
-	-	-	-	-	-	37.5	0.010054	45	0.008655
-	-	-	-	-	-	37.58333	0.010051	45.1	0.008654
-	-	-	-	-	-	37.66667	0.010048	45.2	0.008654
-	-	-	-	-	-	37.75	0.010046	45.3	0.008653
-	-	-	-	-	-	37.83333	0.010043	45.4	0.008653
-	-	-	-	-	-	37.91667	0.010041	45.5	0.008652
-	-	-	-	-	-	38	0.010038	45.6	0.008652
-	-	-	-	-	-	38.08333	0.010036	45.7	0.008652
-	-	-	-	-	-	38.16667	0.010034	45.8	0.008651
-	-	-	-	-	-	38.25	0.010031	45.9	0.00865
-	-	-	-	-	-	38.33333	0.010029	46	0.00865
-	-	-	-	-	-	38.41667	0.010027	46.1	0.008649
-	-	-	-	-	-	38.5	0.010025	46.2	0.008649
-	-	-	-	-	-	38.58333	0.010023	46.3	0.008648
-	-	-	-	-	-	38.66667	0.010021	46.4	0.008648
-	-	-	-	-	-	38.75	0.010019	46.5	0.008647
-	-	-	-	-	-	38.83333	0.010016	46.6	0.008647
-	-	-	-	-	-	38.91667	0.010014	46.7	0.008647
-	-	-	-	-	-	39	0.010012	46.8	0.008646
-	-	-	-	-	-	39.08333	0.010011	46.9	0.008645
-	-	-	-	-	-	39.16667	0.010009	47	0.008645
-	-	-	-	-	-	39.25	0.010007	47.1	0.008645
-	-	-	-	-	-	39.33333	0.010005	47.2	0.008644
-	-	-	-	-	-	39.41667	0.010004	47.3	0.008644
-	-	-	-	-	-	39.5	0.010002	47.4	0.008643
-	-	-	-	-	-	39.58333	0.01	47.5	0.008642
-	-	-	-	-	-	39.66667	0.009999	47.6	0.008642
-	-	-	-	-	-	39.75	0.009997	47.7	0.008642
-	-	-	-	-	-	39.83333	0.009996	47.8	0.008641
-	-	-	-	-	-	39.91667	0.009994	47.9	0.008641
-	-	-	-	-	-	40	0.009992	48	0.00864
-	-	-	-	-	-	40.08333	0.009991	48.1	0.00864
-	-	-	-	-	-	40.16667	0.00999	48.2	0.00864
-	-	-	-	-	-	40.25	0.009988	48.3	0.008639
-	-	-	-	-	-	40.33333	0.009987	48.4	0.008638
-	-	-	-	-	-	40.41667	0.009986	48.5	0.008638

-	-	-	-	-	-	40.5	0.009984	48.6	0.008638
-	-	-	-	-	-	40.58333	0.009983	48.7	0.008637
-	-	-	-	-	-	40.66667	0.009982	48.8	0.008637
-	-	-	-	-	-	40.75	0.009981	48.9	0.008636
-	-	-	-	-	-	40.83333	0.00998	49	0.008636
-	-	-	-	-	-	40.91667	0.009978	49.1	0.008636
-	-	-	-	-	-	41	0.009977	49.2	0.008635
-	-	-	-	-	-	41.08333	0.009976	49.3	0.008635
-	-	-	-	-	-	41.16667	0.009975	49.4	0.008634
-	-	-	-	-	-	41.25	0.009974	49.5	0.008634
-	-	-	-	-	-	41.33333	0.009973	49.6	0.008634
-	-	-	-	-	-	41.41667	0.009972	49.7	0.008633
-	-	-	-	-	-	41.5	0.009971	49.8	0.008633
-	-	-	-	-	-	41.58333	0.00997	49.9	0.008633
-	-	-	-	-	-	41.66667	0.009969	50	0.008632
-	-	-	-	-	-	41.75	0.009969	50.1	0.008632
-	-	-	-	-	-	41.83333	0.009968	50.2	0.008631
-	-	-	-	-	-	41.91667	0.009967	50.3	0.008631
-	-	-	-	-	-	42	0.009966	50.4	0.008631
-	-	-	-	-	-	42.08333	0.009965	50.5	0.008631
-	-	-	-	-	-	42.16667	0.009965	50.6	0.00863
-	-	-	-	-	-	42.25	0.009964	50.7	0.00863
-	-	-	-	-	-	42.33333	0.009963	50.8	0.00863
-	-	-	-	-	-	42.41667	0.009963	50.9	0.008629
-	-	-	-	-	-	42.5	0.009962	51	0.008629
-	-	-	-	-	-	42.58333	0.009961	51.1	0.008629
-	-	-	-	-	-	42.66667	0.009961	51.2	0.008628
-	-	-	-	-	-	42.75	0.00996	51.3	0.008628
-	-	-	-	-	-	42.83333	0.00996	51.4	0.008628
-	-	-	-	-	-	42.91667	0.009959	51.5	0.008628
-	-	-	-	-	-	43	0.009959	51.6	0.008627
-	-	-	-	-	-	43.08333	0.009958	51.7	0.008627
-	-	-	-	-	-	43.16667	0.009958	51.8	0.008627
-	-	-	-	-	-	43.25	0.009957	51.9	0.008626
-	-	-	-	-	-	43.33333	0.009957	52	0.008626
-	-	-	-	-	-	43.41667	0.009956	52.1	0.008626
-	-	-	-	-	-	43.5	0.009956	52.2	0.008626
-	-	-	-	-	-	43.58333	0.009956	52.3	0.008626
-	-	-	-	-	-	43.66667	0.009955	52.4	0.008625
-	-	-	-	-	-	43.75	0.009955	52.5	0.008625
-	-	-	-	-	-	43.83333	0.009955	52.6	0.008625
-	-	-	-	-	-	43.91667	0.009955	52.7	0.008625
-	-	-	-	-	-	44	0.009954	52.8	0.008625
-	-	-	-	-	-	44.08333	0.009954	52.9	0.008624
-	-	-	-	-	-	44.16667	0.009954	53	0.008624
-	-	-	-	-	-	44.25	0.009954	53.1	0.008624
-	-	-	-	-	-	44.33333	0.009953	53.2	0.008624
-	-	-	-	-	-	44.41667	0.009953	53.3	0.008624
-	-	-	-	-	-	44.5	0.009953	53.4	0.008624
-	-	-	-	-	-	44.58333	0.009953	53.5	0.008624
-	-	-	-	-	-	44.66667	0.009953	53.6	0.008623
-	-	-	-	-	-	44.75	0.009953	53.7	0.008623
-	-	-	-	-	-	44.83333	0.009953	53.8	0.008623
-	-	-	-	-	-	44.91667	0.009953	53.9	0.008623
-	-	-	-	-	-	45	0.009953	54	0.008623
-	-	-	-	-	-	-	-	54.1	0.008623
-	-	-	-	-	-	-	-	54.2	0.008623
-	-	-	-	-	-	-	-	54.3	0.008623
-	-	-	-	-	-	-	-	54.4	0.008623
-	-	-	-	-	-	-	-	54.5	0.008623
-	-	-	-	-	-	-	-	54.6	0.008623
-	-	-	-	-	-	-	-	54.7	0.008623
-	-	-	-	-	-	-	-	54.8	0.008623
-	-	-	-	-	-	-	-	54.9	0.008623
-	-	-	-	-	-	-	-	55	0.008623

A.2 Coaxial Geometries

Table A.4 Field line data set of E(x) with x is the distance away from the high voltage electrode, for 10/30, 15/45 and 20/60 mm coaxial geometries with a R_z of 8 µm at 1 kV applied voltage (mesh size: 0.0005 mm minimum element size and 0.5 mm maximum element size).

10/30 mm Configuration		15/45 mm Configuration		20/60 mm Configuration	
x (mm)	E(x) (kV/mm)	x (mm)	E(x) (kV/mm)	x (mm)	E(x) (kV/mm)
0	0.208043585	0	0.134295739	0	0.103676148
0.010528907	0.201454158	0.010364231	0.131324154	0.009961521	0.100652563
0.020881049	0.196850544	0.010555045	0.131273673	0.019385284	0.098603848
0.02109552	0.19670898	0.010753868	0.131202931	0.01938931	0.098556022
0.021316031	0.196647073	0.021084849	0.128702802	0.01939452	0.098575634
0.031526141	0.192864294	0.028821865	0.127405793	0.029485276	0.096734345
0.039317785	0.190772691	0.029242319	0.127348692	0.035280775	0.095958135
0.039755674	0.190519241	0.041335688	0.125532629	0.039959949	0.095290904
0.051849776	0.187780897	0.042657169	0.125484253	0.049530974	0.094351511
0.053164971	0.187504454	0.046233397	0.125006045	0.051673463	0.094096154
0.056863349	0.186932427	0.056458944	0.123928274	0.060818684	0.093364148
0.06692218	0.185282918	0.060082071	0.123689636	0.064104941	0.093149335
0.070252052	0.18484298	0.070245194	0.122880152	0.0701753	0.092747437
0.080608973	0.183504011	0.076634786	0.122498078	0.074173236	0.092520648
0.086162978	0.182918989	0.083773537	0.122077707	0.083203362	0.092063643
0.093898763	0.182148349	0.090342636	0.121733383	0.090017826	0.091773485
0.099396994	0.181640967	0.101612869	0.121219368	0.098464177	0.091442968
0.111527165	0.180677597	0.108902258	0.120924555	0.107721823	0.091155059
0.11705469	0.180261002	0.123572618	0.120404138	0.113900622	0.090955919
0.125747546	0.179674605	0.125219727	0.120342186	0.128352839	0.090606115
0.132523263	0.179210755	0.128678677	0.120235829	0.13048685	0.090536011
0.149393177	0.178253306	0.144248252	0.119762802	0.142842993	0.090286264
0.15327482	0.178074339	0.147405887	0.119699102	0.152206978	0.090113809
0.154155695	0.178027697	0.155800189	0.119466404	0.153685057	0.09006654
0.157022252	0.177840869	0.172093202	0.119050216	0.157241449	0.090008656
0.177962323	0.176797025	0.181907186	0.11884116	0.17562446	0.089700314
0.185584481	0.176463799	0.19562796	0.118532177	0.196978341	0.089394649
0.199233075	0.175849581	0.215928395	0.118123495	0.199436126	0.089368792
0.222215075	0.174895885	0.220290317	0.118033112	0.200216472	0.089347321
0.224525143	0.174798476	0.223747153	0.117970004	0.203145841	0.089310626
0.226135052	0.174744213	0.247865979	0.11751131	0.226917081	0.089009707
0.252856932	0.173688489	0.274461696	0.117041217	0.241519995	0.088841499
0.255897707	0.173581331	0.276295154	0.117009569	0.251364573	0.088725522
0.275172715	0.172857587	0.278016094	0.116979179	0.260458549	0.088628361
0.305442289	0.17177442	0.304151161	0.116534764	0.279374438	0.088423088
0.308807296	0.171653561	0.318047921	0.116303824	0.295058961	0.088263466
0.311368662	0.171564487	0.342773824	0.11590483	0.310895252	0.088101179
0.344902469	0.170406605	0.350433798	0.115779136	0.337404857	0.087844703
0.365836235	0.169709631	0.366095929	0.115534298	0.344479882	0.087776673
0.383066841	0.169134929	0.388293739	0.115186558	0.348387471	0.087739163
0.414631311	0.168111022	0.399425228	0.115015171	0.379773815	0.087444778
0.424405637	0.167792154	0.42874504	0.114567306	0.405391433	0.0872131
0.42917212	0.167644493	0.457655669	0.114135642	0.418122809	0.087097703
0.468196439	0.16640899	0.472859677	0.113908279	0.440352171	0.086901016
0.492517548	0.165657217	0.517816748	0.113252331	0.459791395	0.08672866
0.514922099	0.164965928	0.519588625	0.113224505	0.469953035	0.086640992
0.558338518	0.16365831	0.528928415	0.113090908	0.504256318	0.086344602
0.567079283	0.16339331	0.575897435	0.112420087	0.528239505	0.086140986
0.62232952	0.161770684	0.583224792	0.112312701	0.547239194	0.08598067
0.626305653	0.161649293	0.604705128	0.112013768	0.573136494	0.085763143
0.66038073	0.160674416	0.658009484	0.111270656	0.627080018	0.085317122
0.698789135	0.159579531	0.678331708	0.110989445	0.629259861	0.085299079
0.702372683	0.159475089	0.748064467	0.110044249	0.630880163	0.085286233
0.708620546	0.15930123	0.760837088	0.109871433	0.68914099	0.084812248
0.763061142	0.157786344	0.784662938	0.109555181	0.735342678	0.084443105
0.794922006	0.156915784	0.821117808	0.109070524	0.756671214	0.084272577
0.820570305	0.156219831	0.857156028	0.108599899	0.783707043	0.084060015
0.864233092	0.155054472	0.888631676	0.108188633	0.827708832	0.083713903
0.89022997	0.154363476	0.905466356	0.107972351	0.865069962	0.083424963
0.955104628	0.152677705	0.988114426	0.106917458	0.901751359	0.083141072
0.957561068	0.152613445	1.000027196	0.106765096	0.948732095	0.08278339
0.96006351	0.152549658	1.003495902	0.10672394	0.979346948	0.082550427

1.023217821	0.150946162	1.091110682	0.10563245	0.998522383	0.082406367
1.056386496	0.150122764	1.115091265	0.105340172	1.058147458	0.081959756
1.096966232	0.149118098	1.188208867	0.104451561	1.112044061	0.081561624
1.166218367	0.147443497	1.232824979	0.103919593	1.1683025	0.081148555
1.188939629	0.146898315	1.29731273	0.103155629	1.269382855	0.080420841
1.212021476	0.14635671	1.375709417	0.102247665	1.285890275	0.080301381
1.293329653	0.144463577	1.423679494	0.101695892	1.317554872	0.080078821
1.330681238	0.143608327	1.488685419	0.100964236	1.406111239	0.079455332
1.407803143	0.141878972	1.525271146	0.100552104	1.454032436	0.079124335
1.473332388	0.140447861	1.623592979	0.099471465	1.531668582	0.078590433
1.537045921	0.139072492	1.65542219	0.099124211	1.611063774	0.078053901
1.639451047	0.13693162	1.714286118	0.098496571	1.64926102	0.077798947
1.640427158	0.136911371	1.776818314	0.097829544	1.707954237	0.077408427
1.751290648	0.134661082	1.907705518	0.096471907	1.810928249	0.076734559
1.789216761	0.133914861	1.913990938	0.096406838	1.816843895	0.076695677
1.886107365	0.132026277	1.920709249	0.096338235	1.821124544	0.076668477
1.996180766	0.129952474	2.059171128	0.094945137	1.928588535	0.075978515
2.055725571	0.128855334	2.209039516	0.093485182	2.081564881	0.075018098
2.188986169	0.126464079	2.23233358	0.093257636	2.096574355	0.074925987
2.284406276	0.124822603	2.243084604	0.093158221	2.105432673	0.074869601
2.360941827	0.123510159	2.454941267	0.091179709	2.277496249	0.073824451
2.446601176	0.12210697	2.54941642	0.090326604	2.309108775	0.073635306
2.543736883	0.120521301	2.694973761	0.089039344	2.454125625	0.072777994
2.809164508	0.116410181	2.762594685	0.088457692	2.634335744	0.071746472
2.811502445	0.116396233	2.896937616	0.087312995	2.673837034	0.071519903
2.81206067	0.116370535	3.060256658	0.08596904	2.689060411	0.07143734
2.813244851	0.116353547	3.064103926	0.085938403	2.801678683	0.070815263
3.060809726	0.112793141	3.270964806	0.084293642	2.977477469	0.069850811
3.229200847	0.110504818	3.291049439	0.084132795	3.00370508	0.069715018
3.303884189	0.109496142	3.513637753	0.082443239	3.078739515	0.069319511
3.386393836	0.108438097	3.561003937	0.082088736	3.232966052	0.068511577
3.534888179	0.106535519	3.760603193	0.080637567	3.333882577	0.06799892
3.769778847	0.103704943	3.882936582	0.079782773	3.41678551	0.067575414
3.8723026	0.102460254	4.022860626	0.078806696	3.688912264	0.066240805
4.020934116	0.100826388	4.148963202	0.077967672	3.694763321	0.0662123
4.317726569	0.097569243	4.362857368	0.076552858	4.015861511	0.064701924
4.600219078	0.094747822	4.658798477	0.074706082	4.115838273	0.06424999
4.731940316	0.093432297	4.717940899	0.074336216	4.436732253	0.062829311
4.86051634	0.092248212	4.761606691	0.074081862	4.543937956	0.062369654
5.138846493	0.08968697	5.07869174	0.072215661	4.846112449	0.061106358
5.417424542	0.087322232	5.379900929	0.070543763	4.99883972	0.060495129
5.542865219	0.086256012	5.447522792	0.070167465	5.202279204	0.059687869
5.668337051	0.085270421	5.552953375	0.069616391	5.459560423	0.058707863
5.946421563	0.08308329	5.818051595	0.068225447	5.563348781	0.05831513
6.226477077	0.081035782	5.980860638	0.067417883	5.64970118	0.057997877
6.349941356	0.080133072	6.185641713	0.066403793	5.935195719	0.056966697
6.473017485	0.079296196	6.514971094	0.064856248	6.080081736	0.056461529
6.753828996	0.077385098	6.575604552	0.064573106	6.284349156	0.055758731
7.036450612	0.075588328	6.65540881	0.06421923	6.521289734	0.054969879
7.158133971	0.074814789	6.963275496	0.062852729	6.58387225	0.054762211
7.279666536	0.07409271	7.258168236	0.061611939	6.636875005	0.054590293
7.562798743	0.072409326	7.345392392	0.061244711	6.935797954	0.053636351
7.846205555	0.070828482	7.436617908	0.060880429	7.207851964	0.052802265
7.967665619	0.070151056	7.732017049	0.059699653	7.366724586	0.05232063
8.089125683	0.0695152	8.016283092	0.058620161	7.580564331	0.051699061
8.372532496	0.068030631	8.122125144	0.058218322	7.7996116	0.051064693
8.655939308	0.066632454	8.230738107	0.057826136	7.987945713	0.050543282
8.777399371	0.066033298	8.516178518	0.056795225	8.188529961	0.049987872
8.898859435	0.065468765	8.799555182	0.055820818	8.452847939	0.049286772
9.182266247	0.064150822	8.914264469	0.055426564	8.556067992	0.049012093
9.465673061	0.062905311	9.030806302	0.055044939	8.622406342	0.048843167
9.587133124	0.062371568	9.315825734	0.054111751	8.903313463	0.048126389
9.708593187	0.061866976	9.599842002	0.0532248	9.219268723	0.047348709
9.830053249	0.061362384	9.719079154	0.052852584	9.254930189	0.047262116
9.951513312	0.060857792	9.839302042	0.052494425	9.319744952	0.04710779
10	0.060353201	10.12327414	0.051648438	9.59334825	0.046458487
-	-	10.40677608	0.05084121	9.833961625	0.045907239
-	-	10.52796986	0.05049632	9.937333821	0.045670222
-	-	10.64939463	0.050165722	10.01353555	0.045501583
-	-	10.93282535	0.049393984	10.31266232	0.044840706
-	-	11.21623217	0.048655331	10.60892907	0.044210401
-	-	11.33769223	0.048338855	10.71065288	0.043994199
-	-	11.45915229	0.048035447	10.81356413	0.043783663

-	-	11.74255911	0.047327491	11.10607931	0.043185128
-	-	12.02596592	0.046648459	11.39133421	0.042622737
-	-	12.14742598	0.04635754	11.50220978	0.042404337
-	-	12.26888605	0.046078095	11.61504433	0.042189918
-	-	12.55229286	0.045426105	11.90097844	0.041646876
-	-	12.83569967	0.044799571	12.18481745	0.041126865
-	-	12.95715974	0.04453109	12.30218396	0.040911879
-	-	13.0786198	0.044272891	12.42108355	0.040701812
-	-	13.36202661	0.043670434	12.70539696	0.040199345
-	-	13.64543343	0.04309028	12.98895031	0.039715604
-	-	13.76689349	0.042841722	13.10953703	0.039509896
-	-	13.88835355	0.042602293	13.23065849	0.039310318
-	-	14.17176036	0.042043677	13.51417323	0.038843064
-	-	14.45516718	0.041504912	13.79759316	0.038391504
-	-	14.57662724	0.041274075	13.9189995	0.038198181
-	-	14.6980873	0.041051401	14.04045548	0.038010959
-	-	14.81954737	0.040828727	14.32386373	0.037574349
-	-	14.94100743	0.040606053	14.60727055	0.037151425
-	-	15	0.040383378	14.72873061	0.036970328
-	-	-	-	14.85019067	0.036794773
-	-	-	-	15.13359748	0.036385328
-	-	-	-	15.4170043	0.035988376
-	-	-	-	15.53846436	0.035818308
-	-	-	-	15.65992442	0.035653329
-	-	-	-	15.94333124	0.035268437
-	-	-	-	16.22673805	0.034894799
-	-	-	-	16.34819811	0.034734762
-	-	-	-	16.46965818	0.034579288
-	-	-	-	16.75306499	0.034216684
-	-	-	-	17.0364718	0.033864116
-	-	-	-	17.15793187	0.033713149
-	-	-	-	17.27939193	0.033566274
-	-	-	-	17.56279874	0.033223828
-	-	-	-	17.84620556	0.032890469
-	-	-	-	17.96766562	0.032747723
-	-	-	-	18.08912568	0.032608706
-	-	-	-	18.37253249	0.032284542
-	-	-	-	18.65593931	0.031968733
-	-	-	-	18.77739937	0.031833493
-	-	-	-	18.89885943	0.031701635
-	-	-	-	19.18226625	0.031394198
-	-	-	-	19.46567306	0.031094384
-	-	-	-	19.58713312	0.030966007
-	-	-	-	19.70859319	0.030840704
-	-	-	-	19.83005325	0.0307154
-	-	-	-	19.95151331	0.030590096
-	-	-	-	20	0.030464792

Table A.5 Field line data set of E(x) with x is the distance away from the high voltage electrode, for 10/30 mm configuration, with R_z varied between 8.95-121.8 µm at 1 kV applied voltage (mesh size: 0.0005 mm minimum element size and 0.5 mm maximum element size).

R_z of 8.95 µm		**R_z of 14.65 µm**		**R_z of 46.58 µm**		**R_z of 121.8 µm**	
x (mm)	**E(x) (kV/mm)**	**x (mm)**	**E(x) (kV/mm)**	**x (mm)**	**E(x) (kV/mm)**	**x (mm)**	**E(x) (kV/mm)**
0	0.209564964	0	0.217356486	0	0.246358	0	0.286892407
0.0113326	0.202435833	0.0118	0.209550928	0.051972677	0.212882	0.050951395	0.245706725
0.0225558	0.197481743	0.0239	0.203688477	0.09603643	0.201333	0.08908791	0.230618287
0.0228352	0.197307064	0.0241	0.203577115	0.10634948	0.197696	0.103646548	0.223576071
0.0231194	0.19722623	0.0242	0.203516857	0.114012475	0.196745	0.115368337	0.220715899
0.0343513	0.193125604	0.0362	0.198600947	0.161718065	0.188076	0.155648044	0.208570243
0.0432075	0.190798539	0.0454	0.195801661	0.205159508	0.183645	0.20885555	0.198659789
0.043965	0.190485856	0.046	0.195467229	0.222379421	0.181849	0.221504264	0.195935153
0.0569919	0.187673319	0.0574	0.192487195	0.250734446	0.179602	0.229155796	0.195627248
0.0581966	0.187413665	0.0607	0.191777629	0.285412097	0.176859	0.29616608	0.186239619
0.0618311	0.186889345	0.0719	0.189274252	0.304976269	0.175772	0.311411547	0.185109651
0.0743554	0.184940041	0.0782	0.18821706	0.361008117	0.172576	0.36152448	0.180208994
0.0788748	0.184391157	0.0846	0.18715033	0.403891461	0.170624	0.397214089	0.177514535
0.0913554	0.182881847	0.0925	0.185938516	0.436021676	0.169131	0.431939435	0.174895093
0.100661	0.182023101	0.1043	0.184476446	0.512374438	0.166152	0.500287948	0.17093212
0.1080464	0.181346196	0.1076	0.184066693	0.51800252	0.165879	0.512277004	0.170082063
0.1171435	0.180620866	0.1236	0.182369234	0.533763844	0.165327	0.560857248	0.167713747

0.126244	0.179983742	0.1261	0.182116764	0.603953322	0.162862	0.602690389	0.165761373
0.1290514	0.179781062	0.1478	0.18029613	0.624301771	0.162167	0.612229097	0.165222963
0.1472323	0.178669763	0.1493	0.180186565	0.696316003	0.159872	0.703176531	0.16139597
0.1481005	0.178617193	0.173	0.178556129	0.72611985	0.158916	0.735423854	0.160221465
0.1490058	0.178528301	0.174	0.178500286	0.778747278	0.157375	0.809195724	0.157531923
0.1726941	0.177266208	0.1798	0.178169831	0.837378012	0.155644	0.872800521	0.155454556
0.1797062	0.176925243	0.1971	0.177145822	0.891946572	0.154138	0.923818136	0.153806112
0.1972935	0.176092033	0.2003	0.177001728	0.917051693	0.153436	1.031089468	0.150611102
0.1997517	0.175991967	0.2198	0.175964777	0.9665507	0.152114	1.047642905	0.15015534
0.2159342	0.175274573	0.2305	0.175461024	1.006758363	0.151038	1.149787489	0.147344903
0.2297227	0.174710299	0.2474	0.174663652	1.020551933	0.150692	1.176092379	0.146665282
0.2412812	0.174234917	0.2743	0.173507657	1.126106259	0.147997	1.17930064	0.146535099
0.2603625	0.173501002	0.282	0.173184184	1.173195969	0.146846	1.337594947	0.142562171
0.271661	0.173062042	0.2916	0.172799138	1.316571182	0.143442	1.340105653	0.142509133
0.282587	0.172664977	0.318	0.171749311	1.318059196	0.143399	1.345078737	0.142400149
0.3062701	0.171794021	0.3494	0.170589128	1.320335648	0.143348	1.464849637	0.139600373
0.3244201	0.171163027	0.354	0.170420673	1.470330155	0.139984	1.519016451	0.138384412
0.3443934	0.170464589	0.3592	0.170229946	1.554626408	0.13818	1.60559566	0.136493304
0.3849991	0.169098467	0.3939	0.169000118	1.620861683	0.136776	1.673155019	0.13504508
0.3857657	0.169076968	0.4104	0.168443749	1.735147941	0.134444	1.773631681	0.132994938
0.3872813	0.169021512	0.4425	0.167364941	1.739294446	0.134365	1.832468909	0.131801415
0.4287208	0.167670909	0.4545	0.166964948	1.883266627	0.131537	1.981056242	0.128935625
0.4477318	0.167069157	0.4858	0.165957765	1.916657256	0.130906	1.994572727	0.128694107
0.4733453	0.166258407	0.4999	0.165505917	2.122104966	0.127125	1.998089797	0.128604268
0.5026599	0.165350516	0.5065	0.165297642	2.156188886	0.126513	2.200664445	0.124958312
0.5102029	0.165115765	0.5466	0.164044024	2.318426434	0.123712	2.226865268	0.124472131
0.5189071	0.164851798	0.5864	0.162836467	2.402033925	0.122322	2.278940216	0.123599476
0.5558936	0.163726664	0.5979	0.162488175	2.510291892	0.120553	2.46284507	0.120508198
0.6168912	0.161920224	0.6139	0.162013878	2.633253517	0.118619	2.637732899	0.117765331
0.618613	0.16187507	0.6519	0.160889076	2.681576405	0.117876	2.687964226	0.116971113
0.619239	0.161850002	0.6844	0.159954624	2.821907179	0.115766	2.734933687	0.116279186
0.6216301	0.161781359	0.7116	0.159173183	2.907243084	0.114515	2.916012298	0.11360073
0.6883574	0.159864686	0.7464	0.15819562	3.060901442	0.112344	3.117120085	0.110806574
0.710865	0.159230161	0.7681	0.157585742	3.074702589	0.112146	3.158454439	0.110229461
0.7531139	0.158049994	0.8048	0.156582018	3.249276112	0.109781	3.187110541	0.109861744
0.7925751	0.156967311	0.8398	0.155630483	3.301031598	0.109105	3.43198314	0.10667026
0.8278428	0.156012109	0.8506	0.155340939	3.513019995	0.10638	3.643543495	0.104101303
0.8676919	0.154945877	0.9231	0.153424256	3.772354644	0.103276	3.80860568	0.102112854
0.9427432	0.15298012	0.9538	0.152613739	3.905215472	0.101696	3.989643633	0.100123063
0.9454157	0.152909893	0.9588	0.152488357	4.038476847	0.10025	4.229454887	0.097489466
0.9466968	0.152881051	1.0562	0.150020258	4.301939587	0.097376	4.501288181	0.09476471
0.9511348	0.152763109	1.0709	0.149661223	4.579146357	0.094609	4.629747748	0.093476162
1.0363714	0.150599129	1.1541	0.147625436	4.701478477	0.093388	4.757119704	0.092297853
1.1114911	0.14874986	1.1911	0.146748925	4.815822891	0.092336	5.030052116	0.089774707
1.1276646	0.14835069	1.2432	0.145510493	5.101432871	0.089706	5.312100156	0.087369963
1.135302	0.148170711	1.2848	0.144555342	5.39181013	0.087238	5.430916262	0.086355609
1.2235501	0.14606317	1.352	0.143013361	5.504223388	0.086282	5.549848818	0.085417497
1.2800217	0.144755257	1.4097	0.141735176	5.618028098	0.085387	5.832300822	0.083186212
1.3192171	0.143851985	1.474	0.140313247	5.907122944	0.083111	6.115229565	0.081109777
1.4009752	0.142016092	1.5713	0.138246533	6.192360189	0.081023	6.234811306	0.080232088
1.4027617	0.141976641	1.6144	0.137335313	6.310567612	0.080159	6.355421623	0.079409058
1.4925922	0.140004577	1.6717	0.136167304	6.430177061	0.079345	6.63836373	0.077476455
1.6112197	0.137499338	1.7355	0.134868138	6.71472236	0.077406	6.921024908	0.075673982
1.6288652	0.137127268	1.8364	0.132880186	6.998160794	0.075603	7.042800936	0.074897408
1.680787	0.136075517	1.8748	0.132140535	7.119374753	0.074832	7.16497187	0.074169602
1.7691371	0.134285666	2.0142	0.129509749	7.24084173	0.07411	7.447651313	0.072484245
1.7956177	0.133771858	2.0682	0.128520659	7.524222035	0.072424	7.730258387	0.070904227
1.9320951	0.131129863	2.2146	0.125918618	7.807622677	0.070843	7.852517336	0.070220682
2.0223709	0.129458312	2.2733	0.124890568	7.929086621	0.070165	7.974788136	0.069579287
2.080512	0.128386129	2.3767	0.1231697	8.05054763	0.069529	8.25738414	0.068095809
2.2023388	0.126225172	2.4862	0.121344236	8.333952747	0.068044	8.539981147	0.066699189
2.255071	0.125294733	2.6079	0.119431075	8.617359287	0.066645	8.662250964	0.066094916
2.3614798	0.123505483	2.7156	0.117741289	8.738819375	0.066046	8.784520766	0.06552577
2.432073	0.122312502	2.8746	0.115392594	8.860279445	0.065481	9.067117837	0.064209498
2.4685029	0.1217236	2.9677	0.114030456	9.143686247	0.064163	9.349714916	0.062966006
2.6091129	0.119478634	3.0038	0.113515223	9.427093061	0.062917	9.471984713	0.062427984
2.6819619	0.118346414	3.2187	0.110545197	9.548553124	0.062383	9.59425451	0.061919527
2.8986579	0.115102345	3.3888	0.108328031	9.670013187	0.061878	9.716524306	0.06141107
2.9608259	0.114186093	3.4894	0.107027366	9.791473249	0.061373	9.838794103	0.060902613
3.0426849	0.113052931	3.8111	0.103135472	9.912933312	0.060869	9.9610639	0.060394156
3.2503579	0.110184976	3.8642	0.102483655	10	0.060364	10	0.06
3.4831095	0.107178051	3.9501	0.101535235	-	-	-	-
3.4963881	0.107006198	4.3112	0.097572614	-	-	-	-

3.8415258	0.102831896	4.6268	0.094417662	-	-	-	-
3.8522652	0.102679232	4.7231	0.093456865	-	-	-	-
3.8711326	0.102470786	4.8244	0.092523445	-	-	-	-
4.3004549	0.097740058	5.1299	0.0897103	-	-	-	-
4.622594	0.094512077	5.4195	0.087250603	-	-	-	-
4.7214611	0.093523142	5.5345	0.086272584	-	-	-	-
4.8320373	0.092504194	5.6532	0.08534014	-	-	-	-
5.1327911	0.089731531	5.9387	0.083093965	-	-	-	-
5.4187534	0.087302554	6.2209	0.081029655	-	-	-	-
5.5379994	0.086290155	6.3427	0.08013948	-	-	-	-
5.6588952	0.08533818	6.4649	0.079308246	-	-	-	-
5.9427939	0.083103805	6.7469	0.077388668	-	-	-	-
6.2260584	0.08103193	7.0296	0.075591388	-	-	-	-
6.3473938	0.080144559	7.1514	0.074816748	-	-	-	-
6.4691907	0.079316184	7.2732	0.074093381	-	-	-	-
6.752135	0.077390185	7.5562	0.072410681	-	-	-	-
7.0355086	0.075588458	7.8395	0.070830077	-	-	-	-
7.1569821	0.07481621	7.961	0.070152478	-	-	-	-
7.2784423	0.074094559	8.0825	0.069516544	-	-	-	-
7.5618489	0.072409516	8.3659	0.068031989	-	-	-	-
7.8452555	0.070828664	8.6493	0.066633767	-	-	-	-
7.9667156	0.070151233	8.7707	0.066034586	-	-	-	-
8.0881757	0.069515373	8.8922	0.065470036	-	-	-	-
8.3715825	0.068030797	9.1756	0.064152049	-	-	-	-
8.6549893	0.066632614	9.459	0.062906505	-	-	-	-
8.7764494	0.066033455	9.5805	0.062372747	-	-	-	-
8.8979094	0.06546892	9.7019	0.061868145	-	-	-	-
9.1813162	0.064150972	9.8234	0.061363543	-	-	-	-
9.4647231	0.062905456	9.9449	0.060858941	-	-	-	-
9.5861831	0.062371711	10	0.060354338	-	-	-	-
9.7076432	0.061867118	-	-	-	-	-	-
9.8291032	0.061362525	-	-	-	-	-	-
9.9505633	0.060857932	-	-	-	-	-	-
10	0.060353339	-	-	-	-	-	-

APPENDIX B: STREAMER CRITERION MATLAB CODE

```
clc
clear
data=[%Insert the field line points x and E(x) in two columns];
A=%Use Table 6.1;
B=%Use Table 6.1;
K=%Use Table 6.1;
p=%Desired gas pressure;
voltage= 1:0.01:350; %Expected breakdown voltage should be within the defined range.
for j=1:1:length(voltage)
field=data(:,2)*voltage(j); %Multiply E(x) with the voltage every loop.
 for i=1:1:length(field) %This loop is to calculate the positive α_eff.
  if (field(i)/p) < B
 alpha(i) = 0;
  else
 alpha(i) = A*p*(field(i)/p-B);
  end
x(i)=data(i,1);
 end
integ(j)=trapz(x,alpha); %This is to evaluate the green area shown in Figure 6.3.
 if integ(j)>=K %As per Equation 6.1, breakdown is possible if the integration is greater
than or equal to K.
    Ui=voltage(j) %This voltage represents the streamer inception voltage.
    break
 end
end
```